Improvement of oral antineoplastic therapy by means of pharmacometric approaches & therapeutic drug monitoring

DISSERTATION

zur Erlangung des

naturwissenschaftlichen Doktorgrades der

Julius-Maximilians-Universität Würzburg

vorgelegt von

Bettina Gerner

aus Regensburg

Würzburg

2023

Eingereicht bei der Fakultät für Chemie und Pharmazie am:

……

Gutachter der schriftlichen Arbeit:

1. Gutachter ……

2. Gutachter ……

Prüfer des öffentlichen Promotionskolloquiums:

1. Prüfer ……

2. Prüfer ……

3. Prüfer ……

Tag der Prüfung:

Datum des öffentlichen Promotionskolloquiums:

……

Doktorurkunde ausgehändigt am:

……

Meiner Familie

Wer fragt, ist ein Narr für fünf Minuten.

Wer nicht fragt, bleibt es für immer.

Die vorliegende Arbeit wurde auf Anregung und unter Anleitung von

Herrn Prof. Dr. Oliver Scherf-Clavel

am Lehrstuhl für Pharmazeutische Chemie
des Instituts für Pharmazie und Lebensmittelchemie
der Julius-Maximilians-Universität Würzburg angefertigt.

Danksagung

Allen voran möchte ich *Herrn Prof. Dr. Oliver Scherf-Clavel* für die freundliche Aufnahme in seinen Arbeitskreis, für sein in mich gesetztes Vertrauen und für seine Offenheit neuen und spannenden Projekten gegenüber herzlich danken. Seine Unterstützung während der gesamten Zeit, sei es in Form von Diskussionen und Anregungen oder durch die Möglichkeit an zahlreichen Kongressen, Fort- sowie Weiterbildungen teilzunehmen, hatte einen großen Beitrag zu meiner fachlichen und persönlichen Entwicklung.

Ein weiterer Dank gilt den Mitarbeitern der Endokrinologie des Universitätsklinikums Würzburg. Durch ihr Engagement und die Bereitstellung von Proben und klinischen Daten konnten große Teile der Arbeit angefertigt werden. Hier möchte ich insbesondere Herrn *Prof. Dr. Dr. Matthias Kroiss* und Herrn *Dr. Max Kurlbaum* sowie Frau *Sabine Kendl* und Frau *Michaela Haaf* für ihren stets tatkräftigen Einsatz und für ihre Unterstützung danken.

Herzlichen Dank auch an *Dr. Nora Isberner* von der Medizinischen Klinik und Poliklinik II des Universitätsklinikums Würzburg für Ihre Expertise und Unterstützung bei allen Fragen rund um Ruxolitinib und GvHD.

Dem *Graduate Research Training Program PharMetrX* (Pharmacometric and Computational Disease Modelling) möchte ich danken, dass ich als Training+ Student an den lehrreichen Modulen teilnehmen und so ins Gebiet der Pharmakometrie eintauchen konnte. Das entstandene Netzwerk und der Austausch untereinander sind eine große Bereicherung.

Ein besonderer Dank gilt *Dr. Valerie Nock* von Boehringer Ingelheim, die mich in allen Belangen zur Pharmakometrie enorm unterstützt hat. Vielen Dank, für die Zeit, die du dir so oft genommen hast, meine Projekte und Fragen zu besprechen und für deine stets aufbauenden Worte.

Den Assistenten der klinischen Pharmazie und Pharmakotherapie *Linda Volpp, Florian Lang* und *Charlotte Beier* möchte ich für die professionelle, aber auch sehr unterhaltsame Zusammenarbeit bei der Studierendenbetreuung danken. Auch wenn es oft recht zeitintensiv war, möchte ich die gesammelte Erfahrung auf keinen Fall missen. Auch allen anderen ehemaligen und aktuellen Mitgliedern des Arbeitskreises von Frau Prof. Dr. Högger möchte ich danken. Ich werde unsere gemeinsamen Unternehmungen sowie das ein oder andere Glas Wein in bester Erinnerung behalten. Ohne euch wäre die Zeit in Würzburg nur halb so schön gewesen!

Meinen Bürokollegen, *Alexander Becht, Maximilian Stapf* und *Sebastian Zimmermann* möchte ich für die lustigen Gespräche danken, sie haben den Arbeitsalltag oft ganz besonders gemacht. Vor allem dir, Sebastian, möchte ich danken! Die gegenseitige Unterstützung während unseres gemeinsamen Starts in das Abenteuer Promotion, die vielen Gespräche, während der guten und weniger guten Phasen und unsere Freundschaft hat die gesamte Zeit einmalig gemacht. Ein besonderer Dank geht auch an Alex, für unsere Zeit als WG-Mitglieder und die Freundschaf, die auch nach Ende der gemeinsamen Zeit in Würzburg bestehen bleibt!

Danke *Mahssa*, für unsere lustigen Telefonate und für unseren intensiven Austausch zu allen Fragen rund um die Pharmakometrie.

Meinen *Eltern* und meiner Schwester *Sandra* ein herzliches Dankeschön dafür, dass sie immer für mich da sind und für den schönen Zusammenhalt in allen Lebenslagen.

Der größte Dank gilt meinem Mann, *Simon*. Dafür, dass du mich ermutigt hast, nochmal nach Würzburg zu gehen um zu promovieren und die Zeit der Fernbeziehung mitgetragen hast. Dafür, dass du immer für mich da bist und mich unglaublich unterstützt, nicht nur während der Zeit der Promotion. Zu guter Letzt möchte ich mich auch bei meiner Tochter *Linda* bedanken, dafür, dass sie mir jeden Tag ein Lächeln ins Gesicht zaubert.

Table of Contents

A Introduction

1 Principles of pharmacokinetics, pharmacodynamics and oral drug administration

Pharmacokinetics (PK) is derived from the ancient greek words "pharmakon" (= drug substance, medicine, or poison) and "kinetikos" (= movement) and thus expresses the movement of a drug through the body. PK describes the concentration time course of a drug substance and its metabolites in plasma or any other body fluid or tissue after administration. Simplified it is often paraphrased as "what the body does to a drug". In contrast, the word pharmacodynamics (PD) contains the greek word "dynamikós" which means force or power and describes the effect of a given substance in relation to its concentration in plasma or at the site of action. PD thus is defined as "what the drug does to the body". Based on the drug´s PK and PD properties a relationship between a given dose, the resulting drug concentration in body fluids and the pharmacologic response can be determined and an effect over time course can be established [1] (Figure 1).

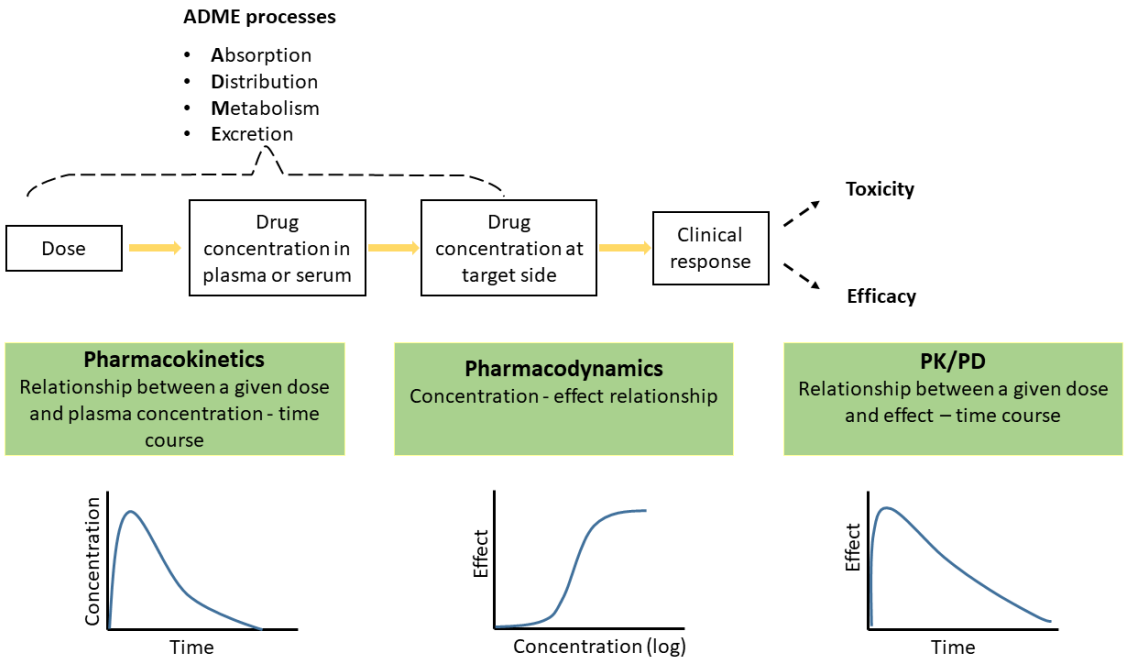

Figure 1. Schematic representation of oral drug administration, time-concentration, concentration-effect, and time-effect relationship.

The concentration-time course is mainly determined by the pharmacokinetic processes of absorption (in case of extravascular administration), distribution, metabolism, and excretion (ADME). In contrast to intravenous (i.v.) administration, only a certain proportion of the given dose may reach the systemic circulation after oral drug administration, expressed by a lower absolute bioavailability [2]. The primary site of drug absorption after oral intake is mainly the small intestine. The bioavailability or systemically available fraction, respectively, of an orally

administered drug is limited for many substances clearly below 100% due to e.g. limited absorption across the gut wall, intestinal metabolism or first-pass elimination by the liver [3,4]. The extent and rate of oral drug absorption will also be influenced by drug release from a solid oral dosage form (e.g., immediate-release versus extended-release), the solubility of the drug substance in the intestinal fluids, its permeability and transporter processes. All these conditions, or rather prerequisites, lead to high inter- and intraindividual variability in drug absorption. This in consequence makes the prediction of systemic exposure, expressed by the area under the concentration-time curve (AUC), on an individual level difficult.

Variability in physiological processes (e.g., gastric emptying time, intestinal transit time, fluid volumes, fasted vs. fed state), differences within the population (age, sex, ethnicity), diseases specificities, drug formulation properties, food-drug interactions or variability in gut-microbiota are possible, but by no means all sources of high variability in PK after oral drug absorption [5-7]. Another process that can contribute to variability in systemic exposure is enterohepatic recirculation (EHC). After intestinal absorption and transfer to the liver via the portal vein, drugs undergoing EHC are recycled via the biliary system to the intestine, where they can be either reabsorbed or finally excreted.

After the drug has reached systemic circulation, the apparent volume of distribution (V_d) is important to quantify its distribution between plasma and other tissues or fluids outside the plasma. V_d is a proportionality constant that relates the measured drug concentration to total drug amount in the body at a given time (Equation (Eq.) 1). It is more a theoretical value ("apparent") rarely reflecting true physiologic volumes. The apparent V_d can vary significantly between patients, based on physiology and pathophysiology (such as body weight, body fat and changes in body composition with aging).

The concept of V_d is strongly linked to plasma protein and tissue binding of a drug. Plasma proteins to which drug binds are mainly albumin and alpha1-acid-glycprotein (AGP) and to a lower extend lipoproteins and α-, β- and γ-globulins [5,8]. Within the vascular space, drugs (mainly basic drugs) can also bind to and distribute into erythrocytes, depending on lipophilicity, pKa and active uptake into erythrocytes. Tissue components which are important for drug distribution are phospholipids, neutral lipids, proteins, and tissue water. Depending on lipophilicity and basicity/acidity, drugs tend to have smaller or greater V_d and as a rule of thumb, a lower V_d is associated with high plasma affinity whereas a higher V_d is associated with high tissue affinity. Acidic drugs mainly bind to plasma albumin and tend to have small V_d. In contrast, basic drugs are more likely to bind to AGP and to erythrocytes and are characterized by a higher V_d. The binding affinity of a drug to plasma proteins influences the fraction of drug that is free, meaning not bound to any plasma protein. The fraction in plasma unbound (f_{up}) is

of great importance for pharmacological efficacy as only unbound, and un-ionized, drugs are able to penetrate membranes and to interact with target proteins such as receptors, channels, and enzymes [9]. Drugs that are highly bound to plasma proteins are very sensitive to changes in plasma protein concentrations. Several factors and conditions, such as stress, pregnancy, surgery, liver dysfunctions or obesity can lead to alterations in plasma protein concentration, especially in AGP concentration but also in plasma albumin concentration [5]. In cancer patients high AGP level and low albumin level can be observed, leading to increased or reduced drug binding to AGP and albumin, which results in clinically relevant alterations in PK, like a higher or lower drug exposure, respectively [10]. Abnormal accumulation of fluid (oedema, ascites, pleural effusion), changing body composition with increasing age (neonates, paediatrics vs. adults and older people) or obesity vs. normal BMI can further contribute to interindividual variability in drug distribution [11]. As the precise knowledge of V_d is crucial for calculating initial dosing(s) [8,12,13], these factors must be considered to prevent patients from over or -underdosing.

$$\mathbf{V_d = \frac{\text{Amount of drug in the body (mg)}}{\text{Plasma concentration of drug } \left(\frac{\text{mg}}{\text{L}}\right)}} \qquad \textbf{Eq. 1}$$

Drug elimination describes the irreversible loss of the active substance and occurs either via metabolism, meaning an enzymatic biotransformation of the drug or through excretion, referring to the removal of the drug via the renal or hepatobiliary route. The rate of elimination is dependent on the unbound drug concentration in a specific fluid, mainly plasma, and the clearance (CL). CL is a proportionality factor, that relates the rate of drug elimination to the drug concentration (Eq. 2). It gives the volume or fluid that is cleared per time unit by elimination and therefore has units of flow (e.g., L/h), whereas elimination describes the rate of loss (e.g. mg/h) [12].

$$\textbf{Rate of elimination = Drug concentration (mg/L) • CL (L/h)} \qquad \textbf{Eq. 2}$$

Only unbound drug is capable to be cleared and the total CL is composed of the sum of all organ CL, with renal and hepatic CL being the most important ones (Eq. 3). CL is directly linked to the organic blood flow and is a key parameter to determine steady state plasma concentrations and maintenance dosing(s) [12,13].

$$\mathbf{CL_{total} = CL_{renal} + CL_{hepatic} + CL_{others}} \qquad \textbf{Eq. 3}$$

A hybrid parameter that includes V_d, clearance and a proportionality constant (ln 2) is the half-life ($t_{1/2}$) (Eq. 4), which describes the time that is needed for a drug concentration to

reach half of its original value. It is commonly used to describe and quantify accumulation, elimination and distribution processes and to predict the time for reaching plasma steady-state concentrations (C_{ss}) [8,13].

$$t_{1/2} = \frac{\ln 2 \cdot V_d}{CL} \qquad \textbf{Eq. 4}$$

Steady state is achieved once the rate of drug input equals the rate of drug elimination. The time to reach steady state depends only on the plasma elimination half-time of the substance and is independent of the given dose. C_{ss} is reached after four (93.8% steady state concentration) to five (96.9% steady state concentration) half-lives [8,14].

Summing up, many aspects of the ADME processes must be considered, when it comes to oral drug administration no matter if the drug is given as tablet, capsule, solution, suspension etc. Every single step is susceptible to between patient but also within patient variability (i.e., variability between two administrations). The more factors exist that influence ADME processes, the higher the risk of inter- and intra-individual variations in observed drug concentrations. This may end up in potential under- or overdosage for the respective patient resulting in either a loss of efficacy or in an increased rate of adverse drug events. Knowledge about the PK and PD principles is valuable to assess the different approaches which were investigated in the present work to improve therapy with oral antineoplastic drugs.

2 Oral targeted antineoplastic therapy

2.1 Paradigm shift to oral targeted therapy

Over the past 20 years, the treatment of cancer and immunological diseases has significantly changed. In 2001, the U.S. Food and Drug Administration (FDA) approved the tyrosine kinase inhibitor (TKI) imatinib for the treatment of chronic myelogenous leukaemia in blast crisis, accelerated phase, or in chronic phase after failure of IFN-alpha therapy [15]. The launch of imatinib is considered to be the first targeted oral anti-cancer therapy and gave the go-ahead for a modern oral targeted anticancer therapy, even though other oral targeted therapy, such as selective estrogen receptor modulators (e.g., tamoxifen), were already approved more than 40 years ago. The use of new oral anticancer drugs has led to a significant improvement in patient care, survival prognosis and patients´ quality of live in various cancers. A high improvement of the overall survival rate due to the introduction of targeted therapy was for example reached in the treatment of chronic myeloid leukaemia, where it increased from 20% up to 80-90% [16,17]. In recent years, new types of cancer treatments have emerged. Different types of novel antineoplastic drugs have been developed, whereby targeted therapy uses drugs to target specific proteins that help cancer cells to survive and grow. Typical types of targeted therapy are small molecule drugs (mainly TKIs) or monoclonal antibodies (mAbs)[18-22].

Until the development of targeted antineoplastic drugs, conventional chemotherapy, along with radiation therapy, was the only approach to treat malignant tumours. The combination of chemotherapy, surgery and radiation therapy still is the treatment of choice for most solid tumours. However, the introduction of targeted antineoplastic drugs expanded treatment options, which can be applied as first-line or second-line therapy for various solid cancers [23] as well as for haematological [24] and immunological malignancies [25]. Furthermore, targeted therapies can be combined with cancer immunotherapy, which offers a number of possible synergies [26]. Targeted therapies are characterized by a remarkable and rapid clinical response in many patients, however long-term success is low, due to a high chance of resistance building. In contrast, a long-lasting tumour regression was observed with immunotherapy, with however a limited overall response rate. Thus, the combination of both therapies merges their advantages and thereby mitigates their respective shortcomings [27].

Even though conventional chemotherapeutics are the backbone of anticancer therapy, their application is limited. These aggressive, poorly selective, and highly cytotoxic agents inflict damage to rapidly dividing cells, but do not distinguish between normal cells and tumour cells, leading to relatively low tumour specificity and high toxicity. In contrast, targeted antineoplastic

drugs are designed more rationally with the aim of interfering with a specific molecular target, typically a protein, which is involved in tumorigenesis and progression [28]. One of the main goals in the development of new targeted cancer therapy is to increase target selectivity to reduce off-target action related side effects. With conventional chemotherapy, a wide range of undesirable effects is seen, depending on the type of cancer, its location, the administered drug and dose, and the constitution of the patient. Typically, blood-forming cells in the bone marrow, hair follicles and mucosal cells in the mouth, digestive tract, and reproductive system are affected. This may lead for example to fatigue, hair loss, mucositis, nausea and vomiting or infertility. It is important to notice that with the introduction of the new targeted compounds, the number and severity of side effects have not necessarily decreased, but overall, targeted antineoplastic drugs are supposed to be well-tolerated, or at least better tolerated than conventional cytotoxic chemotherapy [28,29]. Nevertheless, there are numerous side effects possible, which can lead to dose reduction or therapy discontinuation. In comparison to mAbs kinase inhibitors in general exhibit more and more severe side effects, as they achieve less specific targeting, especially in the case of multi-targeting kinase inhibitors.

2.2 Kinase inhibitors

Protein kinases are enzymes that catalyse the transfer of phosphate groups from adenosine triphosphate to tyrosine, threonine or serine amino acid residues in proteins, which play an important role in various normal cellular signalling processes [20](Figure 2). In cancer cells, activity of protein kinases can be dysregulated due to overexpression and/or genetic alterations such as mutations and translocations, leading to a permanent activation of the proliferative signal and an uncontrolled cell growth [30]. Small molecule kinase inhibitors interrupt the intracellular signalling, which consequently stops the molecular cascade of cell growth, proliferation, migration, and angiogenesis. Depending on their substrate specificity, kinase inhibitors can be divided into serine/threonine kinase inhibitors and tyrosine kinase inhibitors Serine/threonine inhibitors are mainly inhibitors of BRAF, mTOR (mechanistic Target of Rapamycin), MEK (mitogen-activated protein kinase kinase) and CDK (cyclin-dependent kinases). TKIs can be either grouped into receptor tyrosine kinases (RTKs), consisting of an extracellular ligand-binding region, a transmembrane and an intracellular domain, or into non-receptor tyrosine kinases. This subgroup are cytosolic enzymes, thus lack both an extracellular and transmembrane domain (Figure 2). There are at least 58 types of RTKs grouped into 20 subfamilies based on their kinase domain sequence. Vascular endothelial growth factor receptors (VEGFRs), platelet-derived growth factor receptors (PDGFR), the insulin receptor family and the ErbB receptor family (e.g., epidermal growth factor receptor (EGFR) or human epidermal growth factor receptor 2 (HER2)) are representatives of RTK and are suitable targets for targeted therapy, as they are significantly associated with oncogenic aberrations [31,32]. Examples for non-receptor tyrosine kinases are the ABL-family or the JAK-family (example of JAK/STAT see Figure 2). Table 1 shows an overview of frequently addressed targets and examples of corresponding TKI representatives including their indication and year of FDA approval.

Depending on the number of targeted kinases, TKIs can either act as selective single kinase inhibitors or multi-kinase inhibitors, like VEGFR-associated multi-targeted TKIs (e.g., cabozantinib, sorafenib, sunitinib, pazopanib, axitinib). Both mechanisms bring advantages as well as disadvantages, like an improved efficacy or the ability to treat several types of cancer for multi-kinase inhibitors. However, inhibition of multiple targets and off-targets may also be associated with a higher rate of side effects [33-36].Common side effects of TKIs are of haematological nature (e.g. anaemia, thrombopenia and neutropenia), fatigue syndrome and skin disorders, like an acneiform rash which can be seen after administration of EGFR inhibitors or the hand-foot skin reaction and wound healing disorders associated with VEGFR inhibitors [37]. Just as often, gastrointestinal adverse effects, mainly diarrhoea, nausea and vomiting can

occur and are observed more or less frequently with most TKIs [36]. Furthermore, some kinase inhibitors, especially VEGFR inhibitors, can have an impact on the cardiovascular system resulting in e.g., hypertension or arrhythmia and QT-interval prolongation. Depending on their severity, these side effects can lead to dose reductions or treatment interruption. In particular cases, it is therefore advisable to aim for a somewhat lower plasma concentration level, to avoid severe toxicity, which would end up in treatment discontinuation [29,36-38]. Even though TKIs are rationally designed, there are gaps in knowledge, e.g., on PK properties of TKIs, even after approval. Especially the use of TKI in special patient groups (patients with renal or hepatic impairment, children) or the concomitant use of TKI and other compounds, which is quite common in cancer patients, is often analysed in post-marketing PK studies only [39]. Thus, there is a great need to take a closer look at these situations and patients, respectively, and to optimise the therapy if necessary.

Major future challenges are the reduction of off-target - possibly unexpected - toxicity and the prevention of acquired resistance to TKIs, which are more common than de novo resistance. Acquired clinical resistance remains the biggest obstacle to successful long-term therapy, as almost all TKIs are associated with resistance after a certain period of use [40]. Different mechanism for the development of drug resistance have been elucidated and multifactorial drivers seem to be likely [41]. Common mechanism are gene mutations, gene amplifications, overexpression of efflux transporters and activation of bypass pathways [42]. A well-known example of gene mutations are point mutations within the Bcr-Abl kinase domain that affect the ability of imatinib to bind effectively in the ATP pocket. Gene amplification and activation of alternative pathways are for example seen in resistance to first generation EGFR inhibitors (e.g., erlotinib, gefitinib). About 20 % of NSCLC show resistance due to an amplification of the mesenchymal– epithelial transition (MET) factor receptor tyrosine kinase, which activates different EGFR signalling pathways.

Just as the mechanisms of resistance formation are multifaceted, so are the strategies to overcome these mechanisms. One attempt to overcome drug resistance is the development of second or third generation TKIs, which are mainly characterized by higher target affinity and potency, respectively, or which address multiple targets. Other approaches include the combination of TKIs with conventional chemotherapy or immunotherapy (e.g., T lymphocyte-associated antigen 4 (CTLA4) and programmed cell death protein 1 (PD1) antibodies). This can be achieved, for example, through the development of more potent and selective kinase inhibitors, but also through improved patient´s adherence, leading to improved tolerability and decreased toxicity [30,43]. Sufficient knowledge of the drug´s PK behaviour within all steps of the ADME process is of utmost importance to prevent patients from under- or overdosing.

The correlation of plasma (trough) concentrations with adverse events and clinical outcome, respectively, was shown in clinical studies for different kinase inhibitors [44-46]. If there is uncertainty about plasma exposure in individual patients it might be advisable to measure plasma drug concentrations. TDM is certainly more relevant for oral antineoplastic drugs with a narrow therapeutic window (e.g., pazopanib, sunitinib) and potentially less important for those with a wider therapeutic window (e.g., osimertinib, erlotinib) [47]. In the present work, two kinase inhibitors have been analysed in more detail using pharmacometric models and plasma concentrations obtained from TDM have been used to evaluate one of those models.

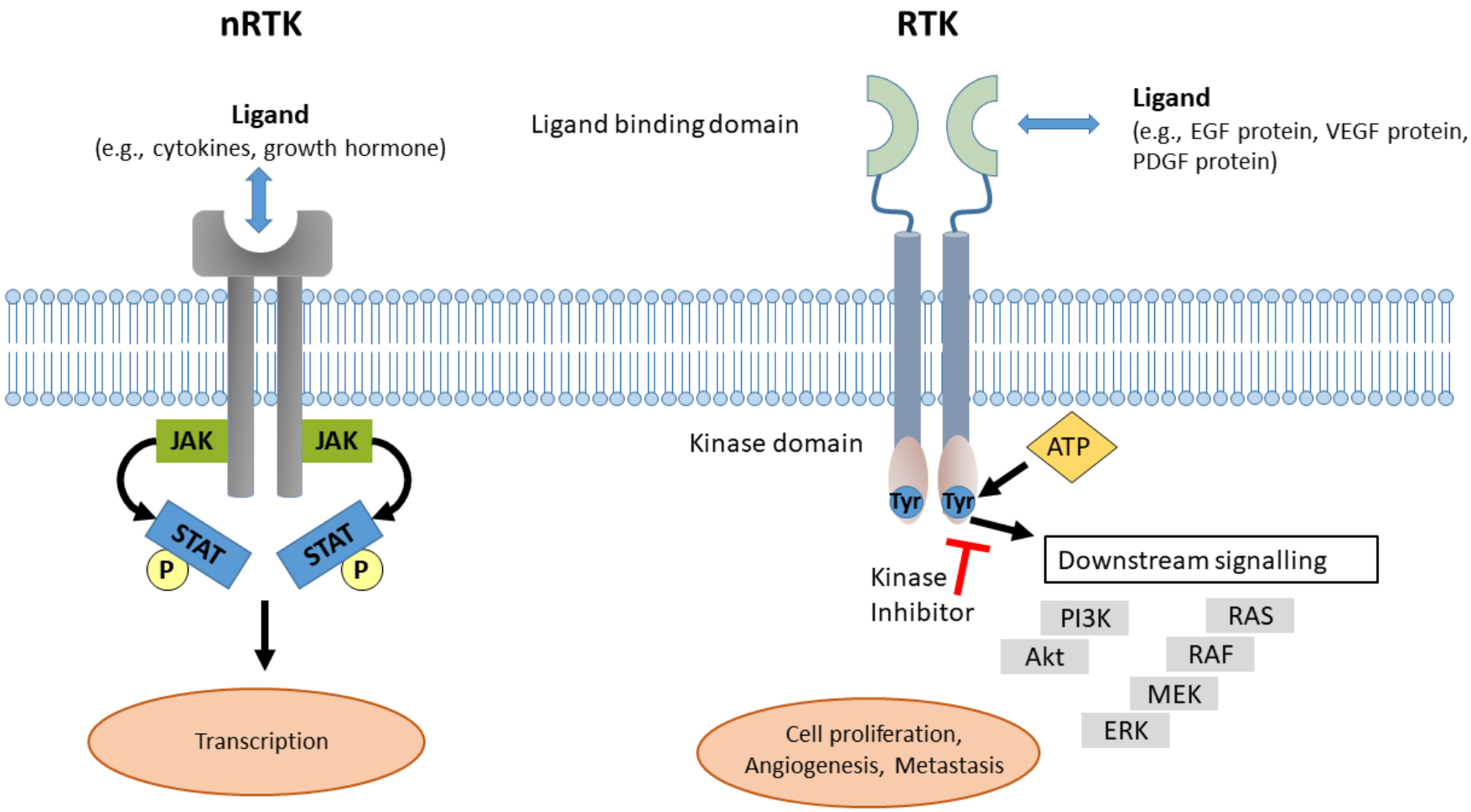

Figure 2. Schematic representation of mechanism of action of a non-receptor tyrosine kinases (nRTK) and receptor tyrosine kinases (RTK), with EGF: endothelial growth factor; VEGF: vascular endothelial growth factor; PDGF: platelet derived growth factor; ATP: adenosine triphosphate; Tyr: tyrosine; RAS/MAPK pathway: mitogen activated protein kinases; PI3K/AKT: phosphoinositide-3-kinase/protein kinase B; JAK/STAT pathway: Janus kinases/Signal transducer and activation of transcription proteins.

Table 1

Overview of TKI targets and examples of corresponding representatives including their indication and year of FDA approval.

Target	Tyrosine kinase inhibitor	Tumour type / indication	FDA approval
BCR-ABL	Imatinib	Chronic myeloid leukaemia	2001
EGFR (ErbB1)	Gefitinib	Various categories of non-small cell lung cancer (NSCLC)	2002
	Erlotinib		2004
	Icotinib		2011
	Afatinib		2013
	Osimertinib		2015
	Dacomitinib		2018
	Alomertinib		2020
KIT	Imatinib[a]	Gastrointestinal stromal tumour (GIST)	2002
	Sunitinib[a]	GIST after disease progression or intolerance to imatinib	2006
VEGFR	Sorafenib[b]	Advanced renal cell carcinoma (RCC)	2005
		Unresectable hepatocellular carcinoma (HCC)	2007
	Sunitinib[c]	GIST, metastatic RCC, pancreatic neuroendocrine tumours	2006, 2006, 2011
	Lenvatinib[d]	Differentiated Thyroid Carcinoma, HCC,	2015, 2018,
		Endometrial Carcinoma	2019
	Cabozantinib[e]	Medullary thyroid cancer, RCC, HCC	2014, 2016
	Axitinib[f]	RCC	2012
	Pazopanib[g]	RCC, soft-tissue sarcoma	2009, 2012
	Tivozanib[h]	RCC	2021
Nonselective inhibition of EGFR (ErbB1 and ErbB2)	Lapatinib	HER2-positive breast cancer	2007
	Neratinib	HER2-positive breast cancer	2017
PDGFR	Sunitinib[i]	GIST after disease progression or intolerance to imatinib	2006
	Avapritinib	Unresectable or metastatic GIST harbouring PDGFRA exon 18 mutation	2020
ALK / ROS1	Crizotinib	Anaplastic lymphoma kinase (ALK)-positive advanced NSCLC, ALK-positive advanced NSCLC	2011
	Lorlatinib		2018
ALK	Alectinib	ALK-positive advanced NSCLC	2014
	Bigatinib	ALK-positive advanced NSCLC	2017
MEK 1/2	Trametinib	Unresectable or metastatic melanoma with a BRAF V600 mutation (monotherapy or combined with dabrafenib)	2013
	Cobimetinib	Unresectable or metastatic melanoma with a BRAF V600 mutation (combined with vemurafenib);	2015,
		Advanced NSCLC with a BRAF V600 mutation (combined with dabrafenib)	2017
FGFR	Erdafitinib	Locally advanced or metastatic urothelial carcinoma	2019
	Pemigatinib	Previously treated, unresectable, locally advanced or metastatic cholangiocarcinoma with a fibroblast growth factor receptor 2 (FGFR2) fusion or other rearrangement	2020
	Infigratinib	Previously treated, unresectable, locally advanced or metastatic cholangiocarcinoma with a FGFR2 fusion or other rearrangement	2021
MET[j]	Capmatinib	MET-mutated[k] advanced NSCLC	2020
	Tepotinib	MET-mutated advanced NSCLC	2021
JAK[l] family	Ruxolitinib	Myelofibrosis, Polycythaemia vera, acute & chronic graft versus host disease	2012, 2014, 2019, 2021
	Deucravacitinib	moderate-to-severe plaque psoriasis in adults	2022

HER2	Tucatinib	HER2-positive breast cancer	2020
RET	Selpercatinib	advanced RET fusion-positive NSCLC, advanced RET fusion-positive thyroid cancer	2020
	Pralsetinib	Advanced RET fusion-positive NSCLC	2020

[a] as part of multi-targeted TKIs
[b] multi targeted inhibition of VEGFR1-3, TIE2, PDGFR, FGFR, BRAF, CRAF, KIT, FLT-3
[c] multi targeted inhibition of VEGFR-1–2, PDGFR, FLT3, KIT
[d] multi targeted inhibition of VEGFR1-3, PDGFR, FGFR 1–4, RET, KIT
[e] multi targeted inhibition of VEGFR1-3, MET, ROS1, RET, AXL, NTRK, KIT
[f] multi targeted inhibition of VEGFR1-3, PDGFR, KIT, FLT-3
[g] multi targeted inhibition of VEGFR, PDGFR, KIT
[h] multi targeted inhibition of VEGFR, c-kit and PDGFR β
[i] most VEGFR-associated multi-kinase inhibitors target PDGFR as well
[k] mesenchymal-epithelial transition factor[l] 'mesenchymal-epithelial transition factor gene exon 14' (METex14) skipping
[l] Janus kinase

2.3 Home-based oral antineoplastic therapy

In general, administration of cancer chemotherapy is a complex medical procedure that involves various risks, causing potential harm to patients. Different ways are possible to apply traditional anticancer drugs, however many of them are given i.v., often with the help of a catheter or a port, in coordinated treatment cycles. Complex therapy regimens, a vulnerable patient population, narrow therapeutic windows of cytotoxic agents and the long list of possible adverse events are reasons, why chemotherapy has to be administered by trained and specialised medical staff to prevent medication errors (e.g. wrong dose, wrong drug, wrong administration route) [48]. For conventional cancer treatment, patients therefore regularly must visit a hospital or a specialised centre to receive their therapy. Some older substances such as methotrexate or mitotane could already be taken orally. However, the route of administration and the treatment setting within cancer therapy changed notably with the introduction and the increasing use of new targeted oral anticancer drugs, first and foremost TKIs [47].

The possibility of taking the substances orally opens several improvements in tumour therapy. Oral administration is not only much more convenient than invasive application, but it also offers patients a higher degree of independence, since they can take the medication anywhere, especially at home. However, home based, oral intake of antineoplastic drugs comes also along with some drawbacks. For classical i.v. chemotherapy administered in a hospital or a specified centre it is ensured that the entire dose is given, respectively reaches the circulating blood system and can be dosed precisely, according to the patient's needs. Therapeutic response of kinase inhibitors is subject to large inter individual variation and depends on different factors, like variability in drug ADME processes or tumour biology [43]. Nonetheless, they are usually dosed at a fixed daily dose. This results in the probability that some patients will show subtherapeutic concentrations, whereas other patients suffer from toxic plasma concentrations

and adverse advents, leading to non-adherence. In consequence, both cases increase the risk of treatment failure. Switching to a long-term daily home-based oral therapy shifts the responsibility for correct and conscientious intake to the patient. To minimize the risk of medication errors and non-adherence, a detailed information and instruction of the patient about the prescribed therapy as well as its correct intake by medical staff is therefore of utmost importance. Even better is an additional intensified clinical pharmacological/pharmaceutical care during treatment with new oral antineoplastic drugs. This was shown in the randomized AMBORA trial, which was investigating the impact of pharmacological/pharmaceutical care on medication safety and patient-reported outcomes during treatment with new oral anticancer agents [49]. In this study, patients of the intervention group were for example counselled on medication management, side effect prevention and management, and adherence. In addition, brochures about common side effects and for patient self-management were handed out to the patients. There was a significant reduction in drug-related problems (i.e., side effects and unresolved medication errors) among patients in the intervention group compared to patients in the control group who received only standard medical care. The number of drug-related problems per patient in week 0 to 12 after treatment initiation was 3.85 ± 2.85 in the intervention group versus 5.81 ± 3.84 in the control group (mean ± standard deviation). It was also shown that treatment satisfaction, an important prerequisite for treatment adherence, with the oral anticancer therapy after 12 weeks was significantly higher in the intervention group than in the control group [49].

Adherence is of great importance to achieve a sufficient and lasting therapeutic effect. The fear or experience of side effects as well as complex treatment regimens or special instructions regarding drug intake (e.g., with a certain meal), might reduce adherence. Adherence can be assessed in different ways, e.g., through self-reporting by patients and caregiver/family member, respectively, electronic monitoring devices or through plasma drug level measurement. A systematic review by Greer et al. about adherences to oral antineoplastic drugs revealed a wide range of observed adherences due to e.g., the diverse methods of adherence measurement but also due to a lack of standardization in defining optimal adherence [50]. According to this review and other literature non-adherence rates between 46% and 100% have been reported [37,50-52]. Reasons for non-adherence are manifold and general principles or predictions about the extent to which patients are adherent are rather difficult to make [50,53]. Patient factors associated with poor adherence are for example marital status (not being married), patient age (both younger and older age) or higher depression. Treatment factors resulting in poor adherence are amongst others higher doses of medication and worse side effects. Furthermore, it was found that adherence to oral antineoplastic drugs significantly declines over time [50]. A

daily oral intake also paves the way for pharmacokinetic difficulties leading for instance to limited absorption of the active substance and subsequently to a reduced efficacy.

Besides, an increased risk of potential adverse reactions for example due to drug-drug interactions (DDI) should be kept in mind. According to a retrospective study by Leeuwen et al, which was investigating the prevalence of DDI in cancer patients taking oral anticancer drugs, in 46% of the 898 patients included in the study, potential DDI were identified [54]. As patients treated with anticancer drugs often suffer from e.g., age-dependent, cancer-dependent, or treatment-dependent comorbidities, they are taking on average five drugs, for instance against tumour pain, nausea, or vomiting [49]. Small molecule inhibitors are mainly metabolized by cytochrome P450 (CYP) enzymes making them susceptible to DDI with CYP inducers or inhibitors like macrolide antibiotics, azole antifungals, St. John´s wort or certain anticonvulsants [22,38]. The concomitant treatment with proton pump inhibitors or histamine-2 receptor antagonists can also lead to reduced absorption of some TKI (e.g. erlotinib [38]), due to their pH-dependent solubility. In the same way, oral absorption can be increased (e.g. nilotinib) or decreased (e.g. dabrafenib or afatinib by certain food intake such as high fat meal)[37,55]. A representative of oral anticancer drugs to which almost all the above-mentioned PK difficulties apply, and which was object of a project within the thesis is mitotane, presented in more detail in the next section.

3 Examples of challenging oral antineoplastic drugs

3.1 Mitotane in Adrenocortical Carcinoma

Adrenocortical carcinoma (ACC) is a very rare but highly aggressive malignant tumour of the adrenal cortex with an annual incidence of 0.7-2.0 cases per million population. Women are slightly more often affected (55-60%) and a peak incidence can be seen in the age of 40-60 years, but in general, ACC can occur at any age [56,57]. In some regions, especially in southern Brazil, there is also a peak incidence in childhood with an annual incidence of about 3.5/million children younger than 14 years [58,59]. An early diagnosis and detection of small adrenal tumours (< 5 cm) is one of the main strategies to fight the disease [60]. Small adrenal tumours are often adrenal incidentalomas. They are usually found by chance during an imaging test, such as an ultrasound or CT scan, which is being done for a problem unrelated to adrenal disease [61]. However, accidental discovery of ACC only occurs in 15-20% of patients [57,62]. On the other hand, the proportion of ACC among all incidentally discovered adrenal masses is low in unselected case series. The clearly larger part of the patients presents with bigger tumours, measuring on average 10 to 13 cm [57]. In general, the diagnosis of ACC is not always trivial. Especially in the case of non-functioning ACC, meaning that there is no adrenal steroid hormone overproduction, symptoms may be absent or unspecific in early stages what makes it more difficult to detect the tumour. Typically, these patients, who constitute up to one third of all ACC patients, present with nonspecific symptoms due to local tumour growth, such as abdominal or back pain [63,64]. About 40% to 60% of patients have clinical hormone excess, which is due to a hormone producing adrenocortical tumour. In this case, hypercortisolism (Cushing syndrome) or mixed Cushing and virilizing syndromes are frequently observed. Androgen, oestrogen and mineralocorticoid excess is less frequent [57]. However, symptoms of hormone excess could be overlooked or not attributed to ACC by physicians and even patients with hormone producing ACC can be diagnosed and subsequently treated at a very late stage.

The differential diagnosis between benign and malignant adrenocortical tumours is challenging, as no single marker can be used to indicate malignancy [45] and both imaging and endocrine workup are required for the diagnosis of malignancy and to assess autonomous hormone secretion [61].The histological diagnosis of malignancy is similarly challenging. The histopathological score proposed by Weiss et al. is the currently most widely used system with a value of 3 or above suggesting malignancy.

ACC tumour-staging follows the classification suggested by ENSAT (European Network for the Study of Adrenal Tumours) [65]. The TNM (tumour, node, metastasis) classification by ENSAT defines four disease stages (Table 2). Stage I and II are localized

tumours with a size of ≤5 cm, respectively > 5cm. In stage III, tumour infiltration into surrounding tissue and/or tumour thrombus in vena cava/renal vein and/or involvement of lymph nodes is the criterion. Stage IV comprises distant metastasis [65]. Until today, no sufficiently effective therapy is available, resulting in poor prognosis and a median overall survival of about 3-4 years referring to all ACC patients [56]. For metastatic disease, five-year survival ranges only from 0% to 28%. Five-year survival rate can be increased up to 50% if the tumour is only locally advanced and up to 80% for tumours limited to the adrenal space [56]. Overall, the prognosis is poor and difficult to predict as there is a high variability in clinical presentation and disease progression. Even in advanced ACC (Stage IV) survival can range from only a few months to several years and in some cases an exceptionally long survival has been reported [57].

Table 2

TNM classification according to the European Network for the Study of Adrenal Tumours (ENSAT) and the Union Internationale Contre le Cancer (UICC) staging system

Stage	Stage definition ENSAT	Stage definition UICC
I	T1, N0, M0	T1, N0, M0
II	T2, N0, M0	T2, N0, M0
III	T1-T2, N1, M0	T1-T2, N1, M0
	T3-T4, N0-N1, M0	T3, N0, M0
IV	T1-T4, N0-N1, M1	T1-T4, N0-N1, M1
		T3, N1, M0
		T4, N0-N1, M0

T1: tumour size ≤ 5cm, T2: tumour size > 5cm, T3: infiltration into surrounding tissue, T4: tumour invasion into adjacent organs (ENSAT + IUCC) or venous tumour thrombus in vena cava or renal vein (only ENSAT), N1: positive lymphnode(s), M0: no distant metastases, M1: presence of distant metastasis

Surgery is the most important intervention in case of localized ACC (Stage I-II-III), and complete surgical resection (RO) plays a key role in achieving long-time survival and is to date the only curative approach [66-68]. Unfortunately, even after complete tumour resection, the rate of local recurrence remains relatively high (19 to 34%) [57] especially in the first two years after surgery and more than half of the patients have a relapse, often with metastases.

To date, mitotane is the only drug approved by the FDA and European Medicines Agency (EMA) for treatment of advanced ACC and is indicated in inoperable tumours of both functional and non-functional types. Mitotane is given orally in 500 mg tablets (Lysodren®; HRA Pharma Paris). It remains the cornerstone of medical treatment in all tumour stages, which is

used in adjuvant as well as in metastatic disease [57,69,70]. For the treatment of advanced ACC, Mitotane is combined with etoposide, doxorubicin, and cisplatin (EDP-M) as first-line therapy based on the results from the FIRM-ACT (First International Randomized Trial in Locally Advanced and Metastatic Adrenocortical Carcinoma Treatment) study. This was a phase III trial, which compared mitotane plus a combination of EDP-M) to mitotane plus streptozocin in patients with advanced ACC. Progression-free survival in patients treated with EDP-M was superior compared with patients treated with mitotane plus streptozocin (5.0 months versus 2.1 months, hazard ratio 0.55, 95% confidence interval 0.43-0.69, P<0.001). However, even with EDP-M the objective response rate is only 23% and disease stabilization is reached in 35% of patients [71].

Mitotanee is a chemical derivative of the insecticide dichlorodiphenyltrichloroethane (DDT) and is also known by its trivial name *o,p'*-DDD (1,1-dichloro-2-(o-chlorophenyl)-2-(p-chlorophenyl)ethane). Figure 3 shows the chemical structure of the target drug mitotane as well as its main metabolites, the corresponding acid *o,p'*-DDA and the unsaturated derivative *o,p'*-DDE [72-74].

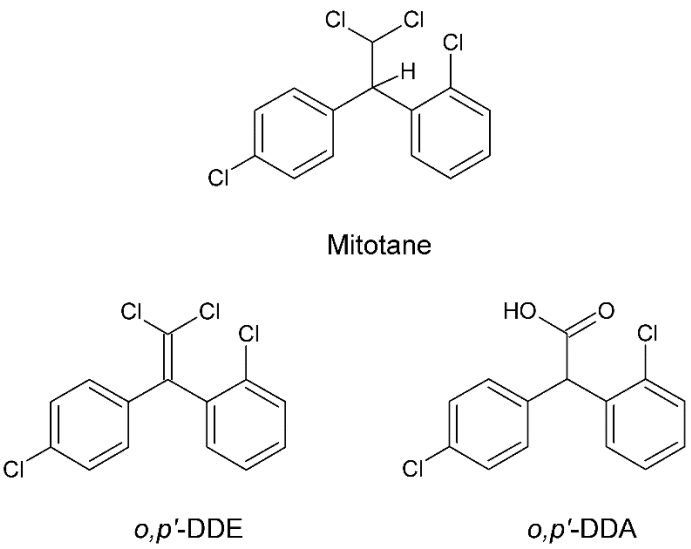

Figure 3. Chemical structure of mitotane and its main metabolites *o,p'*-DDE and *o,p'*-DDA.

Even though Bergenstal et al. introduced mitotane into treatment of ACC already in 1960 [75], its pharmacological mechanism of action has still not completely elucidated. Mitotane can be described as an adrenal cytotoxic agent that has adrenolytic properties and inhibits adrenal steroid synthesis. Mitotane leads to a destruction of the inner zones of the adrenal cortex, the zona fasciculata, and zona reticularis, but not of the zona glomerulosa, which ultimately leads to a loss of steroid secretion of hormones that are under the control of

adrenocorticotrophic hormone (ACTH[70,76]. An inhibition of multiple enzymatic steps of adrenocortical steroid biosynthesis, such as the conversion of 11-deoxycortisol to cortisol through 11ß-hydroxylase (CYP11B1) in the mitochondria of steroidogenic cells, has been reported [70]. However, Chortis et. al did not find any change in 11-deoxycortisol excretion and ruled out an effect of mitotane on 11ß-hydroxylase, but they confirmed an overall down-regulation of steroidogenesis through mitotane [77].

Mitotane has challenging pharmacokinetics. Between 30 and 60% of an orally administered dose seems to be absorbed from the gastrointestinal tract, according to performed studies by Moy et al. and Moolenaar et al. [78-81]. Due to its high lipophilicity, accumulation in fatty tissue leads to elimination half-lives of 18 to 159 days. Mitotane is mainly eliminated in form of its metabolites (see Figure 3) via bile or urine [82]. It is a strong CYP3A4 inducer, coming along with potential DDI with CYP3A4 substrates, like macrolide antibiotics, certain HMG-CoA-reductases or TKIs [83,84]. It is also discussed that mitotane metabolism is affected by CYP3A4 autoinduction [78]. Mitotane has a narrow therapeutic window (targeted average plasma concentration of 14 - 20 mg/l), which further complicates mitotane dosing. Patients with mitotane plasma levels higher than 20 mg/l more frequently suffer from higher rates of adverse events, above all gastrointestinal (e.g., nausea and diarrhoea), endocrinological (e.g., adrenal insufficiency) and central nervous system related (e.g., fatigue, vertigo) side effects. Mitotane plasma concentrations below 14 mg/l, on the other hand, are associated with a reduced objective tumour response rate [57,63]. Mitotane plasma concentrations show a high degree of interindividual and intraindividual variability and at present, dosing decisions are mainly based on clinical experience. At the initiation of the mitotane therapy low or high dose regimens are recommended, depending on the clinical condition of the patient and the aggressiveness of the tumour. In general, it takes about 8 weeks of continuous administration until a steady state concentration is reached in plasma, due to its long $t_{1/2}$. In addition, the extraordinarily long $t_{1/2}$ makes the substance difficult to control and sluggish with respect to changes in plasma concentration after a dose change. To dose mitotane within the therapeutic window and to prevent permanent over- or underdosing, therapeutic drug monitoring (TDM) is essential and determination of mitotane plasma levels is suggested every 2-3 weeks [85].

For some patients, however, it takes several months before they reach therapeutic plasma level, or they do not reach it at all. Especially at the start of treatment it would therefore be helpful to carry out a more intense sampling. Together with model-based simulations patients at risk for not achieving sufficient plasma levels can be identified in this way. It can be assessed whether the therapy should be continued or discontinued, and patients can be prevented from taking this toxic substance for several months without any prospect of success.

TDM of mitotane is offered in Europe to be carried out via the free Lysosafe Service of HRA Pharma. Healthcare professionals can send patients´ plasma samples to the bioanalytical centre of HRA pharma, where the they are assayed by a standardised HPLC analysis method [85]. Since patient plasma is used as a matrix for the determination of mitotane concentration, it requires periodic physician consultations for sampling. Drug monitoring could be greatly simplified, both for the patients and for the treating centres, if the collection of blood samples could be home based and the samples could be directly sent to HRA Pharma by the patients. Home based drug monitoring, as well as a more convenient form of sample collection compared to venous blood sampling and a lower required sample volume, would make mitotane drug monitoring more comfortable and could also contribute to more frequent sampling. To achieve all this, minimally invasive sampling techniques and dried blood analyses could be used, and the feasibility of home-based mitotane drug sampling and monitoring was investigated in the presented thesis.

3.2 Cabozantinib as targeted therapy in Adrenocortical Carcinoma

Due to the poor response rate of conventional cytotoxic chemotherapy or mitotane monotherapy, molecularly targeted therapies gave rise to some hope for the treatment of ACC. A series of different pathways and therapeutic targets have already been studied [62,86]. The protein hormone insulin-like growth factor-2 (IGF2), which promotes tumour cell growth through insulin-like growth factor 1 (IGF-1R) receptor–mediated downstream activation of the protein kinase B (AKT)/mTOR pathway, is known to be overexpressed in most of the ACC tissues [87]. Beside IGF other growth factors and cytokines have been shown to play an important role in the regulation of adrenal growth and function, especially the epithelial growth factor (EGF) and the vascular endothelial growth factor (VEGF). Another approach is addressing the cMET pathway. Overexpression of hepatocyte growth factor and its target cMET was demonstrated in human ACC tissue and down-regulation of MET impaired tumour growth in a xenograft model of ACC [87]. Thus, the focus was or is primarily on drugs addressing the mentioned targets and pathways respectively. Linsitinib and the monoclonal antibodies cixutumumab and figitumumab for example were administered as IGF-1R inhibitors, gefitinib and erlotinib as EGFR inhibitors, bevacizumab as VEGFR inhibitor and temsirolimus in combination with lenalidomide as mTOR inhibitor (Table 3) [57,62,86]. Furthermore, the Wnt/β-catenin pathway, which plays a major role in ACC development, would still offer potential but unfortunately, there is still no targeted therapy to inhibit this pathway specifically [88]. Unfortunately, most of the approaches investigated led to disappointing results as no objective response according to the RECIST (Response Evaluation Criteria in Solid Tumours) criteria or clinical benefit in the form of e.g., progression-free, or overall survival could be demonstrated (Table 3). The same discouraging results were seen with the so far tested multi-kinase inhibitors sorafenib, sunitinib, dovitinib and axitinib, and based on these results none of the investigated TKI is convincing for the treatment of advanced ACC [89-99]. One of the weaknesses in the studies already conducted is the prior or concomitant administration of mitotane. The phase II trial of sunitinib in patients with refractory ACC who were simultaneously treated with mitotane [94] might explain the apparent inefficacy of TKI in these patients. In that study, there was a clear negative impact of the concurrent mitotane therapy on outcome. The median PFS was 2.8 months and only 5/35 patients experienced stable disease whereas 24/35 had progressive disease and 6/35 died. However, these poor results should also be considered in relation to the study population investigated, which only included patients who suffered from significant tumour burden and who had progressive disease despite prior cytotoxic chemotherapy. Serum levels of sunitinib and its active metabolite were measured in seven patients and revealed a negative correlation between mitotane plasma concentration and

the plasma concentration of sunitinib and its active metabolite. These findings support the strong CYP3A4 induction by mitotane [78,83,84], which consequently increased sunitinib clearance and led to significantly lower sunitinib plasma concentrations than expected.

Table 3

Targeted Therapy in ACC

Study	Regimen	Target	No. of patients	PD/SD/PR	OS/PFS (months)
Wortmann et al., [89] case series	Bevacizumab/ Gemcitabine	VEGF	10	10/10 PD	4.1 OS
Quinkler et al., [90] case series	Erlotinib/ Gemcitabine	EGFR	10	9/10 PD 1/10 SD	5.5 OS 2.8 PFS
Samnotra et al., [91] phase II	Gefitinib	EGFR	19	19/19 PD	NR
Ganesan et al., [92] phase I	Temsirolimus/ Lenalidomide	mTOR/ immunomodulatory agent	3	1/3 SD for 6+ months	NR
Naing et al., [93] phase I	Cixutumumab/ Temsirolimus	IGF-1R mTOR	10	4/10 SD for 8+ months	NR
Lerario et al., [95] phase I	Cixutumumab/ Mitotane	IGF-1R	20	7/20 SD	1.5 PFS
Haluska et al., [96] phase I	Figitumumab	IGF-1R	14	8/14 SD but PD after 7 months	
Fassnacht et al., [97] phase III	Linsitinib	IGF-1R, IR	139 (90 allocated to Linsitinib, 90 to placebo)	3/90 PR 1/90 SD	323 vs. 356 days, *P*=0.77, OS 44 vs. 46 days, *P*=0.30, PFS
Berruti et al., [98] phase II	Sorafenib/ Paclitaxel	VEGFR2-3, PDGFR, RAF-1	25	9/25 PD study interrupted	NR
Kroiss et al., [94] phase II	Sunitinib	VEGFR1-2, c-KIT, Fms-like tyrosine kinase 3, PDGFR	35	5/35 SD 24/35 PD	5.4 OS 2.8 PFS
O´Sullivan et al., [99] phase II	Axitinib	VEGFR1-3	13	8/13 SD	26.92 OS 5.48 PFS

ACC adrenocortical carcinoma; *EGFR* epidermal growth factor receptor; *IGF-1R* insulin-like growth factor 1 receptor; *IR* insulin receptor; *mTOR* mammalian target of rapamycin; *NR* not reported; *OS* overall survival; *PD* progressive disease; *PDGFR* platelet-derived growth factor; *PFS* progression free survival; *PR* partial response; *SD* stable disease; *VEGF* vascular endothelial growth factor; *VEGFR* vascular endothelial growth factor receptor.

Another TKI addressing several relevant targets is cabozantinib. It was originally approved by the FDA for the treatment of progressive metastatic medullary thyroid cancer, advanced renal cell carcinoma and hepatocellular carcinoma [100-104]. However, its primary targets, especially cMET (hepatocyte growth factor receptor) and VEGFR2) are known to impair tumour growth also in ACC. By inhibiting both arms of the MET and VEGF axis, cabozantinib prevents from compensatory upregulation of MET and a resultant increase in

tumour growth [105,106]. The substance showed promising results in a case study conducted by Kroiss et al. In that retrospective cohort study, sixteen patients with progressive ACC were treated with cabozantinib after previous mitotane or further systemic therapy. Mitotane was discontinued prior treatment in all patients and plasma levels were < 2 mg/L. Progression-free survival >16 weeks was observed in 50% of the patients and partial response in three patients and stable disease in five patients was seen, respectively. However, eight patients, meaning half of the patients, had tumour progression. During that study, cabozantinib steady-state plasma concentrations of 5 patients were measured, revealing pronounced interindividual variability (IIV) in plasma concentrations, potentially caused by altered CYP3A4 metabolism through previous or concomitant medication [107]. To reduce the interaction potential between mitotane and CYP3A4 substrates, mitotane application was discontinued before starting with the TKI therapy in currently ongoing studies with cabozantinib (Cabozantinib in Advanced Adrenocortical Carcinoma (CaboACC), ClinicalTrials.gov Identifier: NCT03612232.) [108]. These ongoing studies all evaluate the progression free survival at 4 months and the objective response rate of cabozantinib in ACC either in adults or children and young adults (NCT03612232, NCT03370718 and NCT02867592).

Cabozantinib is a substrate of CYP3A4 and undergoes extensive metabolism. Four major cabozantinib metabolites are known, namely Exel 5366 (Amide Cleavage Product), Exel 1644 (6-Desmethyl Amide Cleavage Product Sulfate), Exel 1646 (Monohydroxy Sulfate) and Exel 5162 (N-Oxide). Hepatobiliary elimination seems to be the major route of elimination for the parent substance, whereas the metabolites are also excreted via urine [106,109]. Due to the exclusive elimination via the hepatobiliary pathway, cabozantinib excretion may be impaired by hepatic diseases. However, no investigations for severe hepatic impairment were made so far and recommendations on dose modifications for any hepatic impairment are inconsistent ([106,110-112].

In addition to hepatic impairment, cabozantinib metabolism can be affected by CYP3A4 interactions. The effects of the CYP3A4 inhibitor ketoconazole and the CYP3A4 inducer rifampin on cabozantinib plasma exposure were investigated in two separate studies, revealing increased cabozantinib $AUC_{0\text{-}inf}$ by 38% for the combination with ketoconazole and decreased cabozantinib $AUC_{0\text{-}inf}$ by 77% for the combination with rifampin [111,113]. Co-administration of strong CYP3A4 inducers, however, is assessed differently by the FDA and EMA. According to the FDA the daily cabozantinib dose should be increased by 20 mg (Cabometyx® tablets) and 40 mg (Cometriq® capsules), respectively, if combined with strong CYP3A4 inducers. However, there is no general recommendation to avoid the combination, like it is the case in the EMA Summary of Product Characteristics [111].

After oral administration, either as capsule or tablet, cabozantinib seems to have a high bioavailability, yet no formal determination of absolute bioavailability was conducted so far. Maximum plasma concentrations (C_{max}) occur approximately at 3 to 5 h post-dose. After reaching C_{max} a steep decrease in cabozantinib plasma concentration, followed by a long terminal half-life (~120 h) can be seen in plasma concentration time profiles. In addition, plasma concentration time profiles revealed multiple peaks, starting approximately 24 hours after cabozantinib administration [106,114]. To explain this phenomenon, EHC is assumed, however also other possibilities like absorption in deeper bowel sections or the irregular pattern of gastric emptying might be conceivable [115,116]. To avoid potential cabozantinib over- or underexposure in ACC patients, it is of utmost importance to improve knowledge about the PK properties of the compound and to gain a mechanistic insight into its in vivo behaviour, which was done in project two of the presented thesis. By this, possible sources influencing cabozantinib plasma concentrations can be identified and cabozantinib administration can be adapted accordingly.

3.3 Ruxolitinib in Graft versus Host Disease

Graft-versus-host disease (GvHD) is an inflammatory syndrome that can develop after allogeneic hematopoietic stem cell transplantation (alloHSCT). It occurs when immunocompetent T cells in the donated stem cells or bone marrow (the graft) recognize the recipient (the host) as foreign and subsequently attack the recipient's body cells [117,118]. Although alloHSCT has become the treatment of choice for a variety of hematologic malignancies and benign disorders, GvHD remains one of the major obstacles to successful transplant outcome. GvHD is classified into acute or chronic forms. About half of the alloHSCT patients are affected by acute GvHD [118,119] and 30-70 % suffer from chronic GvHD [117,120], despite prophylaxis with ciclosporin and methotrexate, being administered for a certain period of time after transplantation antagonist [121]. GvHD occurring within the first 100 days post-transplant mostly is considered as acute type and syndromes occurring later are considered chronic, though both forms can overlap and the distinction solely according to the time interval from transplantation is controversial [120,121]. Acute GvHD often affects the skin presenting as an exanthema. [122,123]. Other organs affected are especially liver and the gastrointestinal tract, leading to e.g., hyperbilirubinemia, jaundice, and cholestasis, watery or bloody diarrhoea, nausea, vomiting and loss of appetite. Depending on the number of organs involved and the severity of symptoms, acute GvHD is classified into grade 1 (mild), 2 (moderate), 3 (severe) or 4 (very severe) [118]. A large proportion of patients with acute GvHD

has a high risk of developing chronic GvHD, either directly (progressive) or after a period of resolution [120]. Chronic GvHD can be classified into mild, moderate, or severe forms and mainly involves skin, mouth, liver, or eyes and less frequently the gastrointestinal tract, lung, oesophagus and joints [121].

First-line treatment are systemic high dose glucocorticoids [121,124]. In 30% to 60% of the patients the disease becomes glucocorticoid-refractory or glucocorticoid-dependent, coming along with a poor prognosis [125-127]. The reported 6-month survival estimate of 50% for patients with steroid-refractory acute GvHD and 30% or less of patients surviving beyond 2 years remains low [118]. Until the approval of ruxolitinib, various therapeutic options existed in second-line therapy, (e.g., monoclonal antibodies such as alemtuzumab, daclizumab or infliximab, etanercept, sirolimus and mycophenolate mofetil [117,124,127,128]), but so far only with an unsatisfactory response. With the approval of ruxolitinib, there is now a substance with a significantly improved response, which is meanwhile regularly used as the primary substance in the second line.

Ruxolitinib is a representative of Janus Associated Kinases 1 and 2 (JAK1 and 2) inhibitors and was originally approved in 2012 for the treatment of myelofibrosis and in 2014 for the treatment of polycythaemia vera [119]. Dysregulated JAK1 and JAK2 signalling leads amongst others to high levels of circulating cytokines that activate JAK-STAT pathway. Ruxolitinib inhibits JAK-STAT signalling leading to a decrease in proinflammatory cytokines and chemokines, which are usually elevated in myelofibrosis and other inflammatory conditions, like GvHD. After promising anti-GvHD activity with ruxolitinib in preclinical studies, two randomized phase 3, open-label, multi-centre studies for the treatment of acute (REACH-2 study) and chronic GvHD (REACH-3 study) were conducted and demonstrated improved overall response and longer median failure-free survival in the ruxolitinib groups compared to the control groups receiving best available therapy [127,129]. Thus, the FDA extended ruxolitinib approval to the treatment of steroid refractory acute or chronic GvHD in 2019 and 2021, respectively, and in March 2022 ruxolitinib was approved for the treatment of acute and chronic GvHD also by the EMA [130]. The substance has linear PK and shows high solubility and permeability. Thus is considered a Biopharmaceutical Classification System (BCS) class 1 compound [131]. C_{max} is reached within two hours post dose [131]. In GvHD, 5 to 10 mg ruxolitinib is administered orally twice daily, which is half of the dose given for myelofibrosis. Dose modification is recommended based on safety and depends on platelet count, absolute neutrophil count and total bilirubin elevation [132]. Ruxolitinib is mainly eliminated via metabolism by CYP3A4 (>50%), with additional contribution of CYP2C9, making the substance susceptible to drug-drug interactions. Comedication with CYP3A4 inhibitors (e.g.,

macrolides, triazole antifungals) or dual CYP2C9/3A4 inhibitors (fluconazole) may lead to varying ruxolitinib exposure [133].

Patients who have undergone alloHSCT have an increased risk for invasive fungal infections due to e.g., GvHD, immunosuppressive therapy and neutropenia [134]. Fungal infections play a major role regarding mortality and morbidity after alloHSCT, which is why fungal prophylaxis with posaconazole is standard as long as the patients are on immunosuppressive treatment. Antifungal prophylaxis with azole antimycotics is also restarted when GvHD occurs. Azole antimycotics are known to inhibit relevant CYP enzymes[135,136]. However, FDA and EMA recommendations for ruxolitinib dosing regarding co-medication with strong CYP3A4 inhibitors or dual CYP2C9/3A4 inhibitors are inconsistent. The FDA label distinguishes between different ruxolitinib indications. For GvHD a reduced ruxolitinib starting dose of 5 mg BID (twice a day) if co-administered with fluconazole is recommended. Modifications in ruxolitinib dosing if combined with strong CYP3A4 inhibitors are not proposed. In contrast, the EMA SmPC recommends a general dose reduction of the ruxolitinib dose by 50% with concurrent strong CYP3A4 inhibitors or dual CYP2C9/3A4 inhibitors, regardless of the indication [132,137,138]. Posaconazole has been shown to be superior compared to fluconazole for antifungal prophylaxis in GvHD patients and the concomitant administration with ruxolitinib is frequent after alloHSCT [139,140]. Nonetheless, knowledge on ruxolitinib exposure if combined with posaconazole is scarce and recommendations on dose modifications are based on studies with ketoconazole and fluconazole. In addition to CYP mediated DDI, ruxolitinib metabolism can be altered due to hepatic impairment caused by GvHD. Gastrointestinal involvement as well as co-medication with proton pump inhibitors, impacting the pH dependent solubility of ruxolitinib, can lead to significant variabilities in ruxolitinib disposition [141]. The complexity of the disease, the lack of clinical experience with ruxolitinib, different recommendations on dose modifications and high variability in ruxolitinib plasma concentrations in clinical routine are reasons to further investigate ruxolitinib exposure in different settings, which was part of the presented thesis.

4 Therapeutic drug monitoring

4.1 Main concepts of therapeutic drug monitoring

PK and PD processes can be influenced by a variety of individual, environmental and behavioural factors, leading to variable and potentially unexpected drug concentrations and/or drug responses after a given dose in an individual patient. A clear relationship between the administered dose and the desired pharmacological response is not always straightforward. To overcome this issue and to personalize pharmacotherapy, TDM can be conducted. TDM is the recurring measurement and interpretation of drug concentrations obtained in blood, plasma or other biologic fluids with subsequent dose adaptation and individualization of dosing and dosing schedules (Figure 4). Through this procedure, individual drug therapy is optimized aiming to increase safety and efficacy of a drug therapy.

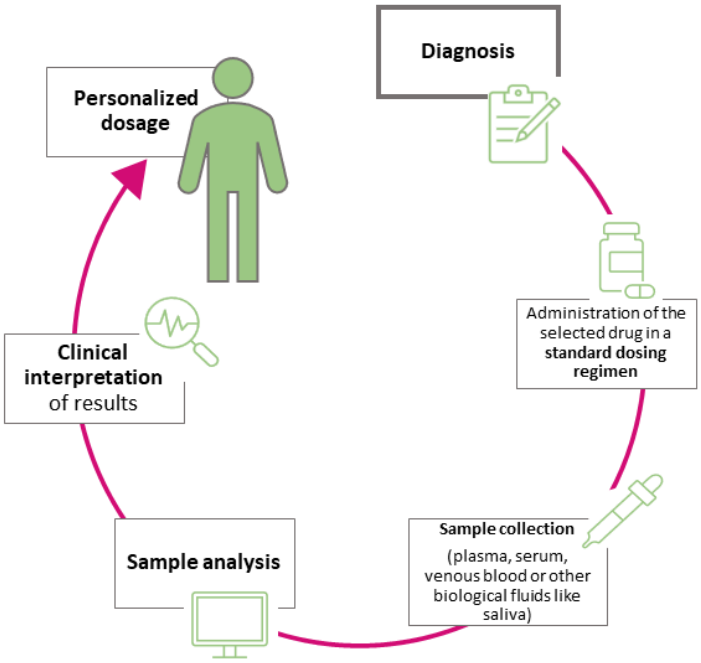

Figure 4. A typical process of the classical therapeutic drug monitoring of a given drug.

TDM is not intended to be applied to all drug substances but especially to those, which are difficult to manage for various reasons. In most cases, drugs predisposed for TDM are characterized by a narrow therapeutic range and/or poorly predictable pharmacokinetics (e.g., due to a saturable metabolism, autoinduction or a saturable binding to plasma or tissue proteins) with marked IIV in PK or PD (> 20%) [142]. Important prerequisites, respectively reasons, to

conduct TDM are the availability of analytical assays that are reliable, cost-effective, and applicable in everyday clinical practice, a low interoccasional/intraindividual variability, and the lack of other, direct methods to monitor the PD of a certain drug. In addition, a well-defined relationship between dose, blood or plasma concentration and therapeutic effect or toxicity [143] is mandatory. Indications for TDM include amongst others the need to evaluate patients´ compliance, therapeutic failure, distinction between drug toxicity and disease symptoms, changes in the main elimination organ (e.g. in the case of kidney diseases) or changes in or additional concomitant medication, which could result in DDI [144]. Typical examples of drug classes and drugs for which one or more of the above indications apply and for which TDM is well established are antidepressants and antipsychotics (e.g. lithium, clozapine) [145-147], immunosuppressives (e.g. cyclosporine, tacrolimus) [148,149], antiepileptics (e.g. valproate, carbamazepine) [150,151], phenytoin [152], theophylline [153] or digoxin [154]. For some anti-infectives (e.g. aminoglycosides, vancomycin) [155,156], in antiretroviral therapy [157] and targeted anticancer therapy [158,159] or in special populations, like neonates or critically ill patients, TDM is supposed to be beneficial [160,161].

It was shown that for a number of substances, amongst others kinase inhibitors, the AUC correlates best to PD responses (efficacy/toxicity) and is a good marker to assess under- or overexposure [162,163]. For practical reasons, however, specific concentrations like C_{max} or trough concentrations (C_{trough} = concentration obtained at the end of a dosing interval, just before the next dose is given) are usually measured in routine clinical practice. In routine TDM, these concentrations are assessed as to whether they are in a predefined therapeutic range, and drug dosing is adjusted accordingly to overcome undesirable dose-effect relationships [143]. The therapeutic range of a drug defines a range of drug concentration, mainly plasma or serum drug concentration, within which the desired clinical effect is most probably achieved. Drug concentrations that lie below a certain threshold are considered as less effective, whereas concentrations above the therapeutic range are associated with higher toxicity (Figure 5). The thresholds for subtherapeutic, therapeutic and toxic effects should not be seen too rigid, as the patient´s specific target goals according to his specific perceived needs should be also considered [164].

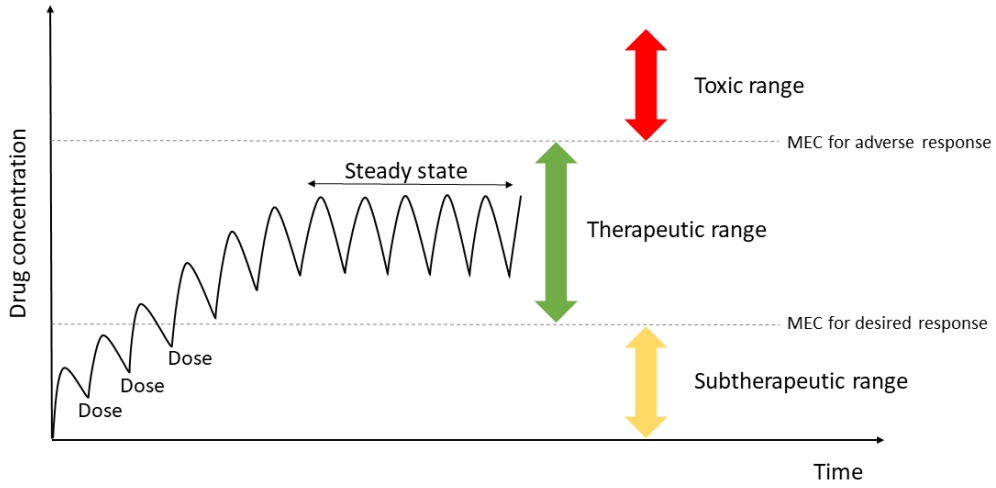

Figure 5. Concept of the therapeutic range. The illustration shows the multiple administration of a drug, reaching a steady state concentration. The steady state concentration lies within the therapeutic range. Drug concentrations below a minimal effective concentration (MEC) for a desired response are within the subtherapeutic range. Drug concentrations above a MEC for an adverse response are within the toxic range.

Usually, blood or plasma measurements are carried out after the drug has reached C_{ss}. For drugs with a long terminal half-live (e.g. mitotane), or if acute drug toxicity is suspected, drug levels can be measured before reaching steady state [143]. Trough levels are characterized by little inter- and intra-individual variability, as variability is mainly associated with absorption and distribution processes and samples taken at the trough therefore contain only sparse information about the PK behaviour of the drug. Nevertheless, measuring C_{trough} has found to be the most feasible in clinical routine. Interpretation of C_{trough} however is strongly linked to correct assumptions of dosing times, which remains a main source of imprecision. With the increased use of oral therapies and outpatient care, it is becoming challenging to measure C_{trough} as sampling times might conflict with patient visit times. Thus, samples would need to be collected at any time point after administrations and extrapolation methods are required to predict C_{min} (minimum concentration) based on plasma samples collected at any time points. [165]. For drugs with large IIV in PK parameters it is however advisable to narrow the sampling window to 3–6 hours before the next drug intake until the end of the dosing interval [165].

4.2 Minimally invasive sampling techniques & dried blood spot analysis

In order to obtain more accurate knowledge about the exposure of patients to an administered drug, it would be desirable to measure 4 to 8 concentrations within a dosing interval. Based on that, the individual AUC [47] can be obtained, which can be further used to

calculate the clearance of the administered drug. With several measured concentrations, a concentration-time profile can be established, which also represents the shape of the PK profile. The AUC itself does not contain any information on the shape of the PK profile and the same AUC value can result in different shapes. However, the concentration-time profile and shape, respectively, allows the evaluation of typical PK aspects such as C_{max}, T_{max} (time point of C_{max}) or C_{min}, which are important parameters to assess effectiveness of the administered dose and the treatment regimen, respectively.

Yet, in clinical practice, it is difficult to realise dense blood sampling, as it is laborious, cost and personnel intensive, and multiple blood collections may not be tolerated by the patient. More flexibility in sampling times and an increase in sampling intensity can be achieved by sampling in an outpatient setting. However, if drug concentrations are measured in venous blood or plasma, home-based sampling is more difficult to realise, as sampling of venous blood by the patients themselves is not feasible.

Despite numerous efforts, alternative matrices like saliva or tears have not yet become standard in clinical settings [166]. Most attempts to use a more accessible matrix than venous blood refer to measurements from capillary blood samples and the implementation of dried blood spot methods (DBS) in TDM. This method was originally introduced by Guthri and Susi in 1963, when they measured phenylalanine associated with phenylketonuria in newborn. They applied a small amount of fresh blood, obtained from heel puncture to a piece of a thick, highly absorbent filter paper. After the blood was air dried, a disc was punched from the centre of the blood spot which was finally analysed [167]. The basic procedure in dried spot analysis and the sub punch method has hardly changed since then. The use of a fixed-diameter sub punch from an absorbent filter paper for quantitative analyses however is associated with some challenges. It must be ensured, that the amount of blood taken from the sub punch is constant and homogeneous in order to conduct reliable and accurate drug concentration measurements. Thus, the traditional subpunch technique is essentially dependent on the blood being evenly distributed when initially spotted. The haematocrit (HCT) of the sampled blood on the other hand has a strong influence on the size of the DBS spot. As the HCT directly affects blood viscosity, a drop of blood with high HCT will spread less far on the surface compared to a drop of blood with low HCT. This ultimately results in high haematocrit dependency of DBS concentrations [168,169]. Newer developments try to overcome these inaccuracies in the DBS analysis caused by the HCT issue, while still delivering the benefits of the minimally invasive sampling procedure. Volumetric absorptive microsampler (VAMS), which consists of an absorbent polymeric tip attached to a moulded plastic handle, wick up a fixed volume (10, 20

or 30 µl) of blood [168,169], irrespective of HCT level. With VAMS, blood, e.g., from a finger prick, can easily and accurately be sampled by dipping the tip directly to the puncture site.

Compared to venous blood sampling, collecting capillary blood from a heel or finger prick is more comfortable as it is less invasive, which implicates less physical and psychological stress on the patient. This in turn can increase patients' acceptance and compliance for a regular monitoring of drug levels. After an appropriate instruction and training by the attending physician, patients can sample capillary blood through a finger prick by themselves. The dried samples can be directly sent to the hospital or analysing laboratory via normal postal systems without further precautions. Thereby, home-based sampling can be carried out almost anytime and anywhere without the need for a physician or nurse to be present. However, this can also only be a supposed advantage, as this new independence is not desired by all patients. Older patients, for example, can be overwhelmed by this and prefer to have their blood taken by a doctor. Minimally invasive sampling techniques require significantly smaller blood volumes (10-30 µl). This makes DBS highly attractive especially for the use in infants and even neonates and for frequent sampling e.g., in critically ill patients. DBS also leads to ethical benefits in rodent PK and toxicokinetic studies. Blood can be easily sampled through the tail vein which strongly improves blood sampling from animals for scientific purpose, [170] .

It is essential to bear in mind, that capillary blood is different to the commonly used matrices, plasma, serum, or venous whole blood. As the sampling site of DBS differs from the sampling site used in normal venous blood sampling, capillary blood rather reflects arterial blood than venous blood, especially when the heel or finger is immersed in warm water to stimulate blood flow. This potentially results in discrepancies between the measured drug concentration from DBS and plasma or venous whole blood, particularly shortly after drug administration, as long as no distribution equilibrium has been achieved [171]. In addition, capillary blood physiologically differs from venous whole blood as it is composed of arterial and venous blood. Due to the sampling from a finger or heel prick it is potentially contaminated with interstitial fluid. In the context of self-sampling by patients, they should be strongly advised to discard the first drop, in order to prevent this contamination [171,172]. A study investigating the feasibility on nilotinib dried blood spot self-sampling revealed that only 77% of the samples collected by CML patients were suitable for analysis, mainly due to a lack of blood flow respectively too small spot sizes [173]. A slightly higher rate of valid DBS samples (more than 90%) was achieved by a population-based study performed in Norway. In this study, again, the biggest problem regarding DBS sampling was insufficient blood flow [174]. To increase blood flow, patients tend to extensively massage and squeeze around the puncture site, which is however likely to result in a dilution of the blood sample with tissue fluid and should therefore be avoided. Furthermore,

patients should be advised that the puncture site should be well cleaned (e.g., with 70% isopropyl alcohol) beforehand to prevent possible contamination of the blood sample. If the measured DBS concentrations are used in the context of TDM as a basis for dose adjustments according to a therapeutic range or a certain threshold value, one must consider that for many substances the therapeutic range mainly refers to plasma concentrations and no reference ranges for capillary blood are available. For a reliable interpretation of capillary drug concentrations, a validated conversion must be established. A suitable relationship between concentrations obtained from DBS and therapeutic ranges based on plasma concentrations is necessary. Measurement of total drug concentrations, whether from plasma or DBS, should always be considered only as a surrogate parameter for the unbound plasma concentration (C_u) as all relevant events in the body related to PK and PD are driven by C_u. It would therefore be a better approach to measure C_u directly, but this is limited in practice by technical issues.

To determine drug plasma concentrations based on DBS measurements, knowledge about the drug´s affinity to constituents within plasma and the blood cells and thus extent of partitioning between the cellular and water components of the blood are necessary. At equilibrium the relationship between C_u and total drug concentration in plasma (Eq. 5) and blood (Eq. 6) are

$$\mathbf{C_p} = \frac{C_u}{f_{up}} \qquad \textbf{Eq. 5}$$

$$\mathbf{C_b} = \left[\frac{1\text{-HCT}}{f_{up}} + \mathbf{HCT} \bullet \mathbf{p}\right] * C_u \qquad \textbf{Eq. 6}$$

where C_p, C_b, C_u are the total plasma, total blood, and unbound concentration, respectively, HCT is the haematocrit, and p is the blood-to-plasma concentration ratio. Thus, the ratio between concentrations measured in blood and in plasma depends on f_{up}, the blood-to-plasma ratio as well as the HCT. If f_{up} is constant, plasma concentration is proportional to unbound concentration. The same holds true for blood concentration if, in addition to f_{up}, HCT and p are also constant [171,172]. If these ideal conditions are given and the blood-to plasma ratio is not subject to time or concentration dependency, either plasma or blood concentration can equally be used to reflect unbound concentration and a linear relationship between plasma and DBS concentration can be established [175,176]. Changes in f_{up}, HCT and p can occur in different situations. Variability in f_{up} can be seen due to alterations in plasma protein concentration (because of stress, surgery, liver dysfunction, pregnancy, cancer etc.) [177]. HCT normally is relatively constant, however cancer patients, and in general critically ill patients, may suffer from partial haemolysis, resulting in lower HCT. Partial haemolysis is also associated with an altered blood-to plasma concentration ratio of the drug, but there is yet little evidence on the

extent of inter- and intra-subject variability of p [171]. In such cases, linear relationships between C_p and C_{DBS} are not reliably given, and nonlinear models for the assessment of DBS vs. plasma concentrations are required. Even though DBS sampling is not free of drawbacks, its advantages over conventional plasma sampling are considerable and feasibility of DBS sampling in therapeutic drug monitoring has been shown for a variety of therapeutic classes of drugs like antiepileptics, antibiotics, antidepressants or antiretrovirals [176]. For the more recent class of targeted antineoplastic drugs, more and more methods are being developed to perform TDM using DBS measurements [176,178-180].

5 Pharmacometric approaches

Pharmacometrics is the iterative science that combines drug, disease and patient/organism information with statistics, mathematics, and computational methods. In general, a model is a simplified representation of a complex biological system and is built for a specific process. Empirical models are data driven, whereas mechanistic models are supposed to give information about the underlying biological system, the disease, and its answer to drug exposure [181]. With pharmacometric models, available information can be analysed to gain a better understanding about the drug-patient-disease interaction. Data obtained from TDM combined with a PK/PD model are valuable to establish a relationship between a given dose, drug concentrations and clinical response and to subsequently describe and predict the effect-time course after administration of a certain dose in a certain population [1]. By that pharmacometrics aims to optimise drug therapy but also to predict new scenarios, such as new dosing regimens or dosing regimens for specific populations (e.g., paediatrics, pregnant women, patients with liver or kidney disease). There are different analysis methods to evaluate PK and PD data and different types of pharmacometric models with different levels of complexity. The right method and model must be selected, based on the available information and on the purpose they are intended to fulfil [182,183].

5.1 Allometric scaling, non-compartmental & compartmental analysis

Allometric scaling is a simple, inexpensive, and fast method based on the relationship between body size of the respective species and a biological process or PK parameter (e.g., clearance). Eq. 7 shows the relationship including the allometric constant *a* (specific to the drug and PK parameter) and the allometric scaling exponent *b* (specific to the PK parameter).

$$\textbf{PK parameter} = a \cdot (\textbf{BW})^{b} \qquad \textbf{Eq. 7}$$

Allometric scaling is especially used for interspecies scaling but also to decide for first in human doses and to predict human drug exposure based on data collected from animals. However, allometric scaling reaches its limits especially for drugs that are highly protein bound, biliary excreted, actively renally secreted, actively metabolized or which have species-specific binding or distribution [184]. One step further goes the concept of in vitro-in vivo extrapolation (IVIVE), which additionally incorporates in vitro information such as drug metabolism, plasma protein binding, permeability, or solubility. However, to gain a mechanistic understanding of ADME processes, to predict and simulate e.g., different dose scenarios in new patient groups,

to investigate the influence of different co-variates or to analyse the effect of different drug-drug interactions, models that incorporate human physiological processes and/or clinical study data are required.

A simple and fast method to evaluate pharmacokinetic parameters and initial exposure characteristics of a drug or metabolite within a single study is the noncompartmental analysis (NCA), which determines PK parameters without assumptions regarding the underlying model structure as the calculation is based on the statistical moments' theory. Based on measured drug concentrations and corresponding concentration-time plots, PK parameters like AUC, C_{max}, T_{max}, V_d, CL and $t_{1/2}$ can be calculated. Drawbacks of NCA are the assumption of linear kinetic and the need of a rich data set per person, which is rarely available in clinical routine. NCA is therefore particularly suitable for non-clinical and toxicology (i.e., animal) studies or early (phase I) clinical trials.

Compartmental models are one of the most frequently used pharmacokinetic models to describe a drug concentration-time course in the body and to simulate absorption, distribution, and elimination processes. In most cases, drug concentrations are measured in plasma, as they are easily accessible and in good relation to the side of effect (e.g., receptor). However, modelling the concentration-time course of other biological fluids, like urine and saliva is conceivable. Depending on the model, the human body is divided into one, two or more hypothetical compartments.

A compartment is a space with a homogenous distribution that is well stirred, which means that the input and output kinetics between two compartments is the same for that compartment. A compartment lumps several organs, which, however, do not necessarily have to be anatomically or physiologically contiguous. The simplest case is a one compartment model, where all organs and tissues of the body are lumped into a single (central) compartment. A given drug enters this central compartment and leaves it after a given time (Figure 6) [2,8].

In the case of a two compartmental model, organs and tissues are divided into a central, well perfused compartment and a peripheral compartment, which is not well perfused. Classically, brain, blood, kidney, and liver are part of the central compartment, whereas fat, skin and muscles are part of the peripheral compartment. A given drug again enters the central compartment and leaves the central compartment. However, the drug also enters the peripheral compartments and recirculation between both compartments occurs with a given rate constant [2] (Figure 6). In some cases, the two compartmental model is extended to a three compartmental model, which allows an even more precise distinction between plasma (central compartment), highly perfused organs and tissues (second compartment) and scarcely perfused organs and tissues (third compartment).

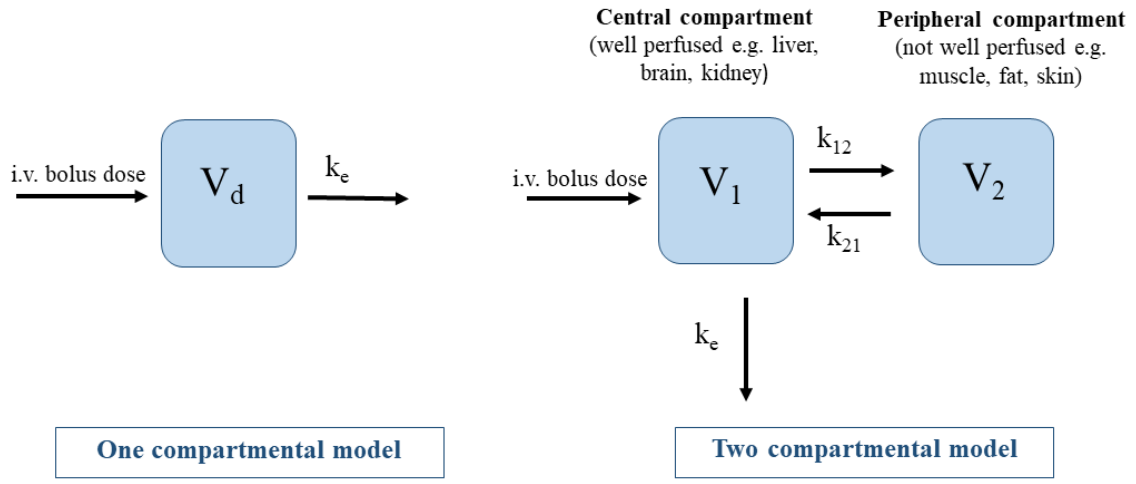

Figure 6. A schematic illustration of a one and a two compartmental model. For the one compartmental model an i.v. bolus dose enters the compartment with a given V_d and leaves the body with a given rate constant k_e. For the two compartmental model, an i.v. bolus dose enters the central compartment, which consists of a given volume V_1. The drug recirculates between the central compartment and the peripheral compartment (with a given volume V_2), with the rate constants k_{12} respectively k_{21}. The drug leaves the central compartment with a rate constant k_e.

5.2 Physiologically based pharmacokinetic modelling

Physiologically based pharmacokinetic (PBPK) models are mathematical models, based on mass balance equations. They can be established to mechanistically describe the PK and PD behaviour of a drug and its metabolites in the body at a very high level of detail. With a PBPK model all relevant ADME processes related to physiological properties of a certain individual or population [8,185] can be considered. PBPK models can be generated during various steps along the drug research and development process but also after approval in clinical routine.

A whole-body PBPK model contains an explicit representation of the organs that are most relevant to the absorption, distribution, excretion, and metabolization of the drug. It is parameterized by physiological and anatomical parameters (e.g. organ volumes, blood flow rates, protein expression levels or tissue composition), drug-specific parameters (e.g. molecular weight, lipophilicity or pKa/pKb values) and parameters that depend on drug as well as on species properties like clearance, protein binding or blood to plasma partition [5,186,187]. PBPK models consists of numerous different compartments representing the respective organs in the body, which are connected via the arterial and venous blood system (Figure 7). A tissue volume or weight and a tissue blood flow rate, which is specific to the species of interest, define every compartment [187,188] (Figure 7). Organs and tissues which are typically represented by PBPK model compartments are heart, lung, brain, stomach, spleen, pancreas, gut, liver, kidney, gonads, thymus, adipose tissue, muscle, bone and skin as these organs are most relevant for ADME processes [187,188]. Existing software packages like SimCYP® (SimCyp Ltd., Sheffield, UK),

GastroPlus® (Simulations Plus Inc., Lancaster, USA) or PKSim® (Bayer Technologies Service, Open Systems Pharmacology, Leverkusen, Germany) can be used to set up a PBPK model. Within the software, there is already a large amount of prior, independent physiological information incorporated, often not only for healthy humans but also for (preclinical) animals like rats, mice, or dogs. Compound specific parameters are usually kept unchanged across different species and extrapolation from one to another species, but also within a species (e.g., patients with and without renal impairment), are done based on extrapolation of physiological and anatomical parameters.

Through the merge of relevant information of the investigated drug but also of the underlying population and the species-specific physiology and biology, the PBPK analysis allows the a priori prediction of plasma and even tissue or organ concentration-time profiles. Two different PBPK modelling approaches are conceivable, depending on data availability and intended application. A pure bottom-up approach can provide a mechanistic understanding of the investigated system but depends on a deep knowledge of ADME processes, high quality in vitro and preclinical data as well as a verified IVIVE. Physicochemical properties of the drug substance could be accessible in reliable quality; however, information on metabolism and transporter processes or on in IVIVE are sometimes not available in sufficient quality. To compensate, clinically observed plasma concentration-time profiles are added to the initial model and parameters that are missing or are subject to uncertainty can be estimated or optimized, respectively, based on the clinical data (middle out approach) using estimation methods like the Levenberg-Marquardt or Monte-Carlo algorithm [189].

In 2018, the FDA published a guideline for best practices in PBPK modeling, model qualification and reporting of modeling studies as there is an increasing number of PBPK use cases and submissions [185]. Even though a PBPK model may comprise several hundreds of ordinary differential equations, the number of independent model parameters for an initial model is usually small (in most cases, fewer than five per compound) but at least basic physicochemical properties (pka, pkb, molecular weight, number of halogens, lipophilicity, and plasma protein binding) of the compound as well as a clearance process, e.g., based on hepatocyte or microsomal assays, must be defined. A further step involves the selection of a suitable method for the calculation of organ/plasma partition coefficients, which describes the drug distribution behavior. Various tissue-composition-based approaches exist for the a priori prediction of tissue partition coefficients such as methods from Rodgers & Rowland [190,191], Schmitt [192], Poulin & Theil [193],Berezhkovskiy [194], which is a revision of the Poulin & Theil method, or Willman et al. [195]. Pure a priori prediction of partition coefficients is however challenging, and the selection of an appropriate method is normally based on a middle

out approach. This means, that based on initial input parameters together with available (pre)-clinical data (i.e., plasma-concentration time profiles), the method which best fits the data is chosen. The overall idea is the consideration of the tissue as a composition of constituents important for drug distribution, such as tissue water, neutral phospholipids and lipids, acidic phospholipids, albumin, lipoproteins and AGP. The distribution of a drug into the tissue is then approximated by the weighted sum of the distribution into relevant tissue constituents. All common existing approaches account for nonspecific binding to tissue components and assume that drugs have access to all constituents as the drug is homogeneously distributed into plasma and each tissue via passive distribution. However, the methods differ in complexity and their underlying assumptions and the required input parameters [196-198]. One of the main points in which the approaches differ is the consideration of ionization. Poulin & Theil and Berezhkovskiy, respectively, as well as Willmann et al, do not consider ionization, whereas the model by Rodgers & Rowland and Schmitt account for the electrostatic interactions between ionized compounds (e.g., moderate-to-strong bases) and anionic phospholipids at physiological pH. Thus, depending on the drug´s basicity or acidity and the degree of ionization at a particular pH, this can have considerable impact. So far, there is no clear "winner" model as each model has pros and cons and the different methods must be tested to find the most suitable one in each case. This was also confirmed by a study published by Utsey et al., in which was found that none of the methods is superior to another, and all partition coefficient methods should be considered [197]. An attempt to provide guidance for the selection of the appropriate method is provided by Yun et al., who developed a decision-tree to classify the most accurate tissue to plasma partition coefficient algorithm based on available input parameters [196]. As the distribution model is compound specific and independent of the considered species or administration protocol, the calculation method for tissue partitioning should not be changed within the modeling process once it was chosen.

As PBPK model building is an iterative (learn and confirm) process, the initial model is continuously evaluated, modified, and refined (Figure 7). By adding more clinical data and/or additional in vitro data, relevant model parameters are identified and adapted to better simulate and predict plasma or tissue concentrations. The model development and application process must be accompanied by sensitivity analyses for key or estimated input parameters, which help to assess uncertainty of these parameters and to investigate the robustness of the PBPK model. If the model and the respective input parameters are well evaluated and verified, the final PBPK model is appropriate to be used for the intended purpose [182,185] (Figure 7). It can be adapted to different species of interests (human, rat, mouse, dog etc.), possible disease conditions (for example liver or renal impairments, different cancer states) or populations with special

physiological conditions like pregnant women, elderly, overweight patients, or children. By that, it can serve as a tool to simulate different hypothesis and to get a deeper understanding of the drug properties in relation to various physiological parameters/circumstances or in combination with other drugs. In two projects of the presented thesis, PBPK models were established and used for the purposes just mentioned.

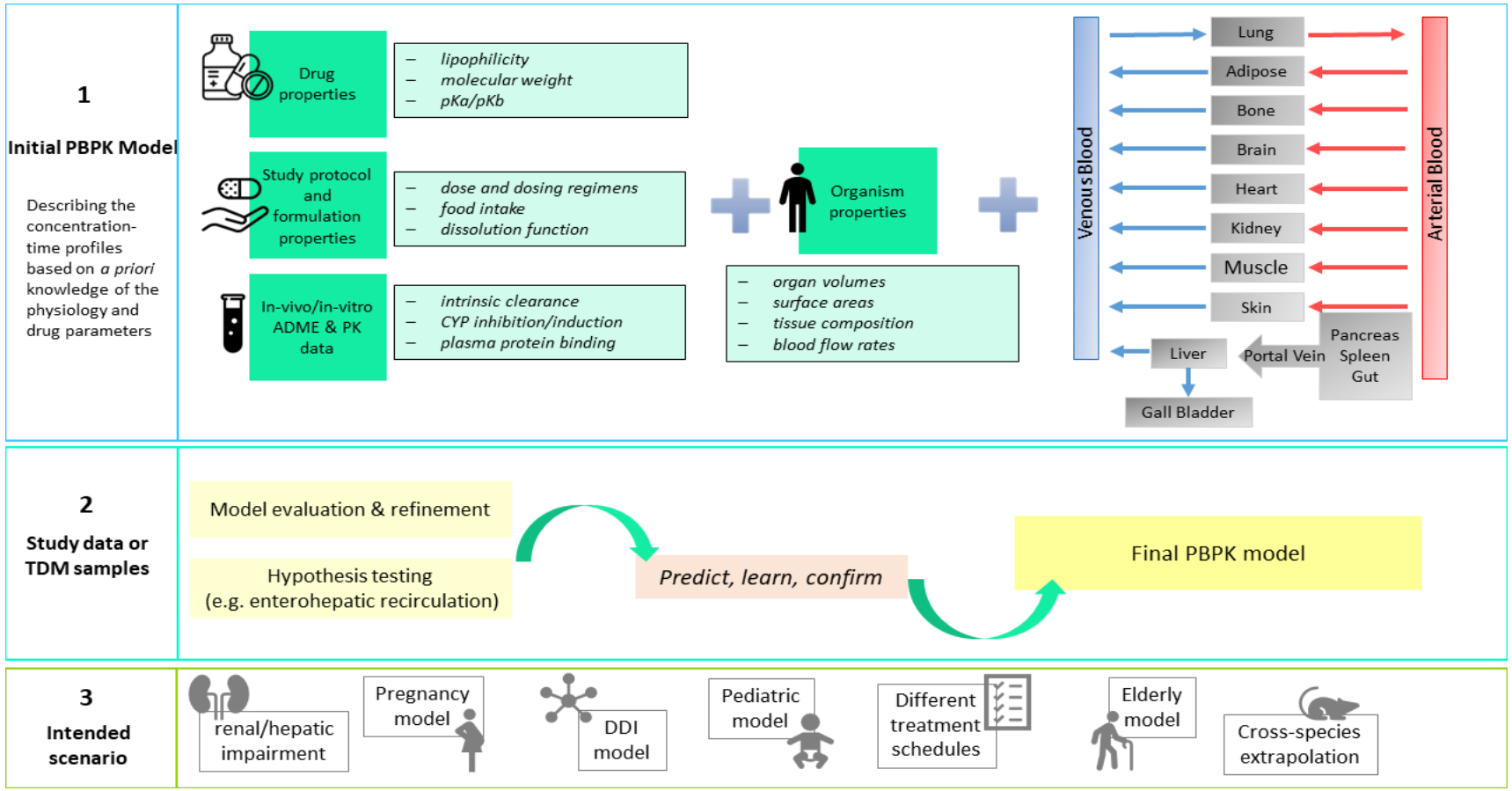

Figure 7. Overview of the input parameters used for an initial PBPK model and exemplary representation of the generic structure of a whole-body PBPK model (1). The initial PBPK model can be evaluated and refined based on e.g., clinical study data, and a continuous learn and confirm cycle occurs until a final PBPK model is validated (2). The final PBPK model can be used in or expanded to, respectively, an intended scenario, such as investigation of renal impairment or DDI (3)

5.3 Population pharmacokinetics

With population pharmacokinetic and pharmacodynamic analyses, typical PK and/or PD behaviour of a drug can be described and at the same time it is possible to assess and quantify variability in drug concentration profiles or drug response within a population and to consider a given residual inter- and intraindividual variability [199,200]. After collecting pharmacokinetic data, either e.g., in the context of a clinical study or during TDM in everyday clinical practice, there are different concepts to estimate pharmacokinetic parameters based on these clinical data. Thus, in contrast to PBPK modelling, this method refers to a top down approach, which is data driven and mainly empirical. The most commonly used methods were introduced already in 1984 by Sheiner et al. [199,201]

- Naïve pooling: all available data are pooled together, pretending that they all originate from one unique individual. Only point estimates for pharmacokinetic parameters are possible and IIV is neglected.
- Standard two-stage approach: this method is divided into two steps. In a first step, each individual is considered separately, and individual PK parameters are obtained based on the individual PK profiles. In a second step, descriptive statistics is applied to obtain point estimates and dispersion parameters of a set of population PK parameters. This approach requires a rich data sampling and a complete pharmacokinetic profile for each individual. In addition, there is a systematic overestimation of interindividual variability as other sources of variability are neglected [202].

Nonlinear mixed-effects modelling (NLME) in the 'population approach' is a special kind of nonlinear regression analysis, which reduces the two steps of the standard two-stage approach into one step. It is a sophisticated method to quantify variability in PK in a study population [203]. The term mixed-effects refers to the simultaneous estimation of fixed-effects (population structural parameters and covariates) and random effects (difference between an individual's parameter value and the population value)[200].

To build a population model, PK or PD data from more than one individual are summarized [204] and analysed simultaneously. One major advantage here is that it is not necessary to have a full dataset, meaning complete concentration-time profiles, for every individual. Even if there are only sparse data for one individual, these data can be incorporated into the model and missing information in the PK or PD profile of one individual can be filled through borrowing it from other individuals. Including data of many individuals enables the generation of a typical population drug concentration-time profile with the respective set of

typical population parameters such as a typical volume of distribution or a typical hepatic/renal clearance (a_{pop}, b_{pop}, k_{pop}) in the first instance. In a second step, the individual concentration-time profile and individual parameter set can be generated for all individuals and the variability within the population can be quantified. Thus, the goal is to characterize the typical pharmacokinetic behaviour of the population and the inter-individual variability at the same time. With the population approach it is possible to investigate the influence of covariates, meaning patient-specific characteristics on model parameters, and finally on the individual drug response or drug concentration.

A NLME typically is composed of several submodels namely a structural model, a covariate model, and a pharmacostatistical model, each of which is explained in more detail below.

The structural model is a mathematical function *f*, that describes the relationship between the independent variable *j* (observation time point) and the dependent variable *y* (observed PK or PD data). The structural model is for example a one-compartmental model containing design variables X (e.g., an administered dose, measurement sampling times) and structural model parameters Φ, like the V_d or the elimination rate constant λ_z. The concentrations y_i for a typical patient of a certain population can be described by Eq.7, where the structural model parameters are the fixed-effects parameters θ, which are elements of the vector Θ. The *j-th* concentration *y* of the *i-th* individual is represented by Eq.8.

$$\mathbf{y_j = f(\Theta, X)} \qquad \textbf{Eq. 7}$$

$$\mathbf{y_{ij} = f(\Phi_i, X_{ij})} \qquad \textbf{Eq. 8}$$

with Φ_i representing the parameter vector that contains the structural model parameters $\phi_{k,i}$ of the *i-th* individual and X_{ij} representing the individual design variables at observation *j* for individual *i*.

The pharmacostatistical model can be subdivided into several hierarchical levels of variability with the IIV and the residual variability being the most important. An optional level of variability gives the intraindividual or interoccasional variability, which allows for the integration of variations in PK from one occasion to another in the same individual (e.g., dose modifications or fluctuation in body weight). The first level of variability mostly is the IIV, also called between subject variability (BSV), which describes the variability between parameter values for a particular individual and the population value of the parameters. BSV mostly is modelled on an exponential scale since PK parameters are supposed to be greater than zero, to avoid non-physiological parameter estimates. For the exponential model, the *k*-th model

parameter for individual *i,* $\phi_{k,i,}$ is the sum of the fixed-effects parameters θ_k and the individual variability parameter $\eta_{k,i}$. and is written as

$$\boldsymbol{\phi}_{k,i} = \theta_k \, e^{\eta_{k,i}} \qquad \textbf{Eq. 9}$$

where η_{ki} represents the random-effects parameter accounting for the difference between the typical (population) parameter θ_k and $\phi_{k,i}$ and is assumed to be normally distributed with mean of 0 and a variance ω_k^2. [203]. The variances of an interindividual variability parameter ω_k^2 k is the k-th diagonal element of the so-called variance-covariance matrix $\boldsymbol{\Omega}$ in a population model. The variance ω_k^2 is the standard deviation on the logarithmic domain and can be expressed as the coefficient of variation (CV%) on the original (linear) scale, according to Eq. 10 [205].

$$\boldsymbol{CV, \%} = \mathbf{100} \bullet \sqrt{\boldsymbol{\omega}_{\mathbf{k}}^{\mathbf{2}}} \qquad \textbf{Eq. 10}$$

A covariance between interindividual variability parameters (ω_k^2 k and ω_{k+1}^2) can be described by the off-diagonal elements of $\boldsymbol{\Omega}$ [181].

The second level of variability is the unexplained residual variability (RUV), termed ε, which accounts for the discrepancy between the model-predicted and the observed value in an individual (e.g., plasma concentration at a certain time). This discrepancy arises due to different reasons like model misspecifications, assay errors or errors in dosing. RUV can be added either as an additive, proportional or combined error depending on the source and nature of error (Eq. 11 - 13)

Additive error:

$$\mathbf{y_{ij}} = \mathbf{f}\left(\boldsymbol{\Phi}_\mathbf{i}, \mathbf{X_{ij}}\right) + \boldsymbol{\varepsilon}_{\mathbf{add,ij}} \qquad \textbf{Eq. 11}$$

Proportional error:

$$\mathbf{y_{ij}} = \mathbf{f}\left(\boldsymbol{\Phi}_\mathbf{i}, \mathbf{X_{ij}}\right) \bullet \left(\mathbf{1} + \boldsymbol{\varepsilon}_{\mathbf{prop,ij}}\right) \qquad \textbf{Eq. 12}$$

Combined error:

$$\mathbf{y_{ij}} = \mathbf{f}\left(\boldsymbol{\Phi}_\mathbf{i}, \mathbf{X_{ij}}\right) \bullet \left(\mathbf{1} + \boldsymbol{\varepsilon}_{\mathbf{prop,ij}}\right) + \boldsymbol{\varepsilon}_{\mathbf{add,ij}} \qquad \textbf{Eq. 13}$$

where y_{ij} is the observation in the *i-th* individual at time j and $f(\Phi_i, Xij)$ denotes model prediction. ε_{add} and ε_{prop} are, similar to the IIV, assumed normally distributed with zero mean and variance σ^2.

One main goal of the population approach is the identification of covariates to explain (in part) variability within the population. Covariates are either patient-specific characteristics,

which can be continuous (e.g., age, weight) or categoric (e.g., sex), (patho)-physiological factors (e.g., disease score, laboratory parameters, genotype) or extrinsic factors such as smoking status or concomitant medications. The influence of a specific covariate on a model parameter θ can be integrated either linear, exponential, additive, exponential or as a power function, also depending on the classification of the covariate (categorical vs. continuous) [200,205].

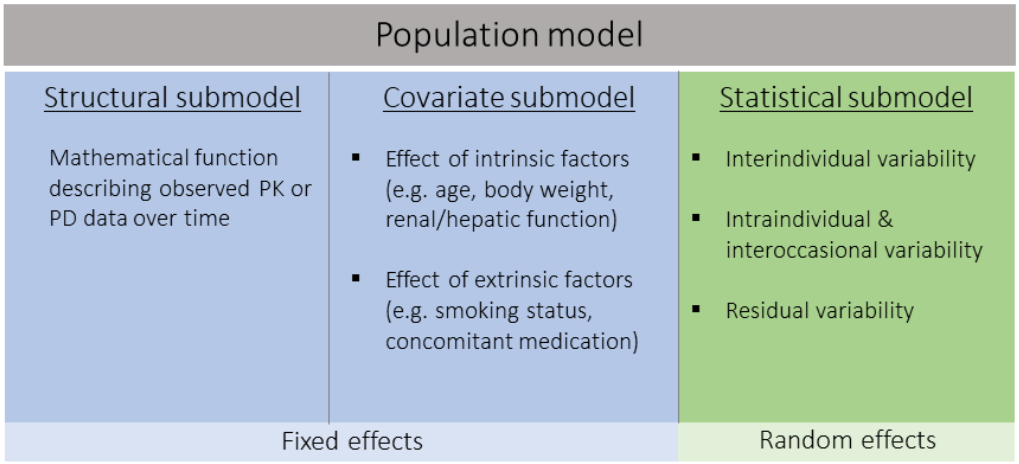

Figure 8. Components of a NLME population model. The structural and covariate submodels refer to the fixed effects of the population model and the statistical submodel is applied to describe the random effects of the population model.

Once a population PK (popPK) model is established based on the mentioned components (Figure 8), it has a wide range of applications. During drug development, popPK models can be used for example to simulate various scenarios, such as different dosing schemes, to optimize trial sample size and PK sampling schedule or to evaluate potential trial designs and optimize dose selection in paediatric trials. They are a helpful tool to determine the variability between individuals, to understand the source of variability and to investigate "what-if" questions. However, simulations to answer "what-if" scenarios can only be done for individuals belonging to a population on which the underlying model is based. All the insights gained from the popPK model, and the simulations, which can be done for individuals belonging to the population ultimately help to optimise the therapy for each individual, e.g., in the frame of model-informed precision dosing.

5.4 Model-informed precision dosing

Model-informed precision dosing (MIPD) is one approach to further improve individual drug therapy based on patient characteristics and (patho-) physiology, comorbidities and comedication as well as disease specificities [206]. Although dose-finding studies are conducted

during drug development, there is limited knowledge regarding dosage and application for many patient groups. Information in the drug label only covers an average standard population upon which published data were generated. Clinical research phase I to III studies are conducted with either healthy volunteers (Phase I) or with volunteers who have the disease or condition in question (Phase II & III) ([207]. However, these volunteers are usually selected according to very strict inclusion criteria that do not represent the breadth of the population and IIV is intentionally kept to a minimum. This approach creates a knowledge gap and uncertainty for the therapeutic use in patients and special subpopulations (e.g., children or the elderly) and numerous scenarios exist, which are not covered by controlled clinical trials. Elderly, pregnant, and breastfeeding women, children, obese or smoker are usually just as little considered as, ethnicity, genetic polymorphisms and patients suffering from various co-morbidities or with a specific health condition (hepatic, renal impairment). Thus, initial dosing and/or dose modifications for these patients and scenarios, are done based on physicians' experience or existing literature and are often off-label.

With MIPD, both, initial dosing as well as subsequent dosing can be improved and adapted according to the patients need. Through the combination of a drug-specific model with patient-specific covariates (e.g., age, height, weight, laboratory parameters like serum creatinine), it is possible to estimate the individual variability in PK and to calculate the probability of target attainment of a certain PK/PD target *a priori*. Thus, an individual dosing strategy can be established before treatment initiation. In a second step, as soon as measured drug concentrations become available, these concentrations can be integrated into the drug-specific model, and a set of individual PK parameters can be derived *a posteriori* [208] using Bayesian approaches. Compared to frequentist statistics, Bayesian statistics allows the integration of prior knowledge about the drug-patient-disease system and typically, the maximum *a posteriori* (MAP) Bayesian estimates, which are the most probable individual parameter values (i.e., the mode of possible PK parameter distribution) are determined. The MAP estimate is a one-point summary of the posterior distribution, which does not give a quantification of the associated uncertainty. If more advanced data assimilation techniques are used, a full Bayesian approach can be performed that enables uncertainty quantification by approximating a full posterior distribution [209].

In many cases MIPD is based on popPK models, although also other approaches, like PBPK modelling and simulation provide a rationale for precise dosing in an individual and thus can be used as a source for a model-informed optimization of drug therapy [206]. Unlike the traditional TDM, which requires sampling in steady-state and sampling of trough levels, drug concentrations sampled at any time and before steady-state is reached can be used for MIPD.

In addition, a single sample is sufficient to estimate individual PK parameters, however precision typically increases with more drug concentration measurements becoming available [208]. Small standard errors of model parameters are indicative of good parameter estimation and express a high precision of the obtained model parameters. A relative standard error (%RSE) for random-effects parameters, reported as CV %, can be calculated according to Eq. 14 [181].

$$RSE_{w_k^2}, cv, \% = \frac{SEw_k^2}{2w_k^2} \bullet 100 \qquad \text{Eq.14}$$

Due to the Bayesian framework that is used in MIPD it is possible to update uncertainty on the variability of the parameters of the population. The prior model can be informed by using TDM data and estimated population parameter can be updated accordingly. With more and more TDM data becoming available the standard error of an estimated parameter gets smaller, leading to less uncertainty and higher prediction, respectively, of the parameters [210].

Applicability of MIPD to optimize dosing in individual patients with appreciable success was shown in several works [206,211-216]. Even though MIPD is regarded as "State of the Art", it is not yet widely used in daily clinical routine [206]. Besides technical, financial, or regulatory hurdles, one of the reasons for the limited use of MIPD in routine clinical practice is the need for dedicated software to develop NLME popPK models, such as NONMEM® (ICON plc, Dublin, Ireland), Monolix™ (Lixoft SAS, Antony, France) or dedicated R packages (e.g., mrgsolve). What they all have in common is that their use requires intensive training and is not suitable for rapid use by end users (i.e. medical staff). [217]. Thus, for an easy application of MIPD at the bedside, dedicated user-friendly tools with a graphical user interface, e.g., in the form of a mobile app or a web-based application are needed. Examples are TDMx, NextDose, DoseMeRx, InsightRX Nova, MwPharm++, PrecisePK, AutoKinetics, BestDose, ID-ODS and Tucuxi [218]. Such tools can then also be used in routine clinical practice. Measured drug concentrations from patients obtained in clinical studies and clinical routine, respectively, were the basis for the development of PK models in the presented thesis. These models can in turn be the basis for optimising the individual dosage for future patients with the aim to achieve drug exposure targets which are associated with desirable clinical outcomes.

B Aim of the work

In this work TDM and pharmacometric methods were explored and used to optimize therapy with oral antineoplastic drugs with critical characteristics and to gain a mechanistic understanding of their PK behaviour to reduce the risk of potential over-or underdosing.

Mitotane, a compound characterized by challenging PK, is an example of a drug where TDM is essential. With the aim to optimize mitotane therapy in ACC, a minimally invasive sampling method, using VAMS technology, should be investigated as a first project.

In order to gain a mechanistic understanding of the compound and to describe its characteristic concentration-time profile, a PBPK model should be developed for the multi kinase inhibitor cabozantinib. Since cabozantinib is metabolized via CYP3A4, it is susceptible to DDI. One goal therefore was to model DDI with the strong CYP3A4 inducer rifampin and compare to validate the model against a published human DDI trial. The cabozantinib model should also be expanded to patients with different levels of hepatic impairment.

In the third project, PBPK models for posaconazole and ruxolitinib should be developed and validated based on clinical data and the impact of the clinically relevant DDI between both compounds should be investigated and compared to plasma exposure obtained from patients with GvHD in a routine clinical setting. Based on the developed PBPK model recommendations should be made for the dose adjustment in case of a combined ruxolitinib and posaconazole treatment for patients with GvHD to avoid ruxolitinib overdoses.

C Results

1 A method for the minimally invasive drug monitoring of mitotane by means of volumetric absorptive microsampling for a home-based therapeutic drug monitoring

Friedl, B., Kurlbaum, M., Kroiss, M., Fassnacht, M., Scherf-Clavel, O.

Reproduced with permission from Springer Nature Analytical and Bioanalytical Chemistry 411(17): 3951-3962, 2019

Abstract

Mitotane is the only currently approved treatment for adrenocortical carcinoma (ACC), a rare endocrine malignancy. Plasma levels within the range of 14 to 20 mg L^{-1} are correlated with higher clinical efficacy and manageable toxicity. Because of this narrow therapeutic index and slow pharmacokinetics, therapeutic drug monitoring is an essential element of mitotane therapy. A small step towards the therapeutic drug monitoring (TDM) by volumetric absorptive microsampling (VAMS) was made with this work. A simple method enabling the patient to collect capillary blood at home for the control of mitotane blood concentration was developed and characterized using MITRA™ VAMS 20 µL microsampler. Dried blood samples were extracted prior to HPLC-UV analysis. Mitotane and the internal standard dicofol (DIC) were detected at 230 nm by ultra-violet detection after separation on a C8 reversed phase column. The assay was validated in the range of 1 to 50 mg L^{-1}. Dried samples were stable at room temperature and at 2–8 °C for 1 week. At 37 °C, a substantial amount of the analyte was lost probably due to evaporation. Hematocrit bias, a common problem of conventional dried blood techniques, was acceptable in the tested range. However, a significant difference in recovery from spiked and authentic patient blood was detected. Comparison of mitotane concentration in dried blood samples (C_{DBS}) by VAMS with venous plasma in patients on mitotane therapy demonstrated poor correlation of C_{DBS} with the concentration in plasma (C_P). In conclusion, application of VAMS in clinical routine for mitotane TDM appears to be of limited value in the absence of a method-specific target range.

Introduction

Adrenocortical carcinoma (ACC) is a rare and aggressive malignancy of the adrenal gland. Surgery is the only curative treatment option but the risk of local recurrence even after complete resection is high and metastatic spread frequent. In advanced stages, ACC has a dismal prognosis with an overall survival of about 12–15 months [1]. Mitotane (o,p'-DDD), an orally administered chemical derivative of the insecticide dichlorodiphenyltrichloroethane (DDT) [2–5], is the only approved drug and applied both in an adjuvant setting and in metastatic disease [2–5]. Because of its high lipophilicity, mitotane exhibits exceptionally unfavorable pharmacokinetics. Accumulation of the compound in fat tissue may lead to elimination half-lives of 18 to 159 days [6]. Mitotane is almost exclusively eliminated in the form of metabolites via bile or urine. Main metabolites are the corresponding acid o,p'-DDA, which can be detected at tenfold higher concentration in blood than mitotane itself, and the unsaturated derivative o,p'-DDE, which is barely detectable in most cases (Fig. 1) [6, 7]. Mitotane has been in use for treatment of ACC for decades and the substance and its metabolites have been the subject of numerous investigations over the past decades [7–9]. Although several studies demonstrated that a mitotane plasma level > 14 mg L^{-1} is associated with significant clinical benefit [10–12], many problematic issues of mitotane treatment, such as dose response effects, lack a certain level of evidence. Furthermore, there is no clear indication that plasma levels of the metabolites are correlated with clinical benefit or toxicity [13]. Due to the nature of the compound, typical toxic effects are common [14] and occur more frequently when high-dose regimens are applied (e.g., gastrointestinal disorder, which might be dose limiting) and at mitotane plasma levels of > 20 mg L^{-1} (e.g., neurotoxicity, hepatic disorder, leucopenia). However, plasma levels > 20 mg l are not associated with improved efficacy [11, 12]. The broad range of observable half-lives and the fact that mitotane plasma levels between 14 and 20 mg L^{-1} are considered as target concentration are reasons that underlie the strong recommendation for therapeutic drug monitoring (TDM) regardless of the selected dosing regimen [6, 15–17]. Furthermore, it is supposed that mitotane metabolism might be affected by autoinduction [18] and the inter-individual bioavailability of mitotane is highly variable [19, 20]. Therefore, mitotane plasma levels should be controlled at the initiation, change, or cessation of the therapy on a regular basis [6, 13]. Depending on the dosing scheme and the individual half-live, a few patients reach target levels within 4–6 weeks, but in the majority of patients, it takes several weeks to months to reach mitotane steady state [21]. Until attaining steady state, the plasma level should be monitored more frequently in order to manage toxicity, especially for high dosing regimens.

To date, the most common methods applied for the TDM of mitotane comprise a suitable sample preparation (protein precipitation, liquid-liquid extraction, and/or solid-phase extraction) followed by chromatographic separation and UV detection [13, 22–25]. Patient plasma is the matrix used in all of these methods to analyze mitotane concentration, which requires periodic physician consultations for sampling. Since the introduction of the dried blood spot in 1963 by Guthrie and Susi [26], many advances in the analysis of dried matrices have been made [27]. One of the more recent milestones is the introduction of sampling devices, which promise to overcome the hematocrit dependence of the sampled blood volume [28–30]. The aim of this work was to test whether the use of one of these volumetric absorptive microsampling devices can replace venous plasma sampling for mitotane TDM. The method was characterized following the recommendations of the European Medicines Agency [31]. After developing and characterizing the method, it was applied to 51 leftover whole blood samples from patients, and mitotane concentrations obtained from these DBS samples were compared to those obtained from conventional plasma samples.

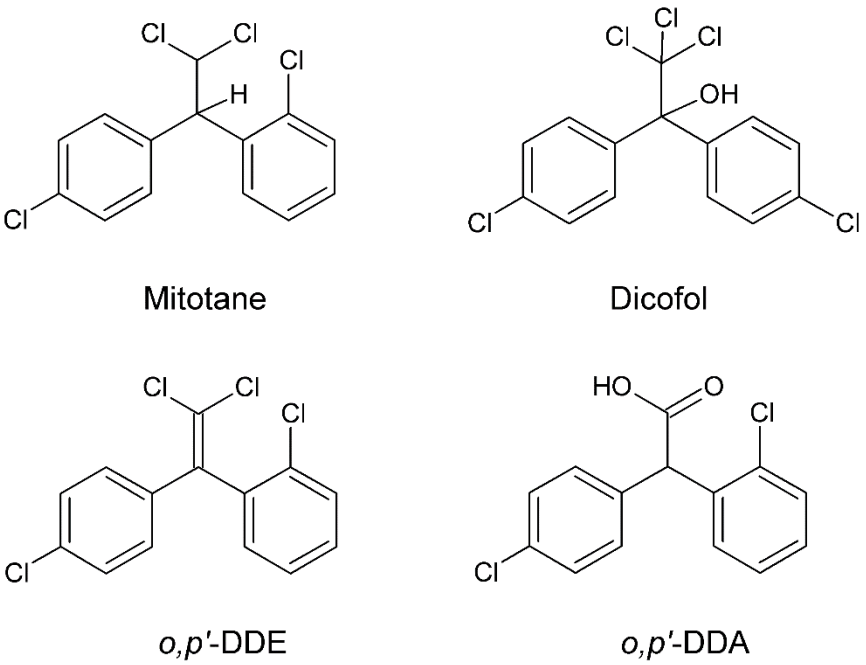

Fig. 1 Chemical structure of the target drug mitotane (MIT), the main metabolites o,p'-DDE and o,p'-DDA, and the internal standard dicofol (DIC)

Materials and methods

Chemicals and reagents

Racemic mitotane (1-(2-chlorophenyl)-1-(4-chlorophenyl)- 2,2-dichlorethan), dicofol (2,2,2-trichloro-1,1-bis(4- chlorophenyl)ethanol), o,p'-DDE, potassium phosphate monobasic, ortho-phosphoric acid 85% for HPLC, and acetonitrile for HPLC gradient grade were purchased from Sigma Aldrich Chemie GmbH (Taufkirchen, Germany), and zinc sulfate heptahydrate and methanol for HPLC gradient grade from VWR International S.A.S. (Fontenay-sous-Bois, France). o,p'-DDA was purchased from Alsachim SAS (Illkirch Graffenstaden, France). Other drug substances were obtained from the local drug bank at the Institute for Pharmacy (Würzburg, Germany). Ultrapure water was produced by a water purification system from Merck Millipore (Schwalbach, Germany). Venous blood with EDTA as anticoagulant was obtained from the blood donation service of the Bavarian Red Cross (Muenchen, Germany).

Equipment and chromatographic procedure

The samples were analyzed using an Alliance (Waters Corp, Milford, MA, USA) 2695 HPLC equipped with 995 photodiode array detector and column thermostat. A LUNA C8 5 μm 150 × 4.6 mm reversed phase column (Phenomenex, Aschaffenburg, Germany) was used as stationary phase. The system was operated in isocratic mode with a flow rate of 1.2 mL min^{-1} and the column kept at 40 °C. The autosampler temperature was set to 25 °C. The mobile phase was composed of water containing 5% (v/v) acetonitrile, acetonitrile containing 5% (v/v) water, and 50 mM potassium dihydrogen phosphate buffer pH adjusted to 2.0 with phosphoric acid 85% at a ratio of 20:70:10 (v/v/v). Ultra-violet detection was performed at 230 nm using the photodiode array detector. The calculation of the concentrations was performed by peak height. The method run time was 15 min. A mixture of 2- propanol and water (50:50 v/v) was used as needle wash solution.

System control and data acquisition were performed with Empower® (Version 3) software. Calibration curves were calculated with the Empower program using a $1/x^2$ weighted linear least-square regression.

Preparation of stock solutions, calibration curve, and quality control samples

Two independent stock solutions for calibrators and quality control samples were prepared in dimethyl sulfoxide (DMSO) to obtain a final concentration of approx. 20 g L^{-1}. These solutions were stored at − 80 °C. Eight calibration and four quality control working solutions were prepared from the stock solutions by serial dilution with DMSO. Twenty-five microliters of

working solution, or DMSO for the blank, was then spiked in 975 µL venous blood (hematocrit adjusted to 0.45) to achieve concentrations of 50, 30, 20, 10, 5, 2.5, 1.5, and 1 mg L^{-1} for the calibrators, and 45, 20, 7, and 1.5 mg L^{-1} for the quality control (QC) samples (QC high, QC medium, QC intermediate, QC low).

After incubation at 37 °C at 400 rpm for 30 min, spiked blood samples (calibrators and quality controls) were absorbed by a 20-µL MITRA™ VAMS device (Neoteryx, Torrance, CA, USA) and dried at ambient temperature (with desiccant) for at least 8 h. Silica gel in PE fleece bag (Tyvek 1059B) was used as desiccant (Wisepac Active Packaging Components Co., Ltd., Shanghai, China).

Sample preparation

Dried blood samples, calibration, and quality control standards were stored at room temperature in a closed container (glass or polypropylene bag) containing desiccant until analysis. The tip of the MITRA™ VAMS device was removed and placed in a polypropylene (PP) tube (2 mL) with round bottom (Eppendorf AG, Hamburg, Germany). After addition of 500 µL internal standard solution (mixture of methanol and 2% (m/V) aqueous zinc sulfate heptahydrate solution 4:1 (v/v) containing 2 mg L^{-1} dicofol), the samples were treated in an ultrasonic bath for 15 min and subsequently shaken for 1 h at 1400 rpm (Thermomixer comfort, Eppendorf AG, Hamburg, Germany). Four hundred fifty microliters of the extracted solution was transferred into a second tube and centrifuged for 5 min (4 °C, 12.000 rcf). Afterwards, 300 µL of the supernatant was transferred to a HPLC vial with PP insert for small volumes (Agilent Technologies, Waldbronn, Germany). One hundred microliters was finally injected onto the chromatographic column. The same extraction procedure was used for liquid blood samples using 20 µL of liquid blood instead of the VAMS device tip.

Method characterization

The method for dried samples was characterized following the recommendations of the European Medicines Agency [31].

The lower limit of quantification (LLOQ) was defined as the concentration of the lowest calibrator with accuracy between 80 and 120% (n = 5) and a precision within 20%. The upper limit of quantitation (ULOQ) was defined as the concentration of the highest calibration level with accuracy between 85 and 115% (n = 5) and a precision within 15%.

Precision and accuracy were evaluated with QC-L (1.5 mg L^{-1}), QC-I (7 mg L^{-1}), QC-M (20 mg L^{-1}), and QC-H (45 mg L^{-1}). Within-run accuracy and precision were determined by measuring a calibration curve with five replicates of every QC in a single run. Between-run

accuracy and precision (% relative standard deviation, %RSD) were assessed by performing a calibration curve with five replicates of each quality control on five different days. The limits for accuracy and precision were ± 15% and ≤ 15% (expressed as relative standard deviation), respectively.

Stability of mitotane in liquid plasma is very well investigated [23, 25, 32]. The stability of standards in liquid blood stored at 2–8 °C was evaluated by comparing 1-week-old standards with freshly prepared ones. Stability of stock solutions in DMSO was tested by comparing freshly prepared solutions in DMSO with 6-month-old solutions kept at − 80 °C.

Short-term stability of the analyte in the dried matrix was tested at different storage conditions. Dried samples were kept with 0.5 g desiccant per sample in tightly closed PP plastic bags for 1 week at 37 °C (93% r.h.), at room temperature (humidity not monitored), and 2–8 °C (humidity not monitored).

Post-preparative stability was assessed by keeping processed samples in their glass vial with PP insert for 24 h in the autosampler at 25 °C.

Six venous blood samples from six individual donors were analyzed as blanks. The absence of interfering peaks was characterized by blank responses < 5% for the internal standard (dicofol) and < 20% of the LLOQ for mitotane. Additionally, the main mitotane metabolites o,p'-DDA and o,p'-DDE as well as likely co-medication (metoclopramide, haloperidol, hydrocortisone, fludrocortisone, prednisone, prednisolone, methylprednisolone, and dexamethasone) were investigated for potential interferences.

Carryover was tested by analyzing blank samples directly after the injection of the highest calibrator (50 mg L^{-1}; n = 5). A mean signal < 20% of the signal at the LLOQ was defined as the absence of carryover effects.

Quality control samples at four different concentrations (48, 20, 7, and 1.5 mg L^{-1}) were prepared with high hematocrit blood (adjusted to 0.55), medium hematocrit blood (adjusted to 0.40), and low hematocrit blood (adjusted to 0.30). Dried blood samples were prepared at least in triplicate and quantified using a calibration curve spiked in blood with an intermediate hematocrit (0.45).

For extraction efficiency, dicofol (IS) and mitotane were diluted in six venous blood samples from six individual donors to yield quality control samples at two different concentrations (MIT 20 mg L^{-1} and 6.5 mg L^{-1}). Afterwards, they were sampled by MITRA™ VAMS device, dried for at least 8 h and extracted. Additionally, dicofol (IS) and mitotane were diluted in a mixture of methanol and 2% (m/V) aqueous zinc sulfate heptahydrate solution 4:1 (v/v) to yield concentrations similar to the dried blood extract, assuming complete extraction of analyte and IS (0.8 and 0.26 mg L^{-1} for MIT and 2 mg L^{-1} for DIC, respectively). All samples

were measured using the described LC method (vide supra). The extraction efficiency was defined as the ratio of peak heights obtained from the processed blood samples (n = 4 for each concentration per patient) and the mean peak heights obtained from the solutions in neat solvent (n = 4 for each concentration).

To evaluate the importance of liquid blood incubation time and condition, blood was spiked with mitotane and dried samples were prepared directly or after incubation at 37 °C, 400 rpm for 30 min at 1.5 and 20 mg L^{-1}. Five replicates for every condition and concentration were prepared. The relative recovery, calculated as IS-corrected peak height ratio (directly prepared divided by after incubation), was reported and interpreted using two-sided student's t test.

Differences in recovery between spiked and patient blood was assessed by comparison of IS-corrected peak height obtained from liquid blood samples compared to dried samples prepared from the same sample at the same time. The relative recovery (dried sample divided by liquid sample) of spiked blood at 1.5 and 20 mg L^{-1} each in five replicates and of six authentic patient samples was calculated. The results were interpreted using ANOVA and Tukey's post hoc test.

Paired plasma and venous blood samples

Fifty-one venous whole blood samples of 7.5 mL using EDTA S-Monovette® (Sarstedt AG & Co. KG, Nümbrecht, Germany) were obtained from patients with adrenal cancer undergoing current or previous treatment at mitotane doses ranging from 0.0 to 6.5 g/day. This study was part of the European Network for the Study of Adrenal Tumors (ENSAT) registry, which has been approved by the ethics committee of the University of Würzburg (approval number 86/03 and 88/11). All patients provided written informed consent. Whole blood was drawn for use in the current study and an aliquot of plasma sample submitted to the Lysosafe® TDM service provided on behalf of the manufacturer, HRA-Pharma (Paris, France). The plasma concentration was determined by a GC-MS method as reported by HRA-Pharma.

Data analysis

Comparison between mitotane MITRA™ and plasma concentrations was realized according to the considerations from the microsampling working group of the International Consortium for Innovation and Quality in Pharmaceutical Development [33]. Patients with missing plasma concentrations, a hematocrit below 0.3, and a plasma or blood level < LLOQ (1 mg L^{-1}) were excluded from analysis. C_{DBS} was plotted against C_P to unveil any nonlinear relationship between the data. A Bland-Altman plot including limits of agreement (mean difference d ± 1.96 SD) was used for the graphical approach to visualize agreement between the actual plasma

concentrations and the predicted plasma concentrations based on MITRA™ measurements. For this purpose, the difference between the predicted plasma concentration (C_{Pred}) and C_P was plotted against the mean of C_{Pred} and C_P [34]. C_{Pred} was calculated by slope only, because the y-intercept was not significantly different from zero. Data analysis was carried out using Microsoft Excel (Microsoft Corporation, Redmond, WA, USA) and R (version 3.4.2) [35] with 'ggplot2,' 'dplyr,' 'readxl,' 'BlandAltmanLeh,' 'mcr,' and 'epiR' packages. The Pearson's product moment correlation coefficient r and the concordance correlation coefficient (CCC) was calculated. CCC determines the agreement on a continuous measure obtained by two methods and was interpreted according to McBride [36] as follows: > 0.99, almost perfect; 0.99–0.95, substantial; 0–0.95, moderate; and < 0.90 poor agreement. A Pearson's product moment correlation was defined as follows: 0 to 0.3 or 0 to − 0.3, weak; 0.3 to 0.7 or − 0.3 to − 0.7, moderate; and 0.7 to 1 or − 0.7 to − 1, strong.

Results

Method characterization

The chromatographic separation was performed within 15 min with dicofol (IS) and mitotane retention times of about 7.9 and 8.8 min, respectively (Fig. 2). Linear regression ($y = ax + b$; mean ± SD of a 0.0143 ± 0.0009, and b 0.0003 ± 0.0014; $n = 5$) with y being the ratio of mitotane peak height to dicofol peak height and x being the concentration in milligram per liter using $1/x^2$ as weighting factor fulfilled the defined criteria. The coefficient of determination was > 0.992 ($n = 5$) and back-calculated calibrator concentrations were within ± 15% (± 20% for the LLOQ) of the nominal concentration. Precision and accuracy were within the acceptance criteria: At the LLOQ (1 mg L^{-1}), 2.37% and 100.4% respectively; at the ULOQ (50 mg L^{-1}), 7.30% and 106.8% respectively. The relative standard deviations of quality controls (Table 1) were between 5.5 and 14% for both intra- and inter-day precision. Investigation of accuracy of quality controls revealed a deviation of less than 15% from the theoretical concentration at each tested concentration level (98.4– 108.1%; Table 1).

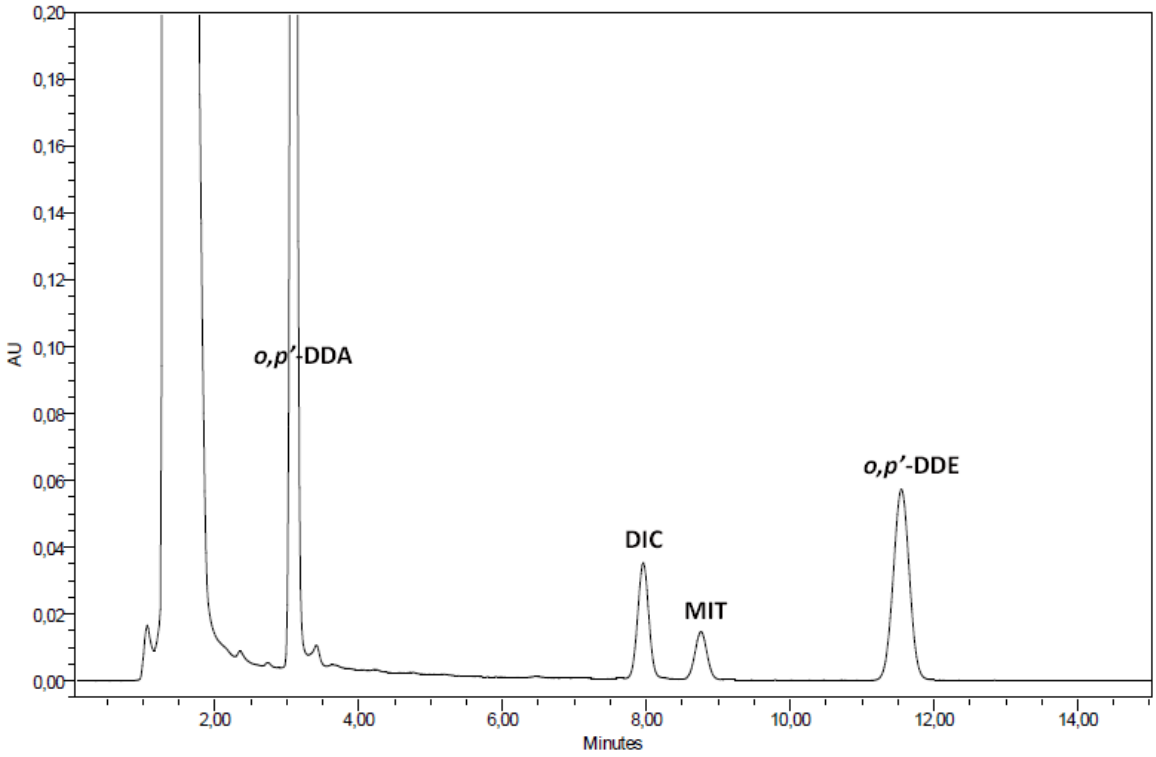

Fig. 2 Chromatogram of a dried blood extract spiked with mitotane at 45 mg L−1 and the main metabolites o,p'-DDE and o,p'-DDA; internal standard: DIC; for chromatographic conditions, see section 2.2

Table 1 Inter-day and intra-day imprecision of mitotane measurements on MITRA™ microsampling device

QC sample	Imprecision (RSD, %)	Accuracy (%)
Inter-day (n = 25)		
QC-L	14.0	107.4
QC-I	13.8	104.9
QC-M	9.7	98.4
QC-H	9.9	102.1
Intra-day (n = 5)		
QC-L)	5.5	108.1
QC-I	8.0	103.0
QC-M	9.4	104.0
QC-H	8.0	103.3

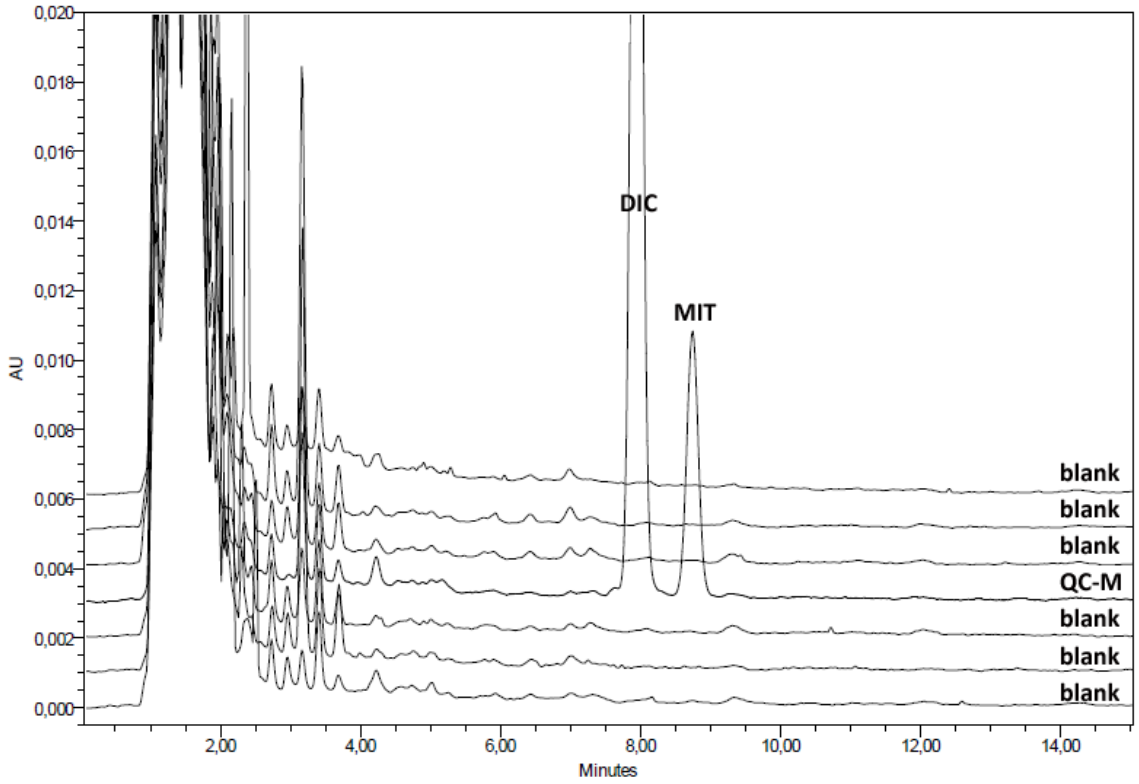

Fig. 3 Overlaid chromatograms of six individual blank samples and a LLOQ sample; internal standard: DIC; mitotane: MIT; for chromatographic conditions, see section 2.2

The analysis of six individual blank samples did not show any interference at the retention time of dicofol (IS) nor at the retention time of mitotane (Fig. 3). Neither did the metabolites o,p'-DDA, o,p'-DDE, nor any of the other investigated drug substances interfere with the peaks due to dicofol (IS) or mitotane.

The analyte and internal standard were stable post-preparation stored for 24 h in the autosampler. Mitotane stock solution was stable for 6 months at − 80 °C. Mitotane (QC-L, QC-M, and QC-H) was stable in liquid blood for at least 1 week at 2–8 °C (accuracy, 103.0–108.1%; precision, 5.5– 9.4%; n = 5 for every QC level). Dried samples with desiccant in a closed PP bag were stable at room temperature and at 2– 8 °C for 1 week. At 37 °C, a substantial amount of the analyte was lost (accuracy, 54.9–72.3%; Table 2).

Table 2 Short-term stability (1 week) of mitotane in MITRA™ microsampling device (n = 3 for every concentration level and condition)

Storage temperature	QC sample	Accuracy (%)	RSD (%)
Room temperature	QC-L	109.9	4.4
	QC-I	110.1	7.0
	QC-M	113.9	5.9
	QC-H	102.7	5.1
2-8 °C	QC-L	101.3	13.1
	QC-I	92.2	9.2
	QC-M	91.4	1.3
	QC-H	112.0	7.1
37 °C	QC-L	54.9	10.7
	QC-I	64.5	5.3
	QC-M	63.6	6.8
	QC-H	72.3	25.3

No carryover effects were observed. There were no peaks present in the blank samples at the retention time of dicofol (IS) nor at the retention time of mitotane when the blank samples were injected directly after the highest calibrator.

Samples prepared from blood with high, medium, or low hematocrit were within the general acceptance criteria for quality control samples (accuracy, 89.8–113.0%; precision, 4.5–10.1%; Table 3). Values obtained for analyte extraction efficiency of samples with high mitotane concentration ranged from 67.0 to 71.5% for mitotane (RSD 5.1–12.7%, n = 4 per patient) and from 98.2 to 99.8% for the internal standard dicofol (Table 4).

Values obtained for analyte extraction efficiency of samples with low mitotane concentration ranged from 84.1 to 94.0% for mitotane (RSD 5.2–9.0%, n = 4 per patient) and from 99.7 to 100.7% for the internal standard dicofol (Table 5).

The relative recoveries of directly sampled VAMS vs. blood samples incubated at 37 °C for 30 min prior to sampling were 94.8 and 106.2% for the 20 mg L^{-1} and the 1.5 mg L^{-1} sample, respectively. Differences in peak height ratio mitotane/IS between the groups were not statistically significant (p = 0.385 and 0.392).

The relative recoveries of dried samples compared to liquid blood samples were 64.7 and 66.3% for the spiked samples at 20 mg L^{-1} and 1.5 mg L^{-1}, respectively. Mean relative recovery of six individuals was 77.3 ± 4.8% (see Fig. 4). The relative recovery in the patient samples was significantly increased (patients vs. high spiked concentration, p = 0.013; patients

vs. low spiked concentration, p = 0.029), whereas no difference between high vs. low spiked concentration was detected (p = 0.909).

Table 3 Hematocrit bias using the 20 µL MITRA™ microsampling device

Hematocrit	QC sample	Accuracy (%)	RSD (%)
Low (0.30)[a]	QC-H	104.2	6.0
	QC-M	107.3	8.7
	QC-I	107.2	9.1
	QC-L	109.4	4.5
Medium (0.40)[b]	QC-H	102.8	7.6
	QC-M	90.6	8.0
	QC-I	89.8	4.9
	QC-L	113.0	7.3
High (0.55)[b]	QC-H	91.0	5.9
	QC-M	92.6	7.0
	QC-I	90.1	6.4
	QC-L	105.3	10.1

[a] n = 3 replicates per concentration level

[b] n = 5 replicates per concentration level

Table 4 Extraction efficiency (EE) of analyte and internal standard from the 20 µL MITRA™ microsampling device for high concentration samples (n = 4 per patient)

	Mitotane		*Dicofol*	
Sample	*EE (%)*	*RSD (%)*	*EE (%)*	*RSD (%)*
Patient No. 1	*67.4*	*5.1*	*99.2*	*0.6*
Patient No. 2	*67.0*	*4.6*	*99.8*	*0.4*
Patient No. 3	*66.6*	*12.7*	*99.0*	*0.7*
Patient No. 4	*71.5*	*9.8*	*98.8*	*0.5*
Patient No. 5	*70.6*	*8.1*	*98.2*	*1.4*
Patient No. 6	*70.4*	*8.1*	*98.3*	*1.2*
average	*68.9*		*98.9*	

Table 5 Extraction efficiency (EE) of analyte and internal standard from the 20 µL MITRA™ microsampling device for low concentration samples (n = 4 per patient)

	Mitotane		Dicofol	
Sample	EE (%)	RSD (%)	EE (%)	RSD (%)
Patient No. 1	85.1	5.2	99.7	0.1
Patient No. 2	84.1	5.2	100.4	0.2
Patient No. 3	86.5	6.3	100.7	0.4
Patient No. 4	94.0	9.0	99.9	0.6
Patient No. 5	88.6	6.0	99.4	1.2
Patient No. 6	86.1	8.4	100.4	0.9
average	87.4		100.1	

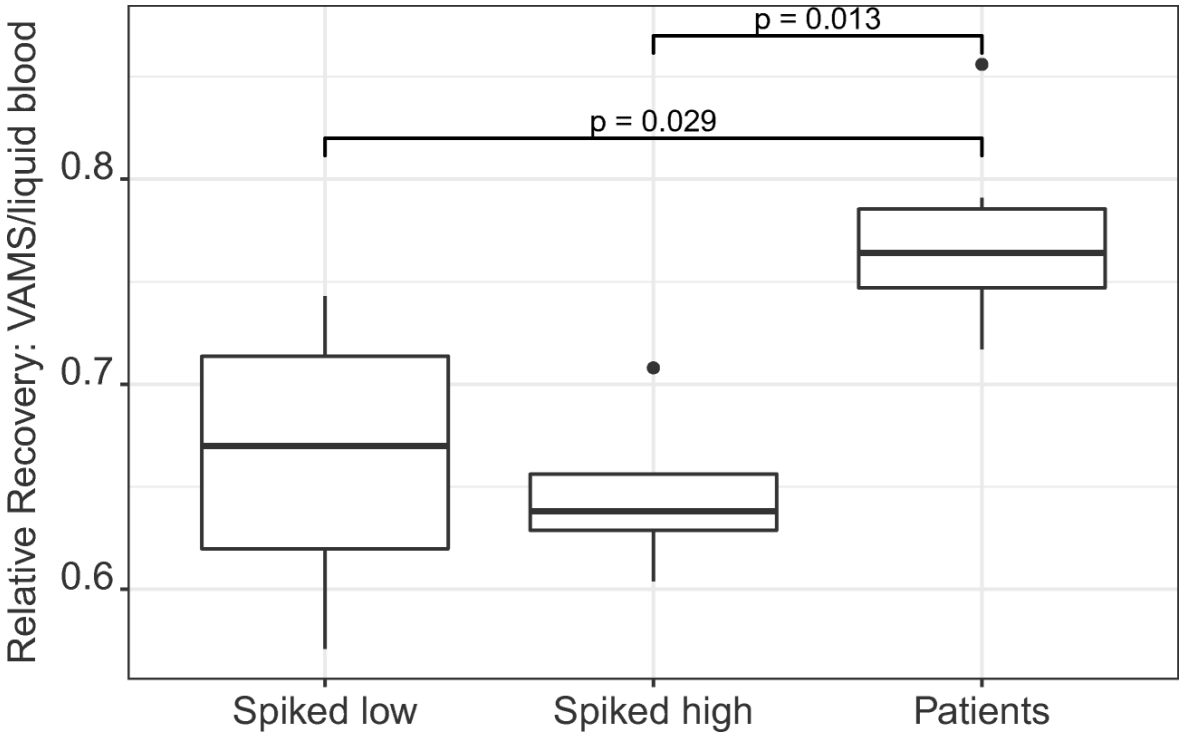

Fig. 4 Boxplot of relative recovery comparing VAMS to liquid blood. The relative recovery of authentic patient samples is significantly increased compared to spiked blood (ANOVA and Tukey's post hoc test). Spiked low 1.5 mg L^{-1} ; spiked high 20 mg L^{-1}

Correlation between paired plasma and venous blood samples

Four of the venous blood samples had a concentration below the defined LLOQ, and in four additional samples, hematocrit level was below the defined hematocrit range. Hence, these samples were excluded from analysis. Mean plasma concentration of the evaluated patient samples was 13.73 mg L^{-1} (SD ± 5.85) and mean whole blood concentration was 9.19 mg L^{-1} (SD ± 4.41). Mean hematocrit was 0.37 and the mean blood to plasma ratio was about 66.9%

(SD ± 15.2) (Table 6; for additional data, see Electronic Supplementary Material (ESM) Table S1).

Furthermore, Table S1 gives data on the difference (%) between patient plasma concentrations and the predicted plasma concentrations, which was − 0.81 ± 22.97%. Agreement between C_{DBS} and C_P was poor ($r = 0.87$, $p < 0.0001$; CCC = 0.60). The slope of the Passing-Bablok regression (C_{DBS} vs. C_P) was 0.72 (Fig. 5). Bland-Altman plots including limits of agreement are shown in Fig. 6. Furthermore, covariates like hematocrit and lipid values (triglycerides, HDL, LDL, and cholesterol levels) were evaluated, as mitotane might alter lipid metabolism of the patients. It has been known for many years that mitotane induces high LDL cholesterol, but also HDL cholesterol and sometimes triglyceride concentrations [37]. The actual mechanism underlying these lipid abnormalities is unknown. There was no correlation between the triglyceride level of the patient and the concentration of mitotane in whole blood as well as in plasma. The same results were obtained for HDL, whereas a negative correlation between LDL values and plasma concentration was observed. However, due to multiple testing and the small sample size, this finding should be considered carefully. No correlation was observed between hematocrit or lipid values, except for LDL, and the measured mitotane concentrations in dried blood or in plasma (Table 7; for graphical representation, see ESM Fig. S1). In addition, it seems that hematocrit values have no impact on the partitioning of mitotane between blood and plasma in the evaluated hematocrit range. However, patients with pathologically low hematocrit level had a high blood to plasma partition ratio showing a moderate correlation. After exclusion of those extreme values, for which the assay was not tested, there was no significant correlation left between blood to plasma ratio and hematocrit (for graphical representation, see ESM Fig. S2).

Table 6 Summary of mitotane plasma and whole blood concentrations, patient's hematocrit level, and the ratio of mitotane concentration between whole blood and plasma measurements

	Plasma concentration	Whole blood concentration	Hematocrit	Ratio blood to plasma
	[mg L^{-1}]	[mg L^{-1}]		[%]
n	41	41	41	41
Mean (± sd)	13.73 (± 5.85)	9.19 (± 4.41)	0.37 (± 0.04)	66.85 (± 15.24)
Median	14.4	9.54	0.37	65.6
Range	1.40 - 31.50	1.07 - 21.02	0.29 - 0.44	30.64 - 96.35

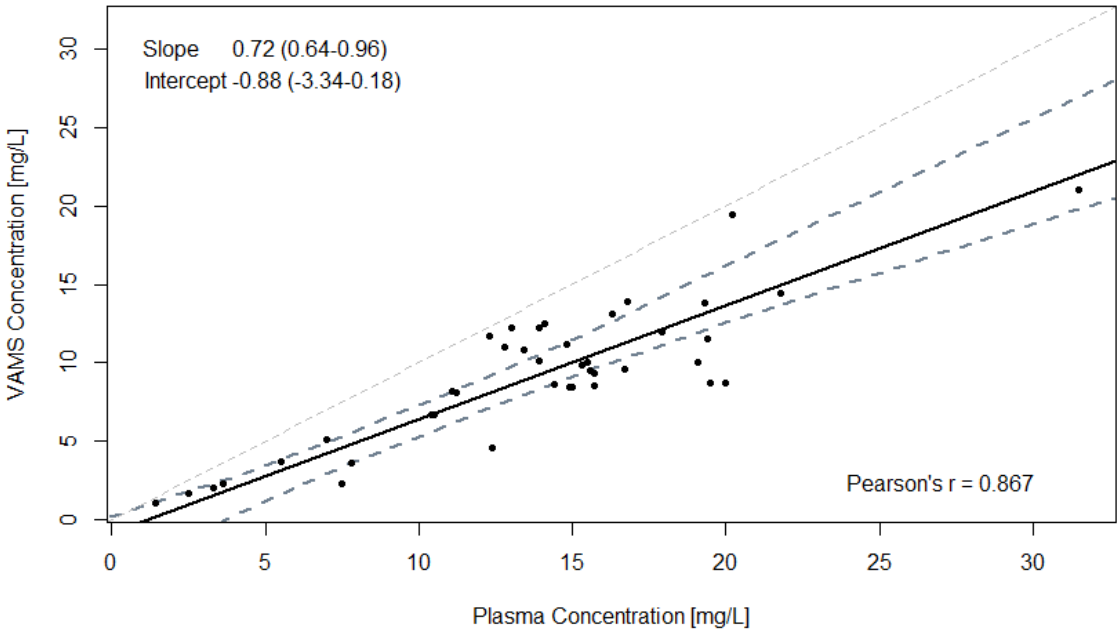

Fig. 5 Passing-Bablok regression analysis of mitotane concentration obtained from MITRA™ and plasma measurements. The solid line represents the regression line with its 95% CIs indicated as dashed lines. The slope and intercept are shown on the upper left of the figure; Pearson's correlation coefficient r is shown in the bottom right of the figure

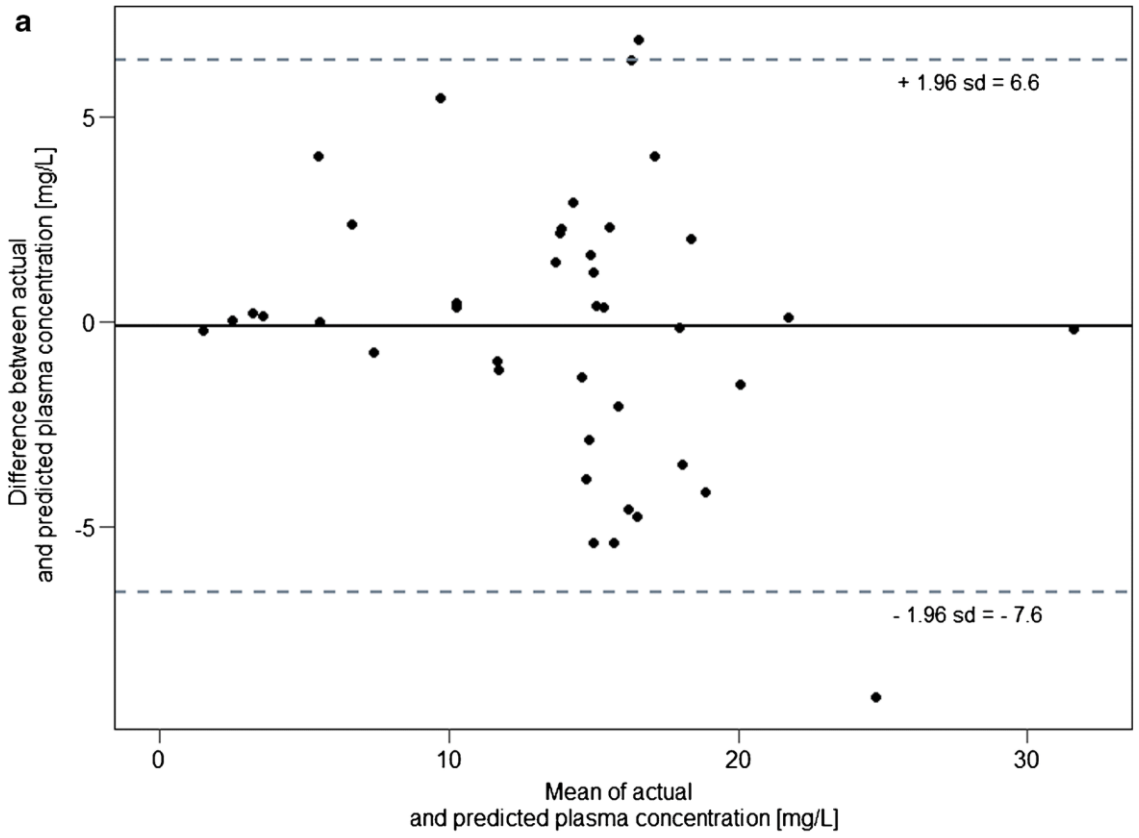
a
+ 1.96 sd = 6.6
- 1.96 sd = - 7.6
Difference between actual
and predicted plasma concentration [mg/L]
5
0
-5
0
10
20
30
Mean of actual
and predicted plasma concentration [mg/L]

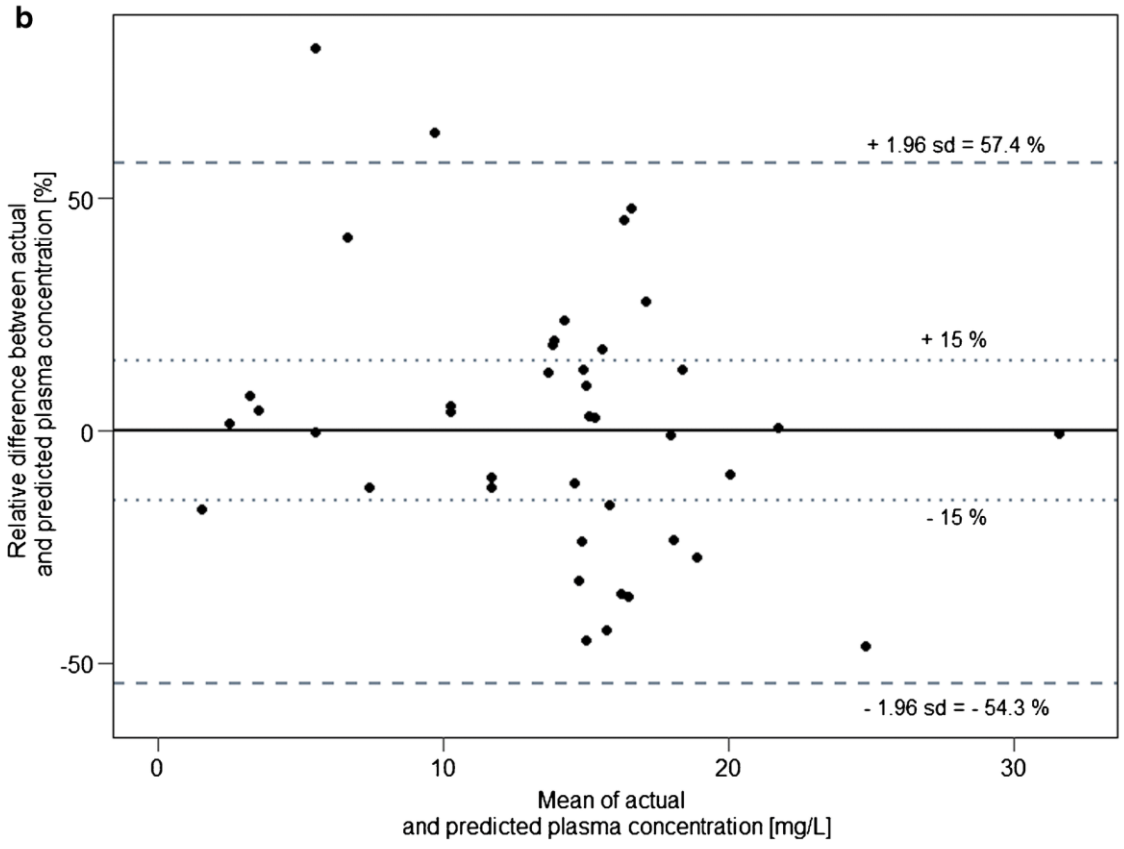
b
+ 1.96 sd = 57.4 %
+ 15 %
- 15 %
- 1.96 sd = - 54.3 %
Relative difference between actual
and predicted plasma concentration [%]
50
0
-50
0
10
20
30
Mean of actual
and predicted plasma concentration [mg/L]

Fig. 6 a Bland-Altman plot comparing results obtained from MITRA™ tips and plasma samples. The solid line represents the mean difference between predicted plasma concentration based on VAMS measurement and the actual plasma concentration. The dashed lines represent the upper and lower limit of agreement (± 1.96 SD). **b** Bland-Altman plot using relative difference vs. mean concentrations. The clinically acceptable limits of ± 15% based on acceptable imprecision of a bioanalytical assay are represented by the dotted lines

Table 7 Pearson's product-moment correlation. Correlation coefficient and corresponding p value for the correlation between hematocrit/lipid values and mitotane plasma respectively blood concentrations

	Plasma		Blood	
	Correlation	p-Value	Correlation	p-Value
Hematocrit	0.071	0.657	0	0.999
Triglycerides	0.296	0.067	0.188	0.251
HDL	0.040	0.813	0.083	0.616
LDL	-0.347	0.031	-0.247	0.129

Discussion

Since the first methods for the monitoring of mitotane were published using gas chromatography in the late 1980s of the last century [12, 32, 38], modern instrumentation has led to a decrease in the volume of matrix needed for the determination. Compared with other methods, the current procedure uses a very low volume of venous blood yielding a dried blood sample (20 μL compared to at least 100 μL plasma) and hence microsampling may represent a novel and more convenient way to monitor mitotane in patients who live far away from the treating cancer center. The MITRA™ VAMS, an approved in vitro diagnostic (IVD), was selected for the present study because of its status as IVD and the favorable handling characteristics. The device is built from a small plastic stick with an attached sphere of absorption agent on the tip of the stick. This sphere turns red as soon as it gets in contact with capillary blood and does not collect more than the intended volume of 10, 20, or 30 μL when handled correctly. After drying, the samples are stable for at least 1 week when shipped at ambient temperature in sealed PP plastic bags containing desiccant (see ESM Fig. S3).

However, in the summer season or in regions with hot climate, the samples should be shipped on ice to reduce loss of analyte due to evaporation (vapor pressure of mitotane is about 0.26 mPa at 30 °C [39]). Another reason for the reduced accuracy after storage at elevated temperature could be due to aging of the sample and related extractability issues not necessarily limited to mitotane [40]. However, since samples stored at room temperature and at 2–8 °C did not show a decrease in accuracy, unlike described by Xie et al. [40], the loss of analyte due to evaporation seems more likely.

Although the samples prepared directly after spiking yielded the same results, incubation of blood at 37 °C for 30 min prior to VAMS sampling was adopted to better reflect the situation in vivo. Furthermore, if the method is expanded to capillary blood, warming of the matrix prior to sampling for CR and QC samples could be crucial to simulate the same viscosity and density of the absorbed blood.

The recovery was comparatively high and no individual influence on extraction efficiency was found in spiked patient samples, expressed by a low RSD. Nevertheless, the recovery from high and low concentration was substantially different (68.9 vs. 87.4%). Since linearity was not an issue, concentration-dependent effects, like saturation of the extraction medium, were unlikely. An explanation could be related to the batch to batch variability of the VAMS device itself. During the experiments, two different batches of devices were used and the „calculated average blood wicking volume" (see CoA) varied as much as from 20.8 to 22.5 µL from batch to batch. The recovery from low concentration was carried out with the latter batch, whereas all the other experiments were conducted using the first batch of VAMS. This should also be considered when measuring patient samples. An in spec variation of wicked blood volume of more than 10% from the nominal value could result in substantial bias, when the VAMS used for calibration comes from a different batch than the VAMS device used for collecting patient samples.

The relative recovery comparing liquid and dried blood of QC low and QC medium supports a recovery of about 70%, assuming a near 100% recovery from liquid samples. Mean relative recovery of patient samples was increased compared to spiked blood. Although the difference was not more than 15%, a substantial amount of variability could be attributed to the difference between spiked and authentic blood samples. As the samples came from critically ill patients, influence of plasma albumin or partial hemolysis cannot be ruled out and the matter needs further attention. In particular, additional investigations are needed whether or not the discrepancy in relative recovery is limited to mitotane and the used method of extraction or if this is a general problem of the VAMS device. However, not the full extent of variation could be attributed to the altered recovery since, in general, the recovery seems to be increased, which does not explain the poor correlation of blood and plasma concentrations. Velghe et al. [41] recently summarized advances in DBS analysis avoiding hematocrit bias and presented other devices for collecting dried samples. Future studies investigating the differences in recovery of spiked vs. authentic samples comparing all available devices are needed to collect evidence whether or not the presented findings are device related, and if so, strategies to cope with the problem will be required.

The blood to plasma ratio found was below 1, indicating that MIT concentration in erythrocytes is below the plasma concentration. This is in concordance with earlier findings in small samples ($n = 1$ and $n = 6$) where the mitotane concentration in red blood cells reached 18 to 25% of the plasma concentration [24, 25]. There is a moderate correlation between C_{DBS} and C_P but the prediction of plasma levels based on Mitra™ measurements is not reliable due to high variability of blood to plasma ratio. As illustrated in Bland-Altman plot (Fig. 6a), there is no obvious relation between the differences of predicted vs. actual plasma concentrations and the mean of predicted vs. actual plasma concentrations. The 95% confidence interval for the predicted plasma concentration ranges from − 7.6 to 6.6 mg L^{-1} , which would be unacceptable for clinical purpose. Figure 6b also underlines the large proportion of samples with a clinically unacceptable bias of more than ± 15% when plasma concentrations were predicted from DBS concentrations.

In conclusion, a nonlinear model may be necessary to relate Mitra™ and plasma concentrations. However, standard deviation for blood to plasma ratio is high (0.67 ± 0.15). Analytical imprecisions of both methods and other unidentified sources of variance might contribute to the observed variation. Additionally, the existence of further covariates, which might lead to a higher binding of mitotane to the erythrocytes in some of the patients, could be another source of uncertainty. For two patients, three subsequent plasma and blood concentration levels were available. Interestingly, in those two patients, plasma and blood levels seem to converge over time after dosage adjustment (see ESM Fig. S4). The hypothesis that blood levels might respond more slowly to dose adjustments (due to partitioning and/or erythrocyte life cycle) compared to plasma concentrations needs to be evaluated in a prospective trial since multiple measurements were only available for these two individuals. Although actual recommendations for the target range refer to plasma concentrations, it is not evident that plasma is the most suitable matrix for the therapeutic drug monitoring of mitotane. The putatively slower reacting blood concentrations might correlate better with adverse reactions or drug response.

In a recently published work by Velghe and Stove [42], the application of VAMS to measure anti-epileptic drugs on leftover patient samples was described. They also demonstrated a high %RSD on the observed blood to plasma ratios, which was between 14 and 20%. The authors concluded that there is a significant level of uncertainty when trying to calculate serum concentrations from VAMS concentrations with an average conversion coefficient. Thus, it should be considered if there is even a need and a possibility to convert blood levels to plasma concentrations and/or how to establish reference ranges in dried blood. Therefore, future

studies analyzing paired patient samples from capillary blood, liquid blood, and plasma in steady state are needed to satisfactorily answer these questions.

Conclusion

In this work, a new method for the quantification of mitotane from dried blood samples is described and the applicability of the developed method using VAMS on leftover real-life patient samples could be demonstrated. In theory, this technique could enable patients and clinicians to perform therapeutic drug monitoring of mitotane in a more convenient way. Patients could collect the samples and send them to the laboratory themselves; thus, there would be no need for regular consultation at the hospital or physician's office for blood or plasma collection purposes, which might reduce treatment costs. Especially during the initial phase of mitotane treatment, more frequent TDM than current standard of care is desirable. More intense sampling could facilitate the prognosis whether a patient will reach satisfactory mitotane concentrations in an acceptable period of time. In combination with model-based simulation, this new method could be a way to decide whether a patient should stay on mitotane treatment or not in order to minimize the number of patients receiving this highly toxic substance while having only minimal chances of reaching therapeutic plasma levels. However, reference ranges in capillary blood would have to be established for a reliable interpretation of the observed concentrations since a simple conversion does not seem to be possible. As of today, therapeutic drug monitoring of mitotane using VAMS is not feasible, because there are too many unanswered questions. Further studies investigating the sources of variation and the clinical implications associated are necessary until the presented concept could become standard in routine care.

Funding information This study was funded by Horphag Research (Europe) Ltd. and in part by the German Research Council (DFG, German Research Foundation) Projektnummer: 314061271 – TRR 205 as well as by an individual grant to M.F. (FA466/4-2) and M.K. (KR4371/ 1-2).

Compliance with ethical standards

Conflict of interest The authors declare that they have no conflict of interest.

Research involving human participants This study was part of the European Network for the Study of Adrenal Tumors (ENSAT) registry, which has been approved by the ethics committee of the University of Würzburg (approval number 86/03 and 88/11).

Informed consent All patients provided written informed consent.

References

1. Fassnacht M, Terzolo M, Allolio B, Baudin E, Haak H, Berruti A, et al. Combination chemotherapy in advanced adrenocortical carcinoma. N Engl J Med. 2012;366(23):2189–97.

2. Cueto C, Brown JH. The chemical fractionation of an adrenocorticolytic drug. Endocrinology. 1958;62(3):326–33. https://doi.org/10.1210/endo-62-3-326.

3. Cueto C, Brown JH, Richardson AP Jr. Biological studies on an adrenocorticolytic agent and the isolation of the active components. Endocrinology. 1958;62(3):334–9. https://doi.org/10.1210/endo-62-3- 334.

4. Terzolo M, Angeli A, Fassnacht M, Daffara F, Tauchmanova L, Conton PA, et al. Adjuvant mitotane treatment for adrenocortical carcinoma. N Engl J Med. 2007;356(23):2372–80. https://doi.org/ 10.1056/NEJMoa063360.

5. Berruti A, Fassnacht M, Baudin E, Hammer G, Haak H, Leboulleux S, et al. Adjuvant therapy in patients with adrenocortical carcinoma: a position of an international panel. J Clin Oncol. 2010;28(23): e401–2. https://doi.org/10.1200/JCO.2009.27.5958.

6. European Medicines Agency. Lysodren: summary of product characteristics. 2009, http://www.ema.europa.eu/docs/en_GB/ document_library/EPAR_-_Product_Information/human/000521/ WC500047235.pdf. Accessed Apr 2018.

7. Kasperlik-Zaluska AA, Cichocki A. Clinical role of determination of plasma mitotane and its metabolites levels in patients with adrenal cancer: results of a long-term follow-up. J Exp Ther Oncol. 2005;5(2):125–32.

8. Hermsen IG, Fassnacht M, Terzolo M, Houterman S, den Hartigh J, Leboulleux S, et al. Plasma concentrations of o,p'DDD, o,p'DDA, and o,p'DDE as predictors of tumor response to mitotane in adrenocortical carcinoma: results of a retrospective ENS@T multicenter study. J Clin Endocrinol Metab. 2011;96(6):1844–51. https://doi. org/10.1210/jc.2010-2676.

9. Hescot S, Paci A, Seck A, Slama A, Viengchareun S, Trabado S, et al. The lack of antitumor effects of o,p'DDA excludes its role as an active metabolite of mitotane for adrenocortical carcinoma treatment. Horm Cancer. 2014;5(5):312–23. https://doi.org/10.1007/ s12672-014-0189-7.

10. Megerle F, Herrmann W, Schloetelburg W, Ronchi CL, Pulzer A, Quinkler M, et al. Mitotane monotherapy in patients with advanced adrenocortical carcinoma. J Clin Endocrinol Metab. 2018;103(4): 1686–95.

11. Baudin E, Pellegriti G, Bonnay M, Penfornis A, Laplanche A, Vassal G, et al. Impact of monitoring plasma 1,1- dichlorodiphenildichloroethane (o,p'DDD) levels on the treatment of patients with adrenocortical carcinoma. Cancer. 2001;92(6):1385–92.

12. van Slooten H, Moolenaar AJ, van Seters AP, Smeenk D. The treatment of adrenocortical carcinoma with o,p'-DDD: prognostic implications of serum level monitoring. Eur J Cancer Clin Oncol. 1984;20(1):47–53.

13. Feliu C, Cazaubon Y, Guillemin H, Vautier D, Oget O, Millart H, et al. Therapeutic drug monitoring of mitotane: analytical assay and patient follow-up. Biomed Chromatogr. 2017;31(11):e3993. https:// doi.org/10.1002/bmc.3993.

14. Daffara F, De Francia S, Reimondo G, Zaggia B, Aroasio E, Porpiglia F, et al. Prospective evaluation of mitotane toxicity in adrenocortical cancer patients treated adjuvantly. Endocr Relat Cancer. 2008;15(4): 1043–53. https://doi.org/10.1677/ERC-08-0103.

15. Terzolo M, Pia A, Berruti A, Osella G, Ali A, Carbone V, et al. Low-dose monitored mitotane treatment achieves the therapeutic range with manageable side effects in patients with adrenocortical cancer. J Clin Endocrinol Metab. 2000;85(6):2234–8. https://doi. org/10.1210/jcem.85.6.6619.

16. Faggiano A, Leboulleux S, Young J, Schlumberger M, Baudin E. Rapidly progressing high o,p'DDD doses shorten the time required to reach the therapeutic threshold with an acceptable tolerance: preliminary results. Clin Endocrinol. 2006;64(1):110–3. https://doi.org/10.1111/j.1365-2265.2005.02403.x.

17. Mauclere-Denost S, Leboulleux S, Borget I, Paci A, Young J, Al Ghuzlan A, et al. High-dose mitotane strategy in adrenocortical carcinoma: prospective analysis of plasma mitotane measurement during the first 3 months of follow-up. Eur J Endocrinol. 2012;166(2):261–8. https://doi.org/10.1530/EJE-11-0557.

18. Arshad U, Taubert M, Kurlbaum M, Frechen S, Herterich S, Megerle F, et al. Enzyme autoinduction by mitotane supported by population pharmacokinetic modelling in a large cohort of adrenocortical carcinoma patients. Eur J Endocrinol. 2018;179(5):287–97.

19. Kerkhofs TM, Derijks LJ, Ettaieb H, Den Hartigh J, Neef K, Gelderblom H, et al. Development of a pharmacokinetic model of mitotane: toward personalized dosing in adrenocortical carcinoma. Ther Drug Monit. 2015;37(1):58–65.

20. Kerkhofs T, Baudin E, Terzolo M, Allolio B, Chadarevian R, Mueller H, et al. Comparison of two mitotane starting dose regimens in patients with advanced adrenocortical carcinoma. J Clin Endocrinol Metab. 2013;98(12):4759–67.

21. Fassnacht M, Kroiss M, Allolio B. Update in adrenocortical carcinoma. J Clin Endocrinol Metab. 2013;98(12):4551–64.

22. Andersen A, Kasperlik-Zaluska AA, Warren DJ. Determination of mitotane (o,p-DDD) and its metabolites o,p-DDA and o,p-DDE in plasma by high-performance liquid chromatography. Ther Drug Monit. 1999;21(3):355–9.

23. Garg MB, Sakoff JA, Ackland SP. A simple HPLC method for plasma level monitoring of mitotane and its two main metabolites in adrenocortical cancer patients. J Chromatogr B Anal Technol Biomed Life Sci. 2011;879(23):2201–5. https://doi.org/10.1016/j. jchromb.2011.06.001.

24. De Francia S, Pirro E, Zappia F, De Martino F, Sprio AE, Daffara F, et al. A new simple HPLC method for measuring mitotane and its two principal metabolites tests in animals

and mitotane-treated patients. J Chromatogr B Anal Technol Biomed Life Sci. 2006;837(1– 2):69–75. https://doi.org/10.1016/j.jchromb.2006.04.005.

25. Mornar A, Sertic M, Turk N, Nigovic B, Korsic M. Simultaneous analysis of mitotane and its main metabolites in human blood and urine samples by SPE-HPLC technique. Biomed Chromatogr. 2012;26(11):1308–14. https://doi.org/10.1002/bmc.2696.

26. Guthrie R, Susi A. A simple phenylalanine method for detecting phenylketonuria in large populations of newborn infants. Pediatrics. 1963;32:338–43.

27. Enderle Y, Foerster K, Burhenne J. Clinical feasibility of dried blood spots: analytics, validation, and applications. J Pharm Biomed Anal. 2016;130:231–43. https://doi.org/10.1016/j.jpba. 2016.06.026.

28. De Kesel PM, Lambert WE, Stove CP. Does volumetric absorptive microsampling eliminate the hematocrit bias for caffeine and paraxanthine in dried blood samples? A comparative study. Anal Chim Acta. 2015;881:65–73. https://doi.org/10.1016/j.aca.2015.04. 056.

29. Denniff P, Spooner N. Volumetric absorptive microsampling: a dried sample collection technique for quantitative bioanalysis. Anal Chem. 2014;86(16):8489–95. https://doi.org/10.1021/ac5022562.

30. Kok MGM, Fillet M. Volumetric absorptive microsampling: current advances and applications. J Pharm Biomed Anal. 2018;147:288– 96. https://doi.org/10.1016/j.jpba.2017.07.029.

31. European Medicines Agency. Guideline on Bioanalytical Method Validation. 2015, https://www.ema.europa.eu/documents/scientificguideline/guideline-bioanalytical-method-validation_en.pdf. Accessed Mar 2018.

32. Inouye M, Mio T, Sumino K. Use of GC/MS/SIM for rapid determination of plasma levels of o,p'-DDD, o,p'-DDE and o,p'-DDA. Clin Chim Acta. 1987;170(2–3):305–14.

33. Evans C, Arnold M, Bryan P, Duggan J, James CA, Li W, et al. Implementing dried blood spot sampling for clinical pharmacokinetic determinations: considerations from the IQ Consortium Microsampling Working Group. AAPS J. 2015;17(2):292–300. https://doi.org/10.1208/s12248-014-9695-3.

34. Bland JM, Altman DG. Statistical methods for assessing agreement between two methods of clinical measurement. Lancet. 1986;1(8476):307–10.

35. R Core Team. R: a language and environment for statistical computing. Vienna: R Foundation for Statistical Computing; 2017.

36. McBride GB. A proposal for strength of agreement criteria for Lin's Concordance Correlation Coefficient. NIWA Client Report; 2005.

37. Shawa H, Deniz F, Bazerbashi H, Hernandez M, Vassilopoulou - Sellin R, Jimenez C, et al. Mitotane-induced hyperlipidemia: a retrospective cohort study. Int J Endocrinol. 2013;2013:624962. https://doi.org/10.1155/2013/624962.

38. Benecke R, Vetter B, De Zeeuw RA. Rapid micromethod for the analysis of mitotane and its metabolite in plasma by gas chromatography with electron-capture detection. J Chromatogr. 1987;417(2):287–94.

39. U.S. Department of Health and Human Services Agency for Toxic Substances and Disease Registry. Toxicological profile for DDT, DDE, and DDD. 2002, https://www.atsdr.cdc.gov/toxprofiles/ tp35.pdf. Accessed Mar 2018.

40. Xie I, Anderson M, Wang M, Xue L, Breidinger S, Goykhman D, et al. Extractability-mediated stability bias and hematocrit impact: high extraction recovery is critical to feasibility of volumetric adsorptive microsampling (VAMS) in regulated bioanalysis. J Pharm Biomed Anal. 2018;156:58–66.

41. Velghe S, Delahaye L, Stove CP. Is the hematocrit still an issue in quantitative dried blood spot analysis? J Pharm Biomed Anal. 2019;163:188–96.

42. Velghe S, Stove CP. Volumetric absorptive microsampling as an alternative tool for therapeutic drug monitoring of first-generation anti-epileptic drugs. Anal Bioanal Chem. 2018;410(9):2331–41.

2 Physiologically Based Pharmacokinetic Modelling of Cabozantinib to Simulate Enterohepatic Recirculation, Drug-Drug Interaction with Rifampin and Liver Impairment

Gerner, B., Scherf-Clavel, O.

Reprinted from Pharmaceutics 13(6): 778, 2021

Abstract

Cabozantinib (CAB) is a receptor tyrosine kinase inhibitor approved for the treatment of several cancer types. Enterohepatic recirculation (EHC) of the substance is assumed but has not been further investigated yet. CAB is mainly metabolized via CYP3A4 and is susceptible for drug–drug interactions (DDI). The goal of this work was to develop a physiologically based pharmacokinetic (PBPK) model to investigate EHC, to simulate DDI with Rifampin and to simulate subjects with hepatic impairment. The model was established using PK-Sim® and six human clinical studies. The inclusion of an EHC process into the model led to the most accurate description of the pharmacokinetic behavior of CAB. The model was able to predict plasma concentrations with low bias and good precision. Ninety-seven percent of all simulated plasma concentrations fell within 2-fold of the corresponding concentration observed. Maximum plasma concentration (C_{max}) and area under the curve (AUC) were predicted correctly (predicted/observed ratio of 0.9–1.2 for AUC and 0.8–1.1 for C_{max}). DDI with Rifampin led to a reduction in predicted AUC by 77%. Several physiological parameters were adapted to simulate hepatic impairment correctly. This is the first CAB model used to simulate DDI with Rifampin and hepatic impairment including EHC, which can serve as a starting point for further simulations with regard to special populations.

1. Introduction

Tyrosine kinase inhibitors (TKI) play an increasingly important role in the therapy of multiple malignancies and the development of compounds targeting, for example, the vascular endothelial growth factor (VEGF)/VEGF receptor (VEGFR) signaling pathway has led to key advances in the treatment of different cancer types [1–3]. One representative of this drug class is the multi-target TKI Cabozantinib (CAB), which is currently approved for the treatment of metastatic medullary thyroid cancer (MTC) [4,5], advanced renal cell carcinoma (RCC) [6,7] and hepatocellular carcinoma (HCC) [8,9]. The primary targets of CAB are MET (hepatocyte growth factor receptor, HGFR) and VEGFR2 (vascular endothelial growth factor receptor 2), which are both important mediators of tumor growth and tumor angiogenesis [10]. In addition to approved indications, CAB is currently investigated in numerous clinical trials, covering a wide range of different cancer types [11]. This could lead to approval in other types of cancer and to additional patient populations being treated with CAB. Thus, it is important to gain a deeper knowledge of the pharmacokinetic (PK) behavior of CAB to ensure the most effective and safe therapy for a broad range of patients. CAB is orally administered once daily either as capsule (Cometriq®) or tablet formulation (Cabometyx®). Maximum plasma concentrations (Cmax) after a single dose occur approximately at 3 to 5 h post-dose. CAB shows a long terminal half-life (~120 h), is highly bound to human plasma proteins (99.7%) and undergoes extensive metabolism as it is a substrate of Cytochrome P450 (CYP3A4) [12]. Four major CAB metabolites can be found in plasma: Exel-5366 (Amide Cleavage Product), Exel-1644 (6-Desmethyl Amide Cleavage Product Sulfate), Exel-1646 (Monohydroxy Sulfate) and Exel-5162 (N-Oxide). An illustration of the chemical structure of CAB and its main metabolites is shown in the Electronic Supplementary Material (ESM) Figure S1. The hepatobiliary elimination seems to be the predominant route of excretion in humans, whereas urinary excretion is only relevant for the CAB metabolites. Metabolites predominantly found in urine were dequinolinyl CAB glucuronide, dequinolinyl CAB sulfate and EXEL-5366 (CAB amide cleavage product) [13].

CAB plasma concentration time profiles are characterized by a rapid decrease in CAB plasma concentration in the first hours followed by a long terminal half-life. In addition, PK studies in human and rats revealed multiple peaks in the plasma concentration time profiles starting approximately 24 h after CAB administration. This phenomenon is most likely due to an enterohepatic circulation (EHC), but not finally confirmed yet [12,14,15], as also other causes, like absorption in deeper bowel sections or the irregular pattern of gastric emptying, might be conceivable [16,17].

CAB is susceptible to drug–drug interactions (DDI), as it is mainly metabolized via CYP3A4. The combination of CAB with Rifampin (RIF), a strong CYP3A4 inducer, resulted

in increased CAB clearance (4.3-fold) and reduced CAB exposure (AUC) by 77% [18]. Therefore, inducers like Rifampin, St. John's Worth, Phenytoin, Carbamazepine or Phenobarbital should be avoided according to the EMA summary of product characteristics (SPC) [19]. In contrast to that, the FDA label does not make a general recommendation to avoid the combination but recommends increasing the daily CAB dose by 20 mg (Cabometyx®) and 40 mg (Cometriq®), respectively. As the hepatobiliary pathway appears to be the main route of elimination for CAB, hepatic dysfunction may have a relevant influence on CAB plasma concentrations. Hepatic diseases can occur in relevant patient populations due to co-medication and disease (e.g., HCC and liver metastases) and is characterized by a loss of functional hepatocytes, resulting in possibly toxic or ineffective plasma concentrations. To investigate different liver disease states, one aim was to expand the PBPK model to patients with mild and moderate liver impairment.

PBPK approaches provide a framework to combine information on physiology, population and drug characteristics, and to extract maximal information from available data to gain a mechanistic understanding of key processes in the PK of a drug [20–23]. One strength of PBPK modelling is the possibility to gain mechanistic insights into pharmacokinetics and in vivo behaviour of a compound by using it as a simulation tool where the focus is less on the quantitative predictions but much more on hypothesis generation and testing [21,24]. Therefore, the aim of this work was to investigate the hypothesis of EHC and to describe the PK of CAB. The PBPK model was also used as a tool to simulate the concomitant administration of RIF and the influence of liver impairment regarding changes in plasma concentration time profiles and drug exposition.

2. Materials and Methods

2.1. Software

The PBPK model was built using PK-Sim® version 8 as part of the open source modeling software Open Systems Pharmacology Suite (Bayer Technology Services, Leverkusen, Germany) [25]. For a detailed insight into the software, the input and output parameter as well as the description of the generic model structure of PK-Sim® refer to Eissing et al. [26], Willmann et al. [27], Kuepfer et al. [28] or the user manual [29]. All published study data were digitized using WebPlotDigitizer (Version 4.3, Ankit Rohatgi, Pacifica, CA, USA). Microsoft Excel 2016 Version 16.0 (Microsoft Corporation, Redmond, WA, USA) and R Studio Version 1.1.383 (RStudio Incorporation, Boston, MA, USA) running R version 3.6.3 (R Foundation for

Statistical Computing, Vienna, Austria, 2020) [30] were used for model performance, statistical calculations and plot generation.

2.2. Clinical Data

Human peroral data from the mass balance study, one bioequivalence study (CAB capsule vs. tablet), one dose proportionality study (20, 40, 60 mg tablet), a DDI study (divided in a Rifampin and Ketoconazole arm), a food effect and a PPI (proton pump inhibitor) effect were digitized and used for model development and evaluation. The model development process was supplemented with intravenous (iv) (5 mg/kg, 10 mg/kg) data from rats, published by Wang et al. [2]. The gathered CAB peroral plasma profiles were split into a training dataset, used for model development and parameter optimization, and a test dataset for model evaluation. Data from the liver impairment study were used to investigate the ability of the model to simulate different hepatic disease states. All human studies used a single dose of either CAB solution, tablet, or capsule covering a dose range from 20 to 140 mg, depending on the study design. A summary of each study regarding the demographics, administration protocols and the allocation to either the training or the test dataset, respectively, or to the DDI and hepatic impairment simulations is given in Table S1 of the ESM. Sampling times of each study are presented in Table S2.

2.3. Workflow and Model Development

The PBPK modelling was performed in a stepwise procedure. Rat iv data were used for the development of an initial PBPK model. All physicochemical data of CAB found through an intensive literature search were used as input parameters. Different methods for the calculation of tissue distribution and cellular permeability were evaluated [31]. The generic rat individual, which is already an integral part of PKSim® was adapted according to the animals used by Wang et al. and implemented in the model. In a second step, simulations for rat intragastric (ig) administration were performed. All input values of the iv model were transferred to the ig model. Relevant input parameters and knowledge from the rat PBPK models were used to build a first human PBPK model. For model building in humans a virtual mean individual according to the demographics of the respective studies mentioned in Table S1 was created and used in these simulations. To account for the second peak in the plasma concentration time profiles, the fast decrease in CAB plasma concentration in the approximately first 20 h, and the long terminal half-life different hypothesis were tested. Different CAB formulations (solution, tablet, and capsule) were investigated separately. For further model development and evaluation, virtual populations containing 100 individuals were created. An implemented PKSim® algorithm

was used to generate a variation of anthropometric parameters within the limits of the ICRP or NHANES database [28,29], respectively. These parameters were kept within the limits of the respective study population. Parameters which were not found in the literature were estimated and single parameters were adjusted according to the observed data. Local sensitivity analysis to evaluate the influence of changes in input parameters on the final PBPK model were conducted, especially if the parameter had been optimized or might have had a strong influence on the model due to the calculation methods in PK-Sim®. Data from the DDI study of CAB with RIF were simulated to verify the implemented CYP3A4 process. To simulate CAB plasma concentration time profiles in mild and moderate hepatic impairment, relevant physiological parameters of the final PBPK model were adapted. A workflow of the model development and evaluation process is given in the ESM (Figure S2). Data of all included rat and human studies are shown in different plots in the ESM (Figures S3–S6). A more detailed description of the observed human and rat plasma concentration time profiles and further information on the model development process can also be found in the ESM.

2.4. Enterohepatic Circulation Modelling

A gallbladder emptying process was implemented in PKSim® and relevant physiological parameters, like the emptying half-time were optimized. To enable biliary excretion and EHC, substrate affinity towards a canalicular efflux transporter like MRP2 (multidrug resistance-associated protein 2) is a prerequisite. MRP2 is an efflux transporter which is predominantly located on the canalicular membrane of the hepatocytes [32] and was included into the model according to the PK-Sim® human gene expression databank because CAB has been found to be a substrate of this transporter [13]. As an assumption, the gallbladder emptying process was activated three times over 24 h, as this process is related to food intake, which was considered to take place in the morning, in the noon and in the evening [33]. A fasted state, meaning no active gallbladder emptying, was assumed for the first hours, as all studies were conducted under fasted conditions.

2.5. Model Evaluation

To evaluate the predictive performance of the model, multiple methods were used [20,34,35]: Visual inspections between observed and simulated plasma concentration time profiles were carried out initially. In addition, predictive performance of the PBPK model was analysed by generating goodness-of-fit plots in which the predicted plasma concentrations was plotted against their corresponding observed values according to the EMA guideline on the reporting of PBPK modelling and simulation [34]. Predicted maximum concentration (C_{max}) and

the predicted area under the systemic drug concentration–time curve from time zero to the time of the last concentration (AUC_{last}) were compared to the respective literature values. Model accuracy and precision was described by using prediction error (PE), mean prediction error (MPE) and mean absolute prediction error (MAPE). The calculations were made according to Equations (1)–(3).

$$PE\ [\%] = \frac{Cpredicted,i - Cobserved,i}{Cobserved,i}\ x\ 100\% \quad (1)$$

$$MPE\ [\%] = \frac{Cpredicted,i - Cobserved,i}{Cobserved,i}\ x\ 100\% \quad (2)$$

$$MAPE\ [\%] = \frac{Cpredicted,i - Cobserved,i}{Cobserved,i}\ x\ 100\% \quad (3)$$

Mean relative deviation (MRD, Equation (4)) of the predicted and observed plasma concentrations was calculated for a quantitative measure of model performance. MRD values ≤2 characterize an adequate model performance and therefore were considered acceptable.

$$MRD = 10^x; x = \sqrt{\frac{1}{n}\sum_{i=1}^{n}(log_{10}c_{predicted,i} - log_{10}c_{observed,i})^2} \quad (4)$$

Abbreviations in Equations (1)–(4) are as follows: $c_{predicted,i}$ = predicted plasma concentration, $c_{observed,i}$ = corresponding observed plasma concentration, n = number of observed values.

2.6. DDI Interaction between CAB and RIF

The developed CAB PBPK model was combined with the Rifampicin PBPK model, developed by Hanke et al. to simulate DDI between CAB and RIF [36]. Clinical study data from a DDI interaction study between CAB and RIF were used and the interaction between CAB and RIF was recreated *in silico*. Multiple dosing simulations for capsule and tablet administration were conducted and for the administration of CAB together with RIF higher CAB daily doses were used (180 mg capsule; 80 mg tablet), according to the FDA recommendation. Regular doses (140 mg capsule; 60 mg tablet) once daily were maintained, if CAB was given alone. The quality of the DDI interaction modelling was evaluated by comparison of the respective plasma concentration-time profile and through calculation and comparison of the ratios of AUC_{last}

(Equation 5) and C_{max} (Equation 6) for the administration of CAB alone or together with its perpetrator.

$$DDI\ AUC_{last}\ ratio = \frac{AUC_{last}\ CAB\ in\ combination\ with\ RIF}{AUC_{last}\ CAB\ alone} \quad (5)$$

$$DDI\ C_{max}\ ratio = \frac{C_{max}\ CAB\ in\ combination\ with\ RIF}{C_{max}\ CAB\ alone} \quad (6)$$

2.7. Hepatic impairment simulations

For the hepatic impairment simulations, individuals and populations (n = 100) with demographic properties according to the respective study data [37] were created. Several physiological changes are relevant in patients with hepatic impairment and were accordingly adapted [38-40]: The portal liver blood flow and the renal blood flow were reduced, the liver blood flow and the blood flows for the remaining organs, except for the brain, were increased according to Edginton et. al. [38]. For the enzyme specific clearance, the activity of CYP3A4 was adapted also based on Edginton et al. A reduced liver volume fraction and different hematocrit values for mild and moderate liver impairment were used. The plasma protein scale factor, which is integrated in PKSim®, was adapted to describe changes in the plasma protein concentration respectively binding. All simulations were done based on a single administration of 60 mg CAB capsule. Evaluation of model performance was conducted via visual appraisal of the plasma concentration-time profile and by comparison of the predicted and observed plasma exposure and C_{max} of the healthy control group and in patients with mild and moderate liver impairment.

3. Results

3.1. Rat intravenous and intragastric simulations

The first simulations were done based on iv data and physicochemical values, which were extracted from literature. The best results for the calculation of tissue distribution and cellular permeability were obtained for the combination of Rodgers & Rowland and the PKSim® standard method. As no further information on specific processes, like CYP metabolism or MRP2 affinity, was available, a total hepatic clearance was assumed as a surrogate and optimized based on the in vivo data [41]. Afterwards, all input values of the iv model were transferred to the ig model. As for the first ig simulations there was an overestimation in plasma

concentration, intestinal permeability and gastrointestinal solubility was optimized to describe the observed data more precisely. The value for plasma protein binding was adopted from humans, as in general there is a good correlation between the protein binding in human and rat plasma [42]. This is also seen for EXEL-1644, which has similar protein binding in rats (99.729% to 99.966%) compared to humans (99.950% to 99.996%) [13]. The final parameters used for the rat PBPK model are shown in Table S3. The iv and the ig model both were able to describe the plasma concentration-time profiles of CAB in rats (Figure 1) and show a high accuracy illustrated by a low bias (MPE range –6.4% to +12.2%) and a good precision (MAPE range 18.4%-33.8%). A MRD of all predicted plasma concentrations ≤ 2 is achieved in all simulations (MRD range 1.27-1.63). Table S4 summarizes the respective PK parameters C_{max} and AUC_{last} as well as the values for MPE, MAPE and MRD.

3.2. Human peroral simulations for different CAB formulations

All drug dependent parameters, e.g. lipophilicity or molecular weight, should be the same across species and were transferred from the rat to the human model. Calculation methods for distribution and cellular permeability should also be the same across different species. Several calculation methods were tested during model development. Best results were also obtained for the Rodgers & Rowland tissue distribution in combination with the PKSim® standard method for the calculation of cellular permeabilities. Parameters, which could not be transferred from the rat simulations, were estimated. These included EHC parameter (gallbladder ejection half-time, time to complete gallbladder refilling, EHC continuous fraction, gallbladder ejection fraction), as well as k_{cat} and K_M for MRP2. In vitro values for k_{cat} and K_M for CYP3A4 were available from a study by Lin et al. [43]. However, the purpose of that study was to elucidate the enzymatic characteristics of different CYP3A4 alleles in vitro. Their K_m value was used more like an internal comparative for different isoenzymes and was determined under non-physiological conditions without taking protein-binding into account, representing rather the free K_m. Both in vitro values were therefore checked and adapted to fit the data and especially for K_m there was a high deviation from the reference value for the reasons stated. Renal, hepatic, and biliary excretion were investigated, but no renal excretion was found for CAB, which is consistent with literature [13]. As a CYP3A4 metabolism and an active MRP2 transport were used in the human model, no additional liver and biliary plasma clearance was implemented. Different CAB formulations (solution, tablet, and capsule) were investigated separately, as they are not bioequivalent. The formulation type "dissolved" was used for the oral solution. This formulation type characterizes the drug as being in solution at the point of oral administration. However, there was no further information on the administered solution in the

original study (e.g., additional solubiliser) and as CAB is a poorly soluble drug, it might be possible that the given solution was more like a suspension than a real solution. Therefore, dissolution at the point of administration might be incomplete and the intestinal absorption may be limited by the solubility, imposing an upper bound to the absorption rate. To mimic the possibly biased solubility and the overestimation of absorbed substance, the gastrointestinal solubility was reduced, just as it was done in the oral simulations for rats. Nevertheless, there was still some overestimation of the CAB plasma concentration, especially for later time points. For the simulation of CAB tablets and capsules, the integrated Weibull function was used to create a tablet respectively capsule formulation and relevant parameter of the Weibull function were adapted to fit the observed data. All parameters used in the final PBPK model are show in Table 1.

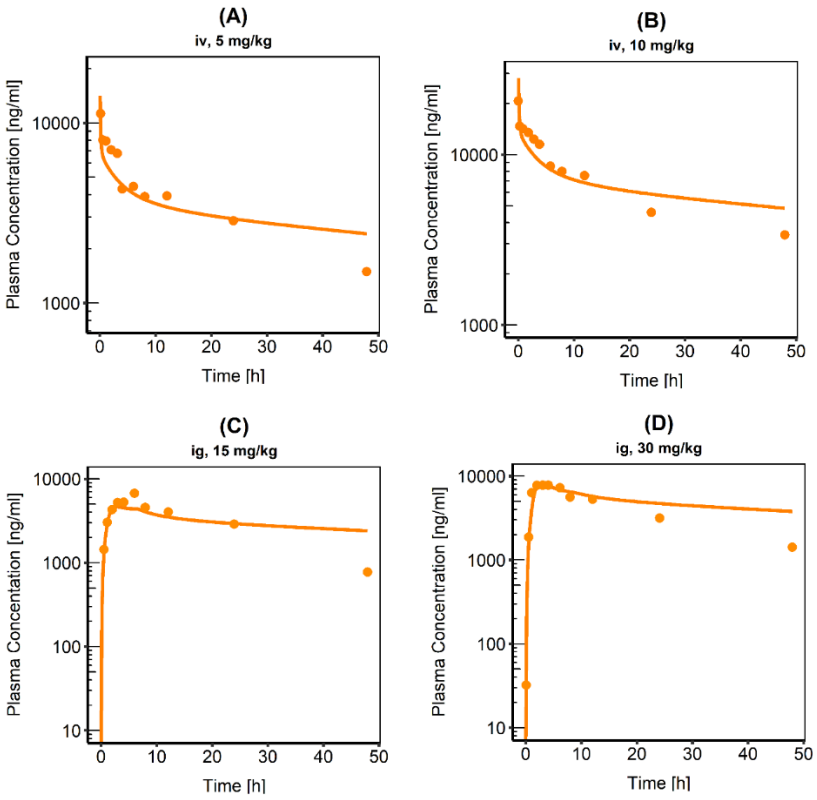

Figure 1. Semilogarithmic plots of plasma concentration-time profiles following (**A**) 5mg/kg intravenous (iv), (**B**) 10 mg/kg iv, (**C**) 15 mg/kg intragastric (ig) or (**D**) 30 mg/kg ig administration of CAB. Observed data are shown as dots, simulations are shown as lines. All data extracted from Wang et al., n = 8 in each case.

Table 1. Summary of the CAB parameters used in the human PBPK model

Parameter	Unit	Value used in PBPK model	Literature value [Reference]	Description
MW	[g/mol]	501.50	501.50 [44]	Molecular weight
pK_a [base]		6.32	6.32 [45]	Acid dissociation constant
fu_p		0.24	0.24 [13]	Fraction unbound in plasma
logP		4.40[a]	5.15 [45]	Lipophilicity
Solubility (pH 6.5)	[10^{-3} mg/mL]	7.72[a]	0.00 [44]	Solubility
K_M CYP3A4	[µmol/L]	0.97[a]	21.32 [43]	Michaelis-Menten constant CYP3A4
k_{cat} CYP3A4	[1/min]	0.67	0.66 [43]	Katalytic rate constant CYP3A4
K_M MRP2	[µmol/L]	10[a]	--	Michaelis-Menten constant MRP2
k_{cat} MRP2	[1/min]	2111.11[a]	--	Transport rate constant MRP2
Reference concentration MRP2	[µmol protein/l in the tissue of highest expression]	0.09	0.06 [46]	Liver reference concentration
Partition coefficients		Rodgers and Rowland	[47,48]	Calculation method cell to plasma coefficients
Cellular permeabilities		PKSim® Standard	[29]	Calculation method permeation across cell membranes
Transcellular intestinal permeability	[10^{-4} cm/min]	1.70[a]	--	Intestinal permeability via transcellular route
Tablet Weibull time	[min]	36.00[a]		Dissolution time (50% dissolved) fasted state
Tablet Weibull shape		1.29[a]		Shape parameter of Weibull function
Capsule Weibull time	[min]	45.00		Dissolution time (50% dissolved) fasted state
Capsule Weibull shape		5.00		Shape parameter of Weibull function
Emptying half-time	[min]	41.44	69.98 [33]	Half-time for gallbladder emptying (exponential release)
EHC continuous fraction		0.1		Fraction of biliary secreted compound continuously entering duodenum
Gallbladder ejection fraction		0.45		Fraction discretely ejected into the duodenum
Refilling time	[min]	241.00	419 [33]	Time to complete gallbladder refilling

[a] Model parameters have been estimated through parameter optimization based on the plasma drug concentrations, *EHC*: Enterohepatic circulation, -- Value not available

The fractions absorbed in different intestine sections were simulated after administration of a CAB 140 mg solution, tablet, and capsule (Figure 2)). In case of the solution, the total fraction absorbed was reached almost instantaneously and the complete dose was absorbed. For the tablet formulation, only about 75% of the dose was absorbed in the first three hours and it took about 30 hours until 95% of the dose was absorbed. For the capsule formulation, a slightly lower fraction was absorbed in the first three hours (65%), which agrees with the lower C_{max} compared to the tablet formulation. After 30 hours, about 82% of the given dose was absorbed, conforming to the relative bioavailability compared to the solution (74-93% for capsule; 97% for tablet) [12]. Plasma concentration-time profiles with and without an integrated EHC after the administration of a 140 mg tablet process are compared in **Fehler! Verweisquelle konnte nicht gefunden werden.**. If no EHC process was included, the observed plasma concentrations were significantly underestimated, and CAB plasma exposure was 2.7 times lower compared to the plasma exposure with an included EHC (23809.01 ng/h/ml vs. 64750.20 ng/h/ml).

3.3. PBPK model evaluation

The final PBPK model was successfully used to describe observed CAB plasma concentrations in healthy volunteers (HVs) after a single oral dose. Simulated plasma profile trajectories were in close concordance with observed data. Linear plots of predicted versus observed plasma concentration time profiles are shown in Figure 4. Semi-logarithmic plots can be found in Figure S7 of the ESM. Figure 5 shows the goodness-of-fit plots comparing predicted to observed plasma concentrations. Ninety-seven percent of all simulated plasma concentrations fall within 2-fold of the corresponding concentration observed. Figure S8 shows the predicted vs. observed area under the concentration time curves from the first to the last data point (AUC_{last}) and maximum plasma concentration (C_{max}) values of all studies. All predicted AUC_{last} and C_{max} values fell within the 2-fold acceptance criterion. Ratios for predicted versus observed AUC_{last} values are between 0.9 and 1.2 and for C_{max} between 0.8 and 1.1. All values can be found in the ESM (Table S5). Results for model bias (mean prediction error), model precision (mean absolute prediction error) and MRD are listed in Table S6. Mean MRD was 1.53 with a range of 1.22 to 1.88, thus all fulfilled the acceptance criterion. Results of the local sensitivity analysis, which was performed based on the simulation of the 140 mg CAB capsule administration, are demonstrated in Figure S9. For a graphical representation of the final model including a detailed view on the EHC, see Figure 6.

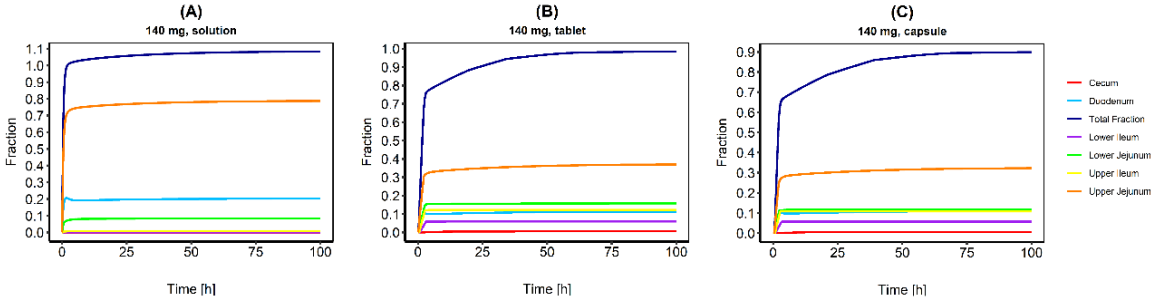

Figure 2. Simulation of the absorbed CAB fractions in different intestine sections after administration of a CAB 140 mg solution (**A**), tablet (**B**) and capsule (**C**).

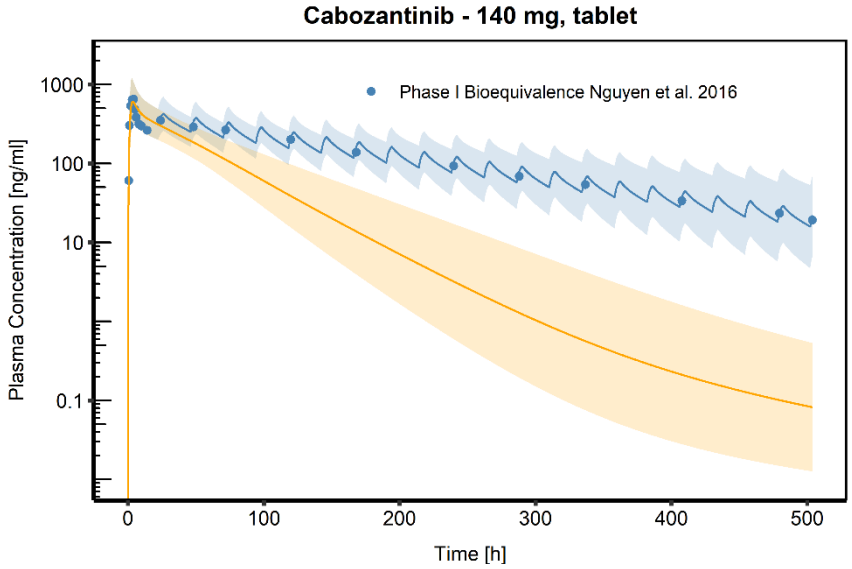

Figure 3. Comparison of simulated CAB venous blood plasma concentration-time profiles (semi-logarithmic) following oral administration of a 140 mg CAB tablet. The blue shaded area represents the geometric mean SD for population simulations with an implemented EHC process. The orange shaded area represents the geometric mean SD for population simulations without an implemented EHC process. Geometric means are shown as blue line (with EHC) respectively as orange line (without EHC). Observed data are shown as blue dots.

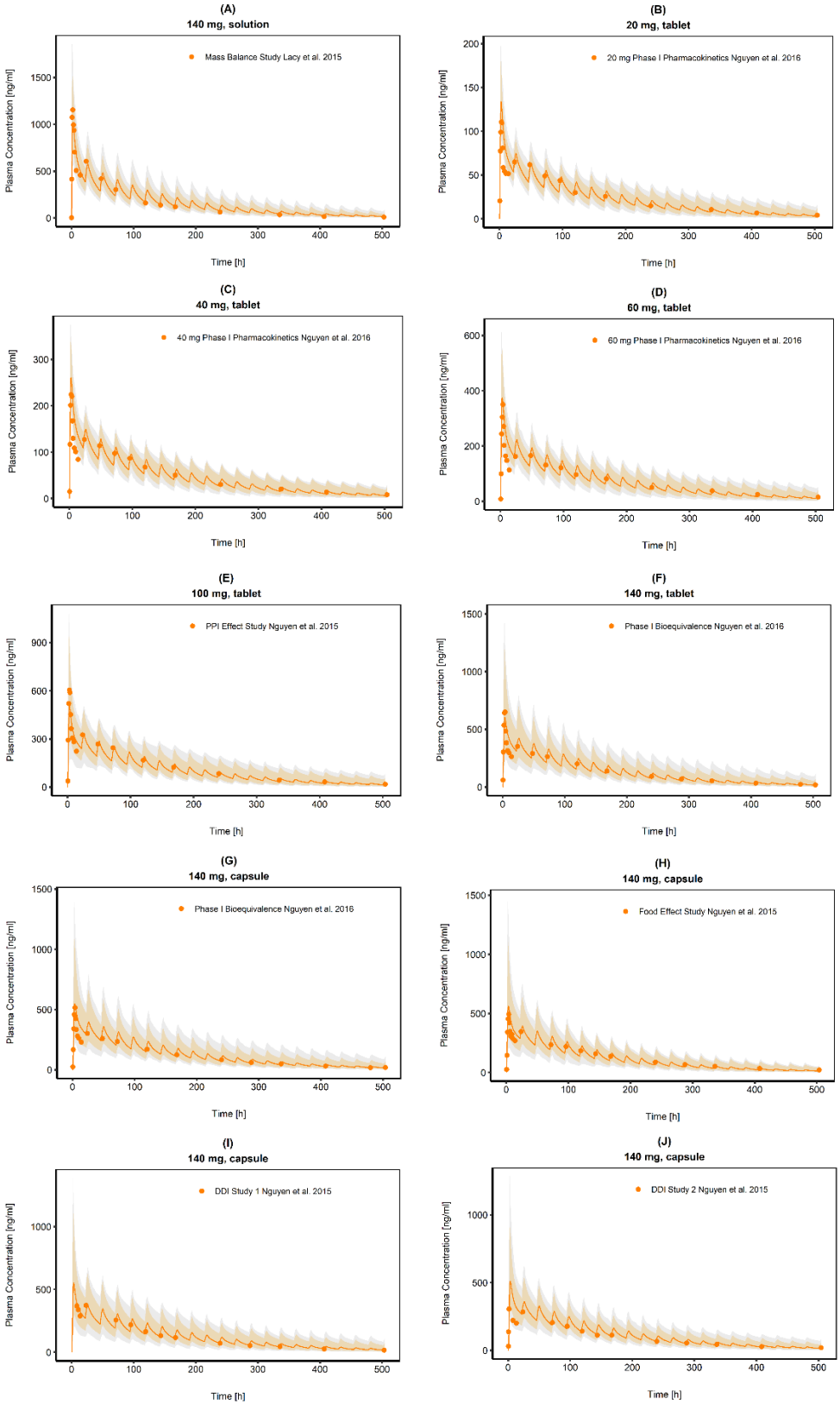

Figure 4. CAB plasma concentration time profiles (linear). (**A**) 140 mg CAB oral solution from a mass balance study, (**B–D**) data from a Phase I study CAB as tablet in 20, 40 and 60 mg oral single dose, (**E**) CAB 100 mg oral single dose as tablet in a PPI effect study, (**F,G**) 140 mg CAB as tablet an capsule formulation from a bioequivalence study, (**H**) 140 mg CAB oral single dose as capsule formulation from a food effect study, (**I,J**) 140 mg CAB oral single dose as capsule formulation from DDI studies with Ketoconazole and Rifampin. Observed data are shown as orange dots. Population simulation (n = 100) geometric means are shown as orange lines; the shaded orange areas represent the predicted population geometric SD. The shaded grey areas represent the 5% to 95% prediction interval.

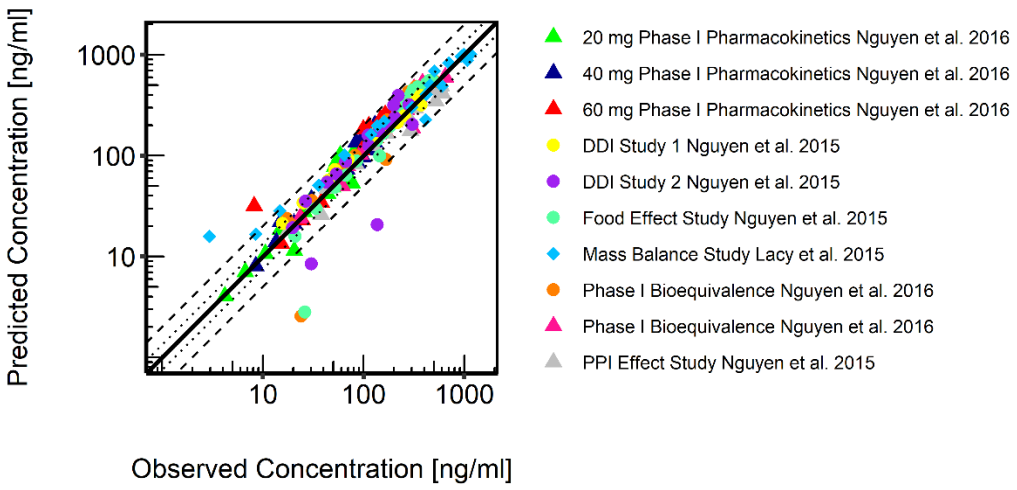

Figure 5. Goodness-of-fit plot for the predicted versus observed CAB plasma concentrations. Tablet formulations are represented by triangles, capsule formulations are represented by dots, the solution is represented by diamonds. The black solid line represents the line of identity; dashed black lines represent a twofold deviation; dotted black lines represent a 1.25-fold deviation.

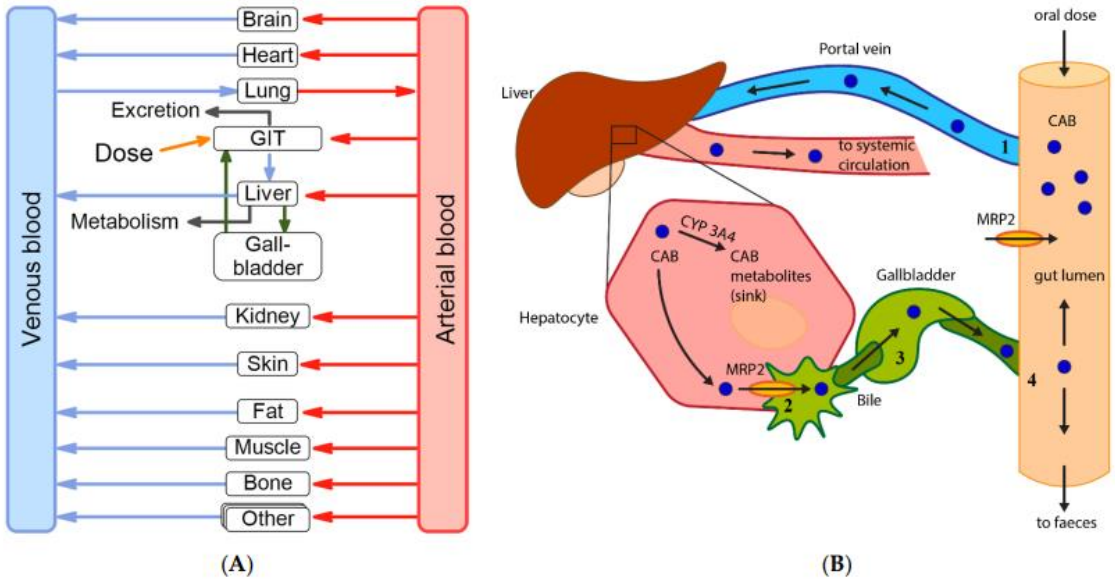

Figure 6. (**A**) Overview of the final PBPK model. Cabozantinib enters the PBPK model via oral administration to the GIT and is eliminated by metabolism and faeces (see (**B**) for further details). Cabozantinib metabolites were not modelled due to insufficient data. GIT: gastro-intestinal-tract (**B**) Schematic illustration of the EHC model of Cabozantinib after oral drug administration: (**1**) after intestinal absorption, CAB is distributed via the hepatic portal vein into the liver; (**2**) once in the liver, a fraction of CAB is excreted into the bile via MRP2 transporter; (**3**) bile is transferred into the gallbladder where it is stored and concentrated; (4) after a given accumulation time, bile is delivered back into the intestine and a fraction of recirculated CAB can be reabsorbed again in the intestine or eliminated with faeces. To model EHC of the drug, active transport processes via MRP2, storage in gallbladder, secretion into the duodenum and reabsorption along the intestine are included in the model. Elimination occurs mainly via hepatic and intestinal (not shown for simplicity) metabolism (CYP 3A4) and faeces. CAB: Cabozantinib; MRP2: multidrug resistance-associated protein 2.

3.4. Simulations of DDI between CAB and RIF

The plasma concentration-time profile after single-dose administration of 140 mg CAB capsule, given either alone or together with its perpetrator RIF, could be described adequately (Figure). There is a tendency to overestimate CAB plasma concentration for later time-points (> 300h), however, all observed, except for the last one, are within the geometric mean SD. The ratio for AUC_{last} of CAB administered together with RIF and CAB administered without RIF was 0.23, which is a reduction in AUC_{last} by 77%. This agrees with the reduced CAB exposure (77%) found by Nguyen et al. [18], which is also stated in the EMA and FDA SPC and label for Cabometyx® and Cometriq®. The DDI C_{max} ratio was 87.00%, which is within 80%—125%, indicating that RIF co-administration does not relevantly influence CAB absorption (Table 2).

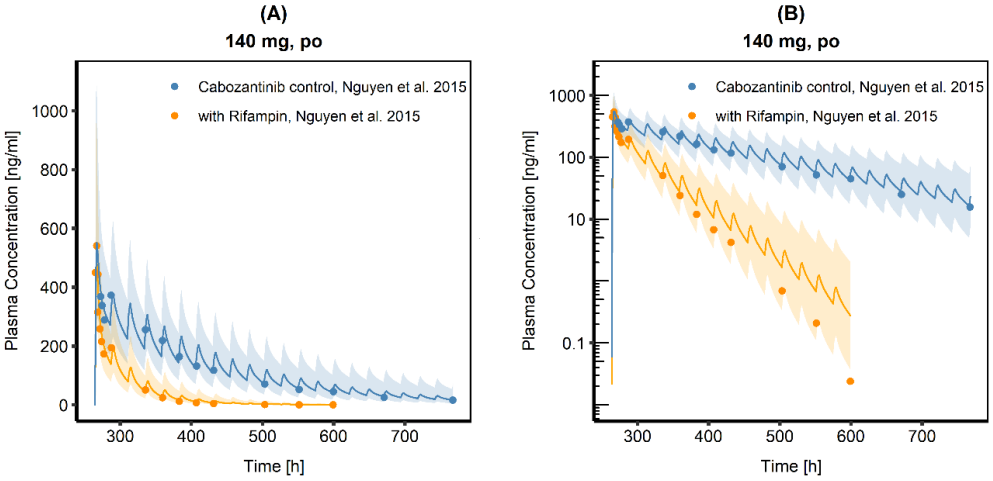

Figure 7. Cabozantinib plasma concentration-time profiles in linear (**A**) and semi-logarithmic (**B**) representation without and with rifampin co-administration. Observed data are shown as dots. Population simulation (n=100) geometric means are shown as lines; the shaded areas represent the predicted population geometric SD.

Table 2. Comparison of AUC_{last} and C_{max} for the administration of CAB, given either alone or in combination with its perpetrator RIF

PK Parameter	CAB with RIF	CAB without RIF	Ratio
AUC_{last}	13624.61	59738.08	0.23
C_{max}	480.46	551.17	0.87

Multiple dosing simulations for CAB tablet (60 mg) and capsule (140 mg), given without RIF, resulted in predicted average steady state plasma concentrations (C_{ss}) of 1197.44 ng/ml respectively 1576.68 ng/ml. Simulations after multiple-dose administration of CAB together with RIF and an increased CAB dose by 20 mg (tablet) respectively 40 mg (capsule) led to C_{ss} of 394.74 ng/ml and 532.41 ng/ml. Thus, even with higher CAB doses, DDI C_{ss} were still about

two-thirds lower compared to the C_{ss} if CAB is given without its perpetrator. Table S7 gives a clearer presentation of all values. Figure S10 shows predicted Css either for CAB capsule or tablet given alone (CAB standard dose) or together with 600 mg RIF (increased CAB dose).

3.5. Investigation of hepatic impairment on CAB plasma exposure

Individuals and populations with mild and moderate liver impairment were created and the model was able to describe CAB plasma exposure in the healthy control group as well as in the diseased populations. An overview of the final physiological parameters changed for mild and moderate liver impairment compared to the healthy control group is given in Table . Figure shows predicted plasma concentration-time profiles for these populations (n = 100) including observed CAB plasma concentrations. In Figure S11 of the ESM, the trajectories are compared in one plot, indicating the higher plasma exposure in mild and moderate liver impairment compared to the control group. AUC_{last} for patients with mild and moderate hepatic impairment was 64% respectively 50% higher compared to HVs (51633 ng/h/ml for mild impairment and 47096 ng/h/ml for moderate impairment vs. 31448 ng/h/ml for the control group). Mean predicted C_{max} is slightly increased in the mild impairment group and slightly lowered in the moderate impairment group. Patients in the mild liver impairment group of the underlying study had a minimal lower fraction of unbound CAB in plasma (fu_p) compared to the control group, whereas patients of the moderate liver impairment group had a higher fu_p compared to the control group. To include this observation, a plasma protein scale factor, which has a strong influence on C_{max} and AUC_{last}, was adapted to describe the plasma concentration-time profile adequately. In case of mild hepatic impairment, plasma protein scale factor was reduced to 0.85 to account for the higher C_{max} seen in these patients. For the moderate hepatic impairment group this scale factor was set to 1.30, which resulted in an increased volume of distribution and consequently in a lower C_{max}. The higher fu_p assumed for the moderate liver impaired population led to an increased clearance, resulting in lower plasma concentration levels throughout the curve and a not quite so high increase in plasma exposure compared to the predicted AUC_{last} for the mild liver impaired population.

Table 3. Physiological changes of parameters associated with hepatic impairment

Parameter	Control group	Mild hepatic impairment	Moderate hepatic impairment
Hematocrit value[b]	0.47[a]	0.39[b]	0.37[b]
Blood flow[b]			
portal	1.00	0.40	0.36
renal	1.00	0.88	0.65
hepatic arterial	1.00	1.30	2.30
other organs	1.00	1.75	2.25
Liver volume fraction[b]	1.00	0.81	0.65
CYP3A4 activity	1.00	1.00	0.40
Plasma protein scale factor	1.00[a]	0.85	1.25

[a] value based on PKSim®, [b] values according to Edginton et al. [38]

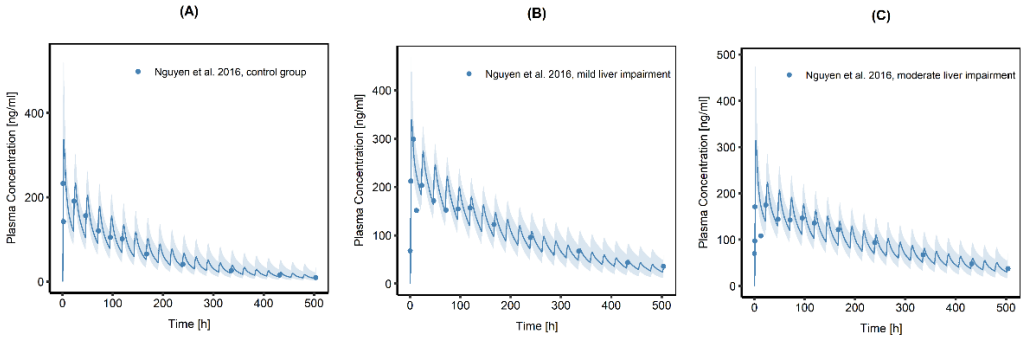

Figure 8. Population simulations (n = 100) of CAB plasma concentration-time profiles after a single dose administration of 60 mg CAB capsule to (**A**) the healthy control group, (**B**) patients with mild liver impairment and (C) patients with moderate liver impairment. Blue dots indicate mean observed plasma concentrations, the blue line represents the population simulations geometric mean of the predicted plasma concentrations; the shaded areas represent the predicted population geometric SD.

4. Discussion

CAB is a new drug, which could be used in other therapeutic areas, besides RCC and HCC, as it is investigated in numerous clinical trials. As an example, the safety and efficacy of CAB in advanced adrenocortical carcinoma is currently evaluated [49]. Despite the increasingly widespread use, not all pharmacokinetic properties of the substance have been fully inspected. In the presented work, a whole-body PBPK model for CAB has been established, which was less used as a precision tool but rather as a tool to serve as a further step to gain insights into the PK properties of the substance. The developed model successfully describes and predicts observed plasma concentration-time profiles of different CAB formulations (solution, capsule and tablet) in a wide dose range (20-140 mg) after single-dose administration in humans and for ig (15-30 mg/kg) and iv (5-10 mg/kg) administration in rats. The inspection of rat plasma concentration-time profiles after ig administration hypothesized nonlinear PK (Figure S3), as for the lower dose, significantly higher plasma concentrations were observed if plotted dose

normalized. This is not the case after iv administration, which led to the conclusion that the nonlinear PK seen in the ig profiles might be associated with drug absorption processes. Optimization of relevant parameter showed that especially in the large intestine but also in the ileum the intestinal solubility was overestimated and reduced accordingly. Inspection of the human plasma concentration-time profiles (Figure S5, Figure S6) reveal a second peak approximately 24 hours after CAB administration. In addition, according to a study by Lacy et al., relatively high ^{14}C-CAB levels in feces at 1 week postdose can be seen. Both phenomena could be justified as a consequence of an EHC of CAB [13,50]. Seventeen metabolites of CAB were identified, of which EXEL-1646 is the only human metabolite that could be back transformed to the parent compound (see ESM Figure S1) [13]. However, in vitro it has been shown that EXEL-1646 will only be transformed into its nonconjugated monohydroxy precursor [13]. In contrast, rat plasma concentration-time profiles don´t show the phenomenon of a second or multiple peak (Figure S3), which might be due to the missing gallbladder in rats and in consequence due to the unincisive EHC. In the CAB assessment report, an EHC of the substance is assumed as most possible cause for the characteristic PK profile of CAB in humans, which is why this process was investigated particularly [51,52]. However, alternative processes might also explain multiple peaks in plasma concentration-time profile and a long terminal half-life combined with a steeper decrease of the plasma concentration at the beginning. For example, absorption processes in deeper intestine sections, like in the upper or lower ileum, could cause a delayed absorption. To verify this possibility, the fractions absorbed in different intestine sections were simulated and confirmed a lower fraction absorbed for the capsule formulation compared to the tablet formulation and solution. This is in accordance with the findings by Lacy et al., who stated that the mean AUC_{0-inf} values for HVs administered a 140 mg cabozantinib capsule dose or tablet dose were 74–93 % and 97 %, respectively, of the corresponding value in the mass balance study where CAB was formulated as a solution [12]. Besides a lower total fraction absorbed, a delay in the absorption process could be detected in the simulations with lower fractions absorbed in the first 24 hours for capsules compared to tablets and to the solution. Nevertheless, the delayed absorption alone could not account for the long terminal half-life. Therefore, the EHC process was implemented into the model, which notably improved its performance. Comparisons of simulations with and without the EHC process highlighted the strong impact of the process on CAB plasma exposure. After all, a combination of delayed intestinal absorption and EHC led to the best description of CAB plasma concentration-time profiles.

The final PBPK model also included an active MRP2 transport processes and CYP3A4 metabolism, two main features characterizing CAB PK and representing possible sources for

drug interactions and resistance [18,41,53]. CAB is mainly used in advanced disease states e.g. in hepatocellular carcinoma, where co-administration of several additional drugs is not uncommon and several authors [9,54] discuss these issues. Interactions with strong CYP3A4 inducers (e.g. Rifampin) or inhibitors (e.g. Ketoconazol) can lead to decreasing or increasing CAB plasma concentrations which may require closer monitoring and dose adjustment [41]. The developed model was used to simulate DDI with RIF and confirmed a decrease of 77% in plasma exposure, when RIF is co-administered with CAB. The model adequately describes the CAB RIF DDI plasma concentration-time profile and is in good agreement with the observed data. The correct prediction of the impact of the perpetrator drug indicates the correct implementation of the relevant elimination pathways of the victim drug and the right amount of drug eliminated via that pathway [55]. After single-dose administration it was not possible to match AUC_{last} values of the control data by only increasing the amount of the single dose, as in that case, C_{max} will also strongly increase, which could have an impact on safety. However, CAB accumulates fivefold by day 15 following daily dosing based on AUC, which should be considered in the treatment of these patients. As no clinical data after multiple-dose administration were available, predicted C_{ss} after multiple dosing for the 60 mg tablet was compared to the C_{ss} published by Castellano et al. [56], to evaluate the ability of the model to simulate multiple dosing correctly. A good agreement between the predicted and published value was found (1197 ng/ml vs. 1123 ng/ml). Steady state simulations for CAB co-administered with RIF indicate that a dose increase by 20 mg (tablet) respectively 40 mg (capsule) is not sufficient to achieve the corresponding CAB plasma levels, when CAB is administered without its perpetrator. Hence, the model presented in this work cannot confirm, that the dose increase recommended by FDA led to equivalent Css (Figure S10). For that reason, EMA advises against using strong CYP3A4 inducer, when patients are treated with CAB in order to avoid subtherapeutic plasma concentrations. However, there may be situations where it is clinically necessary to co-administer both substances and slightly lower CAB plasma levels are still sufficient. To counteract CAB Css that are far below the desired threshold, it might be valuable to conduct therapeutic drug monitoring in patients treated concomitantly with CAB and a strong CYP3A4 inducer like RIF.

Limitations, which could reduce the applicability of the model, should be pointed out. No human iv data were available and the human PBPK model of CAB was developed based on peroral data only. This is generally possible [28] but leads to a number of uncertainties and inaccuracies. State of the art approach is to establish an i.v. model first and to describe distribution and clearance processes independently from drug absorption processes. In a second step the model for p.o. administration can be established based on the i.v. model and parameters

that influence absorption can be estimated with less uncertainty. To overcome this issue, a cross-species sequential approach using rat iv data was pursued. Based on these simulations for the rat, relevant physicochemical properties were evaluated to describe drug distribution. However, clearance processes and especially the EHC process could not be transferred from rat to human, as only few information on rat clearance was available, the rat lacks a gallbladder, and metabolism processes are fundamentally different between rat and human, as stated by Lacy et al. [13]. One shortcoming is that the original study data were not available but only published data. Therefore, for model development only mean plasma concentrations without observed standard deviations could be used, which made it impossible to assess interindividual variability. Lacy et al. reported multiple peaks in the plasma concentration-time profiles after a single oral dose of CAB [12]. However, in the mean plasma concentration time profiles these multiple peaks can´t be really seen, but they might be observed in individual plasma concentration time profiles. In the case of EHC, one might expect peaks already earlier than 24 hours after administration, matching with the food intake of the volunteers, but only two plasma concentration-time profiles show small peaks already approximately nine hours after CAB administration. However, as EHC is characterized by high interindividual variability [57], mean data might not accurately represent the individual course. Model inaccuracy may also result from the periodicity of the complex EHC process, dependent on digestion with high interindividual variability e.g. on bile accumulation, concentration and release into the duodenum. The high variability of the EHC process is also mentioned in a published PBPK model for Sorafenib, another TKI approved for HCC, RCC and MTC. The work of Abbiati et al. highlights the EHC, which causes the characteristic double peak in the plasma concentration-time curves of Sorafenib [50]. In contrast to the CAB model, the model of Abbiati et al. was developed based on mice data and is restricted to the first EHC contribution due to limited available data regarding this process.

Van Erp et al. point out that for TKI "most of the available PK information is based on information obtained from in vitro experiments, animal studies, DDI studies and mass balance studies in HVs with a single dose of the aimed TKI. However, it is difficult to translate the results of these studies to the clinical oncology practice where these drugs are administered on a daily basis […]" [58]. The CAB PBPK model was also developed based on HVs but now gathers all information and combines it with relevant physiological and anatomical processes, which are integrated in the PK Sim® software.

With that, the model could be extended to simulate the plasma exposure in patients with mild and moderate liver impairment. Liver diseases can affect a number of morphological and physiological processes and may have an impact on enterohepatic circulation and biliary

excretion. A decreased uptake into hepatocytes, an altered metabolism and distribution within the hepatocytes as well as reduced transfer mechanism into bile is conceivable. Especially cholestasis can have a significant influence on hepatobiliary excretion, either through biliary obstruction (e.g. caused by duct stones or pancreatic carcinoma) or transporter defects respectively downregulation (e.g. strong downregulation of canalicular MRP2). However, patients in the study of the effect of hepatic impairment on CAB PK were not affected by cholestasis but by liver cirrhosis only [37]. According to Roberts et al. [57], liver cirrhosis rather affects sinusoidal membrane transport systems than canalicular bile transport systems. Therefore, the focus was placed on changes in hepatic blood flow, in cellular enzymatic function and in altered plasma protein binding to simulate patients suffering from mild and moderate liver impairment. According to Nguyen et al. [37], plasma exposure was increased by 81% and 63% in patients with mild respectively moderate liver impairment, compared to healthy subjects. Simulation using the herein presented model yielded a slightly lower increase in plasma exposure by 64% and 50% for mild and moderate liver impairment but it meets the observed tendency, and it has to be noted that hepatic dysfunction varies widely between patients with the same Child-Pugh score. A lower increase in plasma exposure for moderate disease compared to subjects with mild hepatic impairment and a generally lower C_{max} for those patients was justified through Nguyen et al. by a higher fup and a higher interindividual variability. The model was able to describe C_{max} and AUC_{last} in patients with mild and moderate hepatic impairment correctly and can be expanded for further investigations for example in patients with Child-Pugh class C, as there is a knowledge gap for such patients.

It must be considered, that the simulated populations with liver disease contained only male individuals, as the underlying study was conducted exclusively in male subjects. The transferability to females is therefore limited. In addition, patients of the underlying study where considerably older than the individual used for model development (37 years vs. 54 to 58 years). The model was also developed based on an individual with quite lower weight (73.96 kg), respectively BMI, compared to the participants from the hepatic impairment study (mean weight control group: 86.00 kg, mean weight mild hepatic impairment group: 92.40 kg, mean weight moderate hepatic impairment group: 88.50 kg). BMI can have an impact on oral plasma clearance. It was shown that with higher BMI, the CAB apparent clearance decreases [59], which could have also influenced the simulated plasma exposure. A reduction in plasma binding proteins can be associated with different disease states and results in altered fup [60,61]. Slight changes in fup tend to have a higher impact on compounds with excessive protein binding such as CAB because the observed percent change would be large. The presented model revealed a considerable influence of the CAB fu_p on plasma exposure and C_{max}. In relevant patients,

suffering from cirrhosis, it might be valuable to measure this parameter to predict CAB PK more precisely.

CAB is used in cancer patients and several other alterations regarding physiology are conceivable, both because of the disease itself or due to co-medication, and could be adapted in the developed model as it was done for liver cirrhosis [62]. EHC process, CYP3A4 and MRP2 expression and activity can be modified, and the model can therefore serve as a starting point to transfer the results to populations of interest. Comorbidities like cholecystis, cholestasis or cholelithiasis but also diabetes mellitus and renal diseases could influence enterohepatic circulation directly or indirectly and might be subject of future questions [57]. As already stated, CAB plasma levels could be altered through its affinity to MRP2 transporter and it is conceivable to investigate situations, which could lead to alterations in MRP2 expression, like cholestatic liver diseases [63-65], based on the presented model. Concomitant use of drugs that inhibit MRP2 transport could result in higher plasma concentrations whereas a conceivable overexpression of MRP2, e.g. in specific tumours or due to a concomitant use of pregnane X receptor ligand (e.g. Phenobarbital) leads to the opposite [64,66-68]. Both scenarios are more than unfavourable for the patients, as they either can suffer from side effects or less efficacy. As DDI based on the CAB CYP3A4 metabolism are very important, with more data becoming available in future, the model might be used as a basis for further investigations regarding relevant DDI and the associated dose adaptations.

5. Conclusions

A whole body PBPK model for CAB has been built in PK-Sim® including key processes like CYP3A4 metabolism, MRP2 transport and EHC which may influence pharmacokinetic properties of the drug. It comprises in vitro, in vivo and in silico information combined with available CAB plasma concentrations. EHC was found to be the most plausible cause for the characteristic PK profile. The final model is characterized by good precision and low bias. The model was expanded to simulate DDI with RIF and CAB plasma exposure in patients with mild and moderate liver impairment.

PBPK modeling is a convenient tool to mechanistically explore the PK behavior of a drug and the model presented in this work can contribute to gain further insight into CAB absorption, distribution, metabolism and excretion. As a comprehensive software tool was used in this work, it will be convenient to reuse the PBPK model for other scenarios also by non-modeling experts. By that, it serves as a starting point for further studies in specific populations, disease states or with respect to drug interactions (e.g., via CYP3A4). So far, clinical study data are limited, especially with regards to plasma exposure after multiple dosing, but they might be

available in near future with more studies conducted. Future PBPK models could be developed by implementing data from cancer patients or from patients taking relevant co-medication.

Supplementary Materials: The following are available online at www.mdpi.com/xxx/s1, Electronic Supplementary Materials: Additional information on model development and evaluation including Figures S1 S11 and Tables S1-S7.

Author Contributions: "Conceptualization, B.F. and O.SC.; methodology, B.F.; investigation, B.F.; writing—original draft preparation, B.F.; writing—review and editing, B.F. and O.SC.; visualization, B.F. All authors have read and agreed to the published version of the manuscript.

Funding: This research received no external funding.

Acknowledgments: The authors kindly acknowledge Valerie Nock, Boehringer Ingelheim Pharma GmbH & Co. KG, Lisa Alina Kneller, University of Münster, Fatemeh Aghai, University of Würzburg and the PharMetrX Network, for their scientific support and valuable suggestions.

Conflicts of Interest: Bettina Gerner declares no conflict of interest. Oliver Scherf-Clavel reports endowed professorship grant (Horphag Research Ltd.).

References

1. Kurzrock, R.; Sherman, S.I.; Ball, D.W.; Forastiere, A.A.; Cohen, R.B.; Mehra, R.; Pfister, D.G.; Cohen, E.E.; Janisch, L.; Nauling, F.; et al. Activity of XL184 (Cabozantinib), an oral tyrosine kinase inhibitor, in patients with medullary thyroid cancer. *J Clin Oncol* **2011**, *29*, 2660-2666.

2. Markowitz, J.N.; Fancher, K.M. Cabozantinib: a multitargeted oral tyrosine kinase inhibitor. *Pharmacotherapy* **2018**, *38*, 357-369.

3. Neul, C.; Schaeffeler, E.; Sparreboom, A.; Laufer, S.; Schwab, M.; Nies, A.T. Impact of Membrane Drug Transporters on Resistance to Small-Molecule Tyrosine Kinase Inhibitors. *Trends Pharmacol Sci* **2016**, *37*, 904-932.

4. Grüllich, C. Cabozantinib: a MET, RET, and VEGFR2 tyrosine kinase inhibitor. In *Small Molecules in Oncology*; 2014; pp. 207-214.

5. Fallahi, P.; M Ferrari, S.; Di Bari, F.; Materazzi, G.; Benvenga, S.; Miccoli, P.; Antonelli, A. Cabozantinib in thyroid cancer. *Recent Pat Anticancer Drug Discov* **2015**, *10*, 259-269.

6. Singh, H.; Brave, M.; Beaver, J.A.; Cheng, J.; Tang, S.; Zahalka, E.; Palmby, T.R.; Venugopal, R.; Song, P.; Liu, Q. US Food and Drug Administration approval: cabozantinib for the treatment of advanced renal cell carcinoma. *Clin Cancer Res* **2017**, *23*, 330-335.

7. Tannir, N.M.; Schwab, G.; Grünwald, V. Cabozantinib: an active novel multikinase inhibitor in renal cell carcinoma. *Curr Oncol Rep* **2017**, *19*, 14.

8. Abou-Alfa, G.K.; Meyer, T.; Cheng, A.-L.; El-Khoueiry, A.B.; Rimassa, L.; Ryoo, B.-Y.; Cicin, I.; Merle, P.; Chen, Y.; Park, J.-W.; et al. Cabozantinib in Patients with Advanced and Progressing Hepatocellular Carcinoma. *N Engl J Med* **2018**, *379*, 54-63.

9. Deeks, E.D. Cabozantinib: A Review in Advanced Hepatocellular Carcinoma. *Targ Oncol* **2019**, *14*, 107-113.

10. Yakes, F.M.; Chen, J.; Tan, J.; Yamaguchi, K.; Shi, Y.; Yu, P.; Qian, F.; Chu, F.; Bentzien, F.; Cancilla, B.; et al. Cabozantinib (XL184), a novel MET and VEGFR2 inhibitor, simultaneously suppresses metastasis, angiogenesis, and tumor growth. *Mol Cancer Ther* **2011**, *10*, 2298-2308.

11. U.S. National Library of Medicine. ClinicalTrials.gov. Search Term: "Cabozantinib". Available from: https://clinicaltrials.gov/ct2/results?cond=&term=Cabozantinib&cntry=&state=&city=&dist= (accessed on 2020 Sep 09).

12. Lacy, S.A.; Miles, D.R.; Nguyen, L.T. Clinical Pharmacokinetics and Pharmacodynamics of Cabozantinib. *Clin Pharmacokinet* **2017**, *56*, 477-491.

13. Lacy, S.; Hsu, B.; Miles, D.; Aftab, D.; Wang, R.; Nguyen, L. Metabolism and Disposition of Cabozantinib in Healthy Male Volunteers and Pharmacologic Characterization of Its Major Metabolites. *Drug Metab Dispos* **2015**, *43*, 1190-1207.

14. Ren, L.J.; Wu, H.J.; Sun, L.H.; Xu, X.; Mo, L.Y.; Zhang, L.; Zhang, J.Y.; Wu, C.Y. A sensitive LC-MS/MS method for simultaneous determination of cabozantinib and its metabolite cabozantinib N-oxide in rat plasma and its application in a pharmacokinetic study. *Biomed Chromatogr* **2018**, *32*, e4227.

15. Lehr, T.; Staab, A.; Tillmann, C.; Trommeshauser, D.; Schaefer, H.-G.; Kloft, C. A quantitative enterohepatic circulation model. *Clinical pharmacokinetics* **2009**, *48*, 529-542.

16. Metsugi, Y.; Miyaji, Y.; Ogawara, K.-i.; Higaki, K.; Kimura, T. Appearance of double peaks in plasma concentration–time profile after oral administration depends on gastric emptying profile and weight function. *Pharmaceutical research* **2008**, *25*, 886-895.

17. Suttle, A.B.; Pollack, G.M.; Brouwer, K.L. Use of a pharmacokinetic model incorporating discontinuous gastrointestinal absorption to examine the occurrence of double peaks in oral concentration–time profiles. *Pharmaceutical research* **1992**, *9*, 350-356.

18. Nguyen, L.; Holland, J.; Miles, D.; Engel, C.; Benrimoh, N.; O'Reilly, T.; Lacy, S. Pharmacokinetic (PK) drug interaction studies of cabozantinib: Effect of CYP3A inducer rifampin and inhibitor ketoconazole on cabozantinib plasma PK and effect of cabozantinib on CYP2C8 probe substrate rosiglitazone plasma PK. *J Clin Pharmacol* **2015**, *55*, 1012-1023.

19. European Medicines Agency. Cabometyx Summary of Product Characteristics. https://www.ema.europa.eu/en/documents/product-information/cabometyx-epar-product-information_en.pdf (accessed on 2021 Mar 09).

20. U.S. Food and Drug Administration. Physiologically Based Pharmacokinetic Analyses — Format and Content — Guidance for Industry. 2018; https://www.fda.gov/regulatory-information/search-fda-guidance-documents/physiologically-based-pharmacokinetic-analyses-format-and-content-guidance-industry (accessed on 2021 Mar 09).

21. Peters, S.A. *Physiologically-Based Pharmacokinetic (PBPK) Modeling and Simulations: Principles, Methods, and Applications in the Pharmaceutical Industry*, 1st ed.; John Wiley & Sons, Inc.: 2012.

22. Jones, H.; Rowland-Yeo, K. Basic concepts in physiologically based pharmacokinetic modeling in drug discovery and development. *CPT: pharmacometrics & systems pharmacology* **2013**, *2*, 1-12.

23. Schmitt, W.; Willmann, S. Physiology-based pharmacokinetic modeling: ready to be used. *Drug Discovery Today: Technologies* **2004**, *1*, 449-456.

24. Jones, H.M.; Parrott, N.; Jorga, K.; Lavé, T. A novel strategy for physiologically based predictions of human pharmacokinetics. *Clin Pharmacokinet* **2006**, *45*, 511-542.

25. Open Systems Pharmacology. PK-Sim®. Version 7.4.0. Available online: https://github.com/Open-Systems-Pharmacology/Suite/releases/tag/7.4.0 (accessed on 2019 Sep 26).

26. Eissing, T.; Kuepfer, L.; Becker, C.; Block, M.; Coboeken, K.; Gaub, T.; Goerlitz, L.; Jaeger, J.; Loosen, R.; Ludewig, B.; et al. A computational systems biology software platform for multiscale modeling and simulation: integrating whole-body physiology, disease biology, and molecular reaction networks. *Front Physiol* **2011**, *2*, 4.

27. Willmann, S.; Lippert, J.; Sevestre, M.; Solodenko, J.; Fois, F.; Schmitt, W. PK-Sim®: a physiologically based pharmacokinetic 'whole-body' model. *Biosilico* **2003**, *1*, 121-124.

28. Kuepfer, L.; Niederalt, C.; Wendl, T.; Schlender, J.F.; Willmann, S.; Lippert, J.; Block, M.; Eissing, T.; Teutonico, D. Applied Concepts in PBPK Modeling: How to Build a PBPK/PD Model. *CPT Pharmacometrics Syst Pharmacol* **2016**, *5*, 516-531.

29. Open Systems Pharmacology. PK-Sim® software manual. Available online: https://docs.open-systems-pharmacology.org/ (accessed on 2019 Sep 26).

30. R Core Team *R: A language and environment for statistical computing*, R Foundation for Statistical Computing, Vienna, Austria: 2017.

31. Brightman, F.A.; Leahy, D.E.; Searle, G.E.; Thomas, S.J.D.m.; disposition. Application of a generic physiologically based pharmacokinetic model to the estimation of xenobiotic levels in rat plasma. **2006**, *34*, 84-93.

32. Jedlitschky, G.; Hoffmann, U.; Kroemer, H.K. Structure and function of the MRP2 (ABCC2) protein and its role in drug disposition. *Expert Opin Drug Metab Toxicol* **2006**, *2*, 351-366.

33. Baier, V.; Cordes, H.; Thiel, C.; Castell, J.V.; Neumann, U.P.; Blank, L.M.; Kuepfer, L. A Physiology-Based Model of Human Bile Acid Metabolism for Predicting Bile Acid Tissue Levels After Drug Administration in Healthy Subjects and BRIC Type 2 Patients. *Front Physiol* **2019**, *10*.

34. European Medicines Agency. Guideline on the reporting of physiologically based pharmacokinetic (PBPK) modelling and simulation. 2018; https://www.ema.europa.eu/en/reporting-physiologically-based-pharmacokinetic-pbpk-modelling-simulation (accessed on 2020 Mar 12).

35. Kuemmel, C.; Yang, Y.; Zhang, X.; Florian, J.; Zhu, H.; Tegenge, M.; Huang, S.M.; Wang, Y.; Morrison, T.; Zineh, I. Consideration of a credibility assessment framework in model-informed drug development: potential application to physiologically-based pharmacokinetic modeling and simulation. *CPT: pharmacometrics & systems pharmacology* **2020**, *9*, 21-28.

36. Hanke, N.; Frechen, S.; Moj, D.; Britz, H.; Eissing, T.; Wendl, T.; Lehr, T. PBPK models for CYP3A4 and P-gp DDI prediction: a modeling network of rifampicin, itraconazole, clarithromycin, midazolam, alfentanil, and digoxin. *CPT: pharmacometrics & systems pharmacology* **2018**, *7*, 647-659.

37. Nguyen, L.; Holland, J.; Ramies, D.; Mamelok, R.; Benrimoh, N.; Ciric, S.; Marbury, T.; Preston, R.A.; Heuman, D.M.; Gavis, E.; et al. Effect of Renal and Hepatic Impairment on the Pharmacokinetics of Cabozantinib. *J Clin Pharmacol* **2016**, *56*, 1130-1140, doi:10.1002/jcph.714.

38. Edginton, A.N.; Willmann, S. Physiology-based simulations of a pathological condition. *Clinical pharmacokinetics* **2008**, *47*, 743-752.

39. Johnson, T.N.; Boussery, K.; Rowland-Yeo, K.; Tucker, G.T.; Rostami-Hodjegan, A. A semi-mechanistic model to predict the effects of liver cirrhosis on drug clearance. *Clinical pharmacokinetics* **2010**, *49*, 189-206.

40. George, J.; Murray, M.; Byth, K.; Farrell, G.C. Differential alterations of cytochrome P450 proteins in livers from patients with severe chronic liver disease. *Hepatology* **1995**, *21*, 120-128.

41. Martignoni, M.; Groothuis, G.M.; de Kanter, R. Species differences between mouse, rat, dog, monkey and human CYP-mediated drug metabolism, inhibition and induction. *Expert opinion on drug metabolism & toxicology* **2006**, *2*, 875-894.

42. Colclough, N.; Ruston, L.; Wood, J.M.; MacFaul, P.A. Species differences in drug plasma protein binding. *MedChemComm* **2014**, *5*, 963-967.

43. Lin, Q.M.; Li, Y.H.; Lu, X.R.; Wang, R.; Pang, N.H.; Xu, R.A.; Cai, J.P.; Hu, G.X. Characterization of Genetic Variation in CYP3A4 on the Metabolism of Cabozantinib in Vitro. *Chem Res Toxicol* **2019**, *32*, 1583-1590.

44. U.S. Food and Drug Administration. CABOMETYX (cabozantinib) Tablets. Chemistry Review(s) 2015; https://www.accessdata.fda.gov/drugsatfda_docs/nda/2016/208692Orig1s000ChemR.pdf (accessed on 2020 Jan 15).

45. Ipsen Biopharmaceuticals Canada Inc. CABOMETYX Product Monograph. 2019; https://ipsen.com/websites/IPSENCOM-PROD/wp-content/uploads/sites/18/2019/11/21094828/Cabometyx-PM-EN-07Nov2019.pdf (accessed on 2020 Jan 15).

46. Deo, A.K.; Prasad, B.; Balogh, L.; Lai, Y.; Unadkat, J.D. Interindividual variability in hepatic expression of the multidrug resistance-associated protein 2 (MRP2/ABCC2): quantification by liquid chromatography/tandem mass spectrometry. *Drug Metab Dispos* **2012**, *40*, 852-855.

47. Rodgers, T.; Leahy, D.; Rowland, M. Physiologically based pharmacokinetic modeling 1: predicting the tissue distribution of moderate-to-strong bases. *J Pharm Sci* **2005**, *94*, 1259-1276.

48. Rodgers, T.; Rowland, M. Physiologically based pharmacokinetic modelling 2: predicting the tissue distribution of acids, very weak bases, neutrals and zwitterions. *J Pharm Sci* **2006**, *95*, 1238-1257.

49. Kroiss, M.; Megerle, F.; Kurlbaum, M.; Zimmermann, S.; Wendler, J.; Jimenez, C.; Lapa, C.; Quinkler, M.; Scherf-Clavel, O.; Habra, M.A. Objective response and prolonged disease control of advanced adrenocortical carcinoma with cabozantinib. *J Clin Endocrinol Metab* **2020**, *105*, 1461-1468.

50. Abbiati, R.A.; Manca, D. Enterohepatic Circulation Effect in Physiologically Based Pharmacokinetic Models: The Sorafenib Case. *Ind. Eng. Chem. Res.* **2017**, *56*, 3156-3166.

51. European Medicines Agency. Assessment report Cometriq. 2013; https://www.ema.europa.eu/en/documents/assessment-report/cometriq-epar-public-assessment-report_en.pdf (accessed on 2019 Oct 09).

52. European Medicines Agency. CHMP assessment report Cabometyx. 2016; https://www.ema.europa.eu/en/documents/assessment-report/cabometyx-epar-public-assessment-report_en.pdf (accessed on 2019 Oct 09).

53. Schinkel, A.H.; Jonker, J.W. Mammalian drug efflux transporters of the ATP binding cassette (ABC) family: an overview. *Advanced drug delivery reviews* **2012**, *64*, 138-153.

54. D'Angelo, A.; Sobhani, N.; Bagby, S.; Casadei-Gardini, A.; Roviello, G. Cabozantinib as a second-line treatment option in hepatocellular carcinoma. *Expert Rev Clin Pharmacol* **2020**, *13*, 623-629.

55. Fuhr, L.M.; Marok, F.Z.; Hanke, N.; Selzer, D.; Lehr, T. Pharmacokinetics of the CYP3A4 and CYP2B6 Inducer Carbamazepine and Its Drug–Drug Interaction Potential: A Physiologically Based Pharmacokinetic Modeling Approach. *Pharmaceutics* **2021**, *13*, 270.

56. Castellano, D.; Maroto, J.P.; Benzaghou, F.; Taguieva, N.; Nguyen, L.; Clary, D.O.; Jonasch, E. Exposure-response modeling of cabozantinib in patients with renal cell carcinoma: Implications for patient care. *Cancer treatment reviews* **2020**, *89*.

57. Roberts, M.S.; Magnusson, B.M.; Burczynski, F.J.; Weiss, M. Enterohepatic circulation. *Clin. Pharmacokinet.* **2002**, *41*, 751-790.

58. van Erp, N.P.; Gelderblom, H.; Guchelaar, H.-J. Clinical pharmacokinetics of tyrosine kinase inhibitors. *Cancer Treat Rev* **2009**, *35*, 692-706.

59. Miles, D.; Jumbe, N.L.; Lacy, S.; Nguyen, L. Population pharmacokinetic model of cabozantinib in patients with medullary thyroid carcinoma and its application to an exposure-response analysis. *Clinical pharmacokinetics* **2016**, *55*, 93-105.

60. Spinella, R.; Sawhney, R.; Jalan, R. Albumin in chronic liver disease: structure, functions and therapeutic implications. *Hepatology international* **2016**, *10*, 124-132.

61. Carvalho, J.R.; Machado, M.V. New insights about albumin and liver disease. *Annals of hepatology* **2018**, *17*, 547-560.

62. Cheeti, S.; Budha, N.R.; Rajan, S.; Dresser, M.J.; Jin, J.Y. A physiologically based pharmacokinetic (PBPK) approach to evaluate pharmacokinetics in patients with cancer. *Biopharmaceutics & drug disposition* **2013**, *34*, 141-154.

63. Oswald, M.; Kullak-Ublick, G.A.; Paumgartner, G.; Beuers, U. Expression of hepatic transporters OATP-C and MRP2 in primary sclerosing cholangitis. *Liver* **2001**, *21*, 247-253.

64. Pauli-Magnus, C.; Meier, P.J. Hepatobiliary transporters and drug-induced cholestasis. *Hepatology* **2006**, *44*, 778-787.

65. Borst, P.; Zelcer, N.; Van De Wetering, K. MRP2 and 3 in health and disease. *Cancer letters* **2006**, *234*, 51-61.

66. Schrenk, D.; Baus, P.R.; Ermel, N.; Klein, C.; Vorderstemann, B.; Kauffmann, H.-M. Up-regulation of transporters of the MRP family by drugs and toxins. *Toxicol Lett* **2001**, *120*, 51-57.

67. Kullak-Ublick, G.A.; Stieger, B.; Meier, P.J. Enterohepatic bile salt transporters in normal physiology and liver disease. *Gastroenterology* **2004**, *126*, 322-342.

68. Mottino, A.D.; Catania, V.A. Hepatic drug transporters and nuclear receptors: regulation by therapeutic agents. *World journal of gastroenterology: WJG* **2008**, *14*, 7068.

3 A Physiologically-Based Pharmacokinetic Model of Ruxolitinib and Posaconazole to Predict CYP3A4-Mediated Drug–Drug Interaction Frequently Observed in Graft versus Host Disease Patients

Bettina Gerner, Fatemeh Aghai-Trommeschlaeger, Sabrina Kraus, Götz Ulrich Grigoleit, Sebastian Zimmermann, Max Kurlbaum, Hartwig Klinker, Nora Isberner, Oliver Scherf-Clavel

Reprinted from Pharmaceutics 14(12): 2556, 2022

Abstract

Ruxolitinib (RUX) is approved for the treatment of steroid-refractory acute and chronic graft versus host disease (GvHD). It is predominantly metabolized via cytochrome P450 (CYP) 3A4. As patients with GvHD have an increased risk of invasive fungal infections, RUX is frequently combined with posaconazole (POS), a strong CYP3A4 inhibitor. Knowledge of RUX exposure under concomitant POS treatment is scarce and recommendations on dose modifications are inconsistent. A physiologically based pharmacokinetic (PBPK) model was developed to investigate the drug–drug interaction (DDI) between POS and RUX. The predicted RUX exposure was compared to observed concentrations in patients with GvHD in the clinical routine. PBPK models for RUX and POS were independently set up using PK-Sim® Version 11. Plasma concentration-time profiles were described successfully and all predicted area under the curve (AUC) values were within 2-fold of the observed values. The increase in RUX exposure was predicted with a DDI ratio of 1.21 (Cmax) and 1.59 (AUC). Standard dosing in patients with GvHD led to higher RUX exposure than expected, suggesting further dose reduction if combined with POS. The developed model can serve as a starting point for further simulations of the implemented DDI and can be extended to further perpetrators of CYP-mediated PK-DDIs or disease-specific physiological changes.

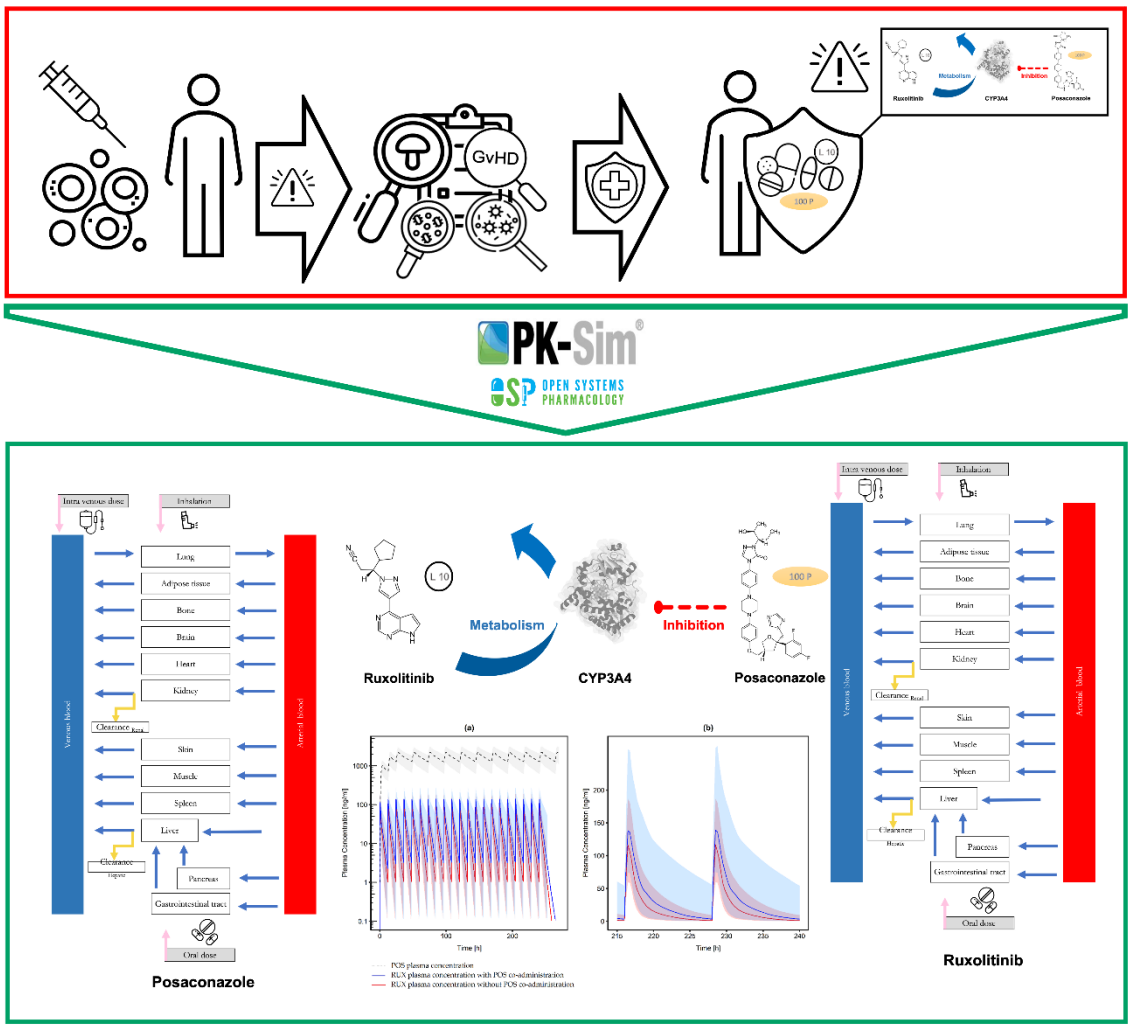

Graphical Abstract

1. Introduction

Ruxolitinib (RUX) is an orally administered multi-kinase inhibitor with potent and selective inhibitory activity against Janus-associated kinases (JAK) 1 and 2 and is approved for the treatment of myelofibrosis and polycythemia vera. In 2019 and 2021, the U.S. Food and Drug Administration (FDA) extended the indication to the treatment of steroidrefractory acute and chronic graft versus host disease (GvHD), respectively. The European Medicines Agency (EMA) approved RUX for the treatment of GvHD in March 2022. GvHD is the most common life-threatening complication after allogeneic hematopoietic stem cell transplantation (allo-HSCT) and a challenge to successful transplant outcomes [1,2]. Acute GvHD mainly affects the skin, liver, and gastrointestinal tract. Despite prophylaxis with immunosuppressive agents, about half of the patients undergoing allo-HSCT develop acute GvHD and 30–70% develop chronic GvHD [1,3–5]. For first-line treatment of moderate to severe acute and chronic GvHD,

systemically high-dosed glucocorticoids are used [6]. However, less than half of the patients treated for acute and only 40–50% of patients treated for chronic GvHD respond to the treatment, respectively [1].

Invasive fungal infections play a major role regarding mortality and morbidity after allo-HSCT [7]. Therefore, antifungal primary prophylaxis is crucial to improve outcomes. Posaconazole (POS) has been shown to be superior to fluconazole for antifungal prophylaxis in GvHD patients and is therefore frequently used [8,9]. It is a potent inhibitor of cytochrome P450 (CYP) 3A4 (IC50 = 1.5 μM) and can lead to a strong increase in the exposure of CYP3A4 substrates [10–12]. POS is classified a Biopharmaceutical Classification System (BCS) Class II compound with solubility-limited pharmacokinetics and slow absorption and distribution. Oral bioavailability of POS is highly dependent on the formulation. RUX is a BCS Class I compound, characterized by high permeability, high solubility, and rapid dissolution. RUX is metabolized by CYP3A4 (>50%) and to a lower extent by CYP2C9. Consequently, RUX elimination is susceptible to drug–drug interactions (DDI) if co-administered with POS, potentially increasing RUX exposure. Very common adverse events of RUX are blood- (e.g., anemia, thrombocytopenia, neutropenia) and lymphatic system disorders. In addition, JAK inhibition increases the probability of invasive fungal infections by impacting immune cells (e.g., dendritic cells, T cells), thus contributing to immunosuppression [13,14]. RUX is commonly dosed 10 mg twice daily (BID) in GvHD patients. Due to the high probability of concomitant administration of strong CY3A4 inhibitors (e.g., calcineurin inhibitors, azoles) a lower RUX dose compared to myelofibrosis treatment was chosen for the pivotal studies in GvHD patients without a formal dose-finding study [15]. Dose adjustment is recommended for safety reasons and is based on platelet count, absolute neutrophil count, and total bilirubin elevation. Increased RUX plasma levels due to CYP3A4 or dual CYP2C9/3A4-inhibition may lead to a higher occurrence of adverse events, which is an additional burden in the vulnerable population of GvHD patients.

However, different recommendations regarding dose adjustments for the combination of RUX with strong CYP3A4 inhibitors (e.g., ketoconazole, POS) or dual CYP2C9/3A4 inhibitors (fluconazole) are given by the FDA and EMA. Based on studies with the FDA index inhibitors ketoconazole and fluconazole, the EMA summary of product characteristics (SmPC) recommends a general dose reduction of the RUX single daily dose by 50% with concurrent strong CYP3A4 inhibitors or dual CYP2C9/3A4 inhibitors, regardless of the indication [15–17]. In contrast, the FDA label distinguishes between myelofibrosis, polycythemia vera, and GvHD. For GvHD patients, a reduced RUX starting dose of 5 mg BID is only recommended if it is co-administered with fluconazole, whereas dose adjustments when used concomitantly with strong CYP3A4 inhibitors are explicitly excluded. So far, no investigations have been

conducted of the combination of RUX and POS. According to FDA and EMA, physiologically based modeling (PBPK) is a powerful tool to qualitatively and quantitatively analyze the impact of DDI and can be used in lieu of clinical studies [16,18–21]. In recent years, drug submissions containing PBPK analyses to investigate DDI have significantly increased (to 60%) [20,22]. In general, FDA analysis of regulatory submissions shows that the PBPK model approach has good performance in predicting the effect of CYP3A4 inhibition on the pharmacokinetics of drug substrates [20,21,23]. So far, PBPK modeling is not applied in the clinical routine even though it can be used to guide dose adjustment by predicting the potential DDI of concurrently administered perpetrators and victims. As no investigations have been conducted of the combination of RUX and POS so far, the aim of this work was to develop a PBPK model to describe changes in RUX exposure due to CYP3A4-inhibition by POS. The developed DDI model was used to compare simulated RUX exposure in healthy individuals to observed concentrations in patients treated for aGvHD or cGvHD in the routine clinical setting.

2. Materials and Methods

2.1. Software

Version 11 of the freely available software PK-Sim®, which is part of the Open Systems Pharmacology Suite (Bayer Technology Services, Leverkusen, Germany) [24], was used for POS and RUX model building. Parameter optimization using the integrated Monte Carlo algorithm and sensitivity analyses were also performed with PK-Sim®. Extraction of clinical study data from published literature was conducted with the semi-automated tool WebPlotDigitizer (Version 4.3, Ankit Rohatgi, Pacifica, CA, USA). For plot generation, R Studio Version 1.1.383 (RStudio Incorporation, Boston, MA, USA) running R version 3.6.3 (R Foundation for Statistical Computing, Vienna, Austria, 2020) [25] was used. All statistical calculations and investigation of model performance were carried out with Microsoft Excel 2016 Version 16.0 (Microsoft Corporation, Redmond, WA, USA).

2.2. Posaconazole Model Development

An extensive literature research was conducted to obtain physicochemical properties (e.g., molecular weight, lipophilicity, pKa, solubility at different pH values) of POS. Human intravenous (i.v.) data from five clinical studies comprising different dose regimens (50 mg, 100 mg, 200 mg, 250 mg, and 300 mg) were used for the development of the initial model [26]. Different methods for the calculation of tissue distribution and cellular permeability were evaluated and values obtained from literature for lipophilicity (LogP) [27], fraction unbound in

plasma(fu_p) [28], and for the catalytic rate constant (kcat) for UGT1A4 [29] were integrated and optimized in a stepwise approach, if necessary. In addition, the influence of glomerular filtration rate (GFR) fraction and biliary clearance was investigated. The model was tested with human i.v. data from a 300 mg single dose (SD) clinical study [30]. POS is available as suspension (SUS) (40 mg/mL), delayed-release SUS (30 mg/mL), delayed release tablet (DR-tablet) (100 mg per tablet) and i.v. formulation (18 mg/mL). The delayed-release SUS was approved only recently (Noxafil® 300 mg PowderMix, FDA: May 2021 and EMA: January 2022) and was therefore not used for model building. As the DR-tablet is less susceptible to changes in gastric conditions or pH-dependent precipitation, two different formulations were modeled for the POS SUS and DR-tablet [31]. The DR-tablet was modeled using concentration-time data from two clinical studies [32,33]. Optimized parameters consisted of intestinal solubility, specific intestinal permeability, and the formulation (time to 50% dissolution, lag time, and dissolution profile). To account for the higher POS exposure after administration of the DR-tablet, the intestinal solubility was adapted in all tablet simulations and fitted to the physiological pH changes along the gastrointestinal tract [34]. POS SUS was modeled using training datasets from two SD [35,36] clinical studies and one multiple dose (MD) [35] clinical study. Particle dissolution was used to model POS SUS. Specific intestinal permeability, solubility at different pH values, and gain per charge were obtained from literature and optimized accordingly to better fit the data. For POS SUS, supersaturation was enabled to account for the precipitation behavior of POS upon entering the small intestine [27]. The precipitated drug was treated as "soluble" so that the precipitated POS amount was added to the solid drug mass. Thereby, the solid fraction available for dissolution and the particle size were increased and the poor solubility in the intestines was modeled more accurately. The thickness of the unstirred water layer and the particle radius were optimized to better simulate the poor solubility of POS SUS in the intestinal pH environment.

The parameters were tested using SD and MD data from clinical studies [32,35,37], as shown in Table S1. Virtual mean human individuals were created according to the demographics of the respective studies and used in the simulations. A summary of each study regarding the demographics, administration protocols, and their assignment to training or test datasets is documented in Table S1 of the Electronic Supplementary Materials (ESM). A schematic workflow of the POS model development and evaluation including optimized parameters is shown in Figure 1.

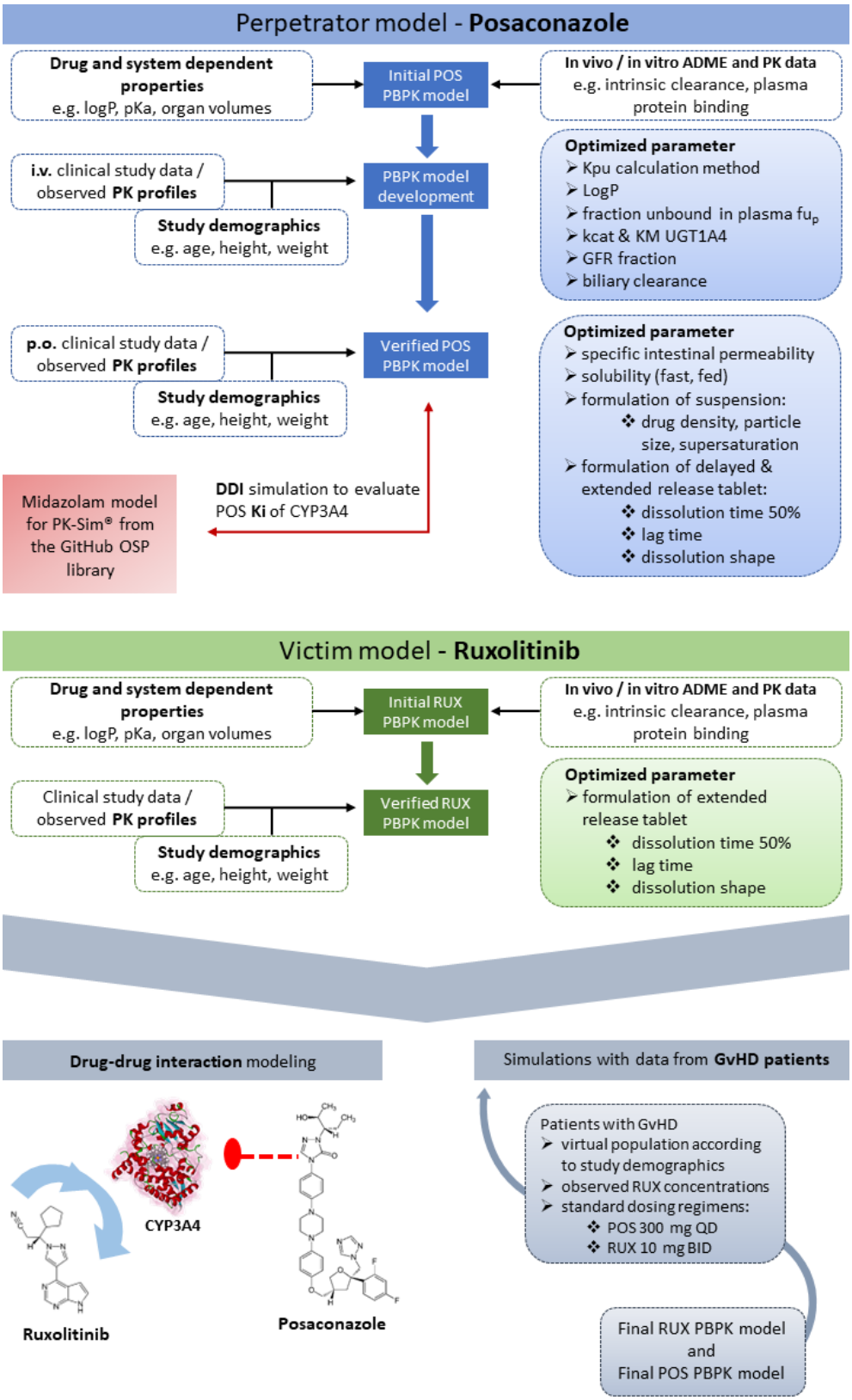

Figure 1. Schematic workflow showing the development and evaluation of the perpetrator (POS) and victim (RUX) PBPK models, which were developed separately. Initial model development started with basic input parameters from the literature. Parameters optimized during model building are shown in the blue and green rectangles, respectively. The final input parameters are given in Tables S2 and S6. The entire model building and evaluation process was supported using clinical study data, used either as training or test dataset (see Tables S1 and S5 for allocation). The final POS and RUX models were applied to simulate DDI between these substances and simulations with data obtained from GvHD patients were conducted (see gray rectangle).

2.3. Ruxolitinib Model Development

Physicochemical data of RUX obtained by extensive literature search were used as initial input parameters. The RUX model was developed based on eleven datasets from three clinical studies, covering a dose range from 10 to 100 mg. In these studies, RUX was administered orally in different dose regimens (QD, BID, TID), in single or multiple dose scenarios. Four SD clinical studies were used as training datasets [38]. Formulation-related parameters were optimized to model the extended-release tablet (time to 50% dissolution, lag time, and shape of dissolution profile) (Figure 1). The model was tested using data from two SD [39] and five MD clinical studies [40]. A summary of each study regarding the demographics, administration protocols, and the allocation to either the training or the test dataset is given in Table S5 of the ESM.

2.4. Model Evaluation

RUX and POS PBPK models were evaluated using various methods according to the guidelines on the reporting of PBPK modeling by the EMA and FDA [19,41]. For a first visual interpretation of the model performance, the trajectories of the predicted plasma concentrations were compared to the respective observed profiles. Goodness-of-fit plots were generated in which the predicted and observed plasma concentrations, predicted and observed maximum concentrations (C_{max}), as well as the predicted areas under the systemic drug concentration–time curve from time zero to the time of the last concentration (AUC_{last}) were compared. Prediction error (PE) (Equation (1)), mean prediction error (MPE) (Equation (2)) and mean absolute prediction error (MAPE) (Equation (3)) were calculated to evaluate model accuracy and precision.

$$PE\ [\%] = \frac{Cpredicted,i - Cobserved,i}{Cobserved,i}\ x\ 100\% \quad (1)$$

$$MPE\ [\%] = \frac{Cpredicted,i - Cobserved,i}{Cobserved,i}\ x\ 100\% \quad (2)$$

$$MAPE\ [\%] = \frac{Cpredicted,i - Cobserved,i}{Cobserved,i}\ x\ 100\% \quad (3)$$

Mean relative deviation (MRD, Equation (4)), defined as the average distance of the observed plasma concentration values from the predicted values on a logarithmic scale [42], was calculated for a quantitative measure of model performance. MRD values ≤ 2 were considered

acceptable and characterize an adequate model performance in the case that the average of the predicted values was equal to or less than a factor of 2 of the observed values.

$$MRD = 10^{x}; x = \sqrt{\frac{1}{n}\sum_{i=1}^{n}(log_{10}c_{predicted,i} - log_{10}c_{observed,i})^{2}} \quad (4)$$

Abbreviations in Equations (1)–(4) are as follows: $c_{predicted,i}$ = predicted plasma concentration, $c_{observed,i}$ = corresponding observed plasma concentration, n = number of observed values. Local sensitivity analysis of single parameters of the POS and RUX models was performed, measured as relative changes of AUC_{last} or C_{max}. The sensitivity analysis of parameters that had been optimized or might have had a strong influence on the models due to the calculation methods in PK-Sim® was conducted with a variation range of 10.0 and a maximum number of 9 steps.

2.5. Drug–Drug Interaction between Posaconazole and Midazolam

To evaluate the inhibitory constant (Ki) of POS for the competitive inhibition of CYP3A4, the developed POS model was combined with a published and evaluated PBPK model for midazolam (MDZ) [43]. Plasma-concentration time profiles from a phase 1 interaction study after i.v. and oral administration of MDZ either given alone or in combination with 200 mg or 400 mg oral POS were used to investigate the effect of oral POS on MDZ exposure. The clinical studies used for DDI modeling of POS and MDZ are summarized in Table S9. The quality of the DDI interaction modeling was evaluated in a stepwise approach. First, the respective plasma concentration-time profiles were visually compared. For a quantitative evaluation, the ratios of AUC_{last} and C_{max} for the administration of i.v. and oral MDZ alone or together with its perpetrator, respectively, were calculated according to Equations (5) and (6). The calculated DDI ratios were compared in each case with the respective values reported by Krishna et al. [44].

$$DDI\ AUC_{last}\ ratio = \frac{AUC_{last}\ MDZ\ in\ combination\ with\ POS}{AUC_{last}\ MDZ\ alone} \quad (5)$$

$$DDI\ C_{max}\ ratio = \frac{C_{max}\ MDZ\ in\ combination\ with\ POS}{C_{max}\ MDZ\ alone} \quad (6)$$

2.6. Simulations in Graft versus Host Disease Patients

We used 278 serum samples from 30 patients with either acute or chronic GvHD receiving any dose regimen of RUX collected between February 2019 and February 2021 at the University Hospital of Würzburg as part of a non-interventional prospective clinical trial. The study was approved by the Ethics Commission of the University of Würzburg (ref 199/18-am). All performed procedures were in accordance with the Declaration of Helsinki. Written informed consent was obtained from all patients. RUX dosage, time of last intake, time of sampling, and additional co-medications were recorded during the study. POS dosage was documented during data collection, yet the time of last intake was missing. It was assumed that POS was taken at the same time as RUX and that the concentrations were obtained in a steady state. RUX and POS concentrations were measured in human serum using previously published liquid chromatography methods [45,46]. As the PBPK model was developed and evaluated for interaction between POS and RUX, the dataset was filtered for patients receiving POS as antifungal prophylaxis. Moreover, patients receiving RUX without any strong or moderate CYP3A4 inhibitor were filtered, and simulations for patients receiving RUX with and without its perpetrator POS were conducted separately. One hundred and sixty-three of the RUX concentrations from 19 patients were obtained under concomitant POS administration; 27 RUX concentrations from 7 patients were obtained without the co-administration of POS. All simulations were based on the standard daily RUX dose of 20 mg daily (10 mg BID). For all simulations in GvHD patients, a virtual population (n = 100) according to the study demographics was built. Information on the baseline patient demographics can be found in Table S10.

3. Results

3.1. Posaconazole PBPK Model Building and Evaluation

The best results were obtained for a combination of the Poulin and Theil distribution methods and PK-Sim® standards for distribution method and cellular permeability, respectively. Based on the i.v. data, values for fu_p, lipophilicity, the katalytic rate constant for UGT1A4, and the specific biliary clearance were optimized to get a better fit of predicted versus observed concentrations. The i.v. model was extended to include oral data after administration of POS suspension (SUS) and delayed release tablet (DR-tablet). The specific permeability calculated based on molecular weight and lipophilicity of the substance within the PK-Sim® software ($1.81 \times 10{-}4$ cm/min) was further optimized in fasted and fed state ($5.05 \times 10{-}5$ cm/min) and used for SUS simulations [47,48]. High-fat or non-fat meal events were modeled with 841 kilo calories (kcal) or 200 kcal, as reported by Courtney et al. [37].

For the DR-tablet simulations, the specific permeability was 4.80 × 10−5 cm/s. POS SUS was modeled using particle dissolution with supersaturation enabled and the DR-tablet was modeled using the Weibull function. Particle radius (1.9 µm), thickness of unstirred water (140 µm), dissolution time (145 min), lag time (30 min), dissolution shape (1.67), and drug density (0.37 g/cm^3) were estimated using parameter identification or improved by manual adjustment. The final parameters used for the POS PBPK model are shown in Table S2.

The final PBPK model was successfully used to describe the observed POS plasma concentrations after single and multiple dose administration of i.v. or oral POS. Simulated plasma profile trajectories were in close concordance with observed data in fasted as well as in fed state. Linear and semilogarithmic plots of predicted versus observed plasma concentration-time profiles after i.v., DR-tablet, or SUS administration are shown in Figure S5a–c and Figure S6a–c, respectively. The model slightly overpredicted low POS plasma concentrations at later times after dosing (see goodness-of-fit plot, Figure S1); 90.44% of all simulated plasma concentrations fell within 2-fold of the corresponding concentrations observed. Separate goodness-of-fit plots for i.v., DR-tablet, and SUS can be found in Figure S2a–c. All predicted AUC_{last} and 95% of the predicted C_{max} values were within the 2-fold acceptance criterion (Figure S3). For the i.v. simulation, a MRD of all predicted plasma concentrations ≤2.0 was achieved in all simulations (MRD range 1.42–1.75) and 87.3% of all simulated plasma concentrations were within 2-fold of the corresponding concentrations observed. The MPE range was −29.65% to 39.60% and the MAPE range was 25.01% to 46.50% (Table S4). Oral simulations of different dosing regimens either in fasted or fed state after DR-tablet or SUS administration had a MRD of 1.52 (1.19–2.36) with 12/13 simulations ≤ 2.0, while 91.72% of simulated plasma concentrations after SUS administration and 91.67% after DR-tablet administration were within 2-fold of the corresponding concentration observed. Ratios for predicted versus observed values were 0.66 to 1.44 (AUC_{last}) and 0.55 to 2.26 (C_{max}) (Table S3). The local sensitivity analysis revealed that variation in lipophilicity had the greatest impact on changes in AUC_{last} after a 100 mg POS single tablet administration, followed by fu_p (Figure S4).

3.2. Ruxolitinib PBPK Model Building and Evaluation

For the RUX PBPK model, several calculation methods for tissue distribution and cellular permeabilities were tested during model development. The best results were obtained for the Rodgers and Rowland tissue distribution [49,50] in combination with the PK-Sim® standard method for the calculation of cellular permeabilities. Drug-dependent parameters such as lipophilicity, solubility, and fu_p found in the literature were appropriate and not adapted. According to Umehara et al., biliary and renal excretion are negligible and were therefore not

implemented into our model [51]. CYP2C9 and CYP3A4 metabolizing enzymes were included and a first order process for the metabolic enzyme activity was chosen, which fully covered RUX elimination. The specific clearance used in the simulations was 0.65 L/µmol/min for the CYP2C9 process and 0.46 L/µmol/min for the CYP3A4 process and was calculated based on the in vitro intrinsic clearance by Umehara et al. [51]. The integrated Weibull function was used to create an extended-release tablet and parameters for the dissolution time (15.0 min) and the dissolution shape (1.10) were adapted to fit the observed data. The best results were obtained for a dissolution time of 15 min and a dissolution shape of 1.10. All input parameters used in the final RUX PBPK model can be found in Table S6. The final RUX PBPK model successfully predicted observed RUX plasma concentrations after single as well as multiple dosing in the investigated populations (see Figure 2 for linear plots and Figure S11 for semilogarithmic plots) and 86.79% of the observed data fell within 2-fold of the corresponding concentration observed (Figure S8). Ratios for predicted versus observed values were 0.68 to 1.12 (AUC_{last}) and 0.65 to 1.04 (C_{max}) (Table S7). The model slightly underpredicted RUX exposure, as 9/11 ratios for predicted versus observed AUC_{last} were < 1. This effect was less distinct for C_{max}. Except for three simulations, all predicted C_{max} values were within +/−10% compared to the observed C_{max}. However, all predicted AUC_{last} and C_{max} values fell within the 2-fold acceptance criterion (Figure S9). The mean MRD was 1.58 (1.20 to 2.23) and 9/11 simulations fulfilled the acceptance criterion. All values for MRD, MPE, and MAPE are listed in Table S8. Local sensitivity analysis showed that the RUX model was most sensitive to fup followed by lipophilicity (see Figure S10).

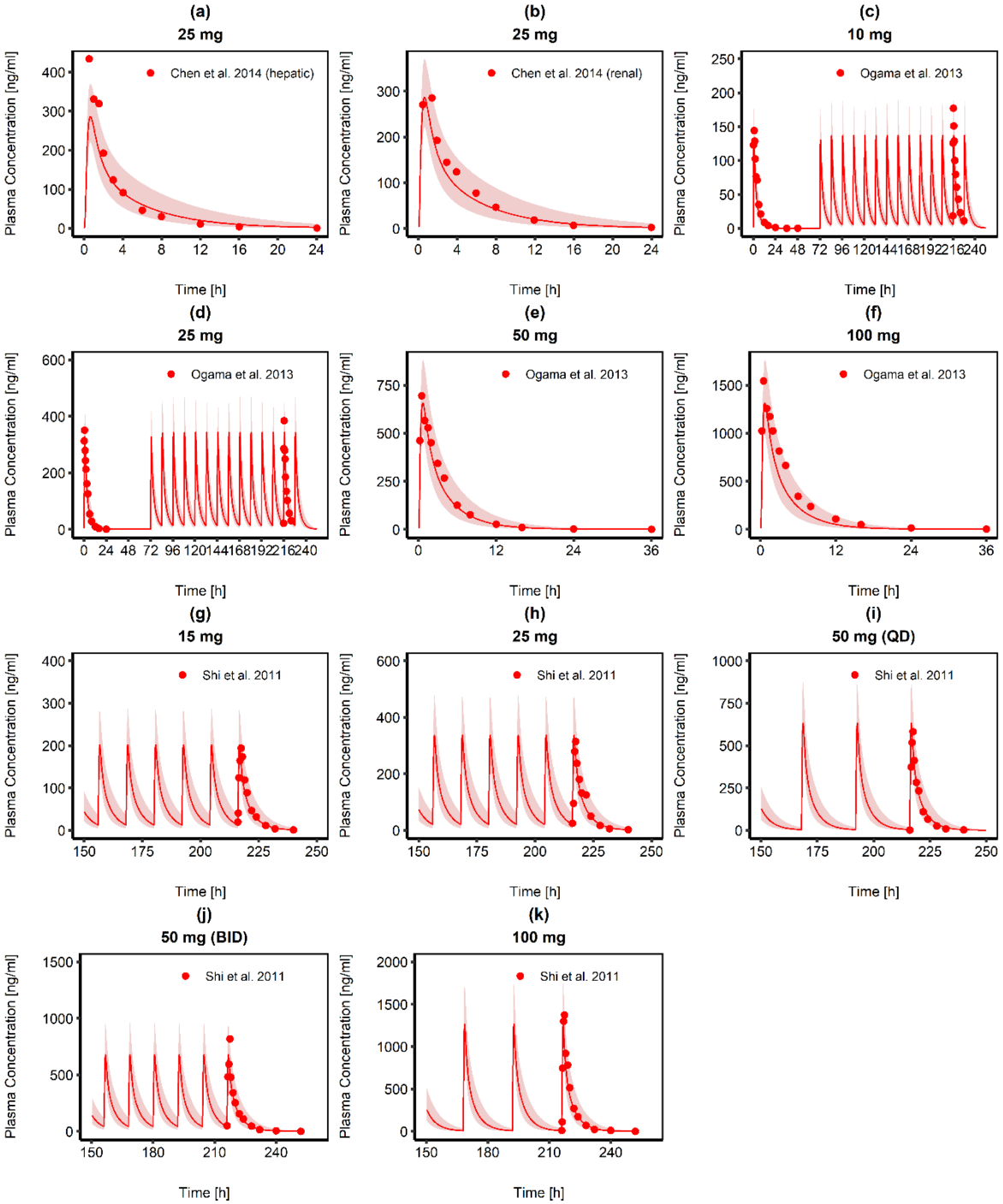

Figure 2. Predicted RUX plasma concentration-time curve profiles (solid red lines) and observed RUX concentrations (red dots), obtained after single (**a,b,e,f**) and multiple RUX tablet (**c,d,g–k**) administration. The red shaded area represents the predicted population geometric standard deviation in each case. The ESM contains detailed information about the study protocols and RUX model performance for each simulation. QD: once daily, BID: twice daily. Source: [38–40].

3.3. Drug–Drug Interaction Modeling

3.3.1. Posaconazole and Midazolam

A competitive inhibition process was assumed for the interaction of POS and MDZ with CYP3A4. POS reversibly binds to CYP3A4 and competes with MDZ for free binding sites.

All input parameters of the POS and MDZ model were transferred, expect for Ki, which was estimated. The Ki start value was taken from the literature (0.42 µM) [52]. Based on the 200 mg and 400 mg MDZ i.v. administration, Ki parameter estimation led to an optimized value of 5.22 × 10−3 µM. Comparison of 200 mg and 400 mg i.v. MDZ administration with and without concomitant POS administration can be found in Figure 3. Calculated DDI ratios for C_{max} and AUC_{last} were comparable to the ratios calculated from the respective clinical study by Krishna et al. [44] (Table 1). As Ki was estimated based on MDZ i.v. administration, as a proof-of-concept, DDI ratios were calculated for data after oral MDZ administration and were comparable to the reported values (Table 1).

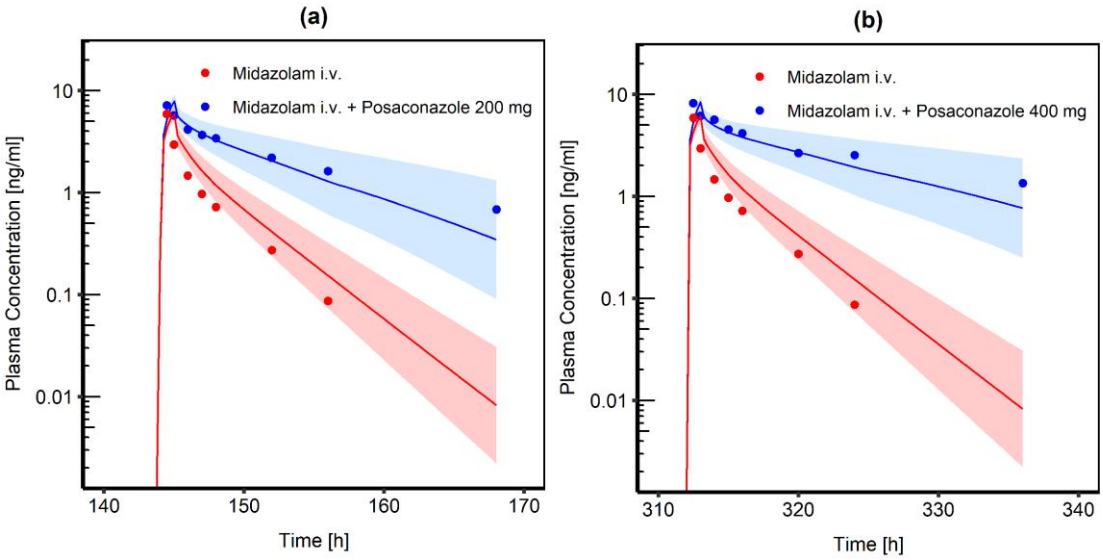

Figure 3. Comparison of simulated MDZ venous blood plasma concentration-time profiles (semilogarithmic) following i.v. administration of 0.4 mg MDZ infusion. The blue shaded area represents the geometric mean SD for population simulations of the resulting MDZ plasma concentrations if co-administered with either (**a**) 200 mg oral POS or (**b**) 400 mg oral POS and an inhibitory constant Ki = 5.22 nmol/L for the CYP3A4 interaction process. The red shaded area represents the geometric mean SD for population simulations without concomitant POS administration. Geometric means are shown as a blue line (with POS administration) or a red line (without POS administration). Observed data are shown as blue and red dots, respectively.

Table 4. DDI ratio for C_{max} and AUC_{last} calculated for the administration of MDZ together with POS.

POS	MDZ 0.4 mg i.v. SD		MDZ 2.0 mg oral SD	
DDI ratio	C_{max}	AUC_{last}	C_{max}	AUC_{last}
200 mg oral SUS	1.42[a]	3.38[a]	2.74[a]	5.54[a]
	1.30[b]	*4.42*[b]	*2.20*[b]	*4.99*[b]
400 mg oral SUS	1.41[a]	4.43[a]	3.02[a]	6.95[a]
	1.68[b]	*6.23*[b]	*2.33*[b]	*5.26*[b]

[a] DDI ratio for C_{max} and AUC_{last} calculated with MDZ and POS model. [b] values taken from literature (in vivo)

3.3.2. Posaconazole and Ruxolitinib

The resulting Ki for the inhibition of CYP3A4 was transferred to the POS model and the model was combined with the developed RUX model for DDI simulations. Simulations with a virtual population receiving 300 mg oral POS DR-tablet and 10 mg BID RUX were conducted and simulated C_{max} for RUX without POS co-administration was 116.31 ng/mL. The median C_{max} for the simulation of RUX plasma concentration if given together with its perpetrator was 20.5% higher (C_{max} = 140.21 ng/mL). Simulated RUX exposure was about 59% higher if co-administered with POS (AUC_{last} = 382.17 ng·h/mL) compared to RUX administration alone (AUC_{last} = 239.88 ng·h/mL). The calculated DDI ratio was 1.21 for C_{max} and 1.59 for AUC_{last}, respectively.

3.4. Simulation of Graft versus Host Disease Patients

In the GvHD study population, a high interindividual variability in observed RUX concentrations was seen, especially shortly after tablet intake (within five hours after RUX administration). We found 64.42% of the observed serum concentrations after 10 mg BID RUX administration in combination with POS were within the 5% to 95% prediction intervals of the corresponding simulation (Figure 4a). Even without concomitant administration of oral POS, model-predicted median RUX serum concentration for the administration of 10 mg RUX BID was lower than the serum concentrations observed in the GvHD patients of the clinical study (Figure 4b). The POS model predicted trough concentrations of 1282.16 ng/mL and maximum plasma concentrations of 2245.70 ng/mL (300 mg QD POS DR-tablet, simulated for day 10), while measured concentrations revealed a median concentration of 2392 ng/mL (range: 21–5808 ng/mL, n = 169, 300 mg QD POS DR-tablet) and 2441 ng/mL (range: 1854–2784 ng/mL, n = 8, 200 mg TID POS SUS) [53]. About half (51.25%) of the observed POS values fell within the 5% to 95% prediction interval of the simulation and 43.75% of the observed POS concentrations were above the predicted range. Simulated and observed POS serum concentrations are displayed in Figure 4c.

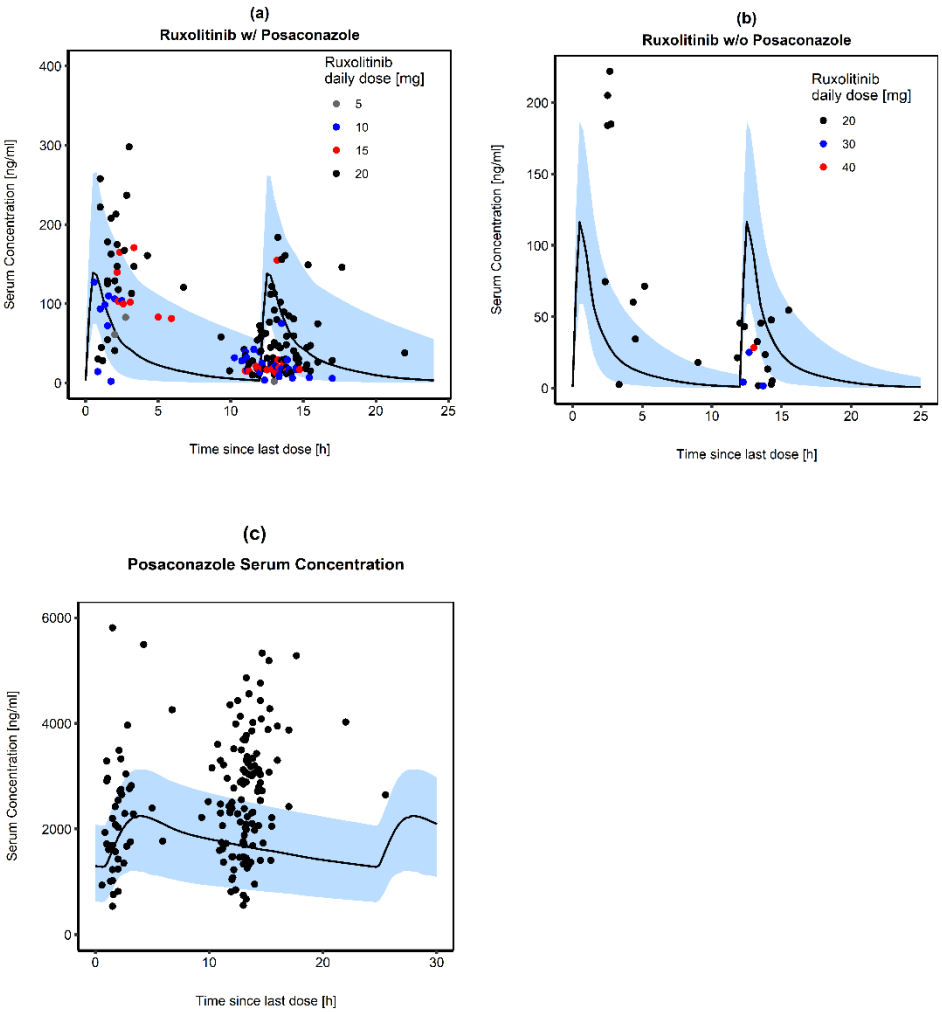

Figure 4. Comparison of simulated RUX serum concentration-time profiles following oral administration (10 mg BID) if (**a**) co-administered with 300 mg oral POS and (**b**) given without its perpetrator. Observed RUX concentrations are shown as dots with different colors, representing different RUX daily doses actually taken by the patients. Median RUX concentrations are shown as a black line in each part. Part (**c**) represents predicted (black solid line) and observed POS concentrations (black dots) after administration of 300 mg oral POS tablet once daily. The blue shaded areas represent the 5% to 95% prediction intervals for population simulations (n = 100) of the resulting RUX and POS plasma concentrations, respectively.

4. Discussion

To the best of our knowledge, this work presents the first PBPK models for POS and RUX using PK-Sim® developed for application in the clinical routine. Seven PBPK models using different PBPK software (SimCYP® (Certara Holdings Ltd., Sheffield, UK) or GastroPlus (SimulationsPlus, Lancaster, CA, USA) have been published for POS [27,54–59]. Only three were developed to model potential DDI with one being developed for application to the clinical routine. The remaining models were developed for the assessment of bioequivalence or to describe POS behavior in the gastrointestinal (GI) tract. In the literature, feasibility of the PBPK approach has been shown for RUX and the index inhibitors ketoconazole and fluconazole using

SimCYP®, and the findings were compared to clinically performed DDI studies as a proof-of-concept to support regulatory submissions [60,61]. However, no investigations on the combination of RUX with POS have been conducted so far; yet this is of significant clinical interest because POS is frequently co-administered with RUX in patients with aGvHD and cGvHD [9].

The developed PBPK DDI model predicted an increase in RUX C_{max} and AUC_{last} by 20.5% and 59%, respectively, due to the concomitant POS administration. Using the web-based DDI predictor (https://www.ddi-predictor.org/, accessed on 9 September 2022) with RUX as substrate and POS 300 mg daily as interactor, an increase in AUC ratio of 1.35 was estimated (95% prediction interval 0.96–1.89). Our AUC_{last} ratio of 1.59 is within the proposed prediction interval.

Using measured RUX and POS concentrations in our study population, we were able to evaluate the predicted concentrations, and 64.42% of the observed RUX concentrations (Figure 4a) and 51.25% of the observed POS concentrations (Figure 4c) were within the prediction intervals. Approximately one-third of the observed values lay outside the prediction intervals for two main reasons. As we used data obtained in daily clinical routines, it was not 100% certain whether all concentrations were really trough levels or whether a new dose had already been taken, as is simulated in Figure 4a. This was especially the case for concentrations observed between 12 and 15 h since the last dose. Secondly, we would like to mention the following: even though the PBPK model included the potential DDI, a greater proportion of the observed RUX concentrations in patients receiving 10 mg RUX BID concomitantly with POS were above the predicted median RUX concentration. The observed data are real-life data and were not obtained within a controlled DDI study. Thus, observed concentrations were not only influenced by the DDI between RUX and POS but also by the complex disease, comorbidities, and numerous further medications taken by the patients. Isberner et al. reported a higher RUX exposure in GvHD patients compared to myelofibrosis patients, which was attributed to a lower clearance, which was also reported by Chen et al. (50% and 66.7%, respectively) [53,62]. Isberner et al. allocated the reduced clearance to further DDI caused by a combination of several moderate and weak CYP3A4 or CYP2C9 inhibitors (e.g., atorvastatin and amiodarone) and changes in hepatic clearance due to liver dysfunction, which is, however, hypothetical.

They also observed an additional reduction of RUX clearance by 15% due to comedication with at least one strong CYP3A4 inhibitor, suggesting that in aGvHD and cGvHD patient dose modification may be necessary [53]. This is in accordance with our findings, as concentrations obtained from patients receiving a lower RUX dose (5 mg QD, BID and TID, respectively) were significantly closer to the predicted median RUX concentration

(Figure 4a) and within the 5% to 95% prediction intervals of the model simulation in healthy individuals (10 mg BID).

Thus, the explicit exclusion of dose reduction in aGvHD and cGvHD patients recommended by the FDA seems to lead to overexposure in a considerable proportion of patients. It may be for this reason that the EMA advises a general dose reduction by approximately 50% of the unit RUX dose if co-administered with strong CYP3A4 inhibitors such as ketoconazole and POS or dual CYP2C9/3A4 inhibitors such as fluconazole. In the EMA SmPC, ketoconazole and POS are both listed as strong CYP3A4 inhibitors without consideration of their exact inhibitory potency towards CYP3A4. However, our study showed that POS has a lower impact on RUX exposure compared to ketoconazole (C_{max} and AUC_{last} 33% and 91%, respectively) [61] and fluconazole (C_{max} and AUC_{last} 47% and 234%) [60], suggesting that a 50% unit dose adjustment may not be appropriate in general for the azoles mentioned and dose modifications should also be adapted to the individual patient, according to his or her further medication and etiopathology.

Taken together, observed concentrations outside the prediction intervals are likely due to imprecisions in the measured values, due to limitations within the model, and due to the physiological specifics of GvHD patients. Deviations between predicted and observed RUX concentrations in the clinical routine may be caused by the study design because time of last dose intake and time of sampling were reported by the patient and the nurse, respectively, which is susceptible to bias. In addition, the primarily aim of the conducted study was to observe RUX concentrations in GvHD patients and measurement of POS concentrations was added by amendment. Therefore, it is not fully clear when POS was taken with respect to sampling. The best approximation was the assumption that POS tablet or SUS were taken at the same time as RUX, which may not be true for all events. In addition, PK studies used to obtain observed concentrations for POS and RUX model development did not contain raw data. A digitizing software was used, which is a common procedure, yet it is a source of potential imprecision. Further, allo-HSCT patients receive extensive co-medication and often have renal or hepatic impairments resulting from chemotherapy, radiation, or GvHD. GvHD also affects the GI mucosa, which may affect the absorption processes, leading to the observed variabilities in the POS and RUX exposure. In addition, the underlying disease and patients are heterogenous. So far, no quantitative disease model for GvHD exists, which is why the specific physiological alterations of these patients could not be quantitatively included in the model. Therefore, a healthy population using the demographics of the GvHD study population was used for the simulations in PK-Sim®. However, this population does not represent every individual and the full complexity of the disease and may explain observed deviations. This approach was

nevertheless chosen, as in vivo DDI studies are usually conducted in healthy individuals and, overall, the model is appropriate to predict the magnitude of DDI. As soon as more precise and quantitative knowledge about the underlying disease-specific physiological alterations is available, physiological parameters within the PBPK model can be adapted, which is a considerable benefit of PBPK modeling.

The final RUX PBPK model is characterized by good model performance, as demonstrated by comparison of predicted to observed plasma concentration-time profiles and the respective goodness-of-fit plots, the calculation of MRD values, as well as the comparison of predicted to observed AUC_{last} and C_{max} values (ESM Figures S8, S9 and S11 and Tables S7 and S8). To simulate DDI between RUX and POS, the Ki value for CYP3A4 inhibition by POS was successfully evaluated using a previously published MDZ model. The initial Ki value of POS found in literature was too high as it underpredicted the CYP inhibition process and consequently MDZ plasma concentrations. The optimized value ($5.22 \times 10{-}3$ μM) was in accordance with the Ki value optimized by Bhantnagar et al. ($5.5 \times 10{-}3$ μM) and in line with in vivo findings by Clearly and colleagues ($5 \times 10{-}3$ μM) [52,54,59].

POS model development was challenging, as in general, in silico prediction of in vivo release and exposure of BCS class II compounds and weak bases is not trivial because the in vivo drug dissolution is highly dependent on the GI physiology (e.g., bile component, amount of fluid, and pH in the GI section), which is dynamic and subject to immense inter- and intra-individual fluctuations [28,63]. The lack of published in-house data from preclinical drug development, sparse data on formulation-specific properties, missing information about the patients and the underlying diseases additionally hampered model building [22]. Nonetheless, POS SUS and the commonly used DR-tablet were successfully integrated in the model, so that the model was appropriate to describe POS exposure. Parameter identification and manual optimization were helpful to appropriately fit concentration-time data to formulation-related parameters so that observed concentration-time profiles were within the prediction intervals. Tissue distribution and cellular permeability logP, fu_p, kcat for UGT1A4, GFR fraction, and biliary clearance, which describe the PK after the absorption, were successfully described based on i.v. data only, so that inaccuracies and bias from drug absorption processes were mostly eliminated.

A high interindividual variability was observed in the measured POS concentrations but they are in accordance with values found in the literature. Cornely et al. reported a mean average concentration of 2370 ng/mL (range: 680–9520 ng/mL, once daily, 3 × 100 mg, DR-tablet, n = 210), a mean minimum plasma concentration of 2110 ng/mL (range: 445–9140 ng/mL, once daily, 3 × 100 mg DR-tablet, n = 210), and a mean maximum plasma concentration of

2390 ng/mL (coefficient of variation (CV) 43%, once daily, 3 × 100 mg, DR-tablet, n = 210) in allo-HSCT recipients [64]. Krishna et al., reported a mean average plasma concentration of 1310 ng/mL (CV 31%, 200 mg, once daily, n = 8, measured on day 14) and 2550 ng/mL (CV 38%, 200 mg twice daily, n = 8, measured on day 22), and 2360 ng/mL (CV 54%, 400 mg once daily, n = 8, measured on day 14) taking the POS DR-tablet. The observed variability in POS PK probably contributes to the observed variability in RUX PK and depending on the POS concentration, the interaction may be more or less pronounced. Based on the model, different tested POS dosage (150 mg, 300 mg, 600 mg QD) resulted in different RUX exposure (337.25, 356.51, 367.70 ng * h/mL, respectively), which is consistent with the underlying mechanism. According to the saturable mechanism of CYP inhibition, no linear but rather a saturable increase in RUX exposure can be assumed.

POS free-base has a weak basicity and is well soluble at a low pH and less soluble at a higher pH (e.g., at fasted state stomach (pH 1) 0.79 mg/mL and 0.001 mg/mL at fed state (pH 7.0)), and the absorption of POS is rate-limited by dissolution [27,36,65,66]. After dissolution in the stomach, a substantial amount of dissolved POS precipitates reaching the intestine and is therefore not available for absorption [27]. The systemic exposure of the SUS is highly dependent on food and its fat content [65]. Compared to the fasted state, AUC is four and 2.6 times greater depending on the fat content (50 g and 14 g of fat, respectively). Considering that time and amount of fat content highly impact POS exposure, it can be concluded that fat enhances dissolution of POS in the intestine. This happens either through emulsion or micelle building or due to the increased release of bile salts or lecithin. The changes in the absorption kinetics by an enhanced dissolution through fat could not be fully described by the model, leading to underprediction of the POS absorption after administration of the SUS with a high-fat or a non-fat meal. This may be attributable to the fact that PK-Sim® only allows definition of food events based on the caloric supply and no input of a specific fat content. A high-fat meal can only be added by assuming that for each g fat, 9 kcal are supplied. This is not a true illustration of the food composition and leads to imprecision. Changing the solid fraction of the meal did not improve model fit and was therefore kept at 0.8.

The POS PBPK model showed a steeper absorption phase in fasted state compared to the observed data for dosing at 800 mg and the initial dose of multiple dosing (see Supplementary Materials, semilogarithmic plots for simulations for Ezzet et al.). This may be explained by the fact, that in fasted state, the precipitation kinetics of POS is crucial and accounts for the high intersubject variability of POS plasma concentrations [35]. This is also backed up by the respective study, which showed an intersubject coefficient of variation for the absorption rate constant and bioavailability of 18–70% and 52–73%, respectively. The PBPK

model does not properly capture the precipitation in the intestines, which leads to the greater absorption. However, the observed deviation is regarded as neglectable for the intended application of the POS PBPK model because the systemic daily exposure for 200 mg multiple dosing is within the prediction interval and in clinical routine an 800 mg single dose is not applied.

Using the calculated or optimized specific permeability for the DR-tablet formulation led both to underprediction in absorption and systemic exposure. Ultimately, the intestinal permeability was adapted to model the higher bioavailability of the DR-tablet. The used specific permeability of 4.80 × 10−5 cm/s is the apparent in vitro CaCo2-cell permeability reported by Hens and colleagues [55]. It is clear that the CaCo-2 cell permeability is not equal to the effective permeability, yet Walraven and colleagues reported an in-house effective permeability of 4.02 × 10−5 cm/s, which was also similar to the CaCo2-cell permeability [67]. The higher specific intestinal permeability was sufficient to simulate a faster uptake of POS upon improved intestinal solubility and supersaturation stability when the DR-tablet was used. Using a lower specific intestinal permeability for POS SUS was sufficient to account for the fact that the dissolved amount of POS that can diffuse over the membrane over time is less if POS SUS is used. The lower specific permeability also reflects that POS is not sufficiently released from the SUS formulation and therefore not highly available for transcellular permeation. Bhatnagar and colleagues developed a PBPK model for application in the clinical routine to predict the DDI between Venetoclax and POS using SimCYP®. They faced the same issue and were able to solve the discrepancy by adjusting the effective permeability (6.41 × 10−4 cm/s), the bile micelle partitioning coefficient, and the intrinsic solubility [54]. Cristofoletti and colleagues developed a PBPK model of POS also using SimCYP® and used 3.7 × 10−4 cm/s as effective permeability [57]. The different values show that depending on the software and the studies used for parameter identification, the intestinal permeability may be different and the calculated value using molecular weight and lipophilicity may not be sufficient to predict the observed data. The observed difficulties are in line with the fact that the two formulations are not interchangeable due to differences in PK resulting from differences in solubility and permeability during GI tract passage. Sensitivity analysis further backs up these findings, as lipophilicity has an outstanding impact on AUC_{last} (−6.81).

In summary, prediction of the PK using PK-Sim® for a poor formulation is not straightforward if data concerning the solubility of the compound and the dissolution of the formulation are not available as model input parameters. Even with in vitro dissolution data, the prediction of in vivo dissolution remains challenging because knowledge about the impact of the dynamic GI environment on drug and formulation behavior is scarce [68]. Garcia et al.,

recently compared the two modeling platforms PK-Sim® and SimCYP®, building comprehensive PBPK models for simvastatin [69]. They found major differences in the implementation of absorption models, with lower complexity and flexibility regarding input of formulation and passive permeability in PK-Sim® compared to SimCYP®. SimCYP®. offers different options for the input of absorption parameters, including built-in correlation methods to scale in vitro measured values as well as the SimCYP® In Vitro data Analysis (SIVA) toolkit [70]. In PK-Sim®, on the other hand, Garcia et al. also had to estimate intestinal passive permeability and formulation dissolution parameters based on available clinical study data, as there were no other options. Expect for one patient, the GvHD study population received the POS DR-tablet and our simulations for that population were done with the DR-tablet accordingly. If POS SUS is administered instead of the DR-tablet, the expected DDI with RUX should be evaluated carefully, as we used different intestinal permeabilities to account for the different formulations. For some study populations, sparse information on the baseline patient demography was available. Only one study reported age, height, weight, and BMI of the study population [30]. One study reported age, height, and weight [33], and five studies reported data for age and either weight, height, or BMI of the study population [26,32,35–37]. To build the virtual populations in PK-Sim®, the missing demographic data were estimated, which led to imprecisions. In addition, the virtual population generated via the implemented PK-Sim® algorithm differs in some cases from the mean individual used for model building, which influences model precision. As an example, the model was able to precisely predict the plasma concentration-time profile of POS for the mean individual created according to Vuletic et al. [36] and simulated concentrations were in close concordance with the observed data (Figure S7). However, a high bias (MPE = 147.64%), low precision (MAPE = 181.61), and a MRD of 2.36 was obtained in the population simulation with the virtual population (Figure S7).

Summing up, the combination of RUX with POS is of significant clinical relevance as an increase of RUX AUX by 60% is associated with higher probability of adverse events due to RUX overexposure. The other way round, it is also conceivable that too low RUX exposure is achieved if, for example, POS is discontinued or exchanged for a substance that is not a CYP3A4 inhibitor (e.g., Amphotericin B). This could result in therapy failure if the RUX dose is not increased accordingly. Our findings showed that using RUX at a standard dosage, if co-administered with POS in GvHD patients, led to higher exposure compared to simulations in a healthy population. Thus, the FDA recommendation should be considered with caution and patients at risk of RUX overexposure or with a high potential of adverse events occurring should be identified, which can be supported by the developed model. The developed POS and RUX PBPK models can be combined with other existing PBPK models of additional perpetrators or

victims in PK-Sim® to describe DDI interaction and applied for dose adjustment in the clinical routine. Future investigations should include the investigation of GvHD-specific physiological alterations, which could be integrated into PBPK models to develop a more accurate GvHD population. In this context, one could also try to distinguish between aGvHD and cGvHD, as the patient populations are often clinically very different, also in terms of co-medication. Additionally, the PBPK models, especially the POS DR-tablet and POS SUS model, should be further validated with measured concentrations from future observational studies.

5. Conclusions

Depending on the regulatory authority and the time of approval, different dose recommendations exist for the combination of RUX with strong CYP3A4 inhibitors, which complicates the application in the clinic. For the application in PK-Sim®, two separate PBPK models for RUX and POS were successfully set up. The PBPK modeling approach was used to predict a DDI scenario for POS and RUX. RUX plasma exposure simulated with the final DDI model was compared to observed concentrations in patients treated for aGvHD or cGvHD in the routine clinical setting, revealing that standard dosing in these patients may not be adequate and reduced RUX doses should be administered depending on the concomitantly administered azoles and their inhibition potency. Due to the complexity of the disease and intake of extensive co-medication, RUX plasma concentration can be higher than expected. It is therefore advisable to monitor plasma levels and adjust RUX dosing accordingly. The DDI model can be expanded to other perpetrators or victims, e.g., fluconazole and could be further optimized by the implementation of physiological changes in GvHD patients, if these are sufficiently investigated. The model can serve as a starting point to implement PBPK modeling in the clinical routine to predict potential DDI in vulnerable patients and to guide dose adjustment.

Supplementary Materials: The following are available online at https://www.mdpi.com/article/10.3390/pharmaceutics14122556/s1,
Electronic Supplementary Materials: Additional information on model development and evaluation including Figures S1–S11 and Tables S1–S10.

Author Contributions: Conceptualization, B.G., F.A.-T., and O.S.-C.; methodology, B.G., F.A.-T., M.K., S.Z.; investigation, B.G., F.A.-T., N.I.; writing—original draft preparation, B.G., F.A.-T.; writing— review and editing, B.G., F.A.-T., N.I., and O.S.-C.; visualization, B.G.;

resources, M.K., S.K., G.U.G., and H.K.; funding acquisition: N.I., O.S.-C., H.K. All authors have read and agreed to the published version of the manuscript.

Funding: This work was supported by the Hector Foundation II, Weinheim, Germany, Fond: STIF-99 ("Individualized cancer therapy with kinase inhibitors using drug monitoring—optimization by minimally invasive at-home sampling").

Institutional Review Board Statement: Not applicable.

Informed Consent Statement: Not applicable.

Data Availability Statement: All modeling files including utilized clinical study data can be found here: https://github.com/Open-Systems-Pharmacology (accessed on 21 November 2022).

Acknowledgments: The authors kindly acknowledge Lukas Kovar and Christoph Hethey for their scientific support and valuable suggestions.

Conflicts of Interest: OSC reports endowed professorship grant (Horphag g Research Ltd.). The remaining authors declare no competing financial or non-financial interests.

References

1. Jamil, M.O.; Mineishi, S. State-of-the-art acute and chronic GVHD treatment. Int. J. Hematol. **2015**, 101, 452–466.

2. Jagasia, M.; Perales, M.-A.; Schroeder, M.A.; Ali, H.; Shah, N.N.; Chen, Y.-B.; Fazal, S.; Dawkins, F.W.; Arbushites, M.C.; Tian, C. Ruxolitinib for the treatment of steroid-refractory acute GVHD (REACH1): A multicenter, open-label phase 2 trial. Blood **2020**, 135, 1739–1749.

3. Zeiser, R.; von Bubnoff, N.; Butler, J.; Mohty, M.; Niederwieser, D.; Or, R.; Szer, J.; Wagner, E.M.; Zuckerman, T.; Mahuzier, B. Ruxolitinib for glucocorticoid-refractory acute graft-versus-host disease. N. Engl. J. Med. **2020**, 382, 1800–1810.

4. Zeiser, R.; Polverelli, N.; Ram, R.; Hashmi, S.K.; Chakraverty, R.; Middeke, J.M.; Musso, M.; Giebel, S.; Uzay, A.; Langmuir, P. Ruxolitinib for glucocorticoid-refractory chronic graft-versus-host disease. N. Engl. J. Med. **2021**, 385, 228–238.

5. Zeiser, R.; Blazar, B.R. Acute graft-versus-host disease—Biologic process, prevention, and therapy. N. Engl. J. Med. **2017**, 377, 2167–2179.

6. Martin, P.J.; Rizzo, J.D.; Wingard, J.R.; Ballen, K.; Curtin, P.T.; Cutler, C.; Litzow, M.R.; Nieto, Y.; Savani, B.N.; Schriber, J.R. First-and second-line systemic treatment of acute graft-versus-host disease: Recommendations of the American Society of Blood and Marrow Transplantation. Biol. Blood Marrow Transplant. **2012**, 18, 1150–1163.

7. Bhatti, Z.; Shaukat, A.; Almyroudis, N.G.; Segal, B.H. Review of epidemiology, diagnosis, and treatment of invasive mould infections in allogeneic hematopoietic stem cell transplant recipients. Mycopathologia **2006**, 162, 1–15.

8. Maertens, J.A.; Girmenia, C.; Brüggemann, R.J.; Duarte, R.F.; Kibbler, C.C.; Ljungman, P.; Racil, Z.; Ribaud, P.; Slavin, M.A.; Cornely, O.A. European guidelines for primary antifungal prophylaxis in adult haematology patients: Summary of the updated recommendations from the European Conference on Infections in Leukaemia. J. Antimicrob. Chemother. **2018**, 73, 3221–3230.

9. Ullmann, A.J.; Lipton, J.H.; Vesole, D.H.; Chandrasekar, P.; Langston, A.; Tarantolo, S.R.; Greinix, H.; Morais de Azevedo, W.; Reddy, V.; Boparai, N.; et al. Posaconazole or fluconazole for prophylaxis in severe graft-versus-host disease. N. Engl. J. Med. **2007**, 356, 335–347.

10. Chen, L.; Krekels, E.H.; Verweij, P.; Buil, J.B.; Knibbe, C.A.; Brüggemann, R.J. Pharmacokinetics and pharmacodynamics of posaconazole. Drugs **2020**, 80, 671–695.

11. Czyrski, A.; Resztak, M.; Swiderski, P.; Brylak, J.; Gł ´ ówka, F.K. The Overview on the Pharmacokinetic and Pharmacodynamic Interactions of Triazoles. Pharmaceutics **2021**, 13, 1961.

12. Lipp, H.P. Clinical pharmacodynamics and pharmacokinetics of the antifungal extended-spectrum triazole posaconazole: An overview. Br. J. Clin. Pharmacol. **2010**, 70, 471–480.

13. Reinwald, M.; Boch, T.; Hofmann, W.-K.; Buchheidt, D. Risk of infectious complications in hemato-oncological patients treated with kinase inhibitors. Biomark. Insights **2015**, 10, BMI.S22430.

14. Mellinghoff, S.C.; Panse, J.; Alakel, N.; Behre, G.; Buchheidt, D.; Christopeit, M.; Hasenkamp, J.; Kiehl, M.; Koldehoff, M.; Krause, S.W. Primary prophylaxis of invasive fungal infections in patients with haematological malignancies: 2017 update of the recommendations of the Infectious Diseases Working Party (AGIHO) of the German Society for Haematology and Medical Oncology (DGHO). Ann. Hematol. **2018**, 97, 197–207.

15. European Medicines Agency (EMA)-Assessment Report Jakavi (Ruxolitinib). Available online: https://www.ema.europa.eu/en/ documents/assessment-report/jakavi-epar-public-assessment-report_en.pdf (accessed on 30 August 2022).

16. U.S. Food and Drug Administration. Clinical Drug Interaction Studies—Cytochrome P450 Enzyme- and Transporter Mediated Drug Interactions Guidance for Industry. 2020. Available online: https://www.fda.gov/regulatory-information/ search-fda-guidance-documents/clinical-drug-interaction-studies-cytochrome-p450-enzyme-and-transporter-mediated drug-interactions (accessed on 5 August 2022).

17. European Medicines Agency. Jakavi Summary of Product Characteristics. Available online: https://www.ema.europa.eu/en/ documents/product-information/jakavi-epar-product-information_en.pdf (accessed on 10 June 2022).

18. U.S. Food and Drug Administration. The Use of Physiologically Based Pharmacokinetic Analyses—Biopharmaceutics Applications for Oral Drug Product Development, Manufacturing Changes, and Controls. 2020. Available online: https://www.fda.gov/regulatory-information/search-fda-guidance-documents/use-physiologically-based-pharmacokinetic-analyses-biopharmaceutics-applications-oral-drug-product (accessed on 5 August 2022).

19. European Medicines Agency. Guideline on the Reporting of Physiologically Based Pharmacokinetic (PBPK) Modelling and Simulation. 2018. Available online: https://www.ema.europa.eu/en/reporting-physiologically-based-pharmacokinetic-pbpk-modelling-simulation (accessed on 28 August 2022).

20. Grimstein, M.; Yang, Y.; Zhang, X.; Grillo, J.; Huang, S.-M.; Zineh, I.; Wang, Y. Physiologically based pharmacokinetic modeling in regulatory science: An update from the US Food and Drug Administration's Office of Clinical Pharmacology. J. Pharm. Sci. **2019**, 108, 21–25.

21. Wagner, C.; Pan, Y.; Hsu, V.; Grillo, J.A.; Zhang, L.; Reynolds, K.S.; Sinha, V.; Zhao, P. Predicting the effect of cytochrome P450 inhibitors on substrate drugs: Analysis of physiologically based pharmacokinetic modeling submissions to the US Food and Drug Administration. Clin. Pharmacokinet. **2015**, 54, 117–127.

22. Darwich, A.; Ogungbenro, K.; Vinks, A.A.; Powell, J.R.; Reny, J.L.; Marsousi, N.; Daali, Y.; Fairman, D.; Cook, J.; Lesko, L.J. Why has model-informed precision dosing not yet become common clinical reality? Lessons from the past and a roadmap for the future. Clin. Pharmacol. Ther. **2017**, 101, 646–656.

23. Luzon, E.; Blake, K.; Cole, S.; Nordmark, A.; Versantvoort, C.; Berglund, E.G. Physiologically based pharmacokinetic modeling in regulatory decision-making at the European Medicines Agency. Clin. Pharmacol. Ther. **2017**, 102, 98–105.

24. Open Systems Pharmacology. PK-Sim®. Version 11.0. Available online: https://github.com/Open-Systems-Pharmacology/ Suite/releases/tag/v11.0 (accessed on 1 May 2022).

25. R Core Team. R: A Language and Environment for Statistical Computing; R Foundation for Statistical Computing: Vienna, Austria, 2017.

26. Kersemaekers, W.M.; van Iersel, T.; Nassander, U.; O'Mara, E.; Waskin, H.; Caceres, M.; van Iersel, M.L. Pharmacokinetics and safety study of posaconazole intravenous solution administered peripherally to healthy subjects. Antimicrob. Agents Chemother. **2015**, 59, 1246–1251.

27. Hens, B.; Pathak, S.M.; Mitra, A.; Patel, N.; Liu, B.; Patel, S.; Jamei, M.; Brouwers, J.; Augustijns, P.; Turner, D.B. In silico modeling approach for the evaluation of gastrointestinal dissolution, supersaturation, and precipitation of posaconazole. Mol. Pharm. **2017**, 14, 4321–4333.

28. Hens, B.; Bolger, M.B. Application of a Dynamic Fluid and pH Model to Simulate Intraluminal and Systemic Concentrations of a Weak Base in GastroPlusTM. J. Pharm. Sci. **2019**, 108, 305–315.

29. Ghosal, A.; Hapangama, N.; Yuan, Y.; Achanfuo-Yeboah, J.; Iannucci, R.; Chowdhury, S.; Alton, K.; Patrick, J.E.; Zbaida, S. Identification of human UDP-

glucuronosyltransferase enzyme (s) responsible for the glucuronidation of posaconazole (Noxafil). Drug Metab. Dispos. **2004**, 32, 267–271.

30. Li, H.; Wei, Y.; Zhang, S.; Xu, L.; Jiang, J.; Qiu, Y.; Mangin, E.; Zhao, X.M.; Xie, S. Pharmacokinetics and Safety of Posaconazole Administered by Intravenous Solution and Oral Tablet in Healthy Chinese Subjects and Effect of Food on Tablet Bioavailability. Clin. Drug. Investig. **2019**, 39, 1109–1116.

31. Kersemaekers, W.M.; Dogterom, P.; Xu, J.; Marcantonio, E.E.; de Greef, R.; Waskin, H.; van Iersel, M.L. Effect of a high-fat meal on the pharmacokinetics of 300-milligram posaconazole in a solid oral tablet formulation. Antimicrob. Agents Chemother. **2015**, 59, 3385–3389.

32. Krishna, G.; Ma, L.; Martinho, M.; O'Mara, E. Single-dose phase I study to evaluate the pharmacokinetics of posaconazole in new tablet and capsule formulations relative to oral suspension. Antimicrob. Agents Chemother. **2012**, 56, 4196–4201.

33. Krishna, G.; Ma, L.; Martinho, M.; Preston, R.; O'Mara, E. A new solid oral tablet formulation of posaconazole: A randomized clinical trial to investigate rising single-and multiple-dose pharmacokinetics and safety in healthy volunteers. J. Antimicrob. Chemother. **2012**, 67, 2725–2730.

34. Fallingborg, J. Intraluminal pH of the human gastrointestinal tract. Dan. Med. Bull. **1999**, 46, 183–196.

35. Ezzet, F.; Wexler, D.; Courtney, R.; Krishna, G.; Lim, J.; Laughlin, M. Oral bioavailability of posaconazole in fasted healthy subjects. Clin. Pharmacokinet. **2005**, 44, 211–220.

36. Vuleti´c, L.; Herceg, M.; Ferderber, K.; Tunji´c, I.; Rizea-Savu, S.; Duna, S.N.; Cetina-Cižmek, B.; Filipovi´c-Gr˘ci´c, J. Single-Dose ˘ Pharmacokinetic Properties and Relative Bioavailability of Different Formulations of Posaconazole Oral Suspension in Healthy Volunteers. Clin. Pharmacol. Drug Dev. **2019**, 8, 827–836.

37. Courtney, R.; Wexler, D.; Radwanski, E.; Lim, J.; Laughlin, M. Effect of food on the relative bioavailability of two oral formulations of posaconazole in healthy adults. Br. J. Clin. Pharmacol. **2004**, 57, 218–222.

38. Ogama, Y.; Mineyama, T.; Yamamoto, A.; Woo, M.; Shimada, N.; Amagasaki, T.; Natsume, K. A randomized dose-escalation study to assess the safety, tolerability, and pharmacokinetics of ruxolitinib (INC424) in healthy Japanese volunteers. Int. J. Hematol. **2013**, 97, 351–359.

39. Chen, X.; Shi, J.G.; Emm, T.; Scherle, P.A.; McGee, R.F.; Lo, Y.; Landman, R.R.; Punwani, N.G.; Williams, W.V.; Yeleswaram, S. Pharmacokinetics and pharmacodynamics of orally administered ruxolitinib (INCB018424 phosphate) in renal and hepatic impairment patients. Clin. Pharmacol. Drug Dev. **2014**, 3, 34–42.

40. Shi, J.G.; Chen, X.; McGee, R.F.; Landman, R.R.; Emm, T.; Lo, Y.; Scherle, P.A.; Punwani, N.G.; Williams, W.V.; Yeleswaram, S. The pharmacokinetics, pharmacodynamics, and safety of orally dosed INCB018424 phosphate in healthy volunteers. J. Clin. Pharmacol. **2011**, 51, 1644–1654.

41. U.S. Food and Drug Administration. Physiologically Based Pharmacokinetic Analyses—Format and Content—Guidance for Industry. 2018. Available online: https://www.fda.gov/regulatory-information/search-fda-guidance-documents/physiologically-based-pharmacokinetic-analyses-format-and-content-guidance-industry (accessed on 28 August 2022).

42. Edginton, A.N.; Schmitt, W.; Willmann, S. Development and evaluation of a generic physiologically based pharmacokinetic model for children. Clin. Pharmacokinet. 2006, 45, 1013–1034. [CrossRef] 43. Frechen, S.; Hanke, N.; Solodenko, J.; Dallmann, A. Midazolam-Model. Available online: https://github.com/Open-Systems-Pharmacology/Midazolam-Model (accessed on 20 May 2021).

44. Krishna, G.; Moton, A.; Ma, L.; Savant, I.; Martinho, M.; Seiberling, M.; McLeod, J. Effects of oral posaconazole on the pharmacokinetic properties of oral and intravenous midazolam: A phase I, randomized, open-label, crossover study in healthy volunteers. Clin. Ther. **2009**, 31, 286–298.

45. Aghai, F.; Zimmermann, S.; Kurlbaum, M.; Jung, P.; Pelzer, T.; Klinker, H.; Isberner, N.; Scherf-Clavel, O. Development and validation of a sensitive liquid chromatography tandem mass spectrometry assay for the simultaneous determination of ten kinase inhibitors in human serum and plasma. Anal. Bioanal. Chem. **2021**, 413, 599–612.

46. Kahle, K.; Langmann, P.; Schirmer, D.; Lenker, U.; Keller, D.; Helle, A.; Klinker, H.; Heinz, W.J. Simultaneous determination of voriconazole and posaconazole concentrations in human plasma by high-performance liquid chromatography. Antimicrob. Agents Chemother. **2009**, 53, 3140–3142.

47. Thelen, K.; Coboeken, K.; Willmann, S.; Dressman, J.B.; Lippert, J. Evolution of a detailed physiological model to simulate the gastrointestinal transit and absorption process in humans, part II: Extension to describe performance of solid dosage forms. J. Pharm. Sci. **2012**, 101, 1267–1280.

48. Thelen, K.; Coboeken, K.; Willmann, S.; Burghaus, R.; Dressman, J.B.; Lippert, J. Evolution of a detailed physiological model to simulate the gastrointestinal transit and absorption process in humans, part 1: Oral solutions. J. Pharm. Sci. **2011**, 100, 5324–5345.

49. Rodgers, T.; Leahy, D.; Rowland, M. Physiologically based pharmacokinetic modeling 1: Predicting the tissue distribution of moderate-to-strong bases. J. Pharm. Sci. **2005**, 94, 1259–1276.

50. Rodgers, T.; Rowland, M. Physiologically based pharmacokinetic modelling 2: Predicting the tissue distribution of acids, very weak bases, neutrals and zwitterions. J. Pharm. Sci. **2006**, 95, 1238–1257.

51. Umehara, K.; Huth, F.; Jin, Y.; Schiller, H.; Aslanis, V.; Heimbach, T.; He, H. Drug-drug interaction (DDI) assessments of ruxolitinib, a dual substrate of CYP3A4 and CYP2C9, using a verified physiologically based pharmacokinetic (PBPK) model to support regulatory submissions. Drug Metab. Pers. Ther. **2019**, 34.

52. Wexler, D.; Courtney, R.; Richards, W.; Banfield, C.; Lim, J.; Laughlin, M. Effect of posaconazole on cytochrome P450 enzymes: A randomized, open-label, two-way crossover study. Eur. J. Pharm. Sci. **2004**, 21, 645–653.

53. Isberner, N.; Kraus, S.; Grigoleit, G.U.; Aghai, F.; Kurlbaum, M.; Zimmermann, S.; Klinker, H.; Scherf-Clavel, O. Ruxolitinib exposure in patients with acute and chronic graft versus host disease in routine clinical practice—A prospective single-center trial. Cancer Chemother. Pharmacol. **2021**, 88, 973–983.

54. Bhatnagar, S.; Mukherjee, D.; Salem, A.H.; Miles, D.; Menon, R.M.; Gibbs, J.P. Dose adjustment of venetoclax when co-administered with posaconazole: Clinical drug-drug interaction predictions using a PBPK approach. Cancer Chemother. Pharmcol. **2021**, 87, 465–474.

55. Hens, B.; Talattof, A.; Paixao, P.; Bermejo, M.; Tsume, Y.; Lobenberg, R.; Amidon, G.L. Measuring the Impact of Gastrointestinal Variables on the Systemic Outcome of Two Suspensions of Posaconazole by a PBPK Model. AAPS J. **2018**, 20, 57.

56. Cristofoletti, R.; Patel, N.; Dressman, J.B. Assessment of Bioequivalence of Weak Base Formulations Under Various Dosing Conditions Using Physiologically Based Pharmacokinetic Simulations in Virtual Populations. Case Examples: Ketoconazole and Posaconazole. J. Pharm. Sci. **2017**, 106, 560–569.

57. Cristofoletti, R.; Patel, N.; Dressman, J.B. Differences in Food Effects for 2 Weak Bases With Similar BCS Drug-Related Properties: What Is Happening in the Intestinal Lumen? J. Pharm. Sci. **2016**, 105, 2712–2722.

58. Chen, K.F.; Chan, L.N.; Lin, Y.S. PBPK modeling of CYP3A and P-gp substrates to predict drug-drug interactions in patients undergoing Roux-en-Y gastric bypass surgery. J. Pharm. Pharm. **2020**, 47, 493–512.

59. Cleary, Y.; Gertz, M.; Morcos, P.N.; Yu, L.; Youdim, K.; Phipps, A.; Fowler, S.; Parrott, N. Model-Based Assessments of CYPMediated Drug–Drug Interaction Risk of Alectinib: Physiologically Based Pharmacokinetic Modeling Supported Clinical Development. Clin. Pharmacol. Ther. **2018**, 104, 505–514.

60. Aslanis, V.; Umehara, K.; Huth, F.; Ouatas, T.; Bharathy, S.; Butler, A.A.; Zhou, W.; Gadbaw, B. Multiple administrations of fluconazole increase plasma exposure to ruxolitinib in healthy adult subjects. Cancer Chemother. Pharmacol. **2019**, 84, 749–757.

61. Shi, J.G.; Fraczkiewicz, G.; Williams, W.V.; Yeleswaram, S. Predicting drug-drug interactions involving multiple mechanisms using physiologically based pharmacokinetic modeling: A case study with ruxolitinib. Clin. Pharmacol. Ther. **2015**, 97, 177–185.

62. Chen, X.; Liu, X.; Wang, P.; Yeleswaram, S. Population Pharmacokinetics of Ruxolitinib in Patients with aGVHD Who Had an Inadequate Response to Corticosteroids. Blood **2019**, 134, 4534.

63. Hansmann, S.; Darwich, A.; Margolskee, A.; Aarons, L.; Dressman, J. Forecasting oral absorption across biopharmaceutics classification system classes with physiologically based pharmacokinetic models. J. Pharm. Pharmacol. 2016, 68, 1501–1515.

64. Cornely, O.A.; Duarte, R.F.; Haider, S.; Chandrasekar, P.; Helfgott, D.; Jimenez, J.L.; Candoni, A.; Raad, I.; Laverdiere, M.; Langston, A.; et al. Phase 3 pharmacokinetics and safety study of a posaconazole tablet formulation in patients at risk for invasive fungal disease. J. Antimicrob. Chemother. **2016**, 71, 1747.

65. European Medicines Agency. Noxafil Summary of Product Characteristics. Available online: https://www.ema.europa.eu/en/ documents/product-information/noxafil-epar-product-information_en.pdf (accessed on 13 September 2022).

66. Gubbins, P.O.; Krishna, G.; Sansone-Parsons, A.; Penzak, S.R.; Dong, L.; Martinho, M.; Anaissie, E.J. Pharmacokinetics and safety of oral posaconazole in neutropenic stem cell transplant recipients. Antimicrob. Agents Chemother. 2006, 50, 1993–1999.

67. Walravens, J.; Brouwers, J.; Spriet, I.; Tack, J.; Annaert, P.; Augustijns, P. Effect of pH and comedication on gastrointestinal absorption of posaconazole: Monitoring of intraluminal and plasma drug concentrations. Clin. Pharmacokinet. **2011**, 50, 725–734.

68. Bermejo, M.; Hens, B.; Dickens, J.; Mudie, D.; Paixao, P.; Tsume, Y.; Shedden, K.; Amidon, G.L. A Mechanistic Physiologically Based Biopharmaceutics Modeling (PBBM) Approach to Assess the In Vivo Performance of an Orally Administered Drug Product: From IVIVC to IVIVP. Pharmaceutics **2020**, 12, 74.

69. Prieto Garcia, L.; Lundahl, A.; Ahlström, C.; Vildhede, A.; Lennernäs, H.; Sjögren, E. Does the choice of applied physiologically based pharmacokinetics platform matter? A case study on simvastatin disposition and drug-drug interaction. CPT Pharmacomet. Syst. Pharmacol. **2022**, 11, 1194–1209.

70. Jamei, M.; Turner, D.; Yang, J.; Neuhoff, S.; Polak, S.; Rostami-Hodjegan, A.; Tucker, G. Population-based mechanistic prediction of oral drug absorption. AAPS J. **2009**, 11, 225–237.

D Final discussion

The projects in this work aimed to support and optimise oral drug therapy of antineoplastic drugs in different therapeutic areas. The drugs that were selected for the projects are characterised above all by special pk properties and a greater or lesser variability in exposure. These particularities result on the one hand from the oral ingestion of the substance, which is in itself already prone to a high degree of variability in drug absorption. On the other hand, the strong metabolism via CYP enzymes (CYP3A4 and partly CYP2C9) plays a major role in the drugs studied, which makes them susceptible to DDI. To reduce the risk of over-or underexposure of the investigated substances, pharmacometric approaches and TDM were applied. In the first project, a minimally invasive method for the TDM of mitotane was evaluated. In the second and third project PBPK models for the TKIs cabozantinib and ruxolitinib, as well as for posaconazole were successfully established. Using these models' mechanistic insights into the PK behaviour of the cabozantinib was gained and the impact of DDI between ruxolitinib and posaconazole on plasma exposure was analysed, respectively.

1 Minimally invasive drug monitoring of mitotane

To evaluate minimally invasive drug monitoring of mitotane, the MITRA™ VAMS, an approved in vitro diagnostic was used for blood sampling. The handling of the device turned out to be easy and practicable. According to the specification, a defined volume of 20 ml should be collected by the MITRA™ VAMS. During the experiments however, it turned out that there were variations, especially when different batches of MITRA™ tips were used and the calculated average blood wicking volume varied as much as from 20.8 to 22.5 µL from batch to batch. This must be kept in mind, if VAMS used for calibration and for patient sampling originate from different batches, as a substantial bias in recovery is given, if the nominal and the wicked blood volume differs more than 10 %.

The small amount of sampled blood may be challenging, as often sensitive methods such as LC-MS/MS are required to measure drug concentration in capillary blood. In the case of Mitotane, however, the dried blood samples could be analyzed with an HPLC-UV method, as there was a sufficiently high mitotane concentration in the wicked blood. This may be beneficial for the application of the method in clinical practice, as LC-MS/MS methods are not widely available in each health care centre.

Dried samples could be stored at room temperature for at least one week, but at higher temperatures (37°C) a substantial amount of analyte was lost, probably due to evaporation. Thus, for example in summer season, samples should be cooled down to mitigate reduced accuracy due to analyte evaporation. Hematocrit bias, a common problem of conventional dried blood spot analysis, was assessed with samples prepared from blood with high (0.55), medium (0.40) and low (0.30) hematocrit. All samples were within the general acceptance criteria for quality control samples (accuracy, 89.8–113.0%; precision, 4.5–10.1%;), pointing out the HCT independency.

Even though the applicability of the developed method using MITRA™ VAMS could be demonstrated, feasibility of mitotane TDM using minimally invasive sampling was not given. This was mainly because no simple conversion from DBS concentrations to plasma concentrations was possible. For mitotane therapy, however, only reference ranges have been established for plasma and not for capillary blood. Thus, a reliable prediction of plasma concentrations based on MITRA™ measurements would be essential but could not be achieved. There was no obvious relation between the differences of predicted vs. actual plasma concentrations and the mean of predicted vs. actual plasma concentrations. The 95% confidence interval for the predicted plasma concentration ranged from − 7.6 to 6.6 mg L^{-1}, which would be unacceptable for clinical purpose. Thus, nonlinear models may be necessary to relate MITRA™ to plasma concentrations or reference ranges in capillary blood would have to be established for feasibility of minimally invasive TDM for mitotane.

2 Physiologically based pharmacokinetic modelling of cabozantinib

The concentration time profile of cabozantinib is characterised by a second peak, a rapid decrease in the first hours and a long terminal half-life. To gain a mechanistic insight into the PK behaviour of the substance and to investigate different reasons leading to the characteristic concentration-time profile a whole-body PBPK model was established. Besides absorption processes in deeper intestine sections and deposition effects, EHC was modelled. EHC, combined with a delayed intestinal absorption, was found to best describe cabozantinib plasma concentration time profiles.

The final PBPK model was used to model DDI between cabozantinib and rifampin and showed a reduced cabozantinib plasma exposure by 77% if co-administered with rifampin. As the FDA label recommends an increased cabozantinib dose if given together with rifampin [112], multiple dose simulations with higher cabozantinib doses were conducted. However, DDI simulations revealed that even with an increased cabozantinib dose, plasma exposure was still two third lower compared to the plasma exposure, if cabozantinib was given without its perpetrator. Based on the simulations, it is advisable to avoid combining cabozantinib with strong CYP inducers like rifampin. If it should be necessary to administer both substances due to clinical reasons, TDM, should be conducted to avoid subtherapeutic plasma exposure.

Since cabozantinib is eliminated mainly via the hepatobiliary route, changes in plasma exposure due to hepatic dysfunction were investigated and the cabozantinib PBPK model was expanded to patients with liver impairments of varying severity. Within the model, physiological parameters were adapted to implement populations with mild and moderate hepatic impairment. Compared to the control group, cabozantinib exposure in the population with mild and moderate hepatic impairment increased by 64% and 50%, respectively. The lower increase in plasma exposure for moderate disease compared to subjects with mild hepatic impairment and a generally lower C_{max} for those patients was justified according to Nguyen et al. by a higher f_{up} and a higher interindividual variability [110]. As f_{up} had a considerable impact on the cabozantinib plasma exposure it might be valuable to measure this parameter in patients suffering from cirrhosis to predict cabozantinib PK more precisely.

3 Physiologically based pharmacokinetic modelling of ruxolitinib and posaconazole

In this project, two separate PBPK models for posaconazole and ruxolitinib were successfully developed and evaluated. As posaconazole and ruxolitinib are commonly co-administered in patients with GvHD, both PBPK models were combined to simulate DDI and to investigate the impact of posaconazole administration on ruxolitinib exposure. This resulted in a 20% increase in ruxolitinib C_{max} and a 59% increase in ruxolitinib exposure. The simulated ruxolitinib plasma concentrations if given together with its perpetrator posaconazole were finally compared to concentrations obtained from patients with GvHD in the clinical routine. 64.42% of the observed serum concentrations after 10 mg twice daily ruxolitinib administration

in combination with posaconazole were within the 5% to 95% prediction intervals of the corresponding simulation, however a greater proportion of the observed ruxolitinib concentrations were above the predicted median ruxolitinib concentration. GvHD is a complex disease and GvHD patients are characterized by heterogeneity with various comorbidities, co-medications, and different pathophysiological conditions. As no quantitative disease model for GvHD was available, all simulations were done with healthy populations, which is one possible explanation for deviations between predicted and observed ruxolitinib concentrations in the clinical routine.

However, even without concomitant administration of oral posaconazole, model-predicted median ruxolitinib serum concentrations were lower than the serum concentrations observed in the GvHD patients. Thus, due to the complex disease and intake of extensive co-medication, ruxolitinib exposure, if administered at a standard dosage, is higher compared to simulations in healthy populations. The ruxolitinib FDA label does not recommend ruxolitinib dose modifications for GvHD patients if given together with strong CYP3A4 inhibitors like posaconazole, yet the simulations carried out could not confirm this statement. In patients at risk of ruxolitinib overdose or with a high potential for adverse events to occur, the standard dose should be taken with caution, and it is advisable to reduce the ruxolitinib dose according to the EMA recommendation.

4 Conclusion

Taken together, (minimally invasive) TDM and pharmacometric approaches such as PBPK modelling were suitable methods to support oral drug administration of antineoplastic drugs. Both approaches aimed to improve knowledge about the right dosing and by that to minimize the risk of potential over-or underexposure of the given drug. The present work thus contributes to optimising the therapy with oral antineoplastic drugs for the individual patient or to adapting it to specific circumstances (e.g., DDI, hepatic impairment), respectively. This is another step towards precision medicine, away from a one-size fits all strategy in cancer therapy.

Especially for newer compounds (i.e., kinase inhibitors) with little clinical experience, PBPK modelling was a valuable tool to gain deeper and mechanistic insight into the pharmacokinetic behaviour of the drug and to draw conclusions about the correct dosage in different situations (e.g., for special populations like GvHD patients or in DDI situations). The PBPK models for cabozantinib, ruxolitinib and posaconazole, respectively, were particularly useful for investigating DDIs.

DDIs are increasingly being evaluated with the help of PBPK modelling. In 2018 and 2019 about 35% and 45%, respectively, of new drug approvals included a PBPK analysis and the most applicated area was DDI (60%) [219]. During clinical development however, DDI investigation is mainly done based on healthy populations without considering the whole complexity of a disease like it is the case in ACC or GvHD. Most of the patients with cancer or immunological malignancies suffer from disease-specific physiological changes and/or take numerous drugs. Thus, there is a need also for future projects to use pharmacometric models to determine the PK/PD or dosage for those patients.

For the cabozantinib model, only data from clinical studies with healthy volunteers could have been used. For the Ruxolitinib PBPK model, plasma concentrations obtained from GvHD patients in daily clinical routine were available and used for model evaluation. Both models however were set up based on healthy individuals, as validated information on disease-specific alterations are missing so far. More effort should therefore be invested in the research of quantitative disease models in the future to improve the precision of the developed models.

To make drug sampling for TDM more convenient and to allow for more frequent sampling, a minimally invasive sampling method for Mitotane was developed. It was however difficult to calculate plasma concentrations from DBS concentrations, and if there are only reference ranges for plasma, measurement from capillary blood is not feasible. This might be a general problem for the application of DBS methods, which are based on capillary blood sampling. Capillary blood physiologically differs from venous whole blood and is potentially contaminated with interstitial fluid. Thus, a one-to-one transfer of the measured capillary blood concentrations to the corresponding plasma concentrations is not possible. To be able to use capillary blood measurements in the form of VAMS for a subsequent dose adjustment, blood to plasma ratios or reference ranges must be determined for the corresponding drugs. Future clinical studies that identify exposure-safety and exposure-effect relationships should include this, as only then DBS measurements can be meaningfully used in routine clinical practice.

In the best case, TDM and pharmacometric models are combined in the sense of a model informed TDM, to guide dose adjustment for individual patients. With more validated pharmacometric models becoming available, an adapted dosage can be administered based on knowledge from these models. However, this also requires corresponding TDM targets and evidence of an exposure-response relationship is a prerequisite for TDM to be useful and recommended. Only based on that, the dosage can be adequately adjusted. Reliable exposure-response relationships are far from available for all new orally targeted antineoplastic drugs and are often only available years after approval [47]. Thus, there is still a need for research here. The projects presented in the dissertation focused mainly on PK issues but looked less at the

PD of the respective substances. Future projects could be expanded to consider PD in addition to PK to establish suitable PD indices, as it is the case for example in the therapy with antibiotics. The collection of real-world data within the framework of TDM provide valuable information which can be used to develop and evaluate pharmacometric models. For future projects, it would be conceivable not only to measure plasma concentrations, but also to measure certain PD biomarkers at the same time. However, a prerequisite for this is that a relevant biomarker is known that is directly related to the clinical effect. Together with information about the individual patient and the underlying disease, such models can then investigate and predict an exposure-response relationship, also for special subpopulations.

To drive adoption of dedicated tools, like mobile or web-based applications in the daily clinical routine, a proper education of the intended end-user is necessary. With these prerequisites, a direct implementation of MIPD at the bedside based on real time drug measurements can succeed. This has not yet become part of the daily clinic routine but is being worked towards in larger and smaller steps. Especially for patients with ACC and GvHD, the presented projects are a further step into the direction of a personalized therapy.

E Summary

Oral antineoplastic drugs are an important component in the treatment of solid tumour diseases, haematological and immunological malignancies. Oral drug administration is associated with positive features (e.g., non-invasive drug administration, outpatient care with a high level of independence for the patient and reduced costs for the health care system). The systemic exposure after oral intake however is prone to high IIV as it strongly depends on gastrointestinal absorption processes, which are per se characterized by high inter-and intraindividual variability. Disease and patient-specific characteristics (e.g., disease state, concomitant diseases, concomitant medication, patient demographics) may additionally contribute to variability in plasma concentrations between individual patients. In addition, many oral antineoplastic drugs show complex PK, which has not yet been fully investigated and elucidated for all substances. All this may increase the risk of suboptimal plasma exposure (either subtherapeutic or toxic), which may ultimately jeopardise the success of therapy, either through a loss of efficacy or through increased, intolerable adverse drug reactions.

TDM can be used to detect suboptimal plasma levels and prevent permanent under- or overexposure. It is essential in the treatment of ACC with mitotane, a substance with unfavourable PK and high IIV. In the current work a HPLC-UV method for the TDM of mitotane using VAMS was developed. A low sample volume (20 µl) of capillary blood was used in the developed method, which facilitates dense sampling e.g., at treatment initiation. However, no reference ranges for measurements from capillary blood are established so far and a simple conversion from capillary concentrations to plasma concentrations was not possible. To date the therapeutic range is established only for plasma concentrations and observed capillary concentrations could not be reliable interpretated.

The multi-kinase inhibitor cabozantinib is also used for the treatment of ACC. However, not all PK properties, like the characteristic second peak in the cabozantinib concentration-time profile have been fully understood so far. To gain a mechanistic understanding of the compound, a PBPK model was developed and various theories for modelling the second peak were explored, revealing that EHC of the compound is most plausible. Cabozantinib is mainly metabolized via CYP3A4 and susceptible to DDI with e.g., CYP3A4 inducers. The DDI between cabozantinib and rifampin was investigated with the developed PBPK model and revealed a reduced cabozantinib exposure (AUC) by 77%. Hence, the combination of cabozantinib with strong CYP inducers should be avoided. If this is not possible, co-administration should be monitored using TDM. The model was also used to simulate cabozantinib plasma concentrations at different stages of liver injury. This showed a 64% and 50% increase in total exposure for mild and moderate liver injury, respectively.

Ruxolitinib is used, among others, for patients with acute and chronic GvHD. These patients often also receive posaconazole for invasive fungal prophylaxis leading to CYP3A4 mediated DDI between both substances. Different dosing recommendations from the FDA and EMA on the use of ruxolitinib in combination with posaconazole complicate clinical use. To simulate the effect of this relevant DDI, two separate PBPK models for ruxolitinib and posaconazole were developed and combined. Predicted ruxolitinib exposure was compared to observed plasma concentrations obtained in GvHD patients. The model simulations showed that the observed ruxolitinib concentrations in these patients were generally higher than the simulated concentrations in healthy individuals, with standard dosing present in both scenarios. According to the developed model, EMA recommended RUX dose reduction seems to be plausible as due to the complexity of the disease and intake of extensive co-medication, RUX plasma concentration can be higher than expected.

F Zusammenfassung

Orale antineoplastische Arzneimittel (OADs) sind ein wichtiger Bestandteil der Behandlung von soliden Tumorerkrankungen, hämatologischen und immunologischen Malignomen. Die orale Verabreichung von Arzneimitteln geht mit positiven Eigenschaften einher (z. B. nicht-invasive Anwendung, ambulante Versorgung mit einem hohen Maß an Unabhängigkeit für den Patienten und geringere Kosten für das Gesundheitssystem). Die systemische Exposition nach oraler Einnahme unterliegt jedoch einer hohen interindividuellen Variabilität, da sie stark von gastrointestinalen Absorptionsprozessen abhängt, die per se durch eine hohe inter- und intraindividuelle Variabilität gekennzeichnet sind. Krankheits- und patientenspezifische Merkmale (z. B. Krankheitszustand, Begleiterkrankungen, Begleitmedikation, Demographie der Patienten) können zusätzlich zu einer Variabilität in den Plasmakonzentrationen zwischen einzelnen Patienten beitragen. Darüber hinaus weisen viele OADs eine komplexe Pharmakokinetik (PK) auf, die noch nicht für alle Substanzen hinreichend untersucht und aufgeklärt wurde. All dies kann das Risiko einer suboptimalen Plasmaexposition (entweder subtherapeutisch oder toxisch) erhöhen, was letztendlich den Therapieerfolg gefährden kann, entweder durch einen Wirkungsverlust oder durch vermehrt auftretende, nicht tolerierbare unerwünschte Arzneimittelwirkungen.

Therapeutisches Drug Monitoring (TDM) kann eingesetzt werden, um suboptimale Plasmaspiegel zu erkennen und eine dauerhafte Unter- oder Überexposition zu verhindern. TDM ist in der Behandlung des Nebennierenrindenkarzinoms (ACC) mit Mitotane, einer Substanz, die sich durch ungünstige PK-Eigenschaften und einer hohen IIV auszeichnet, unerlässlich. In der vorliegenden Arbeit wurde eine HPLC-UV Methode für das TDM von Mitotane aus Trockenblut unter Verwendung volumetrisch absorptiver Mikroprobenahme (VAMS) entwickelt. Bei der entwickelten Methode wurde ein geringes Probenvolumen (20 µl) aus Kapillarblut verwendet, was eine häufigere Probenahme, z. B. zu Beginn der Behandlung, erleichtert. Allerdings gibt es bisher keine Referenzbereiche für Messungen aus Kapillarblut, und eine einfache Umrechnung von Kapillarkonzentrationen in Plasmakonzentrationen erwies sich als schwierig. Bislang ist der therapeutische Bereich nur für Plasmakonzentrationen festgelegt, und beobachtete Kapillarkonzentrationen konnten nicht zuverlässig interpretiert werden.

Der Multi-Kinase-Inhibitor Cabozantinib wird ebenfalls für die Behandlung des ACC eingesetzt. Allerdings sind noch nicht alle PK-Eigenschaften, wie der charakteristische zweite Peak im Konzentrations-Zeit-Profil von Cabozantinib, vollständig untersucht. Um ein mechanistisches Verständnis des Wirkstoffs zu erlangen, wurde ein physiologie basiertes pharmakokinetisches (PBPK) Model entwickelt und verschiedene Theorien zur Modellierung des zweiten Peaks untersucht, wobei sich herausstellte, dass eine enterohepatische Rezirkulation

der Substanz am plausibelsten ist. Cabozantinib wird hauptsächlich über CYP3A4 metabolisiert und ist daher anfällig für Wechselwirkungen mit z. B. CYP3A4-Induktoren. Die DDI zwischen Cabozantinib und Rifampin wurde mit dem entwickelten PBPK-Modell untersucht und ergab eine um 77 % verringerte Cabozantinib-Exposition (AUC). Daher sollte die Kombination von Cabozantinib mit starken CYP-Induktoren vermieden werden. Wenn dies nicht möglich ist, sollte die gemeinsame Verabreichung mittels TDM überwacht werden. Das Modell wurde außerdem verwendet, um die Cabozantinib Plasmakonzentrationen bei unterschiedlicher Schwere einer Leberschädigung zu simulieren. Hier zeigte sich eine um 64 % bzw. 50 % erhöhte Gesamtexposition bei leichter beziehungsweise mittlerer Leberschädigung.

Ruxolitinib wird unter anderem bei Patienten mit akuter (aGvHD) und chronischer (cGvHD) Graft-versus-Host-Erkrankung eingesetzt. Diese Patienten erhalten häufig auch Posaconazol zur Prophylaxe invasiver Pilzerkrankungen, was zu einer CYP3A4-vermittelten DDI zwischen beiden Substanzen führen kann. Unterschiedliche Dosierungsempfehlungen der FDA und der EMA für die Verwendung von Ruxolitinib in Kombination mit Posaconazol erschweren die klinische Anwendung. Um die Auswirkung dieser relevanten DDI zu simulieren, wurden zunächst zwei separate PBPK-Modelle für Ruxolitinib und Posaconazol entwickelt, welche anschließend miteinander kombiniert wurden. Die vorhergesagte Ruxolitinib Exposition wurde mit beobachteten Plasmakonzentrationen von GvHD-Patienten verglichen. Die Modellsimulationen zeigten, dass die beobachteten Ruxolitinib Konzentrationen bei diesen Patienten im Allgemeinen höher waren als die simulierten Konzentrationen bei gesunden Personen, wobei in beiden Szenarien eine Standarddosierung vorlag. Dem Modell zufolge schient die von der EMA empfohlene Reduzierung der RUX-Dosis um 50 % daher plausibler bzw. ausreichend zu sein.

G Appendix

1 List of Publications and Documentation of Authorship

1 **A method for the minimally invasive drug monitoring of mitotane by means of volumetric absorptive microsampling for a home-based therapeutic drug monitoring**

Friedl, B., Kurlbaum, M., Kroiss, M., Fassnacht, M., Scherf-Clavel, O.

Analytical and Bioanalytical Chemistry 411(17): 3951-3962, 2019

doi: 10.1007/s00216-019-01868-1

2 **Physiologically Based Pharmacokinetic Modelling of Cabozantinib to Simulate Enterohepatic Recirculation, Drug-Drug Interaction with Rifampin and Liver Impairment**

Bettina Gerner and Oliver Scherf-Clavel

Pharmaceutics 13(6): 778, 2021

doi: 10.3390/pharmaceutics13060778.

3 **A Physiologically-Based Pharmacokinetic Model of Ruxolitinib and Posaconazole to Predict CYP3A4-Mediated Drug–Drug Interaction Frequently Observed in Graft versus Host Disease Patients**

Bettina Gerner, Fatemeh Aghai-Trommeschlaeger, Sabrina Kraus, Götz Ulrich Grigoleit, Sebastian Zimmermann, Max Kurlbaum, Hartwig Klinker, Nora Isberner and Oliver Scherf-Clavel

Pharmaceutics 14(12): 2556, 2022

doi: 10.3390/pharmaceutics 14122556.

Erklärung zur Autorenschaft

A method for the minimally invasive drug monitoring of mitotane by means of volumetric absorptive microsampling for a home-based therapeutic drug monitoring
Bettina Friedl, Max Kurlbaum, Matthias Kroiss, Martin Fassnacht, Oliver Scherf-Clavel
Analytical and Bioanalytical Chemistry 411(17): 3951-3962, 2019

Bettina Friedl (BF), Max Kurlbaum (MK), Matthias Kroiss (MKr), Martin Fassnacht (MF), Oliver Scherf-Clavel (OSC)

Autor	BF	MK	MKr	MF	OSC	∑ in Prozent
Studiendesign	5	2	3		3	13%
Experimenteller Teil	15	7	5		7	34%
Datenanalyse und Ergebnisinterpretation	14		5	1.5	5	25.5%
Verfassen der Veröffentlichung	10				5	15%
Korrektur der Veröffentlichung		1.5	1.5	1.5	3	7.5%
Koordination der Veröffentlichung					5	5%
Summe						100%

Die Mitautoren der in dieser (teil-)kumulativen Dissertation verwendeten Manuskripte sind sowohl über die Nutzung als auch über die angegebenen Eigenanteile informiert und stimmen dem zu.

Bettina Friedl	Max Kurlbaum	Matthias Kroiss
Hauptautor/in	**Koautor/in**	**Koautor/in**
☒ Verweis: E-Mail hinterlegt	☒ Verweis: E-Mail hinterlegt	☒ Verweis: E-Mail hinterlegt
Martin Fassnacht	Oliver Scherf-Clavel	
Koautor/in	**Korrespondenzautor/in**	
☒ Verweis: E-Mail hinterlegt	☒ Verweis: E-Mail hinterlegt	

Würzburg, 20.03.2023

_____

Prof. Scherf-Clavel

Erklärung zur Autorenschaft

Physiologically Based Pharmacokinetic Modelling of Cabozantinib to Simulate Enterohepatic Recirculation, Drug-Drug Interaction with Rifampin and Liver Impairment
Bettina Gerner and Oliver Scherf-Clavel
Pharmaceutics 13(6): 778, 2021

Bettina Gerner (BG), Oliver Scherf-Clavel (OSC)

Autor	**BG**	**OSC**			**∑ in Prozent**
Studiendesign	5%	2.5			7.5%
Modellentwicklung	30	5			35%
Modellevaluierung und Anwendung	20	5			25%
Verfassen der Veröffentlichung	15	5			20%
Korrektur der Veröffentlichung		7.5			7.5%
Koordination der Veröffentlichung		5			5%
Summe					100%

Die Mitautoren der in dieser (teil-)kumulativen Dissertation verwendeten Manuskripte sind sowohl über die Nutzung als auch über die angegebenen Eigenanteile informiert und stimmen dem zu.

Bettina Gerner	Oliver Scherf-Clavel
Hauptautor/in	**Korrespondenzautor/in**
☒ Verweis: E-Mail hinterlegt	☒ Verweis: E-Mail hinterlegt

Würzburg, 20.03.2023

Prof. Scherf-Clavel

Erklärung zur Autorenschaft

A Physiologically-Based Pharmacokinetic Model of Ruxolitinib and Posaconazole to Predict CYP3A4-Mediated Drug–Drug Interaction Frequently Observed in Graft versus Host Disease Patients

Bettina Gerner, Fatemeh Aghai-Trommeschlaeger, Sabrina Kraus, Götz Ulrich Grigoleit, Sebastian Zimmermann, Max Kurlbaum, Hartwig Klinker, Nora Isberner, Oliver Scherf-Clavel

Pharmaceutics 14(12): 2556, 2022

Bettina Gerner (BG), Fatemeh Aghai-Trommeschlaeger (FAT), Sabrina Kraus (SK), Götz Ulrich Grigoleit (GUG), Sebastian Zimmermann (SZ), Max Kurlbaum (MK), Hartwig Klinker (HK), Nora Isberner (NI), Oliver Scherf-Clavel (OSC)

Autor	BG	FAT	SK	GUG	SZ	MK	HK	NI	OSC	∑ in Prozent
Studiendesign	5	5						2.5	2.5	15%
Klinischer Teil und Datenbeschaffung		1	1	1	1	1	1	1		7%
Modellentwicklung	18	13.5								31.5%
Modellevaluierung und Anwendung	10	7.5								17.5%
Verfassen der Veröffentlichung	10	7.5								17.5%
Korrektur der Veröffentlichung		1.5				1.5		2	2	7%
Koordination der Veröffentlichung	1.5	1.5							1.5	4.5%
Summe										100%

Die Mitautoren der in dieser (teil-)kumulativen Dissertation verwendeten Manuskripte sind sowohl über die Nutzung als auch über die angegebenen Eigenanteile informiert und stimmen dem zu.

Bettina Gerner	Fatemeh Aghai-Trommeschlaeger	Sabrina Kraus
Hauptautor/in	**Koautor/in**	**Koautor/in**
☒ Verweis: E-Mail hinterlegt	☒ Verweis: E-Mail hinterlegt	☒ Verweis: E-Mail hinterlegt
Götz Ulrich Grigoleit	Sebastian Zimmermann	Max Kurlbaum
Koautor/in	**Koautor/in**	**Koautor/in**
☒ Verweis: E-Mail hinterlegt	☒ Verweis: E-Mail hinterlegt	☒ Verweis: E-Mail hinterlegt
Nora Isberner	Oliver Scherf-Clavel	
Koautor/in	**Korrespondenzautor/in**	
☒ Verweis: E-Mail hinterlegt	☒ Verweis: E-Mail hinterlegt	

Würzburg, 20.03.2023 _____

Prof. Scherf-Clavel

2 Conference contributions

Friedl, B., Wahl, O.

A method for the minimally invasive drug monitoring of mitotane

DPhG Jahrestagung **2018**, Hamburg

3 Abbreviations

ACC	adrenocortical carcinoma
ADME	absorption, distribution, metabolism, excretion
AGP	alpha1-acid-glycprotein
alloHSCT	allogeneic hematopoietic stem cell transplantation
AUC	area under the concentration-time curve
BID	twice a day
BCS	biopharmaceutical classification system
C_{max}	maximum plasma concentrations
CL	clearance
C_{ss}	steady state concentration
C_{trough}	trough concentrations
C_u	unbound plasma concentration
CYP	cytochrome P450
DBS	dried blood spot methods
DDI	drug-drug interaction
EGFR	epithelial growth factor receptor
EHC	enterohepatic recirculation
EMA	European Medicines Agency
ENSAT	european network for the study of adrenal tumours
FDA	U.S. food and drug administration
f_{up}	fraction unbound in plasma
GvHD	graft-versus-host disease
HCT	hematocrit
IGF-1R	insulin-like growth factor 1 receptor
i.v.	intravenous
IIV	interindividual variability
IVIVE	in vitro-in vivo extrapolation
JAK1 and 2	Janus Associated Kinases 1 and 2
mAbs	monoclonal antibodies
MAP	maximum a posteriori
MET	hepatocyte growth factor receptor
MIPD	model-informed precision dosing

mTOR	mammalian target of rapamycin
NCA	noncompartmental analysis
NLME	nonlinear mixed-effects modelling/model
NSCLC	non-small cell lung cancer
PBPK	physiologically-based pharmacokinetic
PD	pharmacodynamics
PDGFR	platelet-derived growth factor
PK	pharmacokinetics
popPK	population PK
RTK	receptor tyrosine kinases
RUV	residual variability
SmPC	summary of product characteristics
$t_{1/2}$	half-life
TDM	therapeutic drug monitoring
TNM	tumour, node, metastasis
TKI	tyrosine kinase inhibitor
VAMS	volumetric absorptive microsampler/microsampling
V_d	volume of distribution
VEGF	vascular endothelial growth factor
VEGFR1/2	vascular endothelial growth factor receptor 1/2
TNM	tumour, node, metastasis

87

88

4 Supplementary material

4.1 Supplementary material for results C1

A method for the minimally invasive drug monitoring of mitotane by means of volumetric absorptive microsampling for a home-based therapeutic drug monitoring

Friedl, B., Kurlbaum, M., Kroiss, M., Fassnacht, M., Scherf-Clavel, O.

Reprinted with permission from Springer Nature

Analytical and Bioanalytical Chemistry 411(17): 3951-3962, 2019

Table 1. Measured C_{DBS}, C_P, %Difference between actual plasma concentrations and predicted plasma concentrations (C_{pred} was calculated by dividing the MITRA™ concentration by the slope). MITRA™ samples were analyzed with the developed HPLC-UV method. Plasma concentration was analysed by the Lysosafe® TDM service provided on behalf of the manufacturer, HRA-Pharma (Paris, France)

Patient ID	Conc. MITRA™ [mg/L]	Acutal plasma conc. [mg/L]	Pred. plasma conc. [mg/L]	Difference [%] between pred. plasma conc. and actual plasma conc.	MITRA™ conc. / plasma conc.	Hematocrit
1	11.52	19.4	17.37	10.49	0.59	0.32
2	10.05	15.5	15.15	2.24	0.65	0.43
3	21.02	31.5	31.69	-0.60	0.67	0.34
4	1.64	2.5	2.47	1.09	0.66	0.35
5	< LLOQ	1.2	n.a.	n.a.	n.a.	0.44
6	8.45	15	12.74	15.07	0.56	0.44
7	14.40	21.8	21.71	0.43	0.66	0.40
8	11.74	12.3	17.70	-43.93	0.95	0.37
9	10.11	13.9	15.24	-9.65	0.73	0.39
10	n.a.	n.a.	n.a.	n.a.	n.a.	0.39
11	10.00	19.1	15.07	21.09	0.52	0.33
12	8.70	20	13.12	34.42	0.43	0.40
13	6.53	9	9.85	-9.40	0.73	0.21
14	8.70	19.5	13.12	32.70	0.45	0.39
15	3.60	7.8	5.43	30.43	0.46	0.36
16	9.54	15.6	14.39	7.76	0.61	0.41
17	19.46	20.2	29.35	-45.28	0.96	0.32
18	6.65	10.5	10.03	4.52	0.63	0.40
19	2.06	3.3	3.10	6.10	0.62	0.29
20	8.46	14.9	12.75	14.41	0.57	0.42
21	18.94	20.1	28.56	-42.10	0.94	0.28

Table 1. (continued)

Patient ID	Conc. MITRA™ [mg/L]	Acutal plasma conc. [mg/L]	Pred. plasma conc. [mg/L]	Difference [%] between pred. plasma conc. and actual plasma conc.	MITRA™ conc. / plasma conc.	Hematocrit
22	13.90	16.8	20.96	-24.75	0.83	0.40
23	9.32	15.7	14.06	10.47	0.59	0.39
24	6.67	10.4	10.06	3.25	0.64	0.41
25	2.30	3.6	3.47	3.71	0.64	0.30
26	13.11	16.3	19.77	-21.31	0.80	0.40
27	n.a.	n.a.	n.a.	n.a.	n.a.	0.33
28	9.56	16.7	14.41	13.72	0.57	0.36
29	4.61	12.4	6.95	43.98	0.37	0.41
30	3.66	5.5	5.52	-0.45	0.67	0.36
31	12.51	14.1	18.86	-33.75	0.89	0.29
32	11.96	17.9	18.03	-0.75	0.67	0.37
33	9.90	15.3	14.92	2.48	0.65	0.34
34	< LLOQ	< LLOQ	n.a.	n.a.	n.a.	0.39
35	< LLOQ	< LLOQ	n.a.	n.a.	n.a.	0.44
36	< LLOQ	< LLOQ	n.a.	n.a.	n.a.	0.39
37	10.80	13.4	16.28	-21.47	0.81	0.38
38	8.59	14.4	12.96	10.02	0.60	0.29
39	5.14	7.0	7.74	-10.63	0.73	0.41
40	12.20	13	18.39	-41.46	0.94	0.39
41	8.50	15.7	12.81	18.40	0.54	0.34
42	8.14	11.1	12.28	-10.62	0.73	0.37
43	9.71	9.4	14.64	-55.71	1.03	0.27
44	8.07	11.2	12.17	-8.65	0.72	0.40
45	12.27	13.9	18.50	-33.07	0.88	0.42
46	1.07	1.4	1.61	-15.35	0.77	0.35
47	2.30	7.5	3.47	53.80	0.31	0.37
48	13.82	19.3	20.83	-7.94	0.72	0.35
49	11.04	12.8	16.64	-30.03	0.86	0.40
50	13.23	12.2	19.95	-63.55	1.08	0.23
51	11.18	14.8	16.86	-13.94	0.76	0.32
	Mean ± SD	Mean ± SD	Mean ± SD	Mean ± SD	Mean ± SD	Mean ± SD
	9.19 ± 4.41	13.73 ± 5.85	13.85 ± 6.65	- 0.81 ± 22.97 %	0.67 ± 0.16	0.37 ± 0.04

102

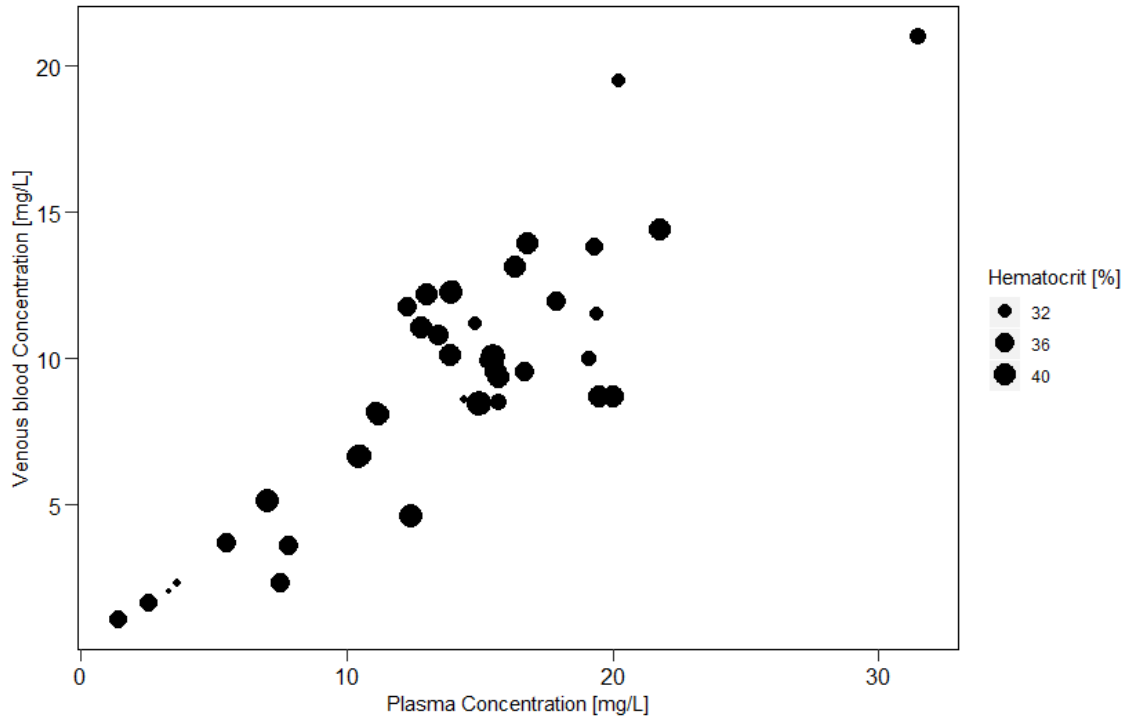

Figure 1. Scatterplot including measured mitotane plasma concentrations, mitotane whole blood concentrations and hematocrit levels of the patients

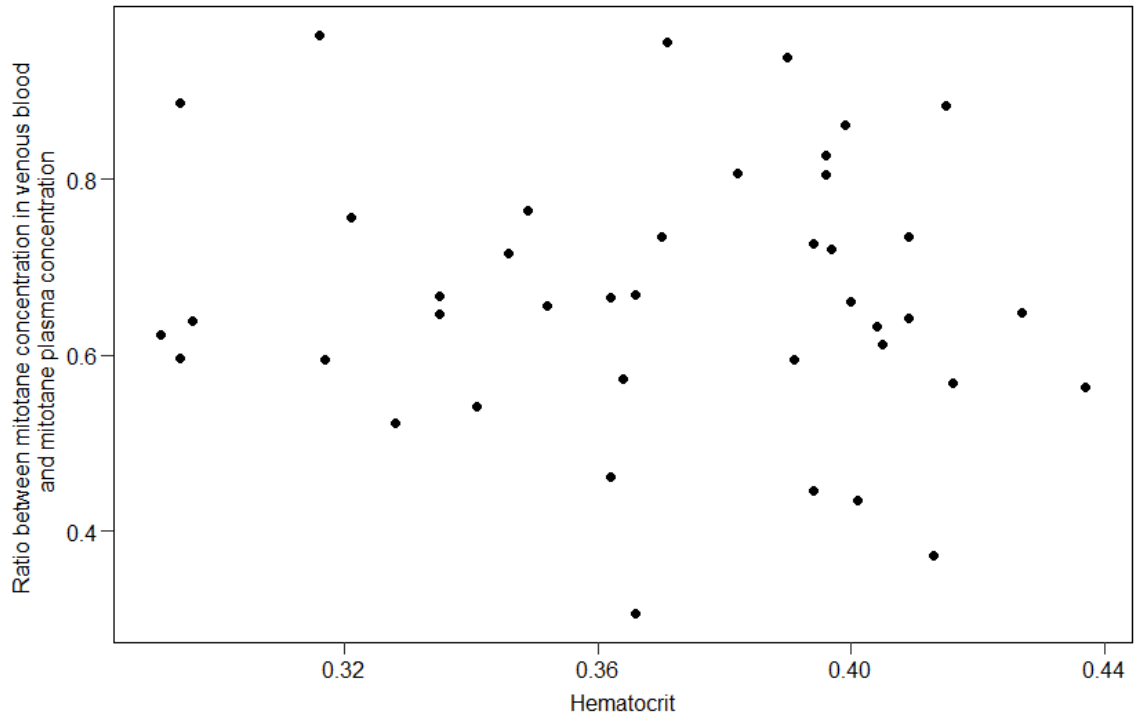

Figure 2. Plot of patients' hematocrit values versus the ratio between measured C_P and C_{DBS} of mitotane (r = - 0.34, $p < 0.05$)

Figure 3. MITRA™ devices loaded with blood samples are boxed in a plastic casing for mechanical stability and packed in a plastic bag (PP) including desiccant for shipment

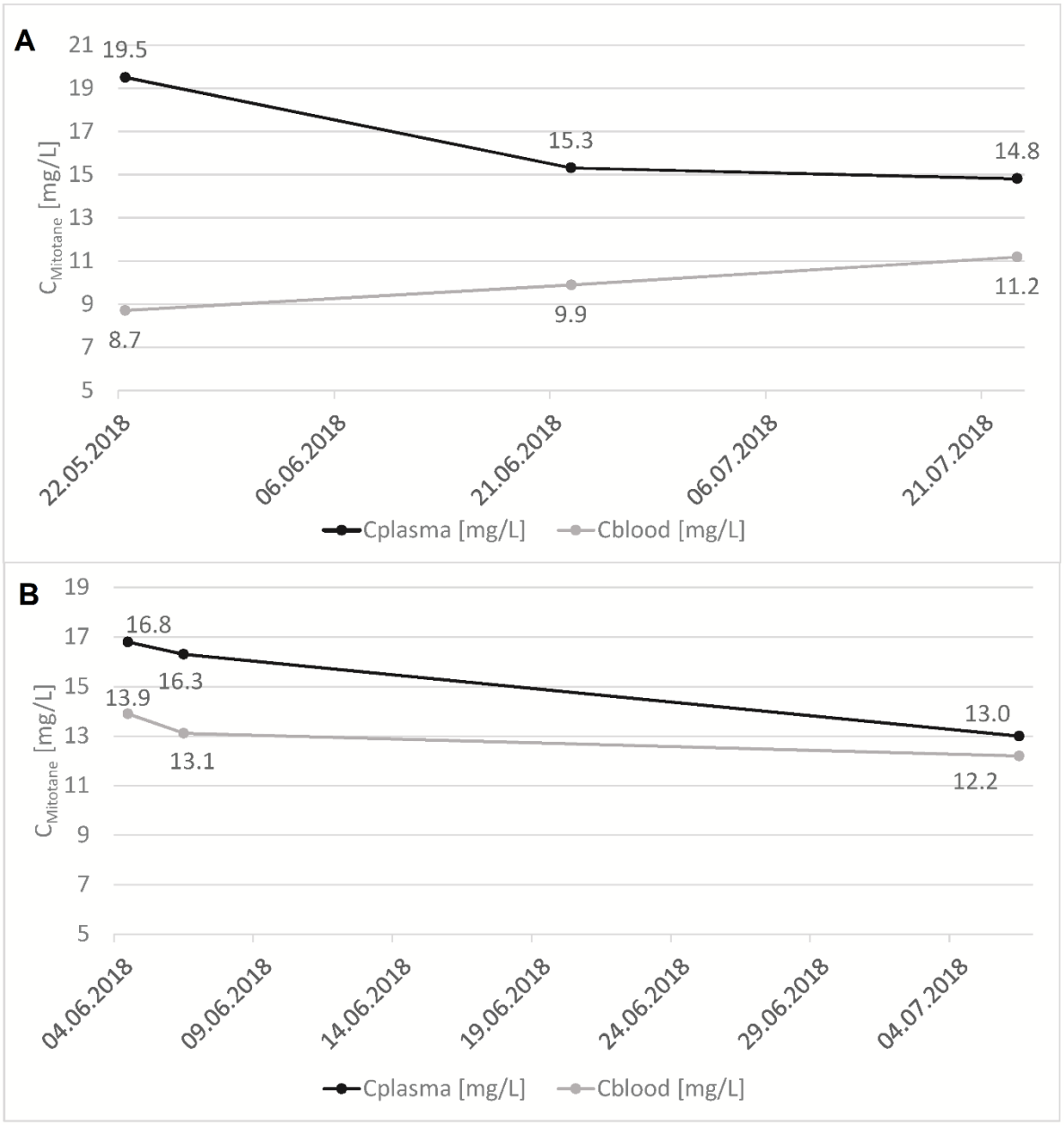

Figure 4. Measured mitotane concentration in plasma vs whole blood. Time course of two different patients: A) in early sustainment phase after dose adjustment

4.2 Supplementary material for results C2

Physiologically Based Pharmacokinetic Modelling of Cabozantinib to Simulate Enterohepatic Recirculation, Drug-Drug Interaction with Rifampin and Liver Impairment

Gerner, B., Scherf-Clavel, O.

Reprinted from Pharmaceutics 13(6): 778, 2021

Contents

Cabozantinib PBPK model development

In this study, a physiologically based pharmacokinetic (PBPK) model for the oral tyrosine kinase inhibitor cabozantinib (CAB) was developed. The substance is extensively metabolized by CYP3A4 and four major CAB metabolites can be found in plasma, namely Exel-5366 (Amide Cleavage Product), Exel-1644 (6-Desmethyl Amide Cleavage Product Sulfate), Exel-1646 (Monohydroxy Sulfate) and Exel-5162 (N-Oxide) (Figure S1). The relevance of membrane transporters for in vivo drug disposition is still unclear [1]. CAB was tested as a substrate for various transporter and was found to be a substrate of MRP2 only [2]. Being a Biopharmaceutics Classification System Class II (BCS II) compound, CAB is characterized by low water solubility and a high cell permeability [3]. As a weak base, only a very small proportion of CAB is charged at the physiological pH of 7.4 and therefore negligible affinity can be expected between CAB and organic anion transporters. Hence, passive diffusion is being considered as the only way for CAB to cross biomembranes in the present model except for the MRP2 mediated active secretion into bile. The PBPK model for CAB was developed to test the hypothesis of EHC and to confirm factors that may influence CAB PK behaviour. The concomitant administration of the strong CYP3A4 inducer Rifampin (RIF) and the influence of liver impairment was investigated regarding changes in plasma concentration-time profiles and exposure. An intensive literature search was conducted for drug-specific model input parameters and 14 plasma concentration time profiles from seven human clinical studies were digitized, divided into a training (n=6) or a test (n=4) dataset and used for model development and evaluation or were used to simulate DDI and liver impairment (Table S1). The model development process was supplemented with intravenous (i.v.) (5 mg/kg, 10mg/kg) data from rats, found in a published work by Wang et al. [4]. All sampling time points for rat and human blood samples [3ml] in each study are given in Table S2. The allocation of human plasma profiles to the training dataset has been done in such a way that i) the broadest possible dose range was covered (20 mg to 140 mg) and ii) both formulations were included (capsule and tablet). For model input parameters which could not be found in literature the parameter identification function in PKSim® was used and model simulations of all training datasets were fitted to the observed data with the integrated Monte Carlo algorithm. The workflow of the CAB PBPK model development from rats to the final CAB PBPK model in humans is shown in Figure S2.

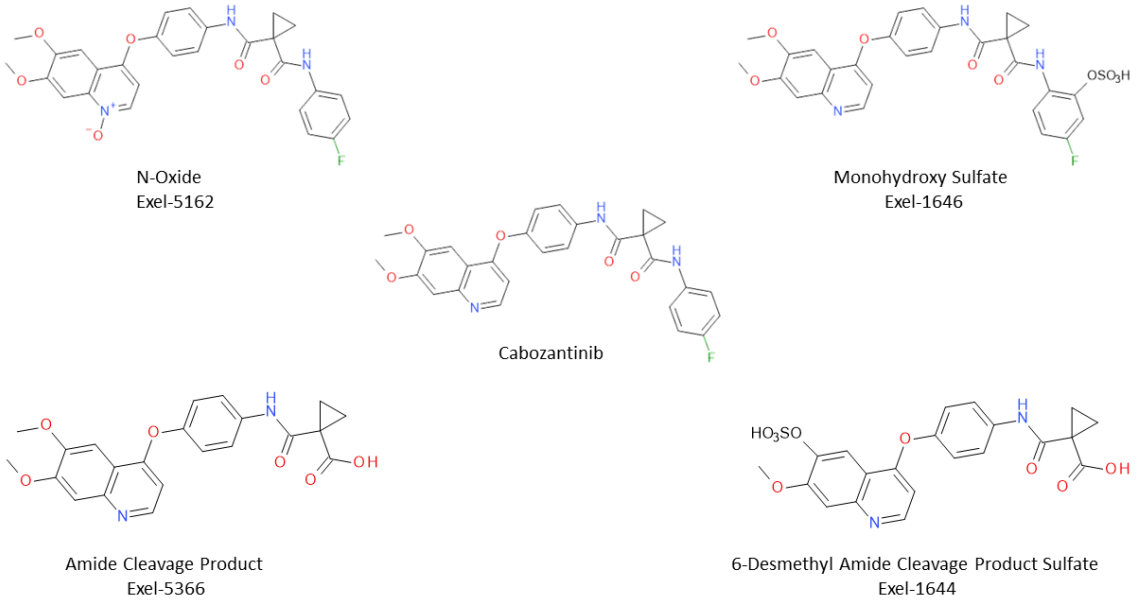

Figure S1. Cabozantinib and its four major plasma metabolites, Exel-5366, Exel-1644, Exel-1646 and Exel-5162.

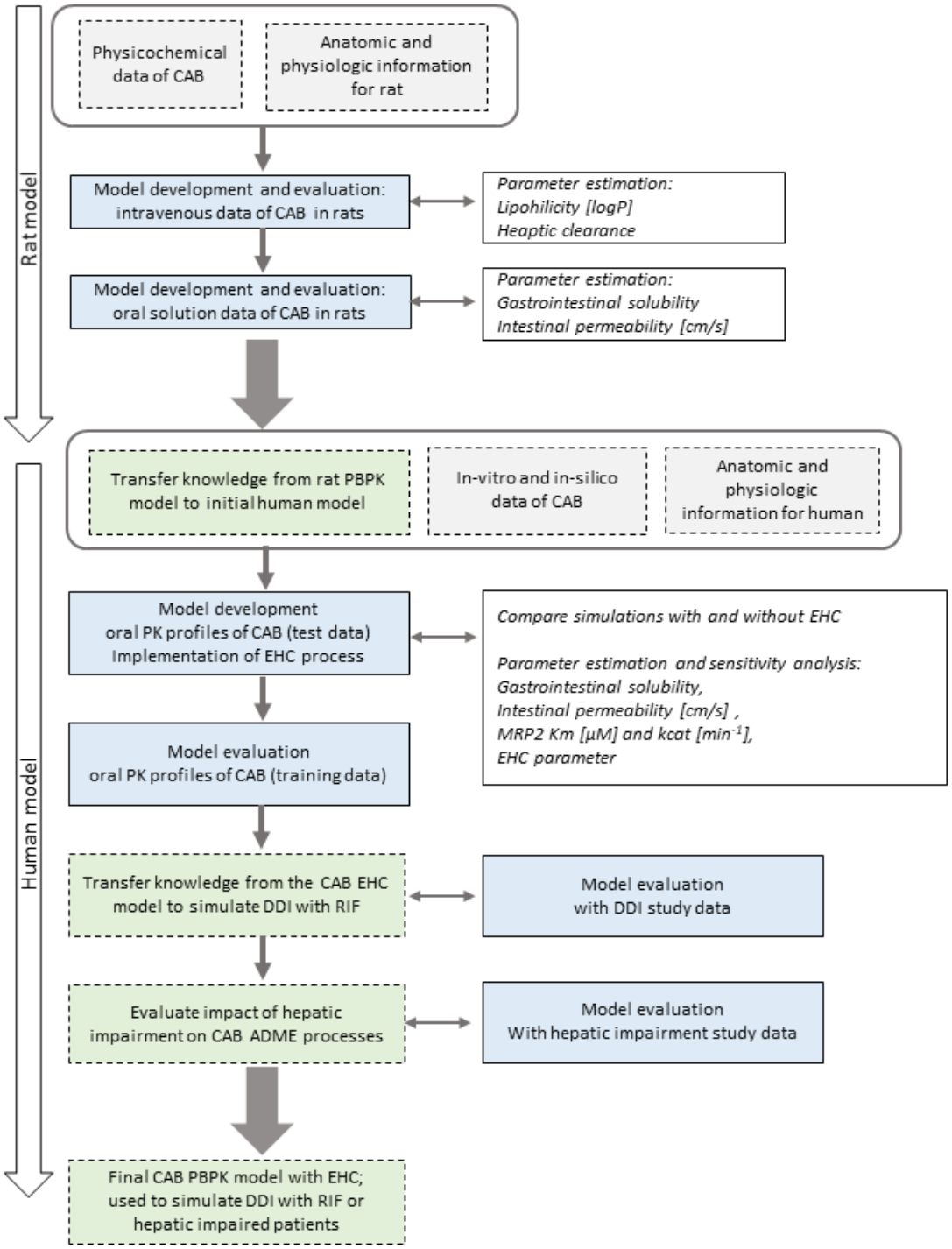

Figure S2. Workflow of the CAB PBPK model development from rats to the final model in humans, which contains enterohepatic circulation process and is capable to model DDI with Rifampin or plasma concentration–time profiles in hepatic impaired patients. *CAB:* cabozantinib; *DDI:* drug-drug interaction; *EHC*: enterohepatic circulation; *RIF:* rifampin.

Table S1. Experimental datasets used for development and evaluation of the base CAB PBPK model, for DDI and hepatic impairment simulations.

Study	Dose [mg]	Treatment	n	Men [%]	Age [yrs]	Weight [kg]	Height [cm]	Dataset	References
PK in rats, Wang et al.	5 mg/kg	iv, SD	8	n.r.	n.r.	n.r.	n.r.	training	[4]
PK in rats, Wang et al.	10 mg/kg	iv, SD	8	n.r.	n.r.	n.r.	n.r.	training	[4]
PK in rats, Wang et al.	15 mg/kg	ig, SD	8	n.r.	n.r.	n.r.	n.r.	training	[4]
PK in rats, Wang et al.	30 mg/kg	ig, SD	8	n.r	n.r.	n.r	n.r.	training	[4]
Mass Balance Study, Lacy et al.	140	po, solution, SD	8	100	n.r. (19-55)	n.r.	n.r.	training	[2]
Phase I PK, Nguyen et al.	20	po, tab, SD	21	52	41 (24-54)	79 (61-112)	168 (151-184)	training	[5]
Phase I PK, Nguyen et al.	40	po, tab, SD	21	52	35 (19-49)	76 (60-97)	166 (152-184)	test	[5]
Phase I PK, Nguyen et al.	60	po, tab, SD	21	52	35 (21-49)	76 (59-93)	165 (145-182)	test	[5]
Phase I BE, Nguyen et al.	140	po, tab, SD	77	42	39 (18-55)	72 (46-108)	164 (146-189)	training	[5]
Phase I BE, Nguyen et al.	140	po, cap, SD	77	42	39 (18-55)	72 (46-108)	164 (146-189)	training	[5]
DDI Study 1, Nguyen et al.	140	po, cap, SD, with RIF	28	57	35 (22-49)	77 (57-111)	n.r.	DDI	[6], Study 1
DDI Study 1, Nguyen et al.	140	po, cap, SD, w/o RIF	28	57	35 (22-49)	77 (57-111)	n.r.	test	[6], Study 1
DDI Study 2, Nguyen et al.	140	po, cap, SD, w/o KET	28	68	39 (22-54)	77 (56-100)	n.r.	training	[6], Study 2
Food Effect Study, Nguyen et al.	140	po, cap, SD, fasted	47	46	38 (18-55)	76 (49-96)	n.r.	training	[7], Study 1
PPI Effect Study, Nguyen et al.	100	po, tab, SD	22	41	38 (25-50)	72 (56-100)	n.r.	test	[7], Study 2
Liver impairment, Nguyen et al.	60	po, cap SD, healthy	10	100	54 (43-65)	89 (65-107)	n.r.	liver	[8]
Liver impairment, Nguyen et al.	60	po, cap SD, mild impairment	8	100	56 (40-65)	92 (71-112)	n.r.	liver	[8]
Liver impairment, Nguyen et al.	60	po, cap SD moderate impairment	8	100	58 (53-62)	86 (66-104)	n.r.	liver	[8]

BE: bioequivalence, *cap*: capsule, *ig:* intragastric, *KET:* Ketoconazol, *n*: number of individuals per study, *n.r.:* not reported, *po*: per os, *RIF:* Rifampin, *SD*: single dose, *tab*: tablet, *w/o*: without. Values in brackets given for age, weight, and height are minima and maxima, all po administrations were given to human subjects

Table S2. Sampling times in minutes for rat and human blood samples in each study

Study	Sampling times [hours]	References
PK in rats, Wang et al.	0, 0.0833, 0.5, 0.75, 1, 2, 3, 4, 6, 8, 24, 48	[4]
Phase I Pharmacokinetics Nguyen et al.	0.5, 1, 2,3, 4, 5, 6, 8, 10, 14, 24, 48, 72, 96, 120, 168, 240, 336, 408, 504 h	[5]
Phase I Bioequivalence Nguyen et al.	0.5, 1, 2, 3, 4, 5, 6, 7,8, 10, 14, 24, 48, 72, 96, 120, 168, 240, 288, 336, 408, 504	[5]
DDI Studies Nguyen et al.	0.5, 1, 2, 3, 4, 5, 6, 7, 8, 9, 10, 14, 24, 72, 96, 120, 144, 168, 240, 288, 336, 408, 504	[6]
Food Effect Study Nguyen et al	0.5, 1, 2, 3, 4, 5, 6, 8, 10, 14, 24, 48, 72, 120, 168, 240, 336, 408, 504	[7], Study 1
PPI Effect Study Nguyen et al.	0.5, 1, 2, 3, 4, 5, 6, 8, 10, 14, 24, 48, 72, 120, 168, 240, 336, 408, 504	[7], Study 2
Liver impairment Study, Nguyen et al.	0.5, 1, 2, 3, 4, 5, 8, 14, 24, 48, 72, 96, 120, 168, 240, 288, 336, 432, 504	[9]

DDI: drug-drug interaction; *PPI:* proton-pump inhibitor

Inspection of rat and human plasma concentration-time data

Plasma concentration-time data after intravenous (iv) and intragastric (ig) administration to Sprague-Dawley rats were extracted from literature [4] and plotted dose normalized (Figure S3) to identify nonlinear properties.

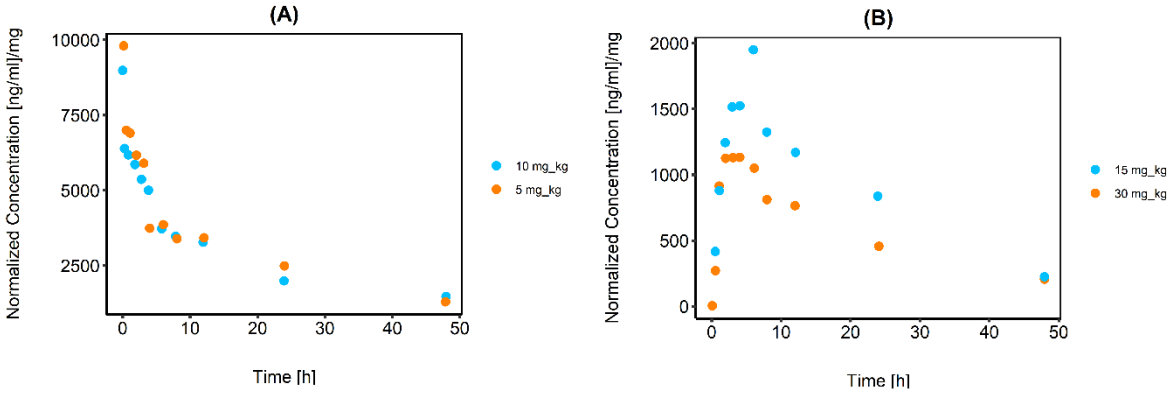

Figure S3. Visual inspection of dose normalized plasma concentration-time curves from 0 to 50 hours for (A) iv administration of 5 mg/kg and 10 mg/kg to Sprague-Dawley rats and (B) intragastric administration of 15 mg/kg and 30 mg/kg to Sprague-Dawley rats.

For all available data in human healthy subjects, dose normalization was performed on the exposure parameters AUC_{0_inf} (area under the concentration–time curves from the first data point to infinity) and C_{max} (maximum concentrations) (

Figure **S4**) to verify linear pharmacokinetics and to gain hints for processes like supersaturation or colon absorption. Dose normalized spaghetti plots in linear and semi-logarithmic scale are shown in Figure S5. In contrast to the plotted rat data, no nonlinear PK could be observed in humans after oral administration, which is consistent with the findings of Lacy et al.[3]. They further describe a significantly lower AUC_{0_inf} when CAB is combined with RIF. Higher systemic exposure is also described for mild and moderate liver impairment by the authors. Figure S5 presents these observations graphically. In addition, concentration-time profiles were plotted after administration of CAB tablets (20, 40, 60, 100 and 140 mg), but without dose normalization (Figure S6). These plots can help to identify existing deposition effects e.g., via binding to proteins or to tissue components. Due to the gradual release of the substance from such a depot, a relatively slow decrease of the plasma concentration at later time points with a long terminal half-life combined with a rapid decrease of the plasma concentration at the beginning would be observed in this case. This effect would be independent of the given dose. As CAB also shows that dichotomy in plasma concentration-time profile, this option was tested, but could not be confirmed as different doses resulted in different plasma concentrations in the second, slowly declining phase. Furthermore, a deposit effect does not automatically explain multiple peaks in plasma concentration-time profiles. As only mean data were available for model development, there might also be a theoretical possibility, that some patients have extraordinary high plasma concentrations after approximately 24 hours, resulting in a general increase of the plasma concentration-time profile at that time. However, because this characteristic peak after 24 hours appears in almost all studies, with different study participants, that theory was excluded.

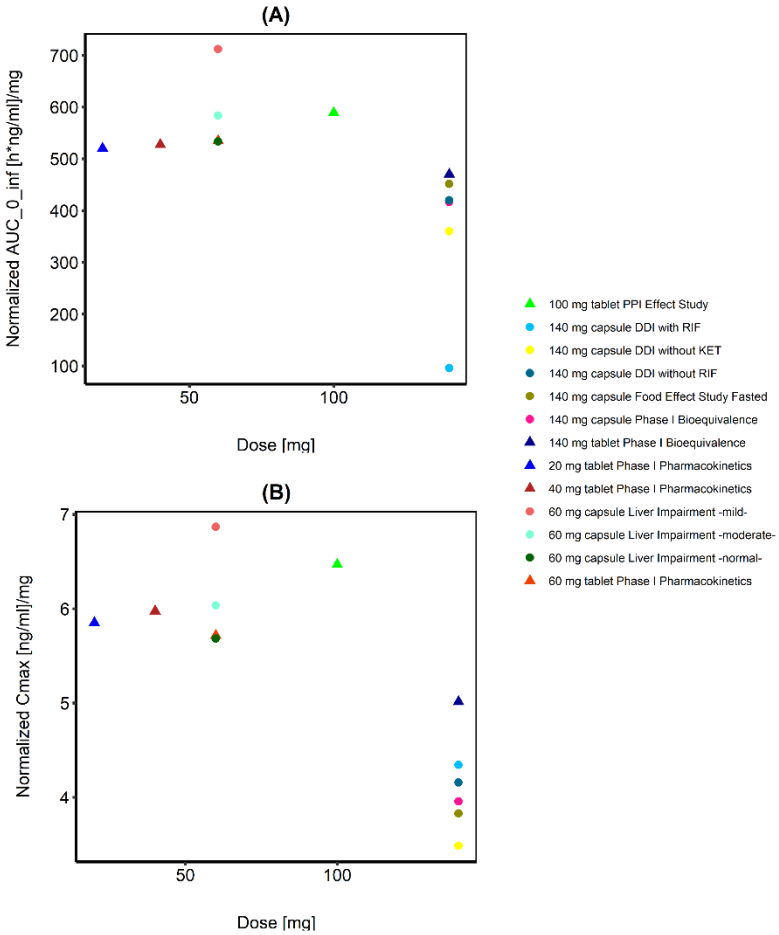

Figure S4. Visual inspection of dose normalized PK parameters versus dose in humans. (A) area under the plasma concentration-time curve from time zero to infinity (AUC_{0_inf}), (B) maximum observed concentration.

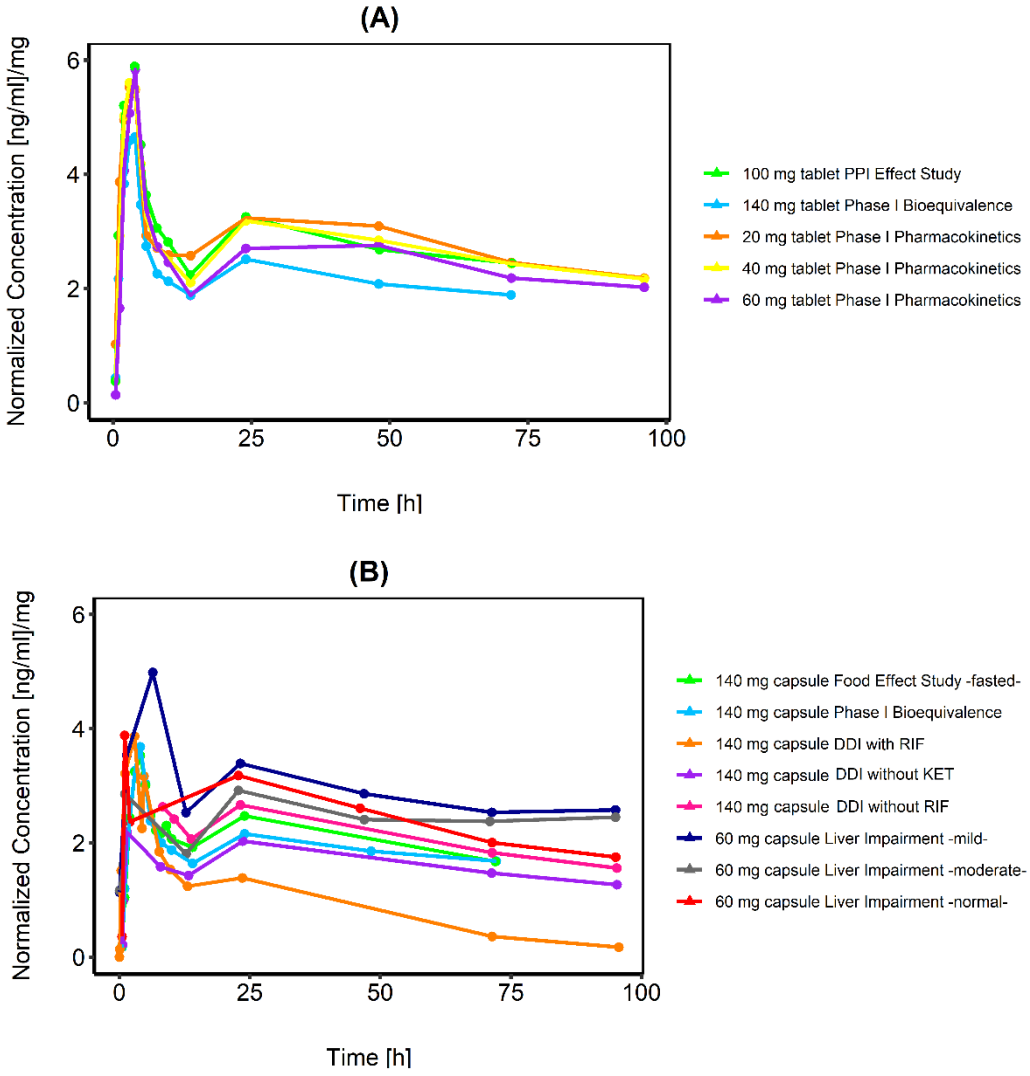

Figure S5. Visual inspection of dose normalized plasma concentration-time curves from 0 to 100 hours for (A) tablet formulations and (B) capsule formulations.

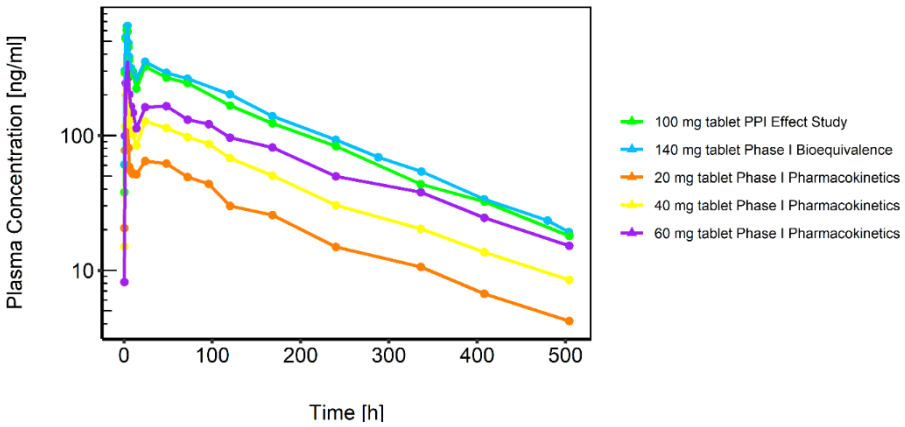

Figure S6. Semilogarithmic plots of plasma concentration-time profiles after single oral administrations of 20, 40, 60 and 100, respectively 140 mg CAB tablet to healthy humans.

Rat intravenous and intragastric simulations

The final parameter used for the rat PBPK model are shown in Table S3. The simulated fraction absorbed for ig 30 mg/kg was lower (0.23) compared to ig 15 mg/kg (0.34) and is in agreement with the nonlinear properties and the lower plasma concentration for the higher dose, which was observed in the dose-normalized plasma concentration-time plots and attributed to differences in drug absorption. Besides the graphical check, model evaluation was done through comparison of the predicted vs observed PK parameters C_{max} and AUC_{last} (Area under the concentration time curve from the first to the last data point) as well as through calculation of the mean prediction error (MPE) and mean absolute prediction error (MAPE) to evaluate bias and prediction of the rat model. Both models show a high accuracy illustrated by a low bias (MPE range – 6.4% to + 12.2%) and a good precision (MAPE range 18.4–33.8%). A mean relative deviation (MRD) of all predicted plasma concentrations ≤ 2 characterize an adequate model performance and was achieved in all simulations (MRD range 1.23-1.63). Table S4 summarizes the respective PK parameters C_{max} and AUC_{last} as well as the values for MPE, MAPE and MRD.

Table S3 Summary of the CAB parameters used in the rat PBPK model

Parameter	Unit	Value used in PBPK model	Literature value [Reference]	Description
MW	[g/mol]	501.50	501.50 [10,11]	Molecular weight
pK_a [base]		6.32	6.32 [12]	Acid dissociation constant
fu_p		0.24	0.24[a] [2]	Fraction unbound in plasma
logP		4.40[b]	5.15 [12]	Lipophilicity
Solubility (pH 6.5)	[10^{-3} mg/mL]	7.72[b]	0.00 [10]	Solubility
$Cl_{hepatic}$	[ml/min/kg]	0.08[b]	--	Total plasma clearance in liver
Partition coefficients		Rodgers and Rowland	[13,14]	Calculation method cell to plasma coefficients
Cellular permeabilities		PKSim® Standard	[15]	Calculation method permeation across cell membranes

[a] based on human plasma protein binding; [b] Model parameters have been estimated through parameter optimization based on the plasma concentrations; -- Value not available

Table S4. Predicted and observed AUC_{last} and C_{max} values of CAB plasma concentrations in rats. Bias (mean prediction error) and precision (mean absolute prediction error) and mean relative deviation.

Route / Dose	AUC_{last}			C_{max}			MPE	MAPE [%]	MRD
	Pred [ng*h/ml]	Obs [ng*h/ml]	Pred/ Obs	Pred [ng/ml]	Obs [ng/ml]	Pred/ Obs			
iv 5 mg/kg	154434.0	152843.8	1.0	14117.0	12392.2	1.1	- 6.4	19.2	1.27
iv 10 mg/kg	309075.4	226769.3	1.4	28232.3	20998.2	1.3	+ 1.9	18.4	1.23
ig 15 mg/kg	141369.9	147716.7	1.0	4681.3	6725.8	0.7	+ 12.2	31.3	1.48
ig 30 mg/kg	237664.6	179824.5	1.3	8019.9	7806.45	1.0	+ 10.4	33.8	1.63

AUC_{last}: Area under the concentration time curve from the first to the last data point*, C_{max}:* maximum plasma concentration, *MAPE:* mean absolute prediction error, *MPE:* mean prediction error, *MRD:* mean relative deviation, *Obs:* observed value, *Pred:* predicted value

Human PBPK model evaluation

In addition to the plots shown in the main manuscript, semi-logarithmic plots of population predictions compared to observed plasma concentration-time profiles are shown in Figure S7. Figure S8 shows the predicted vs. observed AUC_{last} C_{max} values of all studies. Mean predicted and observed AUC_{last} and C_{max} values, model bias (mean prediction error), model precision (mean absolute prediction error) and mean relative deviation (MRD) are listed in Table S5 and Table S6. Results of the local sensitivity analysis, which was made based on the simulation of the 140 mg CAB capsule administration, are demonstrated in Figure S9.

Semi-logarithmic plots

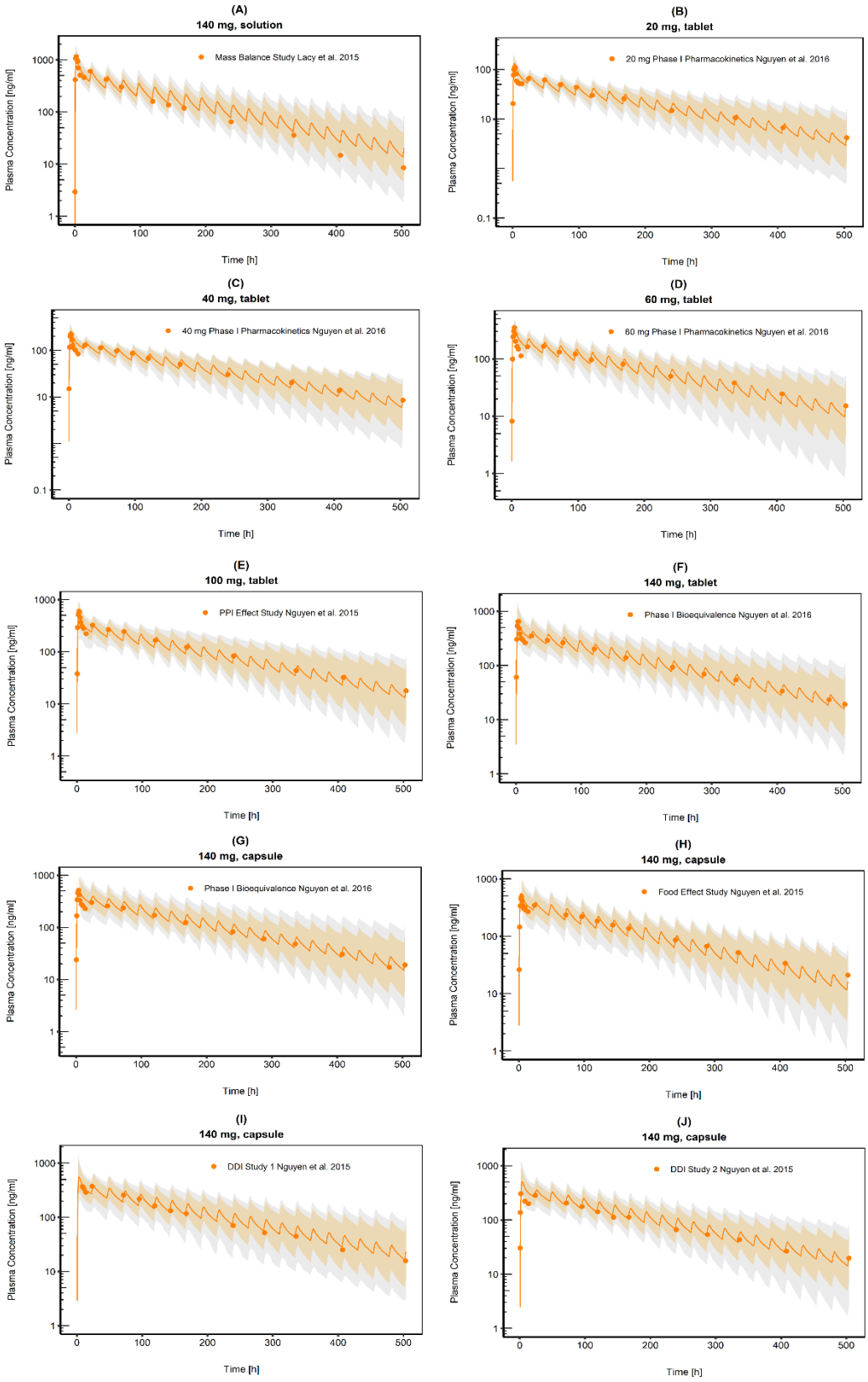

Figure S7. CAB plasma concentration-time profiles (semi-logarithmic). Observed data are shown as orange circles. Population simulation (n=100) geometric means are shown as orange lines; the shaded

orange areas represent the predicted population geometric SD. The shaded grey areas represent the 5 to 95 % prediction interval.

Goodness-of-fit plots for AUC and Cmax

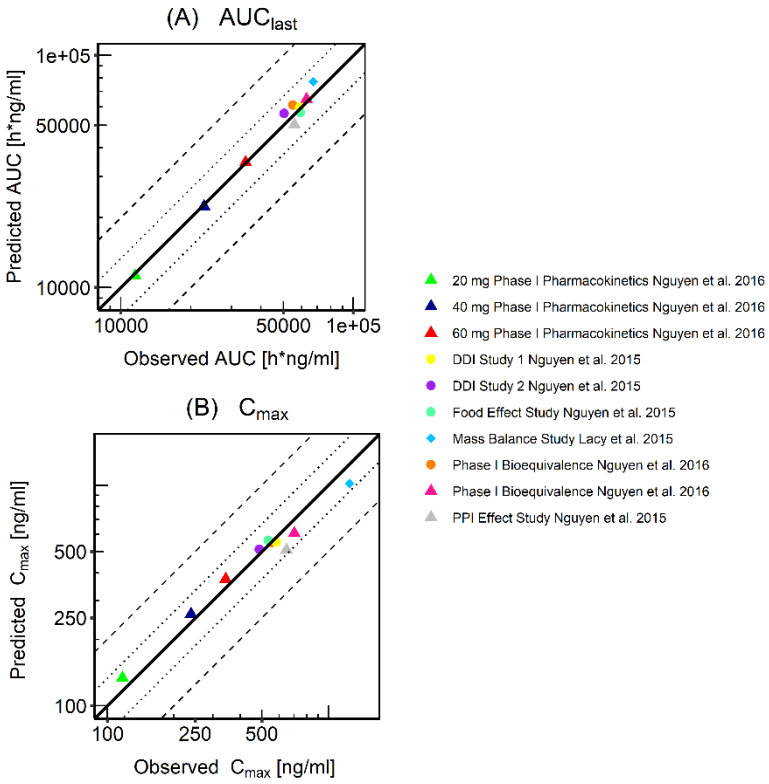

Figure S8. Goodness-of-fit plots for the predicted versus observed (A) AUC_{last} and (B) C_{max}. Tablet formulations are represented by triangles, capsule formulations are represented by dots, the solution is represented by diamonds. In each plot, the black solid line represents the line of identity; dashed black lines represent a twofold deviation; dotted black lines represent a 1.25-fold deviation.

Sensitivity analysis

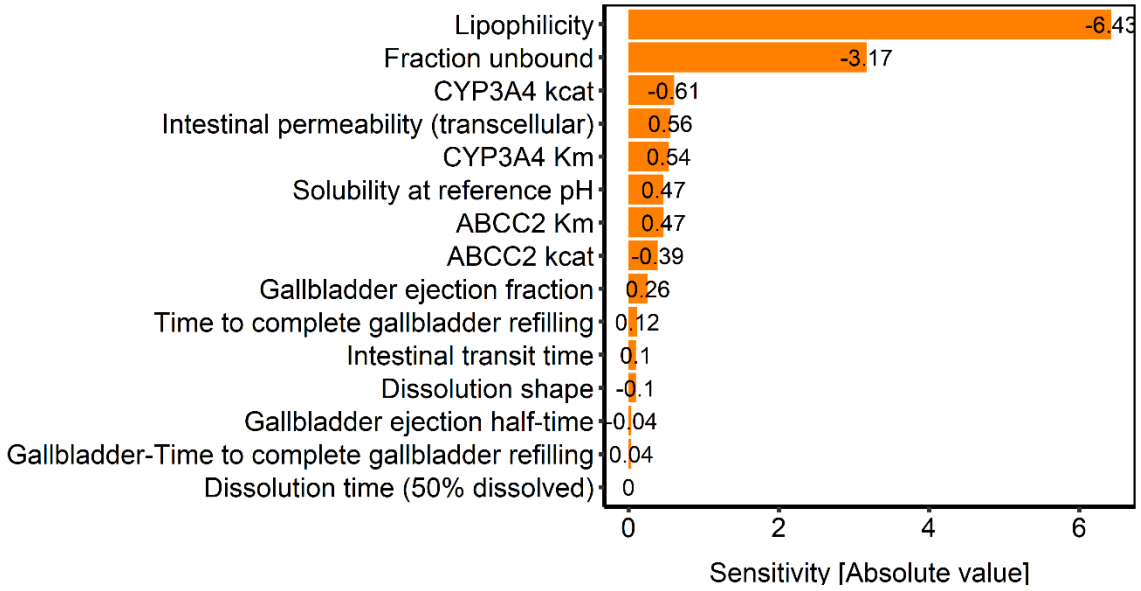

Figure S9. Sensitivity analysis for parameters which were estimated during the model development or which might have an impact due to calculation methods in PK-Sim®. Sensitivity was measured as the relative change of AUC_{last} of a 140 mg CAB capsule single dose administration. Variation range was 10.0 with maximum number of steps = 9. *ABCC2:* MRP2 coding gene, *kcat*: katalytic rate constant, *Km:* Michaelis-Menten constant.

Table S5. Mean predicted and observed pharmacokinetic parameters of CAB after oral single dose of 20, 40, 60, 100 and 140 mg CAB tablet, capsule or solution in healthy volunteers

Dose, Formulation	AUC_{last}			C_{max}			Reference
	Pred [ng*h/ml]	Obs [ng*h/ml]	Pred/Obs	Pred [ng/ml]	Obs [ng/ml]	Pred/Obs	
20 mg, tablet	11245.2	11508.4	1.0	133.7	117.0	1.1	[5]
40 mg, tablet	22636.5	22781.5	1.0	260.2	239.0	1.1	[5]
60 mg, tablet	34579.8	34376.0	1.0	274.9	343.0	1.1	[5]
140 mg, tablet	64750.2	62895.7	1.0	604.8	702.0	0.9	[5]
140 mg, cap	61111.8	54897.1	1.1	541.5	554.0	1.0	[5]
140 mg, cap	59738.1	58800.0[a]	1.0	551.2	582.0	1.0	[6] Study 1
140 mg, cap	56190.1	50400.0[a]	1.1	510.9	488.0	1.1	[6] Study 2
140 mg, cap	56725.8	59200.0	1.0	561.4	536.0	1.1	[7] Study 1
100 mg, tablet	50274.5	55800.0	0.9	507.5	647.0	0.8	[7] Study 2
140 mg, solution	77017.6	67200.0	1.2	1018.7	1250.0	0.8	[2]

AUC_{last}: Area under the concentration time curve from the first to the last data point, *cap:* capsule, *C_{max}:* maximum plasma concentration, *Obs:* observed value, *Pred:* predicted value

[a] reported values are area under the concentration time curve from the first data point to infinity

Table S6. Bias (mean prediction error), precision (mean absolute prediction error) and mean relative deviation (MRD).

Dose, Formulation	MPE	MAPE	MRD	Reference
20 mg, tablet	+ 14.1	24.3	1.32	[5]
40 mg, tablet	+ 20.8	21.7	1.28	[5]
60 mg, tablet	+ 37.2	39.9	1.51	[5]
140 mg, tablet	+ 9.7	18.7	1.24	[5]
140 mg, cap	+ 17.2	30.1	1.75	[5]
140 mg, cap	+ 16.4	19.4	1.22	[6] Study 1
140 mg, cap	+ 10.8	34.9	1.68	[6] Study 2
140 mg, cap	+ 6.8	21.4	1.66	[7] Study 1
100 mg, tablet	- 4.7	13.9	1.88	[7] Study 2
140 mg, solution	+ 43.0	53.3	1.67	[2]

cap: capsule, *MPE:* mean prediction error, *MAPE:* mean absolute prediction error, *MRD:* mean relative deviation

mean MRD	**1.53 (1.22 – 1.88)**
	10/10 with MRD ≤ 2

Simulations of DDI between CAB and RIF

Table S7. Comparison of average CAB steady state plasma concentrations (C_{ss}) after different CAB and RIF administration schemes to evaluate CAB RIF DDI influence on plasma exposure.

Administration scheme	CAB Formulation	CAB C_{ss} (ng/ml)	Ratio CAB alone/ CAB+RIF
60 mg CAB	tablet	1197.44	0.67
80 mg CAB + 600 mg RIF	tablet	394.74	
140 mg CAB	capsule	1576.68	
180 mg CAB + 600 mg RIF	capsule	532.41	0.66

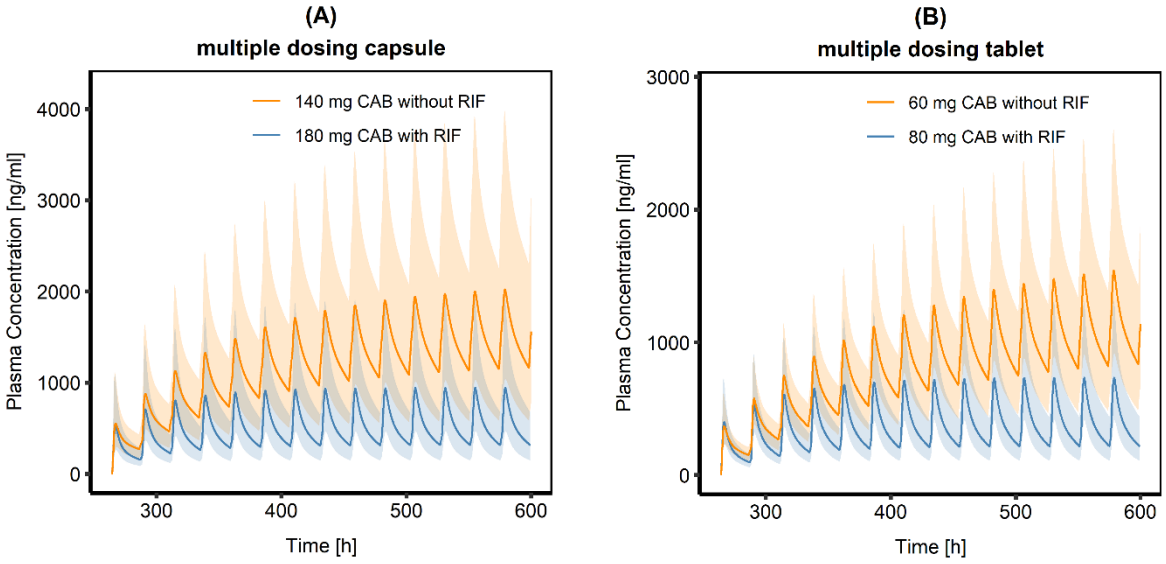

Figure S10. Population simulations (n = 100) of CAB steady state plasma concentration-time profiles. (A) the orange respectively blue line represents the population simulations geometric mean of the predicted plasma concentration after administration of a 140 mg CAB capsule alone (orange line) or a 180 mg CAB capsule with co-administration of 600 mg RIF (blue line). (B) the orange respectively blue line represents the population simulations geometric mean of the predicted plasma concentration after administration of a 60 mg CAB tablet alone (orange line) or a 80 mg CAB tablet with co-administration of 600 mg RIF (blue line). CAB and RIF were administered once daily in each case. CAB administration started on day 11 to account for the run-in period of RIF administration alone until reaching a RIF steady state concentration. The shaded areas represent the predicted population geometric SD in each case.

Investigation of hepatic impairment on CAB plasma exposure

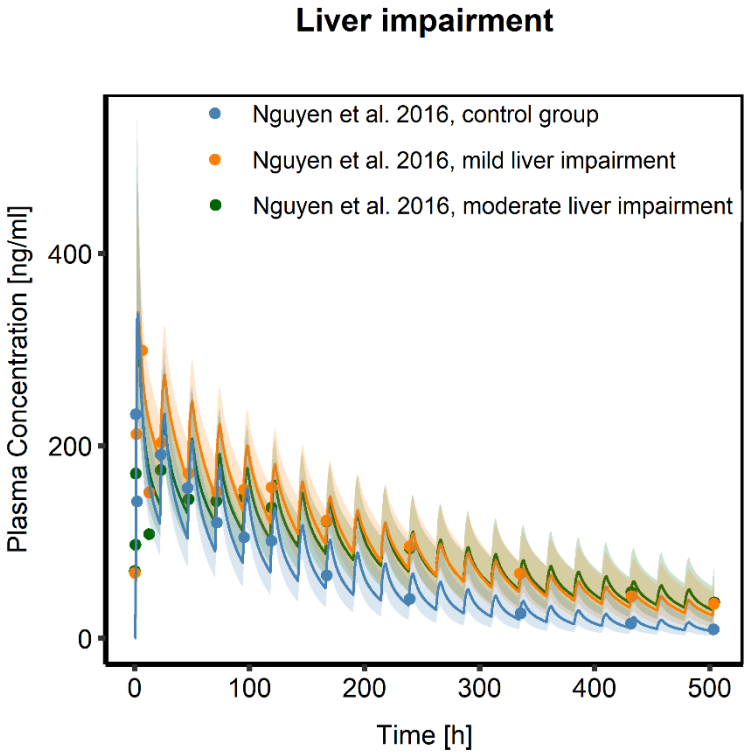

Figure S11. Comparison of simulated plasma concentration-time profiles after a single administration of 60mg CAB capsule to a healthy control group and a mild and moderate liver impaired population; n = 100 in each case. Blue, orange and green dots represent the observed plasma concertation in the respective group; the blue, orange and green line indicate the population simulations geometric mean of the predicted plasma concentration; the shaded areas represent the predicted population geometric SD.

References

1. Neul, C.; Schaeffeler, E.; Sparreboom, A.; Laufer, S.; Schwab, M.; Nies, A.T. Impact of Membrane Drug Transporters on Resistance to Small-Molecule Tyrosine Kinase Inhibitors. *Trends Pharmacol Sci* **2016**, *37*, 904-932.
2. Lacy, S.; Hsu, B.; Miles, D.; Aftab, D.; Wang, R.; Nguyen, L. Metabolism and Disposition of Cabozantinib in Healthy Male Volunteers and Pharmacologic Characterization of Its Major Metabolites. *Drug Metab Dispos* **2015**, *43*, 1190-1207.
3. Lacy, S.A.; Miles, D.R.; Nguyen, L.T. Clinical Pharmacokinetics and Pharmacodynamics of Cabozantinib. *Clin Pharmacokinet* **2017**, *56*, 477-491.
4. Wang, X.; Wang, S.; Lin, F.; Zhang, Q.; Chen, H.; Wang, X.; Wen, C.; Ma, J.; Hu, L. Pharmacokinetics and tissue distribution model of cabozantinib in rat determined by UPLC-MS/MS. *J Chromatogr B Analyt Technol Biomed Life Sci* **2015**, *983-984*, 125-131, doi:10.1016/j.jchromb.2015.01.020.
5. Nguyen, L.; Benrimoh, N.; Xie, Y.; Offman, E.; Lacy, S. Pharmacokinetics of cabozantinib tablet and capsule formulations in healthy adults. *Anti-Cancer Drugs* **2016**, *27*, 669-678.
6. Nguyen, L.; Holland, J.; Miles, D.; Engel, C.; Benrimoh, N.; O'Reilly, T.; Lacy, S. Pharmacokinetic (PK) drug interaction studies of cabozantinib: Effect of CYP3A inducer rifampin and inhibitor ketoconazole on cabozantinib plasma PK and effect of cabozantinib on CYP2C8 probe substrate rosiglitazone plasma PK. *J Clin Pharmacol* **2015**, *55*, 1012-1023.
7. Nguyen, L.; Holland, J.; Mamelok, R.; Laberge, M.K.; Grenier, J.; Swearingen, D.; Armas, D.; Lacy, S. Evaluation of the effect of food and gastric pH on the single-dose pharmacokinetics of cabozantinib in healthy adult subjects. *J Clin Pharmacol* **2015**, *55*, 1293-1302.
8. Nguyen, L.; Holland, J.; Ramies, D.; Mamelok, R.; Benrimoh, N.; Ciric, S.; Marbury, T.; Preston, R.A.; Heuman, D.M.; Gavis, E. Effect of renal and hepatic impairment on the pharmacokinetics of cabozantinib. *The Journal of Clinical Pharmacology* **2016**, *56*, 1130-1140.
9. Nguyen, L.; Holland, J.; Ramies, D.; Mamelok, R.; Benrimoh, N.; Ciric, S.; Marbury, T.; Preston, R.A.; Heuman, D.M.; Gavis, E.; et al. Effect of Renal and Hepatic Impairment on the Pharmacokinetics of Cabozantinib. *J Clin Pharmacol* **2016**, *56*, 1130-1140, doi:10.1002/jcph.714.

10. U.S. Food and Drug Administration. Cometriq (cabozantinib) Capsules. Chemistry Review(s) 2012; https://www.accessdata.fda.gov/drugsatfda_docs/nda/2012/203756Orig1s000ChemR.pdf (accessed on 2020 Jan 15).
11. U.S. Food and Drug Administration. CABOMETYX (cabozantinib) Tablets. Chemistry Review(s) 2015; https://www.accessdata.fda.gov/drugsatfda_docs/nda/2016/208692Orig1s000ChemR.pdf (accessed on 2020 Jan 15).
12. Ipsen Biopharmaceuticals Canada Inc. CABOMETYX Product Monograph. 2019; https://ipsen.com/websites/IPSENCOM-PROD/wp-content/uploads/sites/18/2019/11/21094828/Cabometyx-PM-EN-07Nov2019.pdf (accessed on 2020 Jan 15).
13. Rodgers, T.; Leahy, D.; Rowland, M. Physiologically based pharmacokinetic modeling 1: predicting the tissue distribution of moderate-to-strong bases. *J Pharm Sci* **2005**, *94*, 1259-1276.
14. Rodgers, T.; Rowland, M. Physiologically based pharmacokinetic modelling 2: predicting the tissue distribution of acids, very weak bases, neutrals and zwitterions. *J Pharm Sci* **2006**, *95*, 1238-1257.
15. Open Systems Pharmacology. PK-Sim® software manual. Available online: https://docs.open-systems-pharmacology.org/ (accessed on 2019 Sep 26).

4.3 Supplementary material for results C3

A Physiologically-Based Pharmacokinetic Model of Ruxolitinib and Posaconazole to Predict CYP3A4-Mediated Drug–Drug Interaction Frequently Observed in Graft versus Host Disease Patients

Bettina Gerner, Fatemeh Aghai-Trommeschlaeger, Sabrina Kraus, Götz Ulrich Grigoleit, Sebastian Zimmermann, Max Kurlbaum, Hartwig Klinker, Nora Isberner, Oliver Scherf-Clavel

Reprinted from Pharmaceutics 14(12): 2556, 2022

Contents

1. Posaconazole

1.1 Clinical studies

All clinical studies used for posaconazole PBPK model building and evaluation are summarized in Table S1.

Table S8. Posaconazole clinical study data used for model development and evaluation

Study	Dose [mg]	Treatment	n	Men [%]	Age [yrs]	Weight [kg]	Height [cm]	BMI [kg/m^2]	Dataset	References
Kersemaekers et al. (2015)	50	iv, SD (30 min)	72	46	18-65	n.r.	n.r.	19-35	training	[1]
Kersemaekers et al. (2015)	100	iv, SD (30 min)	72	46	18-65	n.r.	n.r.	19-35	training	[1]
Kersemaekers et al. (2015)	200	iv, SD (30 min)	72	46	18-65	n.r.	n.r.	19-35	training	[1]
Kersemaekers et al. (2015)	250	iv, SD (30 min)	72	46	18-65	n.r.	n.r.	19-35	training	[1]
Kersemaekers et al. (2015)	300	iv, SD (30 min)	72	46	18-65	n.r.	n.r.	19-35	training	[1]
Li et al. (2019)	300	iv, SD (30 min)	18	67	32.5 (20-44)	63 (51-76)	166 (149-178)	22.9 (19-24)	test	[2]
Krishna et al. (2012a)	200	po, tab, SD/MD	10	50	47.7 (33-59)	74.85 (61-100)	165.60 (156-175)	n.r.	training	[3]
Krishna et al. (2012a)	400	po, tab, SD/MD	9	67	43.8 (31-56)	72.89 (61-86)	168.78 (155-181)	n.r.	test	[3]
Krishna et al. (2012b)	100	po, tab, SD (fasting)	16	50	31.4 (19-45)	n.r.	n.r.	26.1 (21.3-30.5)	training	[4]
Krishna et al. (2012b)	100	po, tab, SD (fed)	16	50	31.4 (19-45)	n.r.	n.r.	26.1 (21.3-30.5)	training	[4]
Krishna et al. (2012b)	100	po, sus, SD (fasting)	16	50	31.4 (19-45)	n.r.	n.r.	26.1 (21.3-30.5)	test	[4]
Krishna et al. (2012b)	100	po, sus, SD (fed)	16	50	31.4 (19-45)	n.r.	n.r.	26.1 (21.3-30.5)	test	[4]
Ezzet et al. (2005)	800	po, sus, QD	18	100	36 (26-44)	81.9 (63.6-100)	n.r.	n.r.	training	[5]
Ezzet et al. (2005)	400	po, sus, BID	18	100	36 (26-44)	81.9 (63.6-100)	n.r.	n.r.	training	[5]
Ezzet et al. (2005)	60	po, sus, QID	18	100	36 (26-44)	81.9 (63.6-100)	n.r.	n.r.	test	[5]
Vuletić et al. (2019)	400	po, sus, SD	20	75	34.4 (20-51)	n.r.	n.r.	24.7 (20.5-29.8)	training	[6]

Study	Dose [mg]	Treatment	n	Men [%]	Age [yrs]	Weight [kg]	Height [cm]	BMI [kg/m²]	Dataset	References
Courtney et al. (2003)	200	po, sus SD (high-fat breakfast)	20	100	n.r. (22-45)	n.r.	n.r.	n.r.	training	[7]
Courtney et al. (2003)	200	po, sus SD (non-fat breakfast)	20	100	n.r. (22-45)	n.r.	n.r.	n.r.	training	[7]
Courtney et al. (2003)	200	po, sus SD (fasting)	20	100	n.r. (22-45)	n.r.	n.r.	n.r.	training	[7]

n: number of individuals per study, *n.r.:* not reported, *iv*: intravenous, *po*: per os, *SD*: single dose, *MD*: multiple doses, *tab*: tablet, *sus*: suspension, *QD*: once daily, *BID*: twice daily, *TID*: three times a day, *w/o*: without. Values in brackets given for age, weight, and height are minima and maxima, all po administrations were given to human subjects

1.2 Drug-dependent parameters

The drug dependent parameters used in the final posaconazole PBPK model are summarized in Table S2.

Table S9. Summary of the POS parameters used in the final PBPK model

Parameter	Unit	Value used in PBPK model	Literature value [Reference]	Description
MW	[g/mol]	700.80	700.8 [8]	Molecular weight
pK_a 1 [base]		3.60	3.6 [8][220]	First acid dissociation constant
pK_a 2 [base]		4.60	4.6 [8]	Second acid dissociation constant
fu_p [%]		2.00	2.00 [8]	Fraction unbound in plasma
logP		4.58[a]	4.6 [8]	Lipophilicity
Solubility (pH 6.5)	[10^{-3} mg/mL]	7.72a	70, 10.2, 0.98, 2.8 [8]	Solubility
Partition coefficients		Poulin & Theil	[9,10]	Calculation method cell to plasma coefficients
Cellular permeabilities		PKSim® Standard	[11].	Calculation method permeation across cell membranes
Specific intestinal permeability	[cm/min]	5.05×10^{-5}	1.18×10^{-4} [12,13]	For SUS simulations
Specific intestinal permeability	[cm/s]	4.80×10^{-5}		For DR-tablet simulations
k_{cat} UGT1A4	[1/min]	16.52	16.9±0.55 [14]	Katalytic rate constant UGT1A4
K_M UGT1A4	[µmol/L]	15.90	15.9±1.19 [14]	Michaelis-Menten constant UGT1A4

[a] Model parameters have been estimated through parameter optimization based on the plasma concentrations;
-- Value not available

1.3 Model evaluation

1.3.1 Goodness-of-fit plots of predicted vs observed plasma concentrations

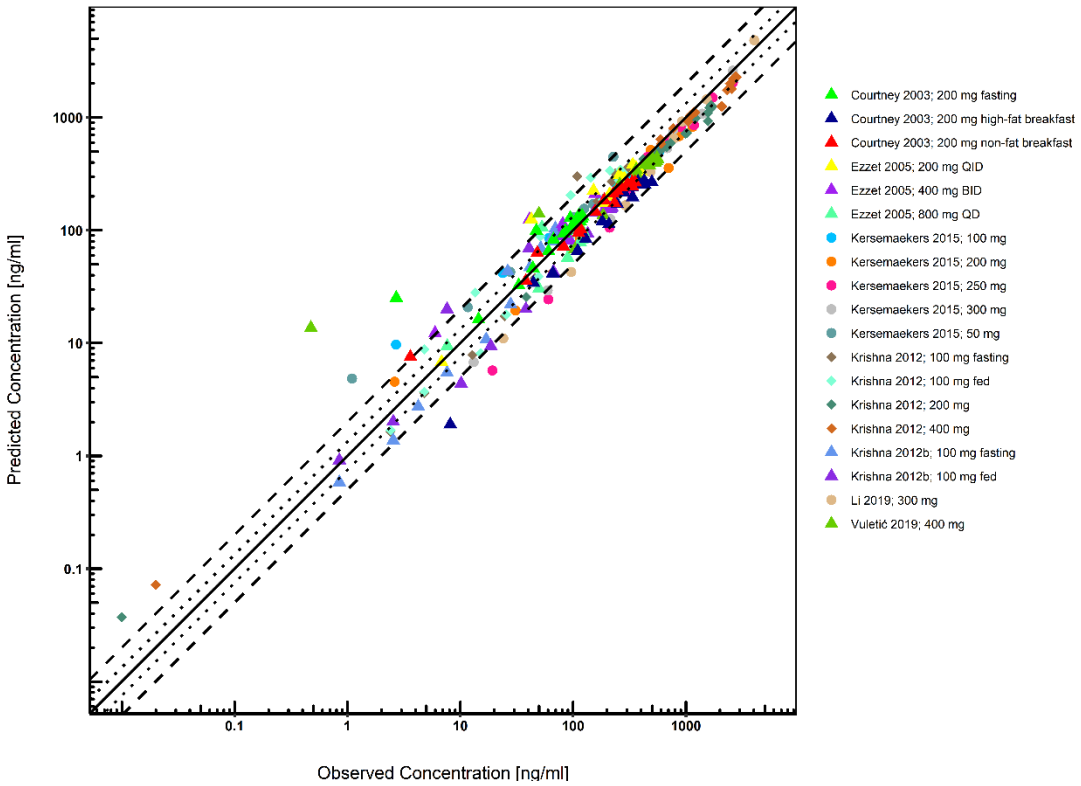

Figure S1. Predicted versus observed POS concentrations for i.v. (dots), DR-tablet (diamonds) and SUS (triangles). The black solid line marks the line of identity. Black dotted lines indicate 1.25-fold, black dashed lines indicate 2-fold deviation.

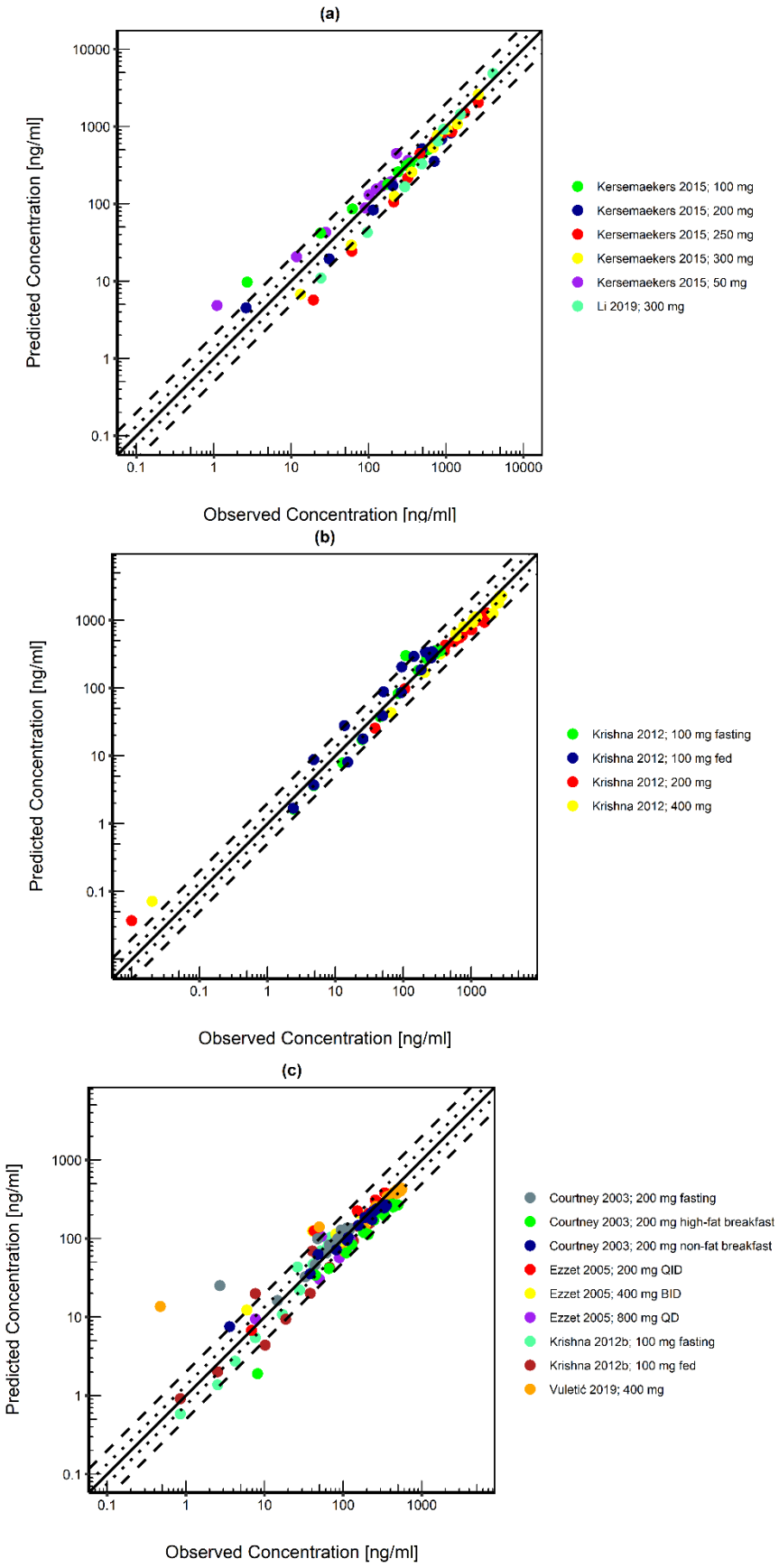

Figure S2. (**a**) predicted versus observed POS concentrations for i.v. administration; (**b**) predicted versus observed POS concentrations for DR-tablet; (**c**) predicted versus observed POS concentrations for SUS administration The black solid line marks the line of identity. Black dotted lines indicate 1.25-fold, black dashed lines indicate 2-fold deviation.

1.3.2 Goodness of fit plot AUC_{last} and C_{max}

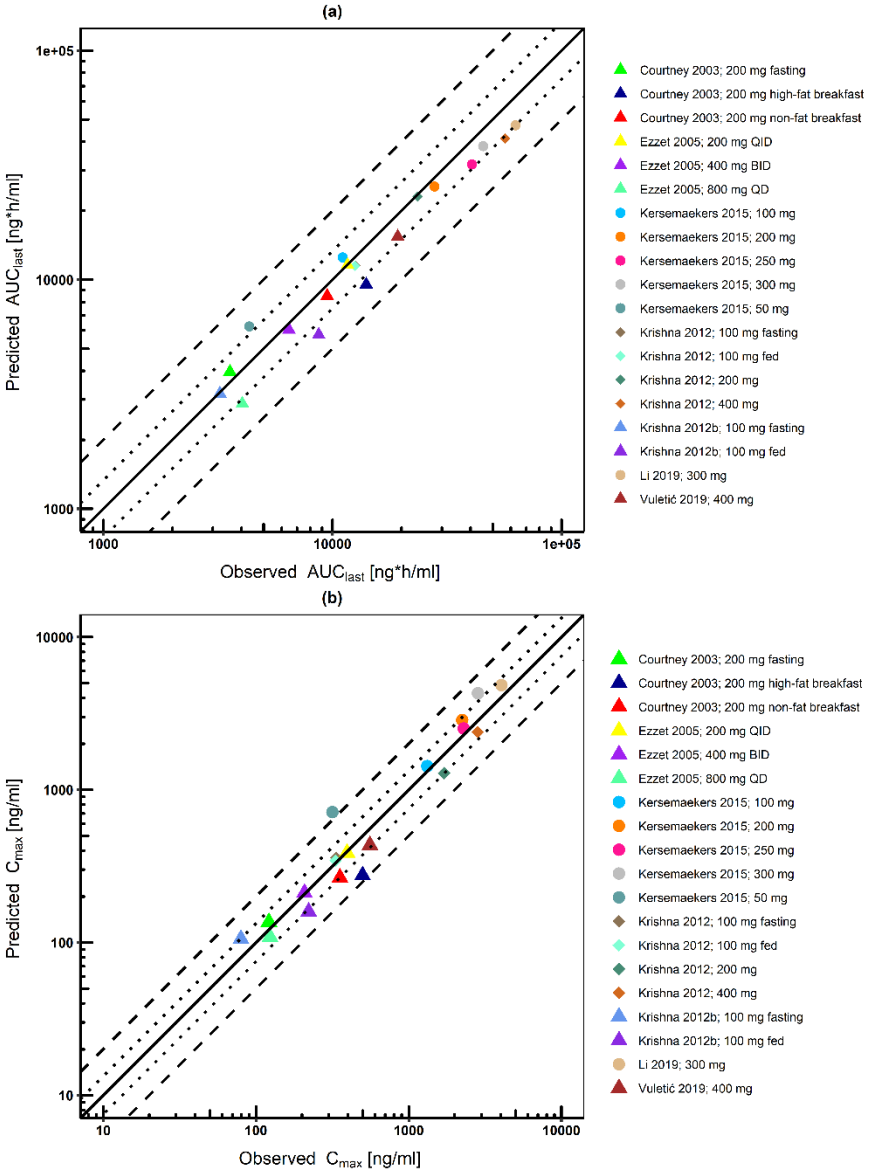

Figure S3. Predicted versus observed POS (**a**) AUC_{last} and (**b**) C_{max} values. Each symbol represents the AUC_{last} or C_{max} of a different profile. I.v. administrations are represented by diamonds, DR-tablet is represented by triangles, the SUS is represented by dots. The black solid line marks the line of identity. Black dotted lines indicate 1.25-fold, black dashed lines indicate 2-fold deviation. AUC_{last}: area under the plasma concentration–time curve from the time of administration to the last data point, C_{max}: maximum plasma concentration

1.3.3 Comparison of predicted and observed AUC_{last} and C_{max}

Table S3. Predicted and observed pharmacokinetic parameters of POS after intravenous and oral administration

Route, Dose	AUC_{last}			C_{max}			Reference
	Pred [ng*h/ml]	Obs [ng*h/ml]	Pred/Obs	Pred [ng/ml]	Obs [ng/ml]	Pred/Obs	
iv, 30 min, 50 mg	6246.8	4337.6	1.44	714.03	316.58	2.26	Kersemaekers et al. 2015 [1]
iv, 30 min, 100 mg	12495.58	11071.89	1.13	1428.07	1322.21	1.08	Kersemaekers et al. 2015 [1]
iv, 30 min, 200 mg	25488.31	27887.93	0.91	2856.20	2241.43	1.27	Kersemaekers et al. 2015 [1]
iv, 30 min, 250 mg	31852.54	40600.00	0.78	2519.31	2291.27	1.10	Kersemaekers et al. 2015 [1] [221]
iv, 30 min, 300 mg	38243.1	45500.00	0.84	4284.4	2840.00	1.51	Kersemaekers et al. 2015 [1]
iv, 30 min, 300 mg	47181.13	62938.74	0.75	4846.02	4043.35	1.20	Li et al. 2019 [2]
oral, tab, MD, 200 mg	25593.18	23560.84-	1.09	1459.45	1705.64	0.86	Krishna et al. 2012 [3]
oral, tab, MD, 400 mg	52149.22	56581.78	0.92	2997.58	2829.40	1.06	Krishna et al. 2012 [3]
oral, tab (fasting), 100 mg	11473.41	12567.66	0.91	376.18	336.28	1.12	Krishna et al. 2012 [4]
oral, tab (fed), 100 mg	12518.61	12555.30	1.00	333.56	332.410	1.0	Krishna et al. 2012 [4]
oral, sus (fasting), 100 mg	3184.2	3224.18	0.99	105.6	79.66	1.33	Krishna et al. 2012 [4] [222]
oral, sus (fed), 100 mg	5748.17	8706.51	0.66	159.5	221.19	0.72	Krishna et al. 2012 [4]
oral, sus, QD, 800 mg	2873.80	4038.40	0.71	108.9	123.62	0.88	Ezzet et al. 2005 [5]
oral, sus, BID, 400 mg	6050.90	6453.20	0.94	211.20	207.60	1.02	Ezzet et al. 2005 [5]
oral, sus, QID, 200 mg	11591.95	11625.10	1.00	386.10	394.32	0.98	Ezzet et al. 2005 [5]
oral, sus, 400 mg	15399.68	19261.75	0.80	435.00	557.35	0.78	Vuletic et al. 2019 [6]
oral, sus, (fasting), 200 mg	3962.51	3566.30	1.11	136.07	121.58	1.12	Courtney et al. 2003 [7]
oral, sus, (high fat breakfast), 200 mg	9523.2	14021.83	0.68	275.48	498.26	0.55	Courtney et al. 2003 [7]

oral, sus, (non-fat breakfast), 200 mg	8496.86	9474.29	0.90	266.48	354.85	0.75	Courtney et al. 2003 [7]

AUC_{last}: Area under the concentration time curve from the first to the last data point, *cap:* capsule, *C_{max}:* maximum plasma concentration, *Obs:* observed value, *Pred:* predicted value, iv: intravenous, *sus:* suspension, *tab:* tablet, *MD:* multiple dosing, *QD*: once daily, *BID*: twice daily; *TID:* three times a day

1.3.4 Bias, prediction and mean relative deviation of plasma predictions

Table S10. Bias (mean prediction error), precision (mean absolute prediction error) and mean relative deviation (MRD).

Route	Dose [mg]	MPE [%]	MAPE [%]	MRD	Reference
Intravenous					
iv, 30 min	50	33.98	34.38	1.42	Kersemaekers et al. 2015 [1]
iv, 30 min	100	39.60	46.50	1.63	Kersemaekers et al. 2015 [1]
iv, 30 min	200	-12.49	30.05	1.46	Kersemaekers et al. 2015 [1]
iv, 30 min	250	-29.65	29.65	1.75	Kersemaekers et al. 2015 [1] [221]
iv, 30 min	300	-25.00	25.01	1.50	Kersemaekers et al. 2015 [1]
iv, 30 min	300	-23.55	28.52	1.61	Li et al. 2019 [2]
mean MRD				**1.56 (1.42 – 1.75)** **6/6 with MRD ≤ 2**	
Oral					
oral, tablet	200	-11.84	16.02	1.24	Krishna et al. 2012 [3]
oral, tablet	400	3.70	14.67	1.19	Krishna et al. 2012 [3]
oral, tablet (fasting)	100	1.54	22.51	1.31	Krishna et al. 2012 [4]
oral, tablet (fed)	100	34.04	39.26	1.48	Krishna et al. 2012 [4]
oral, sus (fasting)	200	6.86	33.29	1.43	Krishna et al. 2012 [4] [222]
oral, sus (fed)	200	-6.82	40.50	1.63	Krishna et al. 2012 [4]
oral, sus, QD	800	-11.24	33.87	1.47	Ezzet et al. 2005 [5]
oral, sus, BID	400	25.07	36.47	1.46	Ezzet et al. 2005 [5]
oral, sus, QID	200	10.22	17.83	1.30	Ezzet et al. 2005 [5]
oral, sus	400	147.64	181.61	2.36	Vuletic et al. 2019 [6]
oral, sus, (fasting)	200	66.57	66.72	1.80	Courtney et al. 2003 [7]
oral, sus, (high fat breakfast)	200	-36.85	36.85	1.75	Courtney et al. 2003 [7]
oral, sus, (non-fat breakfast)	200	-3.26	20.77	1.29	Courtney et al. 2003 [7]
mean MRD				**1.52 (1.19 – 2.36)** **12/13 with MRD ≤ 2**	

iv: intravenous, *sus:* suspension; *tab:* tablet; *QD*: once daily; *BID*: twice daily; *TID*: three times a day; *MPE:* mean prediction error*, MAPE:* mean absolute prediction error, *MRD:* mean relative deviation

1.3.5 Sensitivity analysis

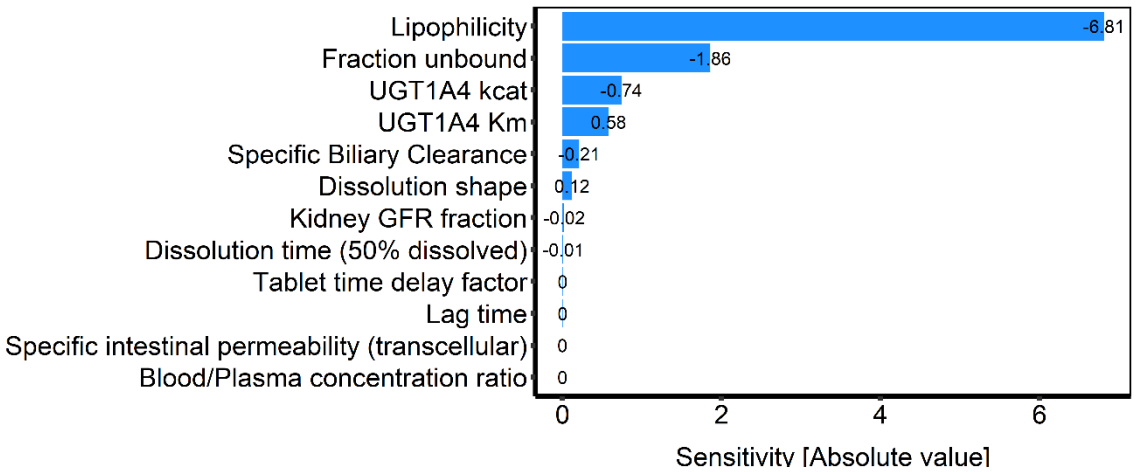

Figure S4. Sensitivity analysis for parameters which were estimated during the model development or which might have an impact due to calculation methods in PK-Sim®. Sensitivity was measured as the relative change of AUC_{last} of a 100 mg POS tablet single dose administration in fasted state. Variation range was 10.0 with maximum number of steps = 9.

1.3.6 Linear Plots

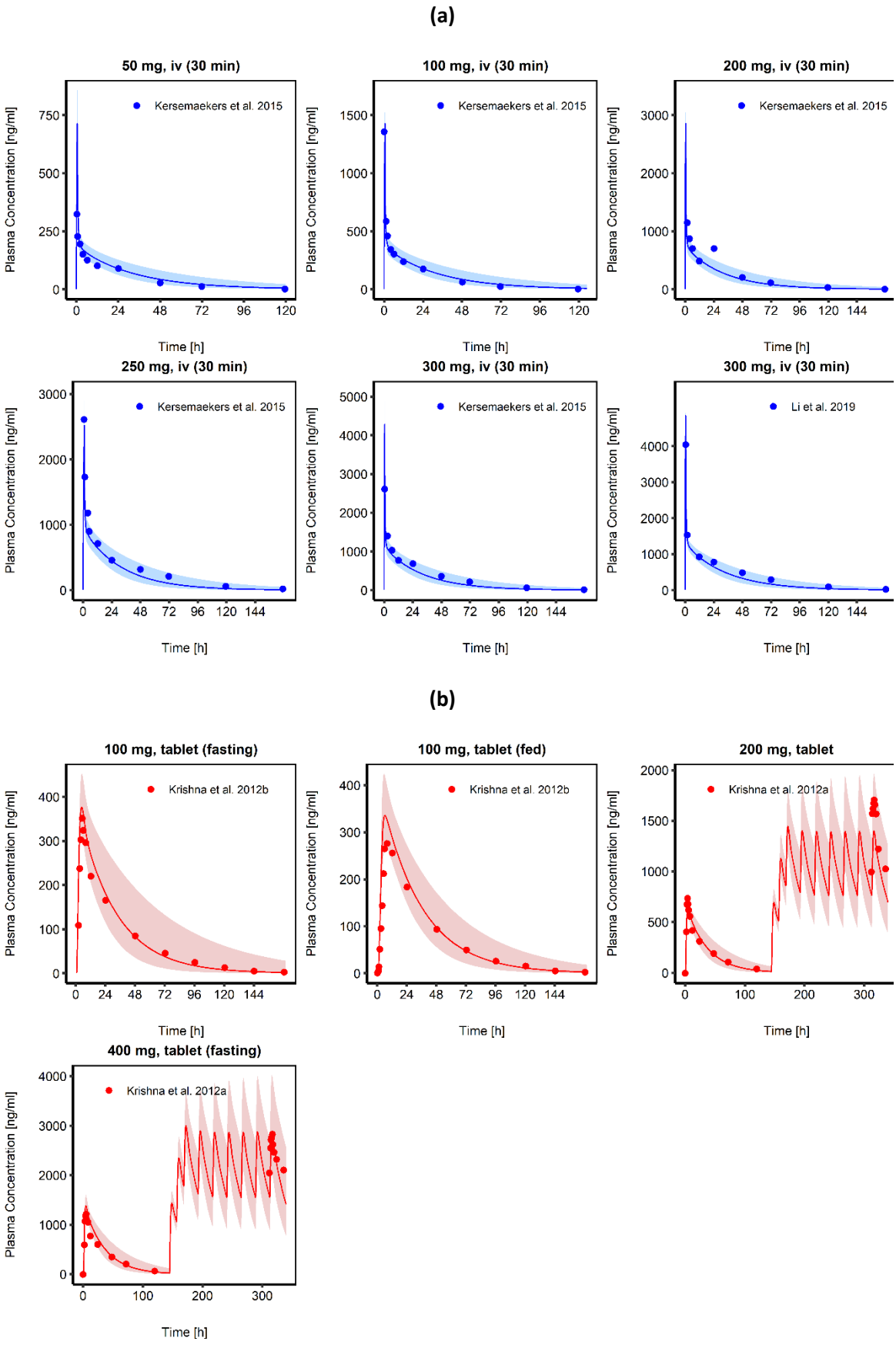

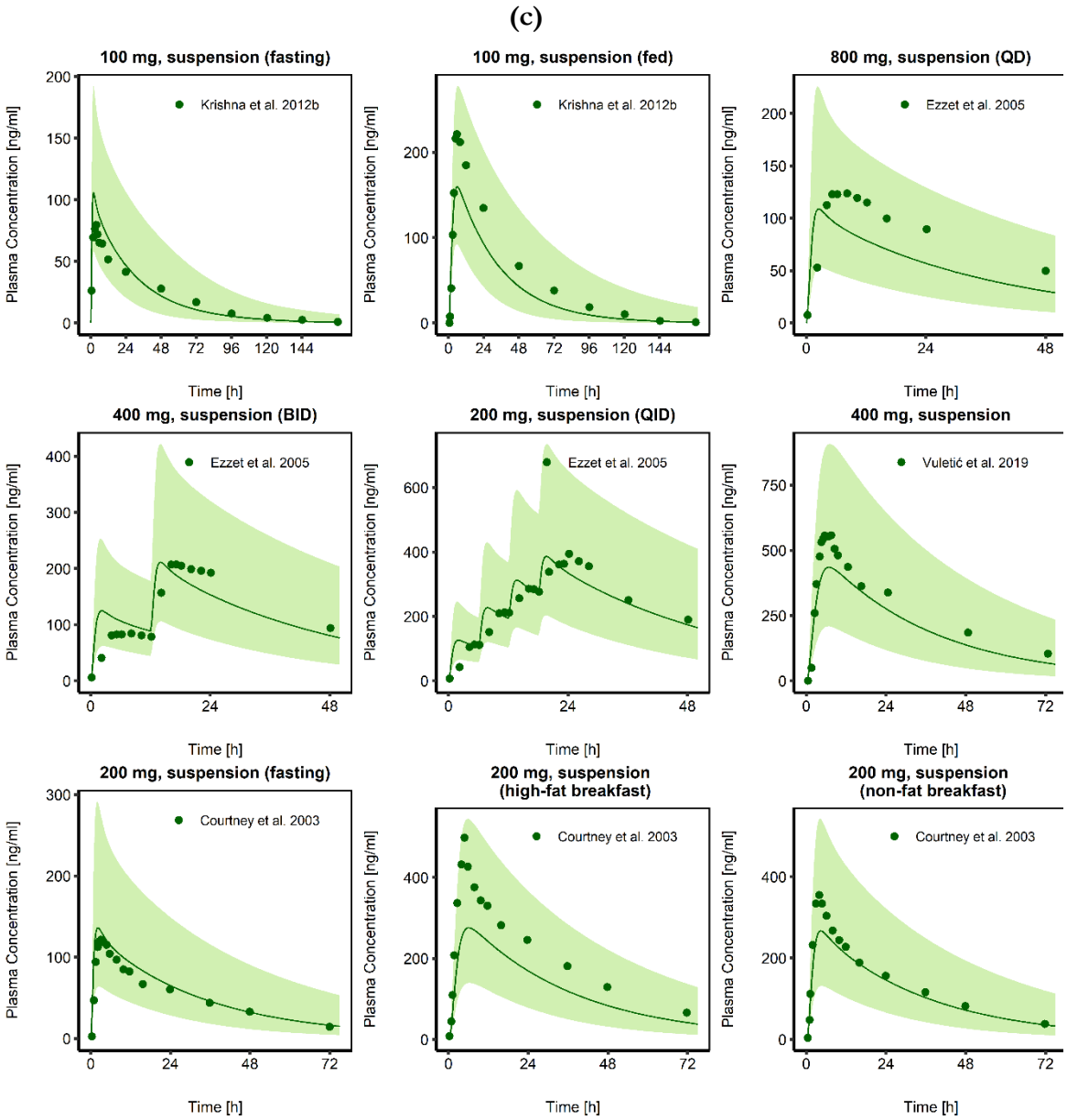

Figure S5. POS plasma concentration-time profiles (linear) after (**a**) i.v administration of POS, (**b**) POS DR-tablets and (**c**) POS SUS. Observed data are shown as blue (i.v.), red (DR-tablet) and green (SUS) circles. Population simulation (n=100) geometric means for each administration type are shown as blue, red and green lines, respectively. The shaded areas represent the predicted population geometric SD.

1.3.7 Semilogarithmic Plots

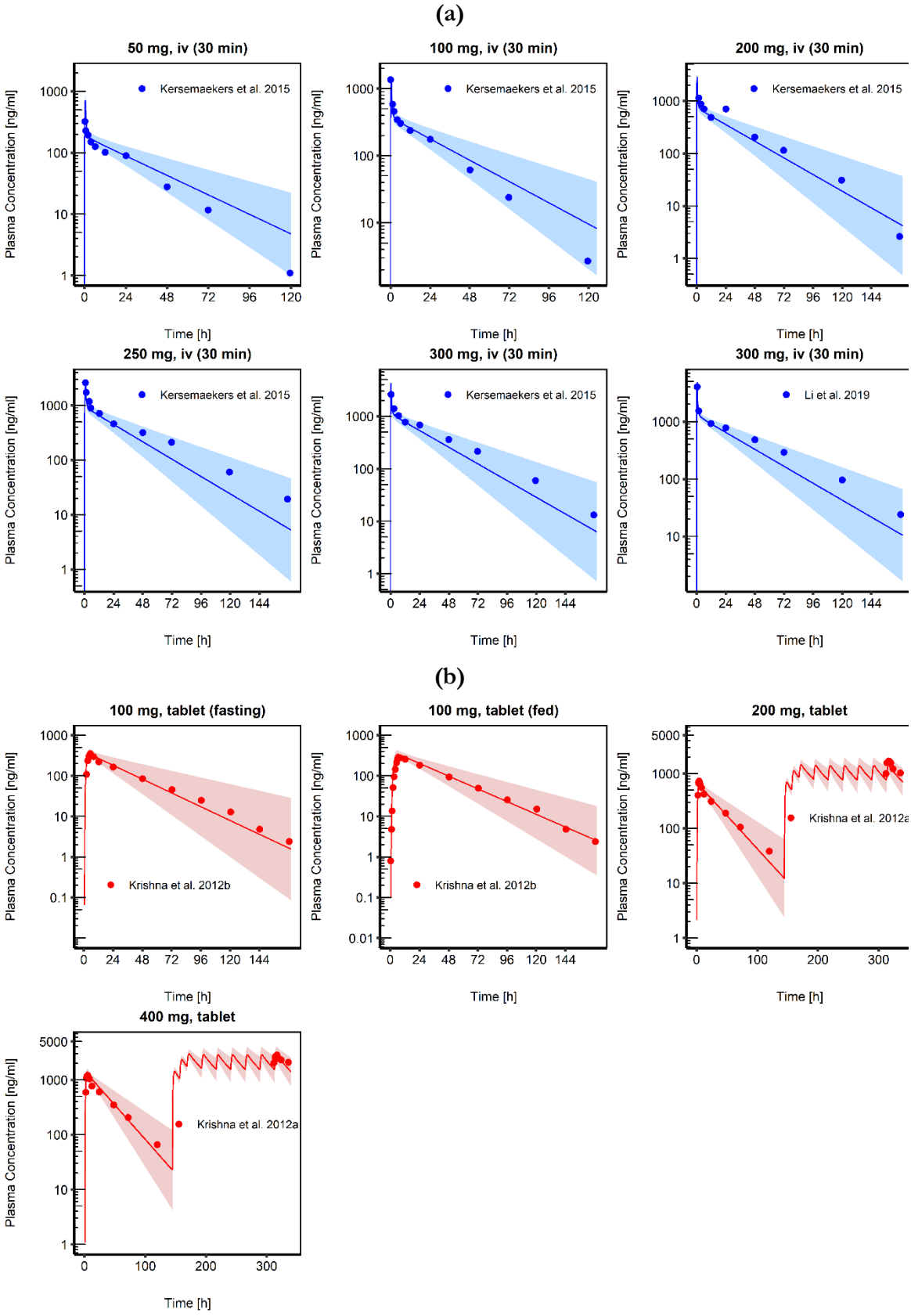

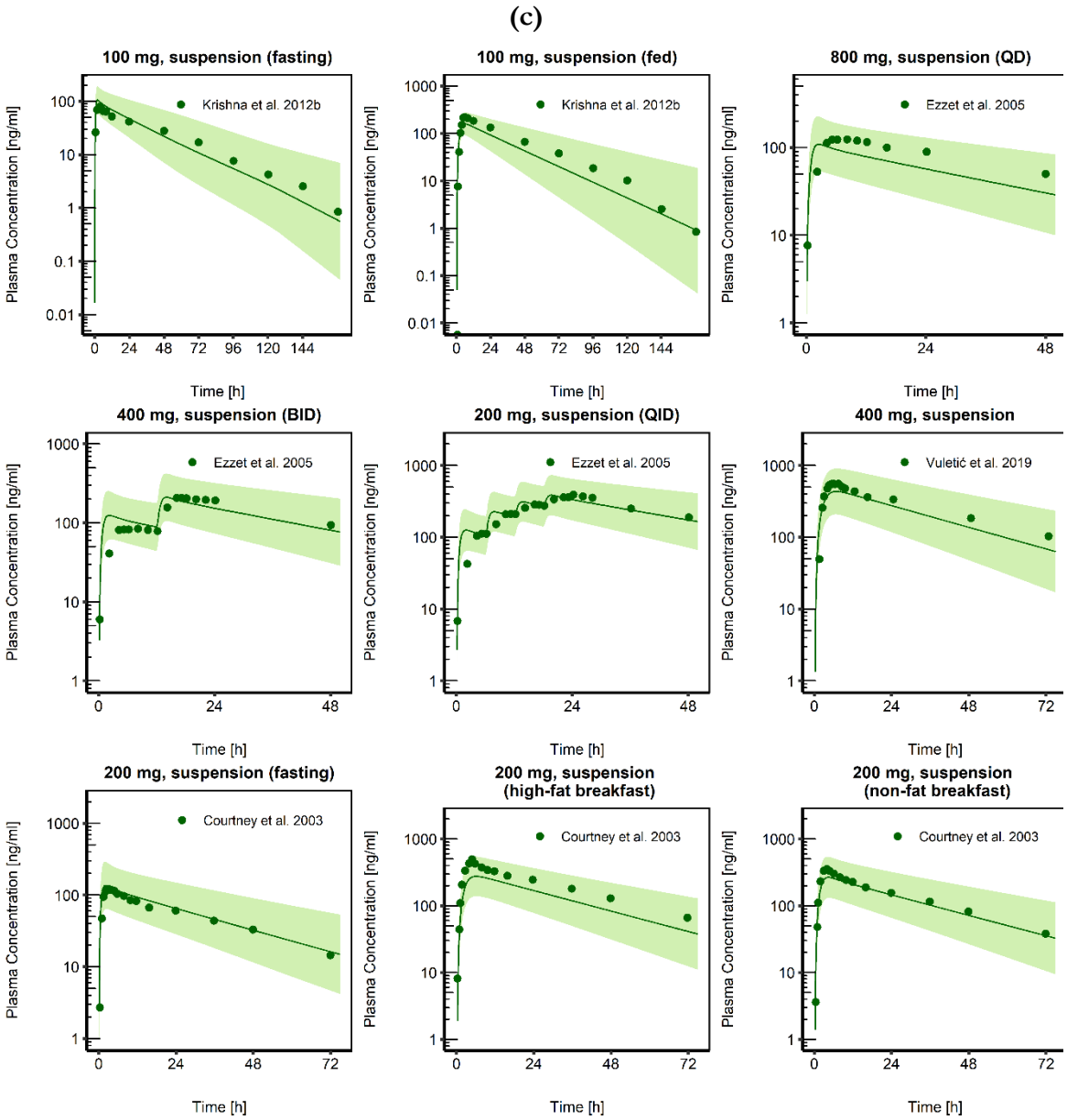

Figure S6. POS plasma concentration-time profiles (semi-logarithmic) after (**a**) i.v. administration of POS, (**b**) POS DR-tablets and (**c**) POS SUS. Observed data are shown as blue (i.v.), red (DR-tablet) and green (SUS) circles. Population simulation (n=100) geometric means for each administration type are shown as blue, red and green lines, respectively. The shaded areas represent the predicted population geometric SD.

1.3.8 Comparison of individual and population simulation

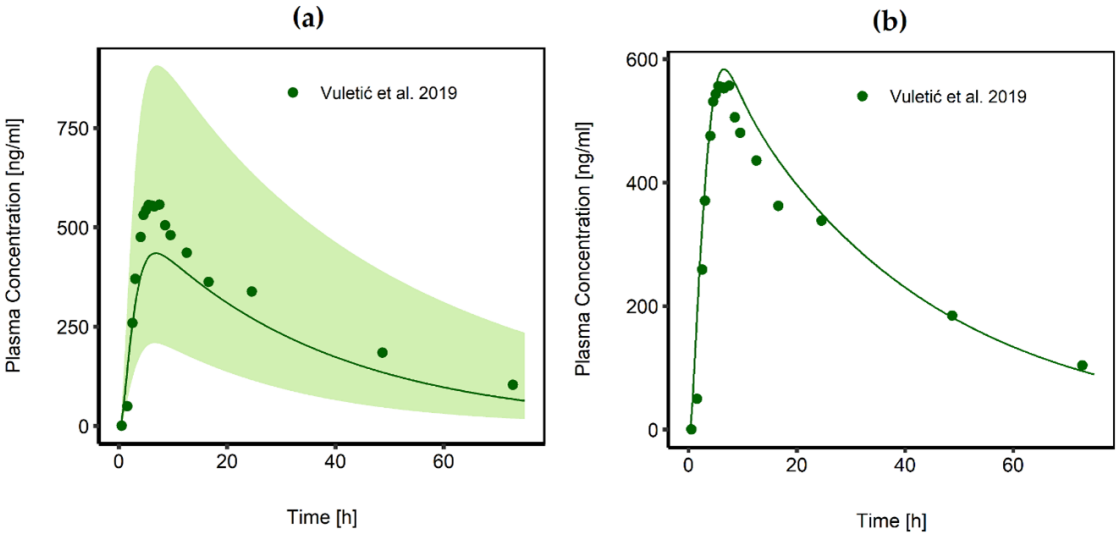

Figure S7. Comparison of predicted POS plasma concentration after administration of a 400 mg POS suspension single dose in (**a**) a virtual population (n = 100) created with the algorithm integrated in PKSim according to the patient demographics in the study conducted by Vuletic et al. **[223]** and predicted plasma concentration in (**b**) the mean induvial of the mentioned study. The green line represents the predicted geometric mean plasma concentration in the population respectively the predicted plasma concentration obtained for the individuum; the shaded area represents the geometric standard deviation for the population simulation; observed data are represented by green dots in each profile.

2. Ruxolitinib

2.1 Clinical studies

Table S5. Clinical studies used for the development of the Ruxolitinib PBPK model.

Study	Dose [mg]	Treatment	n	Men [%]	Age [yrs]	Weight [kg]	Height [cm]	BMI [kg/m²]	Dataset	References
Chen et al. (2014), hepatic	25	po, tab, SD	8	62.5	53 (45–59)	78.4 (61.8–93.2)	n.r.	27.5 (24.2–31.5)	test	[15]
Chen et al. (2014), renal	25	po, tab, SD	8	75	49 (22–69)	80.2 (64.7–89.8)	n.r.	26.9 (23.1–29.7)	test	[15]
Ogama et al. (2013)	10	po, tab, SD+MD	8	100	27 (20-41)	60.95 (52.5–75.9)	171.0 (159–182)	20.91 (18.8–24.5)	training	[16]
Ogama et al. (2013)	25	po, tab, SD+MD	8	100	27 (20-41)	60.95 (52.5–75.9)	171.0 (159–182)	20.91 (18.8–24.5)	training	[16]
Ogama et al. (2013)	50	po, tab, SD	8	100	27 (20-41)	60.95 (52.5–75.9)	171.0 (159–182)	20.91 (18.8–24.5)	training	[16]
Ogama et al. (2013)	100	po, tab, SD	8	100	27 (20-41)	60.95 (52.5–75.9)	171.0 (159–182)	20.91 (18.8–24.5)	training	[16]
Shi et al. (2011)	15	po, tab, BID, MD	71	77.5	29 (18-54)	75.1 (51.1-98.5)	n.r.	24.8 (19.8-29.6)	training	[17]
Shi et al. (2011)	25	po, tab, BID, MD	71	77.5	29 (18-54)	75.1 (51.1-98.5)	n.r.	24.8 (19.8-29.6)	test	[17]
Shi et al. (2011)	50	po, tab, QD, MD	71	77.5	29 (18-54)	75.1 (51.1-98.5)	n.r.	24.8 (19.8-29.6)	test	[17]
Shi et al. (2011)	50	po, tab, BID, MD	71	77.5	29 (18-54)	75.1 (51.1-98.5)	n.r.	24.8 (19.8-29.6)	test	[17]
Shi et al. (2011)	100	po, tab, QD, MD	71	77.5	29 (18-54)	75.1 (51.1-98.5)	n.r.	24.8 (19.8-29.6)	test	[17]

n: number of individuals per study, *n.r.*: not reported, *po*: per os, *SD*: single dose, *MD*: multiple doses, *QD*: once daily, *BID*: twice daily, *w/o*: without. Values in brackets given for age, weight, and height are minima and maxima,

2.2 Drug-dependent parameters

Table S11. Summary of the RUX parameters used in the final PBPK model

Parameter	Unit	Value used in PBPK model	Literature value [Reference]	Description
MW	[g/mol]	306.00	306.0 [18]	Molecular weight
pK_a [base]		3.89	3.89 [18]	Acid dissociation constant
fu_p [%]		3.30	3.30 [224]	Fraction unbound in plasma
logP		2.81	2.81 [18]	Lipophilicity
Solubility (pH 6.5)	[10^{-3} mg/mL]		0.3 [19]	Solubility
Partition coefficients		Rodgers & Rowland	[9,10]	Calculation method cell to plasma coefficients
Cellular permeabilities		PKSim® Standard	--	Calculation method permeation across cell membranes
Specific intestinal permeability	[10^{-4} cm/s]	5.40	5.4 [19]	
CYP 2C9 in vitro CL/recombinant enzyme	[µl/min/pmol rec. enzyme]	0.65	0.648 [18]	In vitro metabolic rate in the presence of CYP2C9
CYP 3A4 in vitro CL/recombinant enzyme	[µl/min/pmol rec. enzyme]	0.46	0.463 [18]	In vitro metabolic rate in the presence of CYP3A4
GFR Fraction		1.0	--	Fraction of filtered drug in the urine
Tablet Weibull time	[min]	15	--	Dissolution time (50 % dissolved)
Tablet Weibull shape		1.10	--	Dissolution profile shape

[a] model parameters have been estimated through parameter optimization based on the plasma concentrations;
-- Value not available

2.3 Model evaluation

2.3.1 Goodness-of-fit plots of predicted vs observed plasma concentrations

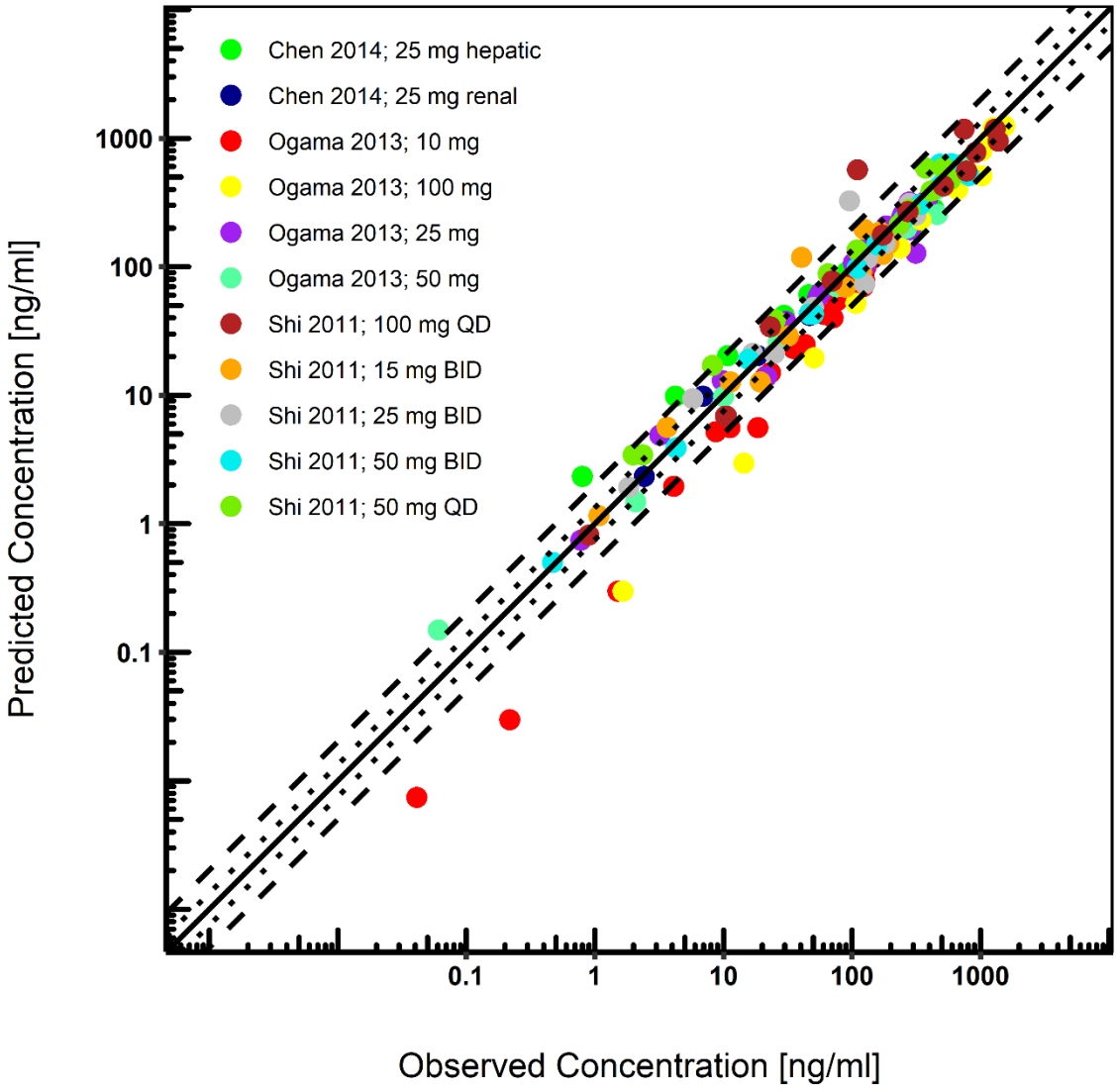

Figure S8. Predicted versus observed RUX concentrations after oral administration. Each dot represents measured plasma concentrations of the respective study The black solid line marks the line of identity. Black dotted lines indicate 1.25-fold, black dashed lines indicate 2-fold deviation.

2.3.2 AUC_{last} and C_{max} goodness-of-fit plots

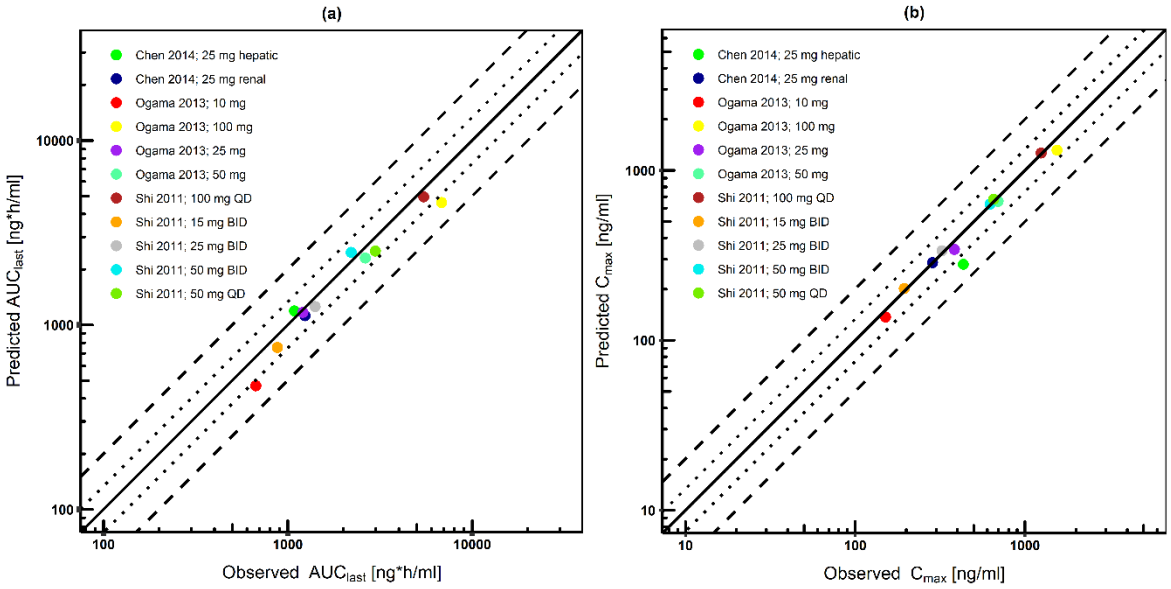

Figure S12. (**a**) Predicted versus observed ruxolitinib AUC_{last}. and (**b**) predicted versus observed ruxolitinib maximum concentration (C_{max}). Each symbol represents C_{max} respectively AUC_{last} of a different profile The black solid line marks the line of identity. Black dotted lines indicate 1.25-fold, black dashed lines indicate 2-fold deviation.

2.3.3 Comparison of predicted and observed AUC_{last} and C_{max}

Table S7. Predicted and observed pharmacokinetic parameters of RUX after oral administration

Route, Dose	AUC_{last}			C_{max}			Reference
	Pred [ng*h/ml]	Obs [ng*h/ml]	Pred/Obs	Pred [ng/ml]	Obs [ng/ml]	Pred/Obs	
po, tab, SD, 25 mg	1191.6	1085.92	1.10	279.95	433.93	0.65	Chen et al. (2014), hepatic [15][225]
po, tab, SD, 25 mg	1122.52	1237.86	0.91	286.28	285.44	1.00	Chen et al. (2014), renal [15]
po, tab, SD+MD, 10 mg	468.48	670.76	0.70	137.15	150.94	0.91	Ogama et al. (2013) [16]
po, tab, SD+MD, 25 mg	1171.21	1207.14	0.97	342.88	384.35	0.89	Ogama et al. (2013) [16]
po, tab, SD, 50 mg	2305.43	2632.77	0.88	657.33	695.28	0.95	Ogama et al. (2013) [226]
po, tab, SD, 100 mg	4610.86	6827.36	0.68	1314.66	1544.16	0.85	Ogama et al. (2013) [16]
po, tab, BID, MD, 15 mg	754.78	877.97	0.86	201.94	194.62	1.04	Shi et al. (2011) [17]
po, tab, BID, MD, 25 mg	1257.97	1406.70	0.89	336.56	324.37	1.04	Shi et al. (2011) [17]
po, tab, QD, MD, 50 mg	2471.90	2207.04	1.12	633.37	622.98	1.02	Shi et al. (2011) [17]
po, tab, BID, MD, 50 mg	2517.59	2983.86	0.84	677.41	654.45	1.04	Shi et al. (2011) [17]
po, tab, QD, MD, 100 mg	4944.03	5457.58	0.91	1265.54	1245.98	1.02	Shi et al. (2011) [17]

AUC_{last}: Area under the concentration time curve from the first to the last data point, *cap:* capsule, *C_{max}:* maximum plasma concentration, *Obs:* observed value, *Pred:* predicted value, *tab:* tablet, *SD:* single dose, *MD:* multiple dosing, *QD*: once daily, *BID*: twice daily

2.3.4 Bias, prediction and mean relative deviation of plasma predictions

Table S8. Bias (mean prediction error), precision (mean absolute prediction error) and mean relative deviation (MRD) of the RUX PBPK model.

Route	Dose [mg]	MPE	MAPE	MRD	Reference
po, tab, SD	25	33.29	54.81	1.68	Chen et al. (2014), hepatic [15][225]
po, tab, SD	25	-7.27	17.70	1.24	Chen et al. (2014), renal [15]
po, tab, SD+MD	10	-39.83	39.83	2.18	Ogama et al. (2013) [16]
po, tab, SD+MD	25	-0.19	17.96	1.32	Ogama et al. (2013) [16]
po, tab, SD	50	-1.21	24.72	1.40	Ogama et al. (2013) [226]
po, tab, SD	100	-40.92	40.92	2.23	Ogama et al. (2013) [16]
po, tab, BID, MD	15	14.77	37.18	1.49	Shi et al. (2011) [17]
po, tab, BID, MD	25	18.69	38.75	1.54	Shi et al. (2011) [17]
po, tab, QD, MD	50	31.23	36.82	1.43	Shi et al. (2011) [17]
po, tab, BID, MD	50	-4.72	14.30	1.20	Shi et al. (2011) [17]
po, tab, QD, MD	100	25.20	50.99	1.71	Shi et al. (2011) [17]
mean MRD				**1.58 (1.20 – 2.23)** **09/11 with MRD ≤ 2**	

tab: tablet; *SD:* single dose, *MD*: multiple doses, *QD*: once daily; *BID*: twice daily; M*PE:* mean prediction error, *MAPE:* mean absolute prediction error, *MRD:* mean relative deviation

2.3.5 Sensitivity analysis

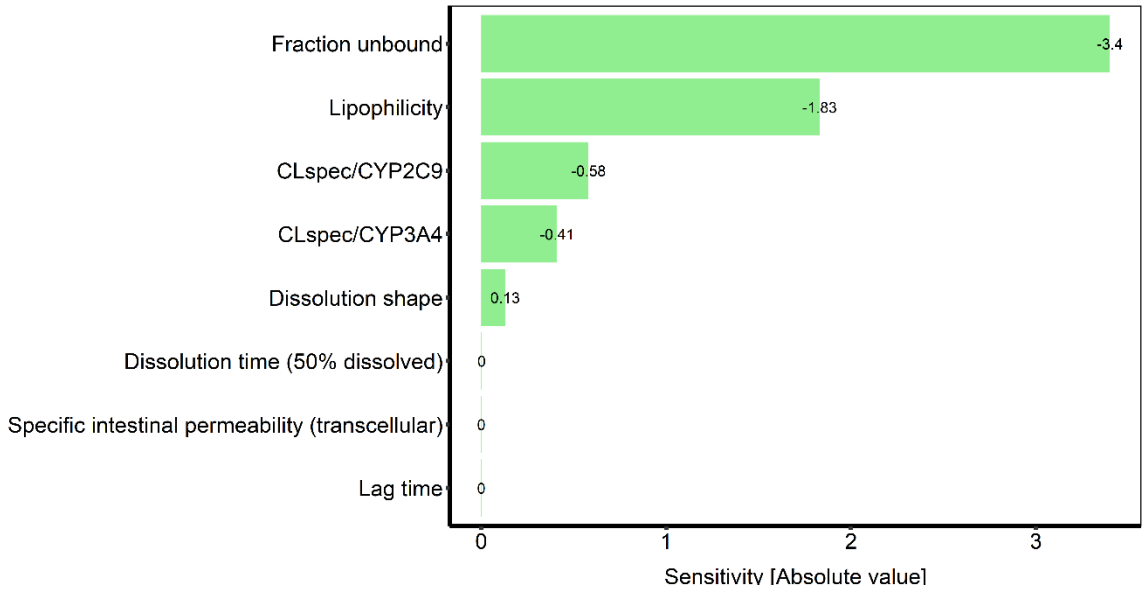

Figure S10. RUX sensitivity analysis for parameters which were estimated during the model development or which might have an impact due to calculation methods in PK-Sim®. Sensitivity was measured as the relative change of AUC_{last} of a 50 mg RUX BID tablet administration in fasted state. Variation range was 10.0 with maximum number of steps = 9.

2.3.6 Semilogarithmic plots

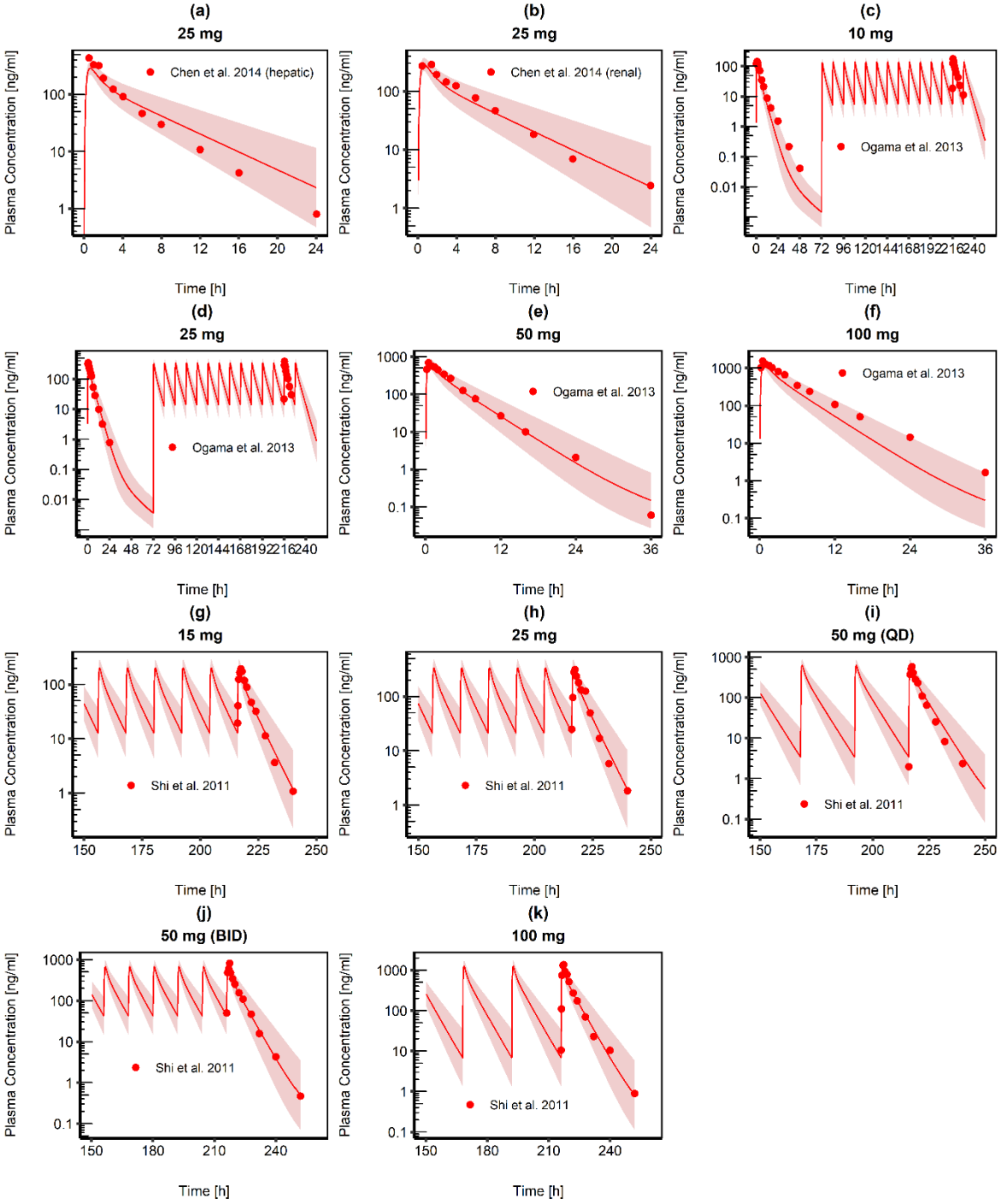

Figure S11. RUX plasma concentration-time profiles (semi-logarithmic) after administration of RUX tablet. Observed data are shown as red dots. Population simulation (n=100) geometric means are shown as red lines; the shaded areas represent the predicted population geometric SD.

3 Drug-drug interaction simulation posaconazole and midazolam

3.1 Clinical studies

Table S9. Clinical studies used for the investigation and evaluation of the inhibitory constant of POS for CYP3A4.

Study	Dose [mg]	MDZ Treatment	n	Men [%]	Age [yrs]	Weight [kg]	Height [cm]	BMI [kg/m^2]	References
Krishna et al. (2009)	0.4 mg MDZ + 200 mg POS	i.v., 30 min	12	92	42.8 (28-53)	80.6 (69.4-94.9)	n.r.	25.6 (22.7-28.8)	[20]
Krishna et al. (2009)	0.4 mg MDZ + 400 mg POS	i.v., 30 min	12	92	42.8 (28-53)	80.6 (69.4-94.9)	n.r.	25.6 (22.7-28.8)	[20]
Krishna et al. (2009)	0.4 mg MDZ	i.v., 30 min	12	92	42.8 (28-53)	80.6 (69.4-94.9)	n.r.	25.6 (22.7-28.8)	[20]
Krishna et al. (2009)	2 mg MDZ + 200 mg POS	oral	12	92	42.8 (28-53)	80.6 (69.4-94.9)	n.r.	25.6 (22.7-28.8)	[20]
Krishna et al. (2009)	2 mg MDZ + 200 mg POS	oral	12	92	42.8 (28-53)	80.6 (69.4-94.9)	n.r.	25.6 (22.7-28.8)	[20]

4 Simulation of graft-versus-host disease patients

Table S12. Baseline patient demographics

Patient characteristic	No. of patients	%
Total	24	
Age [yrs], mean (range)	53 (22–80)	
Weight [kg], mean (range)	73.8 (43.0–111.0)	
Height [cm], mean, (range)	174 (156-196)	
BMI [kg/m^2], mean (range)	24.4 (16.2–43.4)	
Male	13	54.2
Female	11	45.8
RUX with POS	19[a]	79.2
RUX without POS	7[a]	29.2

[a] two patients were treated with RUX alone and in combination with POS

5 References

1. Kersemaekers, W.M.; van Iersel, T.; Nassander, U.; O'Mara, E.; Waskin, H.; Caceres, M.; van Iersel, M.L. Pharmacokinetics and safety study of posaconazole intravenous solution administered peripherally to healthy subjects. Antimicrob. Agents Chemother. **2015**, 59, 1246-1251, doi:10.1128/AAC.04223-14.

2. Li, H.; Wei, Y.; Zhang, S.; Xu, L.; Jiang, J.; Qiu, Y.; Mangin, E.; Zhao, X.M.; Xie, S. Pharmacokinetics and Safety of Posaconazole Administered by Intravenous Solution and Oral Tablet in Healthy Chinese Subjects and Effect of Food on Tablet Bioavailability. Clin. Drug. Investig. **2019**, 39, 1109-1116, doi:10.1007/s40261-019-00833-1.

3. Krishna, G.; Ma, L.; Martinho, M.; Preston, R.; O'mara, E. A new solid oral tablet formulation of posaconazole: a randomized clinical trial to investigate rising single-and multiple-dose pharmacokinetics and safety in healthy volunteers. J. Antimicrob. Chemother. **2012**, 67, 2725- 2730.

4. Krishna, G.; Ma, L.; Martinho, M.; O'Mara, E. Single-dose phase I study to evaluate the pharmacokinetics of posaconazole in new tablet and capsule formulations relative to oral suspension. Antimicrob. Agents Chemother. **2012**, 56, 4196-4201.

5. Ezzet, F.; Wexler, D.; Courtney, R.; Krishna, G.; Lim, J.; Laughlin, M. Oral bioavailability of posaconazole in fasted healthy subjects. Clin. Pharmacokinet. **2005**, 44, 211-220.

6. Vuletić, L.; Herceg, M.; Ferderber, K.; Tunjić, I.; Rizea-Savu, S.; Duna, S.N.; Cetina-Čižmek, B.; Filipović-Grčić, J. Single-Dose Pharmacokinetic Properties and Relative Bioavailability of Different Formulations of Posaconazole Oral Suspension in Healthy Volunteers. Clin. Pharmacol. Drug Dev. **2019**, 8, 827-836.

7. Courtney, R.; Wexler, D.; Radwanski, E.; Lim, J.; Laughlin, M. Effect of food on the relative bioavailability of two oral formulations of posaconazole in healthy adults. Br. J. Clin. Pharmacol. **2004**, 57, 218-222.

8. Hens, B.; Pathak, S.M.; Mitra, A.; Patel, N.; Liu, B.; Patel, S.; Jamei, M.; Brouwers, J.; Augustijns, P.; Turner, D.B. In Silico Modeling Approach for the Evaluation of Gastrointestinal Dissolution, Supersaturation, and Precipitation of Posaconazole. Mol Pharm **2017**, 14, 4321-4333, doi:10.1021/acs.molpharmaceut.7b00396.

9. Rodgers, T.; Leahy, D.; Rowland, M. Physiologically based pharmacokinetic modeling 1: predicting the tissue distribution of moderate-to-strong bases. Journal of pharmaceutical sciences **2005**, 94, 1259-1276.

10. Rodgers, T.; Rowland, M. Physiologically based pharmacokinetic modelling 2: predicting the tissue distribution of acids, very weak bases, neutrals and zwitterions. Journal of pharmaceutical sciences **2006**, 95, 1238-1257.

11. Open Systems Pharmacology. PK-Sim®. Version 11.0. Available online: https://github.com/Open-Systems-Pharmacology/Suite/releases/tag/v11.0 (accessed on 2022 May 01).

12. Thelen, K.; Coboeken, K.; Willmann, S.; Dressman, J.B.; Lippert, J. Evolution of a detailed physiological model to simulate the gastrointestinal transit and absorption process in humans, part II: extension to describe performance of solid dosage forms. Journal of pharmaceutical sciences **2012**, 101, 1267-1280.

13. Thelen, K.; Coboeken, K.; Willmann, S.; Burghaus, R.; Dressman, J.B.; Lippert, J. Evolution of a detailed physiological model to simulate the gastrointestinal transit and absorption process in humans, part 1: oral solutions. Journal of pharmaceutical sciences **2011**, 100, 5324-5345.

14. Ghosal, A.; Hapangama, N.; Yuan, Y.; Achanfuo-Yeboah, J.; Iannucci, R.; Chowdhury, S.; Alton, K.; Patrick, J.E.; Zbaida, S. Identification of human UDP-glucuronosyltransferase enzyme(s) responsible for the glucuronidation of posaconazole (Noxafil). Drug Metab Dispos **2004**, 32, 267-271, doi:10.1124/dmd.32.2.267.

15. Chen, X.; Shi, J.G.; Emm, T.; Scherle, P.A.; McGee, R.F.; Lo, Y.; Landman, R.R.; Punwani, N.G.; Williams, W.V.; Yeleswaram, S. Pharmacokinetics and pharmacodynamics of orally administered ruxolitinib (INCB018424 phosphate) in renal and hepatic impairment patients. Clin. Pharmacol. Drug Dev. **2014**, 3, 34-42.

16. Ogama, Y.; Mineyama, T.; Yamamoto, A.; Woo, M.; Shimada, N.; Amagasaki, T.; Natsume, K. A randomized dose-escalation study to assess the safety, tolerability, and pharmacokinetics of ruxolitinib (INC424) in healthy Japanese volunteers. Int. J. Hematol. **2013**, 97, 351-359.

17. Shi, J.G.; Chen, X.; McGee, R.F.; Landman, R.R.; Emm, T.; Lo, Y.; Scherle, P.A.; Punwani, N.G.; Williams, W.V.; Yeleswaram, S. The pharmacokinetics, pharmacodynamics, and safety of orally dosed INCB018424 phosphate in healthy volunteers. J. Clin. Pharmacol. **2011**, 51, 1644-1654.

18. Umehara, K.; Huth, F.; Jin, Y.; Schiller, H.; Aslanis, V.; Heimbach, T.; He, H. Drug-drug interaction (DDI) assessments of ruxolitinib, a dual substrate of CYP3A4 and CYP2C9,

using a verified physiologically based pharmacokinetic (PBPK) model to support regulatory submissions. Drug Metab Pers Ther **2019**, 34, doi:10.1515/dmpt-2018-0042.

19. Shi, J.G.; Fraczkiewicz, G.; Williams, W.V.; Yeleswaram, S. Predicting drug-drug interactions involving multiple mechanisms using physiologically based pharmacokinetic modeling: a case study with ruxolitinib. Clin Pharmacol Ther **2015**, 97, 177-185, doi:10.1002/cpt.30.

20. Krishna, G.; Moton, A.; Ma, L.; Savant, I.; Martinho, M.; Seiberling, M.; McLeod, J. Effects of oral posaconazole on the pharmacokinetic properties of oral and intravenous midazolam: a phase I, randomized, open-label, crossover study in healthy volunteers. Clin. Ther. **2009**, 31, 286-298.

H References

1. Derendorf, H; Meibohm, B. Modeling of pharmacokinetic/pharmacodynamic (PK/PD) relationships: concepts and perspectives. Pharmaceutical research 1999, 16, 176-185.

2. Schiffter, HA. Pharmakokinetik-Modelle und Berechnungen; Wissenschaftliche Verlagsgesellschaft Stuttgart: 2015.

3. Alqahtani, MS; Kazi, M; Alsenaidy, MA; et al. Advances in oral drug delivery. Frontiers in Pharmacology 2021, 12, 618411.

4. Kim, J; De Jesus, O. Medication Routes of Administration. In StatPearls; StatPearls Publishing: 2022.

5. Peters, SA. Physiologically-based pharmacokinetic (PBPK) modeling and simulations : principles, methods, and applications in the pharmaceutical industry; John wiley & Sons, Inc., Hoboken, New Jersey: Volume 1.

6. Martinez, MN; Amidon, GL. A mechanistic approach to understanding the factors affecting drug absorption: a review of fundamentals. The Journal of Clinical Pharmacology 2002, 42, 620-643.

7. Vinarov, Z; Abdallah, M; Agundez, JA; et al. Impact of gastrointestinal tract variability on oral drug absorption and pharmacokinetics: An UNGAP review. European Journal of Pharmaceutical Sciences 2021, 162, 105812.

8. Thomas N. Tozer, MR. Essentials of Pharmacokinetics and Pharmacodynamics, 2 ed.; Wolters Kluwer: 2016.

9. Watanabe, R; Esaki, T; Kawashima, H; et al. Predicting fraction unbound in human plasma from chemical structure: improved accuracy in the low value ranges. Molecular pharmaceutics 2018, 15, 5302-5311.

10. Cheeti, S; Budha, NR; Rajan, S; et al. A physiologically based pharmacokinetic (PBPK) approach to evaluate pharmacokinetics in patients with cancer. Biopharmaceutics & drug disposition 2013, 34, 141-154.

11. Holford, NHG. Pharmacokinetics & Pharmacodynamics: Rational Dosing & the Time Course of Drug Action. Basic & Clinical Pharmacology 2018, 41-55.

12. Holford, N; Yim, D-S. Volume of Distribution. Translational and Clinical Pharmacology 2016, 24.

13. Beringer, PM. Revised edition of: Basic clinical pharmacokinetics / Michael E. Winter 5th ed. 2010; Philadelphia : Wolters Kluwer Health: 2018.

14. Benet, LZ; Zia-Amirhosseini, P. Basic principles of pharmacokinetics. Toxicologic pathology 1995, 23, 115-123.

15. Dagher, R; Cohen, M; Williams, G; et al. Approval summary: imatinib mesylate in the treatment of metastatic and/or unresectable malignant gastrointestinal stromal tumors. Clin Cancer Res 2002, 8, 3034-3038.

16. Daskalakis, M; Feller, A; Noetzli, J; et al. Potential to improve therapy of Chronic Myeloid Leukemia (CML), especially for patients with older age: incidence, mortality, and survival rates of patients with CML in Switzerland from 1995 to 2017. Cancers 2021, 13, 6269.

17. Kantarjian, H; O'Brien, S; Jabbour, E; et al. Improved survival in chronic myeloid leukemia since the introduction of imatinib therapy: a single-institution historical experience. Blood, The Journal of the American Society of Hematology 2012, 119, 1981-1987.

18. Zahavi, D; Weiner, L. Monoclonal antibodies in cancer therapy. Antibodies 2020, 9, 34.

19. May, P; Figgins, B. Oral anticancer therapy: a comprehensive assessment of patient perceptions and challenges. J Community Support Oncol 2016, 14, 112-116.

20. Arora, A; Scholar, EM. Role of tyrosine kinase inhibitors in cancer therapy. Journal of Pharmacology and Experimental Therapeutics 2005, 315, 971-979.

21. A Baudino, T. Targeted cancer therapy: the next generation of cancer treatment. Current drug discovery technologies 2015, 12, 3-20.

22. Gerber, DE. Targeted therapies: a new generation of cancer treatments. American family physician 2008, 77, 311-319.

23. Hou, J; He, Z; Liu, T; et al. Evolution of molecular targeted cancer therapy: mechanisms of drug resistance and novel opportunities identified by CRISPR-Cas9 screening. Frontiers in Oncology 2022, 908.

24. Hamilton, A; Gallipoli, P; Nicholson, E; et al. Targeted therapy in haematological malignancies. The Journal of Pathology: A Journal of the Pathological Society of Great Britain and Ireland 2010, 220, 404-418.

25. Jung, SM; Kim, W-U. Targeted immunotherapy for autoimmune disease. Immune Network 2022, 22.

26. Vanneman, M; Dranoff, G. Combining immunotherapy and targeted therapies in cancer treatment. Nature reviews cancer 2012, 12, 237-251.

27. Yu, C; Liu, X; Yang, J; et al. Combination of immunotherapy with targeted therapy: theory and practice in metastatic melanoma. Frontiers in immunology 2019, 10, 990.

28. Pottier, C; Fresnais, M; Gilon, M; et al. Tyrosine kinase inhibitors in cancer: breakthrough and challenges of targeted therapy. Cancers 2020, 12, 731.

29. Schirrmacher, V. From chemotherapy to biological therapy: A review of novel concepts to reduce the side effects of systemic cancer treatment. International journal of oncology 2019, 54, 407-419.

30. Bhullar, KS; Lagarón, NO; McGowan, EM; et al. Kinase-targeted cancer therapies: progress, challenges and future directions. Molecular cancer 2018, 17, 1-20.

31. Yamaoka, T; Kusumoto, S; Ando, K; et al. Receptor tyrosine kinase-targeted cancer therapy. International journal of molecular sciences 2018, 19, 3491.

32. Hsu, JL; Hung, M-C. The role of HER2, EGFR, and other receptor tyrosine kinases in breast cancer. Cancer and Metastasis Reviews 2016, 35, 575-588.

33. Lemmon, MA; Schlessinger, J. Cell signaling by receptor tyrosine kinases. Cell 2010, 141, 1117-1134.

34. Roskoski, R. Properties of FDA-approved small molecule protein kinase inhibitors: A 2022 update. Pharmacological research 2021, 106037.

35. Cohen, P; Cross, D; Jänne, PA. Kinase drug discovery 20 years after imatinib: Progress and future directions. Nature reviews drug discovery 2021, 20, 551-569.

36. Hartmann, JT; Haap, M; Kopp, H-G; et al. Tyrosine kinase inhibitors-a review on pharmacology, metabolism and side effects. Current drug metabolism 2009, 10, 470-481.

37. Schlichtig, K; Dürr, P; Dörje, F; et al. New oral anti-cancer drugs and medication safety. Deutsches Ärzteblatt International 2019, 116, 775.

38. Terada, T; Noda, S; Inui, K-i. Management of dose variability and side effects for individualized cancer pharmacotherapy with tyrosine kinase inhibitors. Pharmacology & therapeutics 2015, 152, 125-134.

39. van Erp, NP; Gelderblom, H; Guchelaar, H-J. Clinical pharmacokinetics of tyrosine kinase inhibitors. Cancer treatment reviews 2009, 35, 692-706.

40. Zhong, L; Li, Y; Xiong, L; et al. Small molecules in targeted cancer therapy: Advances, challenges, and future perspectives. Signal transduction and targeted therapy 2021, 6, 201.

41. Ellis, LM; Hicklin, DJ. Resistance to targeted therapies: refining anticancer therapy in the era of molecular oncology. Clinical Cancer Research 2009, 15, 7471-7478.

42. Sierra, JR; Cepero, V; Giordano, S. Molecular mechanisms of acquired resistance to tyrosine kinase targeted therapy. Molecular cancer 2010, 9, 1-13.

43. Huang, L; Jiang, S; Shi, Y. Tyrosine kinase inhibitors for solid tumors in the past 20 years (2001–2020). Journal of hematology & oncology 2020, 13, 1-23.

44. Kurata, Y; Miyauchi, N; Suno, M; et al. Correlation of plasma crizotinib trough concentration with adverse events in patients with anaplastic lymphoma kinase positive non-small-cell lung cancer. Journal of Pharmaceutical Health Care and Sciences 2015, 1, 1-5.

45. Tsuchiya, N; Igarashi, R; Suzuki-Honma, N; et al. Association of pharmacokinetics of axitinib with treatment outcome and adverse events in advanced renal cell carcinoma patients. 2015.

46. Rousset, M; Dutriaux, C; Bosco-Lévy, P; et al. Trough dabrafenib plasma concentrations can predict occurrence of adverse events requiring dose reduction in metastatic melanoma. Clinica Chimica Acta 2017, 472, 26-29.

47. Mueller-Schoell, A; Groenland, SL; Scherf-Clavel, O; et al. Therapeutic drug monitoring of oral targeted antineoplastic drugs. European journal of clinical pharmacology 2021, 77, 441-464.

48. Schwappach, D; Wernli, M. Medication errors in chemotherapy: incidence, types and involvement of patients in prevention. A review of the literature. European journal of cancer care 2010, 19, 285-292.

49. Dürr, P; Schlichtig, K; Kelz, C; et al. The randomized AMBORA trial: Impact of pharmacological/pharmaceutical care on medication safety and patient-reported outcomes during treatment with new oral anticancer agents. Journal of Clinical Oncology 2021, 39, 1983-1994.

50. Greer, JA; Amoyal, N; Nisotel, L; et al. A systematic review of adherence to oral antineoplastic therapies. The oncologist 2016, 21, 354-376.

51. Marin, D; Bazeos, A; Mahon, F-X; et al. Adherence is the critical factor for achieving molecular responses in patients with chronic myeloid leukemia who achieve complete cytogenetic responses on imatinib. Journal of clinical oncology 2010, 28, 2381.

52. Noens, L; Van Lierde, M-A; De Bock, R; et al. Prevalence, determinants, and outcomes of nonadherence to imatinib therapy in patients with chronic myeloid leukemia: the ADAGIO study. Blood, The Journal of the American Society of Hematology 2009, 113, 5401-5411.

53. Mathes, T; Pieper, D; Antoine, S-L; et al. Adherence influencing factors in patients taking oral anticancer agents: a systematic review. Cancer epidemiology 2014, 38, 214-226.

54. Van Leeuwen, R; Brundel, D; Neef, C; et al. Prevalence of potential drug–drug interactions in cancer patients treated with oral anticancer drugs. British journal of cancer 2013, 108, 1071-1078.

55. Gay, C; Toulet, D; Le Corre, P. Pharmacokinetic drug-drug interactions of tyrosine kinase inhibitors: A focus on cytochrome P450, transporters, and acid suppression therapy. Hematological oncology 2017, 35, 259-280.

56. Fassnacht, M; Dekkers, OM; Else, T; et al. European Society of Endocrinology Clinical Practice Guidelines on the management of adrenocortical carcinoma in adults, in collaboration with the European Network for the Study of Adrenal Tumors. European journal of endocrinology 2018, 179, G1-G46.

57. Else, T; Kim, AC; Sabolch, A; et al. Adrenocortical carcinoma. Endocr Rev 2014, 35, 282-326.

58. Sandrini, R; Ribeiro, RC; DeLacerda, L. Childhood adrenocortical tumors. The Journal of Clinical Endocrinology & Metabolism 1997, 82, 2027-2031.

59. Pianovski, MAD; Maluf, EMCP; de Carvalho, DS; et al. Mortality rate of adrenocortical tumors in children under 15 years of age in Curitiba, Brazil. Pediatric Blood & Cancer 2006, 47, 56-60.

60. Sturgeon, C; Shen, WT; Clark, OH; et al. Risk assessment in 457 adrenal cortical carcinomas: how much does tumor size predict the likelihood of malignancy? Journal of the American College of Surgeons 2006, 202, 423-430.

61. Fassnacht, M; Arlt, W; Bancos, I; et al. Management of adrenal incidentalomas: European society of endocrinology clinical practice guideline in collaboration with the European network for the study of adrenal tumors. European journal of endocrinology 2016, 175, G1-G34.

62. Jasim, S; Habra, MA. Management of adrenocortical carcinoma. Current oncology reports 2019, 21, 20.

63. Fassnacht, M; Allolio, B. Clinical management of adrenocortical carcinoma. Best practice & research Clinical endocrinology & metabolism 2009, 23, 273-289.

64. Allolio, B; Fassnacht, M. Clinical review: Adrenocortical carcinoma: clinical update. J Clin Endocrinol Metab 2006, 91, 2027-2037.

65. Fassnacht, M; Johanssen, S; Quinkler, M; et al. Limited prognostic value of the 2004 International Union Against Cancer staging classification for adrenocortical carcinoma. Cancer 2009, 115, 243-250.

66. Datta, J; Roses, RE. Surgical management of adrenocortical carcinoma: an evidence-based approach. Surgical Oncology Clinics 2016, 25, 153-170.

67. Libé, R. Adrenocortical carcinoma (ACC): diagnosis, prognosis, and treatment. Frontiers in Cell and Developmental Biology 2015, 3, 45.

68. Fassnacht, M; Assie, G; Baudin, E; et al. Adrenocortical carcinomas and malignant phaeochromocytomas: ESMO-EURACAN Clinical Practice Guidelines for diagnosis, treatment and follow-up. Ann Oncol 2020, 31, 1476-1490.

69. Megerle, F; Herrmann, W; Schloetelburg, W; et al. Mitotane monotherapy in patients with advanced adrenocortical carcinoma. The Journal of Clinical Endocrinology & Metabolism 2018, 103, 1686-1695.

70. Paragliola, RM; Torino, F; Papi, G; et al. Role of mitotane in adrenocortical carcinoma–review and state of the art. European endocrinology 2018, 14, 62.

71. Fassnacht, M; Terzolo, M; Allolio, B; et al. Combination chemotherapy in advanced adrenocortical carcinoma. New England Journal of Medicine 2012, 366, 2189-2197.

72. U.S. Food and Drug Administration. Lysodren Label. 2017; https://www.accessdata.fda.gov/drugsatfda_docs/label/2017/016885s027lbl.pdf (accessed on 2022 Nov 20).

73. Mornar, A; Sertić, M; Turk, N; et al. Simultaneous analysis of mitotane and its main metabolites in human blood and urine samples by SPE-HPLC technique. Biomedical Chromatography 2012, 26, 1308-1314.

74. European Medicines Agency. Lysodren Summary of Product Characteristics. 2009; https://www.ema.europa.eu/en/medicines/human/EPAR/lysodren (accessed on 2022 Nov 15).

75. Bergenstal, DM; Hertz, R; Lipsett, MB; et al. Chemotherapy of adrenocortical cancer with o, p' DDD. Annals of Internal Medicine 1960, 53, 672-682.

76. Waszut, U; Szyszka, P; Dworakowska, D. Understanding mitotane mode of action. J Physiol Pharmacol 2017, 68, 13-26.

77. Chortis, V; Taylor, AE; Schneider, P; et al. Mitotane therapy in adrenocortical cancer induces CYP3A4 and inhibits 5α-reductase, explaining the need for personalized glucocorticoid and androgen replacement. The Journal of Clinical Endocrinology & Metabolism 2013, 98, 161-171.

78. Arshad, U; Taubert, M; Kurlbaum, M; et al. Enzyme autoinduction by mitotane supported by population pharmacokinetic modelling in a large cohort of adrenocortical carcinoma patients. Eur J Endocrinol 2018, 179, 287-297.

79. Moy, RH. Studies of the pharmacology of o, p'DDD in man. The Journal of Laboratory and Clinical Medicine 1961, 58, 296-304.

80. Moolenaar, A; Van Slooten, H; Van Seters, A; et al. Blood levels of o, p'-DDD following administration in various vehicles after a single dose and during long-term treatment. Cancer Chemotherapy and Pharmacology 1981, 7, 51-54.

81. Haider, MS; Ahmad, T; Groll, J; et al. The challenging pharmacokinetics of mitotane: an old drug in need of new packaging. European Journal of Drug Metabolism and Pharmacokinetics 2021, 46, 575-593.

82. Laboratoire HRA Pharma. Product Monograph Lysodren. 2018; https://pdf.hres.ca/dpd_pm/00064841.PDF (accessed on 2022 Nov 20).

83. Kroiss, M; Quinkler, M; Lutz, WK; et al. Drug interactions with mitotane by induction of CYP3A4 metabolism in the clinical management of adrenocortical carcinoma. Clin Endocrinol (Oxf) 2011, 75, 585-591.

84. van Erp, NP; Guchelaar, H-J; Ploeger, BA; et al. Mitotane has a strong and a durable inducing effect on CYP3A4 activity. European Journal of Endocrinology 2011, 164, 621.

85. Raber, W. Mitotane (Lysodren®) in der Therapie des Nebennierenrindenkarzinoms. Journal für Klinische Endokrinologie und Stoffwechsel 2019, 12, 146-153.

86. Konda, B; Kirschner, LS. Novel targeted therapies in adrenocortical carcinoma. Current opinion in endocrinology, diabetes, and obesity 2016, 23, 233.

87. Phan, LM; Fuentes-Mattei, E; Wu, W; et al. Hepatocyte Growth Factor/cMET Pathway Activation Enhances Cancer Hallmarks in Adrenocortical CarcinomaHGF/cMET Pathway and Adrenocortical Carcinoma. Cancer research 2015, 75, 4131-4142.

88. Alyateem, G; Nilubol, N. Current status and future targeted therapy in adrenocortical cancer. Frontiers in Endocrinology 2021, 12, 613248.

89. Wortmann, S; Quinkler, M; Ritter, C; et al. Bevacizumab plus capecitabine as a salvage therapy in advanced adrenocortical carcinoma. European Journal of Endocrinology 2010, 162, 349.

90. Quinkler, M; Hahner, S; Wortmann, S; et al. Treatment of advanced adrenocortical carcinoma with erlotinib plus gemcitabine. The Journal of Clinical Endocrinology & Metabolism 2008, 93, 2057-2062.

91. Samnotra, V; Vassilopoulou-Sellin, R; Fojo, A; et al. A phase II trial of gefitinib monotherapy in patients with unresectable adrenocortical carcinoma (ACC). Journal of Clinical Oncology 2007, 25, 15527-15527.

92. Ganesan, P; Piha-Paul, S; Naing, A; et al. Phase I clinical trial of lenalidomide in combination with temsirolimus in patients with advanced cancer. Investigational new drugs 2013, 31, 1505-1513.

93. Naing, A; Kurzrock, R; Burger, A; et al. Phase I trial of cixutumumab combined with temsirolimus in patients with advanced cancer. Clinical Cancer Research 2011, 17, 6052-6060.

94. Kroiss, M; Quinkler, M; Johanssen, S; et al. Sunitinib in refractory adrenocortical carcinoma: a phase II, single-arm, open-label trial. The Journal of Clinical Endocrinology & Metabolism 2012, 97, 3495-3503.

95. Lerario, AM; Worden, FP; Ramm, CA; et al. The combination of insulin-like growth factor receptor 1 (IGF1R) antibody cixutumumab and mitotane as a first-line therapy for patients with recurrent/metastatic adrenocortical carcinoma: a multi-institutional NCI-sponsored trial. Hormones and Cancer 2014, 5, 232-239.

96. Haluska, P; Worden, F; Olmos, D; et al. Safety, tolerability, and pharmacokinetics of the anti-IGF-1R monoclonal antibody figitumumab in patients with refractory adrenocortical carcinoma. Cancer chemotherapy and pharmacology 2010, 65, 765-773.

97. Fassnacht, M; Berruti, A; Baudin, E; et al. Linsitinib (OSI-906) versus placebo for patients with locally advanced or metastatic adrenocortical carcinoma: a double-blind, randomised, phase 3 study. The lancet oncology 2015, 16, 426-435.

98. Berruti, A; Sperone, P; Ferrero, A; et al. Phase II study of weekly paclitaxel and sorafenib as second/third-line therapy in patients with adrenocortical carcinoma. European Journal of Endocrinology 2012, 166, 451.

99. O'Sullivan, C; Edgerly, M; Velarde, M; et al. The VEGF inhibitor axitinib has limited effectiveness as a therapy for adrenocortical cancer. The Journal of Clinical Endocrinology & Metabolism 2014, 99, 1291-1297.

100. Fallahi, P; M Ferrari, S; Di Bari, F; et al. Cabozantinib in thyroid cancer. Recent Patents on Anti-Cancer Drug Discovery 2015, 10, 259-269.

101. Grüllich, C. Cabozantinib: a MET, RET, and VEGFR2 tyrosine kinase inhibitor. Small Molecules in Oncology 2014, 207-214.

102. Singh, H; Brave, M; Beaver, JA; et al. US Food and Drug Administration approval: cabozantinib for the treatment of advanced renal cell carcinoma. Clinical Cancer Research 2017, 23, 330-335.

103. Tannir, NM; Schwab, G; Grünwald, V. Cabozantinib: an active novel multikinase inhibitor in renal cell carcinoma. Current oncology reports 2017, 19, 1-8.

104. Abou-Alfa, GK; Meyer, T; Cheng, A-L; et al. Cabozantinib in patients with advanced and progressing hepatocellular carcinoma. New England Journal of Medicine 2018, 379, 54-63.

105. Markowitz, JN; Fancher, KM. Cabozantinib: a multitargeted oral tyrosine kinase inhibitor. Pharmacotherapy: The Journal of Human Pharmacology and Drug Therapy 2018, 38, 357-369.

106. Lacy, SA; Miles, DR; Nguyen, LT. Clinical pharmacokinetics and pharmacodynamics of cabozantinib. Clinical pharmacokinetics 2017, 56, 477-491.

107. Kroiss, M; Megerle, F; Kurlbaum, M; et al. Objective response and prolonged disease control of advanced adrenocortical carcinoma with cabozantinib. The Journal of Clinical Endocrinology & Metabolism 2020, 105, 1461-1468.

108. Kroiß, M; Goebeler, M-E; Röser, C; et al. CaboACC: Cabozantinib beim fortgeschrittenen Nebennierenkarzinom nach Versagen der Standardtherapie. In Proceedings of the Forum, 2019; pp. 376-378.

109. Lacy, S; Hsu, B; Miles, D; et al. Metabolism and disposition of cabozantinib in healthy male volunteers and pharmacologic characterization of its major metabolites. Drug Metabolism and Disposition 2015, 43, 1190-1207.

110. Nguyen, L; Holland, J; Ramies, D; et al. Effect of renal and hepatic impairment on the pharmacokinetics of cabozantinib. The Journal of Clinical Pharmacology 2016, 56, 1130-1140.

111. European Medicines Agency. Cabometyx Summary of Product Characteristics. https://www.ema.europa.eu/en/documents/product-information/cabometyx-epar-product-information_en.pdf (accessed on 2021 Mar 09).

112. U.S. Food and Drug Administration. Cometriq Label. 2016; https://www.accessdata.fda.gov/drugsatfda_docs/label/2016/208692s000lbl.pdf (accessed on 2021 Mar 09).

113. Nguyen, L; Holland, J; Miles, D; et al. Pharmacokinetic (PK) drug interaction studies of cabozantinib: effect of CYP3A inducer rifampin and inhibitor ketoconazole on cabozantinib plasma PK and effect of cabozantinib on CYP2C8 probe substrate rosiglitazone plasma PK. The Journal of Clinical Pharmacology 2015, 55, 1012-1023.

114. Ren, Lj; Wu, Hj; Sun, Lh; et al. A sensitive LC–MS/MS method for simultaneous determination of cabozantinib and its metabolite cabozantinib N-oxide in rat plasma and its application in a pharmacokinetic study. Biomedical Chromatography 2018, 32, e4227.

115. Metsugi, Y; Miyaji, Y; Ogawara, K-i; et al. Appearance of double peaks in plasma concentration–time profile after oral administration depends on gastric emptying profile and weight function. Pharmaceutical research 2008, 25, 886-895.

116. Suttle, AB; Pollack, GM; Brouwer, KL. Use of a pharmacokinetic model incorporating discontinuous gastrointestinal absorption to examine the occurrence of double peaks in oral concentration–time profiles. Pharmaceutical research 1992, 9, 350-356.

117. Jamil, MO; Mineishi, S. State-of-the-art acute and chronic GVHD treatment. International journal of hematology 2015, 101, 452-466.

118. Zeiser, R; Blazar, BR. Acute graft-versus-host disease—biologic process, prevention, and therapy. New England Journal of Medicine 2017, 377, 2167-2179.

119. Jagasia, M; Zeiser, R; Arbushites, M; et al. Ruxolitinib for the treatment of patients with steroid-refractory GVHD: an introduction to the REACH trials. Immunotherapy 2018, 10, 391-402.

120. Lee, SJ; Vogelsang, G; Flowers, ME. Chronic graft-versus-host disease. Biology of Blood and Marrow Transplantation 2003, 9, 215-233.

121. Socié, G; Ritz, J. Current issues in chronic graft-versus-host disease. Blood, The Journal of the American Society of Hematology 2014, 124, 374-384.

122. Goker, H; Haznedaroglu, IC; Chao, NJ. Acute graft-vs-host disease: pathobiology and management. Experimental hematology 2001, 29, 259-277.

123. Jacobsohn, DA; Vogelsang, GB. Acute graft versus host disease. Orphanet journal of rare diseases 2007, 2, 1-9.

124. Martin, PJ; Rizzo, JD; Wingard, JR; et al. First-and second-line systemic treatment of acute graft-versus-host disease: recommendations of the American Society of Blood and Marrow Transplantation. Biology of Blood and Marrow Transplantation 2012, 18, 1150-1163.

125. Westin, JR; Saliba, RM; De Lima, M; et al. Steroid-refractory acute GVHD: predictors and outcomes. Advances in hematology 2011, 2011.

126. MacMillan, ML; Weisdorf, DJ; Wagner, JE; et al. Response of 443 patients to steroids as primary therapy for acute graft-versus-host disease: comparison of grading systems. Biology of Blood and Marrow Transplantation 2002, 8, 387-394.

127. Zeiser, R; von Bubnoff, N; Butler, J; et al. Ruxolitinib for glucocorticoid-refractory acute graft-versus-host disease. N. Engl. J. Med. 2020, 382, 1800-1810.

128. Xhaard, A; Rocha, V; Bueno, B; et al. Steroid-refractory acute GVHD: lack of long-term improved survival using new generation anticytokine treatment. Biology of Blood and Marrow Transplantation 2012, 18, 406-413.

129. Zeiser, R; Polverelli, N; Ram, R; et al. Ruxolitinib for glucocorticoid-refractory chronic graft-versus-host disease. N. Engl. J. Med. 2021, 385, 228-238.

130. Martini, DJ; Chen, Y-B; DeFilipp, Z. Recent FDA Approvals in the Treatment of Graft-Versus-Host Disease. The Oncologist 2022.

131. Shi, JG; Chen, X; McGee, RF; et al. The pharmacokinetics, pharmacodynamics, and safety of orally dosed INCB018424 phosphate in healthy volunteers. The Journal of Clinical Pharmacology 2011, 51, 1644-1654.

132. European Medicines Agency. Assessment report Jakavi. 2022; https://www.ema.europa.eu/en/documents/assessment-report/jakavi-epar-public-assessment-report_en.pdf (accessed on 2022 Jun 10).

133. Shi, JG; Chen, X; Emm, T; et al. The effect of CYP3A4 inhibition or induction on the pharmacokinetics and pharmacodynamics of orally administered ruxolitinib (INCB018424 phosphate) in healthy volunteers. The Journal of Clinical Pharmacology 2012, 52, 809-818.

134. Bhatti, Z; Shaukat, A; Almyroudis, NG; et al. Review of epidemiology, diagnosis, and treatment of invasive mould infections in allogeneic hematopoietic stem cell transplant recipients. Mycopathologia 2006, 162, 1-15.

135. Yamaguchi, Y; Akiyoshi, T; Kawamura, G; et al. Comparison of the inhibitory effects of azole antifungals on cytochrome P450 3A4 genetic variants. Drug metabolism and pharmacokinetics 2021, 38, 100384.

136. Saad, AH; DePestel, DD; Carver, PL. Factors influencing the magnitude and clinical significance of drug interactions between azole antifungals and select immunosuppressants. Pharmacotherapy: The Journal of Human Pharmacology and Drug Therapy 2006, 26, 1730-1744.

137. U.S. Food and Drug Administration. Clinical Drug Interaction Studies —Cytochrome P450 Enzyme- and Transporter-Mediated Drug Interactions Guidance for Industry. 2020; https://www.fda.gov/regulatory-information/search-fda-guidance-documents/clinical-drug-interaction-studies-cytochrome-p450-enzyme-and-transporter-mediated-drug-interactions (accessed on 2022 Aug 05).

138. European Medicines Agency. Jakavi Summary of Product Characteristics. https://www.ema.europa.eu/en/documents/product-information/jakavi-epar-product-information_en.pdf (accessed on 2022 Jun 10).

139. Maertens, JA; Girmenia, C; Brüggemann, RJ; et al. European guidelines for primary antifungal prophylaxis in adult haematology patients: summary of the updated recommendations from the European Conference on Infections in Leukaemia. Journal of Antimicrobial Chemotherapy 2018, 73, 3221-3230.

140. Ullmann, AJ; Lipton, JH; Vesole, DH; et al. Posaconazole or fluconazole for prophylaxis in severe graft-versus-host disease. New England Journal of Medicine 2007, 356, 335-347.

141. Isberner, N; Kraus, S; Grigoleit, GU; et al. Ruxolitinib exposure in patients with acute and chronic graft versus host disease in routine clinical practice—A prospective single-center trial. Cancer Chemotherapy and Pharmacology 2021, 88, 973-983.

142. Abrantes, JA; Jönsson, S; Karlsson, MO; et al. Handling interoccasion variability in model-based dose individualization using therapeutic drug monitoring data. British journal of clinical pharmacology 2019, 85, 1326-1336.

143. Kang, J-S; Lee, M-H. Overview of therapeutic drug monitoring. The Korean journal of internal medicine 2009, 24, 1.

144. Gross, AS. Best practice in therapeutic drug monitoring. British journal of clinical pharmacology 2001, 52, 5-9.

145. Fiaturi, N; Greenblatt, DJ. Therapeutic Drug Monitoring of Antidepressants. In Antidepressants: From Biogenic Amines to New Mechanisms of Action, Macaluso, M., Preskorn, S.H., Eds.; Springer International Publishing: Cham, 2019; pp. 115-133.

146. Mitchell, PB. Therapeutic drug monitoring of psychotropic medications. British journal of clinical pharmacology 2001, 52, 45-54.

147. Hiemke, C; Baumann, P; Bergemann, N; et al. AGNP consensus guidelines for therapeutic drug monitoring in psychiatry: update 2011. Pharmacopsychiatry 2011, 44, 195-235.

148. Kahan, BD; Keown, P; Levy, GA; et al. Therapeutic drug monitoring of immunosuppressant drugs in clinical practice. Clinical therapeutics 2002, 24, 330-350.

149. Brunet, M; Van Gelder, T; Åsberg, A; et al. Therapeutic drug monitoring of tacrolimus-personalized therapy: second consensus report. Therapeutic drug monitoring 2019, 41, 261-307.

150. Patsalos, PN; Spencer, EP; Berry, DJ. Therapeutic drug monitoring of antiepileptic drugs in epilepsy: a 2018 update. Therapeutic drug monitoring 2018, 40, 526-548.

151. Johannessen Landmark, C; Johannessen, SI; Patsalos, PN. Therapeutic drug monitoring of antiepileptic drugs: Current status and future prospects. Expert opinion on drug metabolism & toxicology 2020, 16, 227-238.

152. Ludden, TM. Nonlinear pharmacokinetics. Clinical pharmacokinetics 1991, 20, 429-446.

153. Ogilvie, RI. Clinical pharmacokinetics of theophylline. Clinical pharmacokinetics 1978, 3, 267-293.

154. Grześk, G; Stolarek, W; Kasprzak, M; et al. Therapeutic drug monitoring of digoxin–20 years of experience. Pharmacological Reports 2018, 70, 184-189.

155. Ye, Z-K; Tang, H-L; Zhai, S-D. Benefits of therapeutic drug monitoring of vancomycin: a systematic review and meta-analysis. PloS one 2013, 8, e77169.

156. Roberts, JA; Norris, R; Paterson, DL; et al. Therapeutic drug monitoring of antimicrobials. British journal of clinical pharmacology 2012, 73, 27-36.

157. Aarnoutse, RE; Schapiro, JM; Boucher, CA; et al. Therapeutic drug monitoring. Drugs 2003, 63, 741-753.

158. Gao, B; Yeap, S; Clements, A; et al. Evidence for therapeutic drug monitoring of targeted anticancer therapies. Journal of clinical oncology 2012, 30, 4017-4025.

159. Decosterd, LA; Widmer, N; Zaman, K; et al. Therapeutic drug monitoring of targeted anticancer therapy. Biomarkers in medicine 2015, 9, 887-893.

160. Pauwels, S; Allegaert, K. Therapeutic drug monitoring in neonates. Archives of disease in childhood 2016, 101, 377-381.

161. Jager, NG; van Hest, RM; Lipman, J; et al. Therapeutic drug monitoring of anti-infective agents in critically ill patients. Expert review of clinical pharmacology 2016, 9, 961-979.

162. Paci, A; Veal, G; Bardin, C; et al. Review of therapeutic drug monitoring of anticancer drugs part 1–cytotoxics. European journal of cancer 2014, 50, 2010-2019.

163. Widmer, N; Bardin, C; Chatelut, E; et al. Review of therapeutic drug monitoring of anticancer drugs part two–targeted therapies. European journal of cancer 2014, 50, 2020-2036.

164. Jelliffe, RW; Neely, M. Individualized drug therapy for patients: basic foundations, relevant software and clinical applications; Academic Press: 2016.

165. Janssen, JM; Dorlo, TP; Beijnen, JH; et al. Evaluation of extrapolation methods to predict trough concentrations to guide therapeutic drug monitoring of oral anticancer drugs. Therapeutic Drug Monitoring 2020, 42, 532-539.

166. Hutchinson, L; Sinclair, M; Reid, B; et al. A descriptive systematic review of salivary therapeutic drug monitoring in neonates and infants. British journal of clinical pharmacology 2018, 84, 1089-1108.

167. Guthrie, R; Susi, A. A simple phenylalanine method for detecting phenylketonuria in large populations of newborn infants. Pediatrics 1963, 32, 338-343.

168. De Kesel, PM; Lambert, WE; Stove, CP. Does volumetric absorptive microsampling eliminate the hematocrit bias for caffeine and paraxanthine in dried blood samples? A comparative study. Analytica chimica acta 2015, 881, 65-73.

169. Denniff, P; Spooner, N. Volumetric absorptive microsampling: a dried sample collection technique for quantitative bioanalysis. Analytical chemistry 2014, 86, 8489-8495.

170. Enderle, Y; Foerster, K; Burhenne, J. Clinical feasibility of dried blood spots: Analytics, validation, and applications. Journal of Pharmaceutical and Biomedical Analysis 2016, 130, 231-243.

171. Rowland, M; Emmons, GT. Use of dried blood spots in drug development: pharmacokinetic considerations. The AAPS journal 2010, 12, 290-293.

172. Emmons, G; Rowland, M. Pharmacokinetic considerations as to when to use dried blood spot sampling. Bioanalysis 2010, 2, 1791-1796.

173. Boons, CC; Timmers, L; Janssen, JJ; et al. Feasibility of and patients' perspective on nilotinib dried blood spot self-sampling. European Journal of Clinical Pharmacology 2019, 75, 825-829.

174. Sakhi, AK; Bastani, NE; Ellingjord-Dale, M; et al. Feasibility of self-sampled dried blood spot and saliva samples sent by mail in a population-based study. BMC cancer 2015, 15, 1-9.

175. Evans, C; Arnold, M; Bryan, P; et al. Implementing dried blood spot sampling for clinical pharmacokinetic determinations: considerations from the IQ Consortium Microsampling Working Group. 2015, 17, 292-300.

176. Antunes, MV; Charão, MF; Linden, R. Dried blood spots analysis with mass spectrometry: potentials and pitfalls in therapeutic drug monitoring. Clinical biochemistry 2016, 49, 1035-1046.

177. Peters, SA. Physiologically-Based Pharmacokinetic (PBPK) Modeling and Simulations: Principles, Methods, and Applications in the Pharmaceutical Industry, 1st ed.; John Wiley & Sons, Inc.: 2012.

178. Zimmermann, S; Aghai, F; Schilling, B; et al. Volumetric absorptive microsampling (VAMS) for the quantification of ten kinase inhibitors and determination of their in vitro VAMS-to-plasma ratio. Journal of Pharmaceutical and Biomedical Analysis 2022, 211, 114623.

179. Opitz, P; Zimmermann, S; Mc Laughlin, AM; et al. Development and validation of a bioanalytical method for the quantification of axitinib from plasma and capillary blood using volumetric absorptive microsampling (VAMS) and on-line solid phase extraction (SPE) LC-MS. Journal of Pharmaceutical and Biomedical Analysis 2022, 221, 115033.

180. Isberner, N; Gesierich, A; Balakirouchenane, D; et al. Monitoring of Dabrafenib and Trametinib in Serum and Self-Sampled Capillary Blood in Patients with BRAFV600-Mutant Melanoma. Cancers 2022, 14, 4566.

181. Henrich, A. Pharmacometric modelling and simulation to optimise paclitaxel combination therapy based on pharmacokinetics, cumulative neutropenia and efficacy. 2018.

182. Workgroup, EM; Marshall, SF; Burghaus, R; et al. Good Practices in Model-Informed Drug Discovery and Development: Practice, Application, and Documentation. CPT Pharmacometrics Syst Pharmacol 2016, 5, 93-122.

183. Kim, TH; Shin, S; Shin, BS. Model-based drug development: application of modeling and simulation in drug development. Journal of Pharmaceutical Investigation 2017, 48, 431-441.

184. Huang, Q; Riviere, JE. The application of allometric scaling principles to predict pharmacokinetic parameters across species. Expert opinion on drug metabolism & toxicology 2014, 10, 1241-1253.

185. U.S. Food and Drug Administration. Physiologically Based Pharmacokinetic Analyses — Format and Content — Guidance for Industry. 2018; https://www.fda.gov/regulatory-information/search-fda-guidance-documents/physiologically-based-pharmacokinetic-analyses-format-and-content-guidance-industry (accessed on 2022 Aug 28).

186. Zhuang, X; Lu, C. PBPK modeling and simulation in drug research and development. Acta Pharm Sin B 2016, 6, 430-440.

187. Kuepfer, L; Niederalt, C; Wendl, T; et al. Applied concepts in PBPK modeling: how to build a PBPK/PD model. CPT: pharmacometrics & systems pharmacology 2016, 5, 516-531.

188. Jones, H; Rowland-Yeo, K. Basic concepts in physiologically based pharmacokinetic modeling in drug discovery and development. CPT: pharmacometrics & systems pharmacology 2013, 2, 1-12.

189. Open Systems Pharmacology. PK-Sim® software manual. Available online: https://docs.open-systems-pharmacology.org/ (accessed on 2019 Sep 26).

190. Rodgers, T; Leahy, D; Rowland, M. Physiologically based pharmacokinetic modeling 1: predicting the tissue distribution of moderate-to-strong bases. Journal of pharmaceutical sciences 2005, 94, 1259-1276.

191. Rodgers, T; Rowland, M. Physiologically based pharmacokinetic modelling 2: predicting the tissue distribution of acids, very weak bases, neutrals and zwitterions. Journal of pharmaceutical sciences 2006, 95, 1238-1257.

192. Schmitt, W. General approach for the calculation of tissue to plasma partition coefficients. Toxicology in vitro 2008, 22, 457-467.

193. Poulin, P; Theil, FP. A priori prediction of tissue: plasma partition coefficients of drugs to facilitate the use of physiologically-based pharmacokinetic models in drug discovery. Journal of pharmaceutical sciences 2000, 89, 16-35.

194. Berezhkovskiy, LM. Volume of distribution at steady state for a linear pharmacokinetic system with peripheral elimination. Journal of pharmaceutical sciences 2004, 93, 1628-1640.

195. Willmann, S; Lippert, J; Schmitt, W. From physicochemistry to absorption and distribution: predictive mechanistic modelling and computational tools. Expert opinion on drug metabolism & toxicology 2005, 1, 159-168.

196. Yun, YE; Cotton, CA; Edginton, AN. Development of a decision tree to classify the most accurate tissue-specific tissue to plasma partition coefficient algorithm for a given compound. Journal of pharmacokinetics and pharmacodynamics 2014, 41, 1-14.

197. Utsey, K; Gastonguay, MS; Russell, S; et al. Quantification of the impact of partition coefficient prediction methods on physiologically based pharmacokinetic model output using a standardized tissue composition. Drug Metabolism and Disposition 2020, 48, 903-916.

198. Graham, H; Walker, M; Jones, O; et al. Comparison of in-vivo and in-silico methods used for prediction of tissue: plasma partition coefficients in rat. Journal of Pharmacy and Pharmacology 2012, 64, 383-396.

199. Sheiner, LB. The population approach to pharmacokinetic data analysis: rationale and standard data analysis methods. Drug metabolism reviews 1984, 15, 153-171.

200. Mould, DR; Upton, R. Basic concepts in population modeling, simulation, and model-based drug development. CPT: pharmacometrics & systems pharmacology 2012, 1, 1-14.

201. Steimer, J-L; Mallet, A; Golmard, J-L; et al. Alternative approaches to estimation of population pharmacokinetic parameters: comparison with the nonlinear mixed-effect model. Drug metabolism reviews 1984, 15, 265-292.

202. Ette, EI; Williams, PJ. Population pharmacokinetics II: estimation methods. Annals of Pharmacotherapy 2004, 38, 1907-1915.

203. Bonate, PL. Nonlinear mixed effects models: theory. In Pharmacokinetic-pharmacodynamic modeling and simulation; Springer: 2011; pp. 233-301.

204. Duffull, SB; Wright, DF; Winter, HR. Interpreting population pharmacokinetic-pharmacodynamic analyses–a clinical viewpoint. British journal of clinical pharmacology 2011, 71, 807-814.

205. Nock, V. Pharmacometric modelling of processes in the haematopoietic system and blood: Leukocyte progenitor proliferation and maturation in vitro and in cancer patients and erythrocyte ageing in diabetic patients. 2013.

206. Darwich, A; Ogungbenro, K; Vinks, AA; et al. Why has model-informed precision dosing not yet become common clinical reality? Lessons from the past and a roadmap for the future. Clinical Pharmacology & Therapeutics 2017, 101, 646-656.

207. Sonawane, R; Wagh, R; Dhumane, JR; et al. The Stages of Drug Discovery and Development Process. Asian Journal of Pharmaceutical Research and Development 2019, 7, 62-67.

208. Wicha, SG; Märtson, AG; Nielsen, EI; et al. From therapeutic drug monitoring to model-informed precision dosing for antibiotics. Clinical Pharmacology & Therapeutics 2021, 109, 928-941.

209. Maier, C; Hartung, N; de Wiljes, J; et al. Bayesian data assimilation to support informed decision making in individualized chemotherapy. CPT: pharmacometrics & systems pharmacology 2020, 9, 153-164.

210. Maier, C; de Wiljes, J; Hartung, N; et al. A continued learning approach for model-informed precision dosing: updating models in clinical practice. CPT: Pharmacometrics & Systems Pharmacology 2022, 11, 185-198.

211. Marsousi, N; Samer, CF; Fontana, P; et al. Coadministration of ticagrelor and ritonavir: toward prospective dose adjustment to maintain an optimal platelet inhibition using the PBPK approach. Clinical Pharmacology & Therapeutics 2016, 100, 295-304.

212. Leroux, S; Jacqz-Aigrain, E; Biran, V; et al. Clinical utility and safety of a model-based patient-tailored dose of vancomycin in neonates. Antimicrobial agents and chemotherapy 2016, 60, 2039-2042.

213. Smits, A; De Cock, R; Allegaert, K; et al. Prospective evaluation of a model-based dosing regimen for amikacin in preterm and term neonates in clinical practice. Antimicrobial agents and chemotherapy 2015, 59, 6344-6351.

214. Janssen, EJ; Välitalo, PA; Allegaert, K; et al. Towards rational dosing algorithms for vancomycin in neonates and infants based on population pharmacokinetic modeling. Antimicrobial agents and chemotherapy 2016, 60, 1013-1021.

215. Krekels, EH; Tibboel, D; De Wildt, SN; et al. Evidence-based morphine dosing for postoperative neonates and infants. Clinical pharmacokinetics 2014, 53, 553-563.

216. Neely, M; Philippe, M; Rushing, T; et al. Accurately achieving target busulfan exposure in children and adolescents with very limited sampling and the BestDose software. Therapeutic drug monitoring 2016, 38, 332.

217. Keizer, RJ; Ter Heine, R; Frymoyer, A; et al. Model-informed precision dosing at the bedside: scientific challenges and opportunities. CPT: pharmacometrics & systems pharmacology 2018, 7, 785-787.

218. Kantasiripitak, W; Van Daele, R; Gijsen, M; et al. Software tools for model-informed precision dosing: how well do they satisfy the needs? Frontiers in pharmacology 2020, 11, 620.

219. Zhang, X; Yang, Y; Grimstein, M; et al. Application of PBPK modeling and simulation for regulatory decision making and its impact on US prescribing information: an update on the 2018-2019 submissions to the US FDA's office of clinical pharmacology. The Journal of Clinical Pharmacology 2020, 60, S160-S178.

220. Hens, B; Pathak, SM; Mitra, A; et al. In Silico Modeling Approach for the Evaluation of Gastrointestinal Dissolution, Supersaturation, and Precipitation of Posaconazole. Mol Pharm 2017, 14, 4321-4333.

221. Kersemaekers, WM; van Iersel, T; Nassander, U; et al. Pharmacokinetics and safety study of posaconazole intravenous solution administered peripherally to healthy subjects. Antimicrob. Agents Chemother. 2015, 59, 1246-1251.

222. Krishna, G; Ma, L; Martinho, M; et al. Single-dose phase I study to evaluate the pharmacokinetics of posaconazole in new tablet and capsule formulations relative to oral suspension. Antimicrob. Agents Chemother. 2012, 56, 4196-4201.

223. Vuletić, L; Herceg, M; Ferderber, K; et al. Single-Dose Pharmacokinetic Properties and Relative Bioavailability of Different Formulations of Posaconazole Oral Suspension in Healthy Volunteers. Clin. Pharmacol. Drug Dev. 2019, 8, 827-836.

224. Umehara, K; Huth, F; Jin, Y; et al. Drug-drug interaction (DDI) assessments of ruxolitinib, a dual substrate of CYP3A4 and CYP2C9, using a verified physiologically based pharmacokinetic (PBPK) model to support regulatory submissions. Drug Metab Pers Ther 2019, 34.

225. Chen, X; Shi, JG; Emm, T; et al. Pharmacokinetics and pharmacodynamics of orally administered ruxolitinib (INCB018424 phosphate) in renal and hepatic impairment patients. Clin. Pharmacol. Drug Dev. 2014, 3, 34-42.

226. Ogama, Y; Mineyama, T; Yamamoto, A; et al. A randomized dose-escalation study to assess the safety, tolerability, and pharmacokinetics of ruxolitinib (INC424) in healthy Japanese volunteers. Int. J. Hematol. 2013, 97, 351-359.